ЖУРНАЛ
ПРИКЛАДНОЙ ХИМИИ

Volume 32, No. 6
June 1959

JOURNAL OF
APPLIED CHEMISTRY
OF THE USSR

(ZHURNAL PRIKLADNOI KHIMII)

IN ENGLISH TRANSLATION

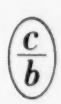

CONSULTANTS BUREAU, INC.

Volume 32, No. 6

June, 1959

JOURNAL OF
APPLIED CHEMISTRY
OF THE USSR

(ZHURNAL PRIKLADNOI KHIMII)

A publication of the Academy of Sciences of the USSR

IN ENGLISH TRANSLATION

Year and issue of first translation:
Vol. 23, No. 1 January 1950

	U. S. and Canada	*Foreign*
Annual subscription	*$60.00*	*$65.00*
Annual subscription for libraries of nonprofit academic institutions	*20.00*	*25.00*
Single issue	*7.50*	*7.50*

Printed in the United States of America

JOURNAL OF APPLIED CHEMISTRY OF THE USSR

Volume 32, Number 6 June, 1959

CONTENTS

CONTENTS (continued)

CONTENTS (continued)

EFFECT OF ELECTROLYTE ADDITIONS ON THE HARDENING OF $3\,CaO \cdot Al_2O_3$

P. P. Budnikov and R. D. Azelitskaya

Much attention has been devoted recently to accelerated hardening of Portland cement, as this problem is associated with the use of articles sooner after their manufacture, decrease of costs, and increase of the productivity of concrete and ferroconcrete works.

Many different methods have been recommended for accelerating the hardening of Portland cement; among these, addition of electrolytes occupies an important position.

The hardening of Portland cement has been studied for a number of years by A. A. Baikov, V. A. Kind, V. N. Yung, Yu. M. Butt, P. P. Budnikov, S. D. Okorokov, and others, but many problems relating to the nature of the processes and properties and composition of the products formed in the hardening of cement have not been finally solved.

The number of unsolved problems is increased if the hardening of Portland cement under the influence of added electrolytes is considered.

The purpose of the present work was to study the effects of small amounts of added electrolytes on the hardening of C_3A* as one of the constituents of Portland cement clinker.

This paper contains the results of a study of the changes in the strength of C_3A and of its rate of hydration in presence of salts of alkali and alkaline-earth metals.

The C_3A used in the investigation was synthesized in the laboratory in a kerosene kiln.

Specimens for strength testing were made from a 1:3 mortar, molded under a pressure of 400 kg/cm^2 in the form of 2 × 2 × 2 cm cubes. The C_3A was ground to pass completely through a No. 85 sieve; a Volsk sand fraction passing through a No. 400 sieve and retained on a No. 200 sieve was used.

The hydration rate of C_3A was studied by determination of the "calcination loss" of specimens made from cement paste of W/C = 0.89.

Data on the effects of small amounts of salts of alkali and alkaline-earth metals on the strength of C_3A are presented in Table 2.

Small amounts of electrolytes (0.1 and 0.5%) were added. We consider that, in accordance with the amount added, electrolytes may have a dual function in the hardening of C_3A. Electrolytes in small amounts change the conditions of interaction between C_3A grains and water. Since this interaction commences, in general, on the grain surface, and electrolytes influence the process, we consider that electrolytes may be classed as surface-active substances.

Electrolytes added in large amounts may enter into chemical reactions with the hydration products of C_3A to form new compounds, which also influence the properties of hydrated C_3A. This dual function of electrolytes has been noted by other authors [1, 2].

* $C_3A = 3CaO \cdot Al_2O_3$.

TABLE 1

Effect of Small Amounts of Added Electrolytes on the Strength of C_3A

Nature and amount (%) of additive	Compressive strength (kg/cm^2)			
	3 days	7 days	28 days	3 months
No addition	37	43	39	91
0.1 K_2CO_3	22	16	18	41
0.5 K_2CO_3	3	3	3	11
0.1 K_2SO_4	13	12	12	41
0.5 K_2SO_4	22	13	6	33
0.1 $CaCl_2$	33	31	62	79
0.5 $CaCl_2$	31	35	41	90
0.1 $CaSO_4$	19	17	40	70
0.5 $CaSO_4$	16	18	38	71
0.1 $CaCO_3$	25	25	22	51
0.5 $CaCO_3$	25	29	29	90

TABLE 2

Effects of Small Amounts of Added Electrolytes on the Rate of Hydration of C_3A

Nature and amount (%) of additive	Amount of bound water (%)					
	3 days	7 days	28 days	3 months	6 months	1 year
No addition	21.67	23.69	25.93	26.91	28.42	28.46
0.1 K_2CO_3	21.42	25.73	26.66	27.15	28.71	28.46
0.5 K_2CO_3	19.94	21.60	23.29	26.11	28.61	28.27
0.1 K_2SO_4	21.02	22.41	25.40	27.09	28.40	28.19
0.5 K_2SO_4	21.80	23.25	25.27	27.14	28.90	28.45
0.1 $CaCl_2$	20.92	22.57	25.83	27.49	29.11	28.58
0.5 $CaCl_2$	20.45	20.96	24.64	27.91	29.18	28.52
0.1 $CaSO_4$	18.30	21.13	24.72	26.99	28.02	28.21
0.5 $CaSO_4$	21.20	22.47	26.06	27.15	28.73	28.16
0.1 $CaCO_3$	22.11	22.30	25.47	27.42	29.00	28.51
0.5 $CaCO_3$	22.30	23.37	25.14	27.15	29.14	28.43

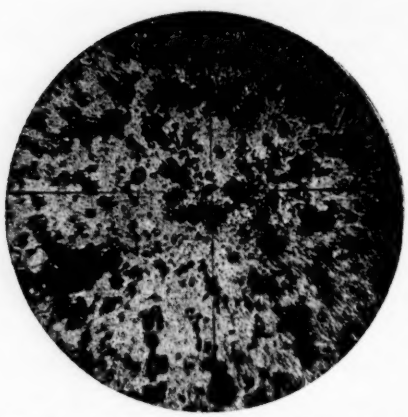

Fig. 1. Hydrated C_3A in ordinary light; magnification 120.

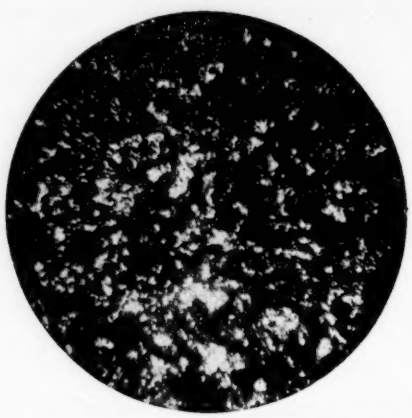

Fig. 2. Hydrated C_3A in polarized light; magnification 120.

In this investigation we were mainly concerned with the influence of electrolytes as surface-active substances on the hardening of C_3A.

From the data in Table 1 it may be concluded that additions of salts of alkali and alkaline-earth metals in the proportions of 0.1 and 0.5% on the weight of C_3A have an adverse effect on the strength increase of the mineral.

Data on the effects of small amounts of electrolytes on the hydration rate of C_3A are presented in Table 2.

Consideration of the above results leads to the following conclusions.

In most cases additions of alkali and alkaline-earth metals (0.1 and 0.5%) decrease the amount of bound water during the first stages of hardening (up to 28 days) relative to the amount of bound water in C_3A without additives. After 28 days the amount of bound water begins to increase (in specimens with added electrolytes) and approaches the amount of bound water in pure C_3A.

In the 90-180 day period the amount of bound water in C_3A with these additives exceeds the amount of bound water in pure C_3A.

After 180 days of hydration the amount of bound water in specimens with additives begins to decrease and approaches the value for pure C_3A.

It is known that when C_3A is hydrated under normal temperature conditions hexagonal crystals of $2CaO \cdot Al_2O_3 \cdot 8H_2O$ and $4CaO \cdot Al_2O_3 \cdot 13H_2O$ are formed; these are unstable and gradually they recrystallize into cubic $3CaO \cdot Al_2O_3 \cdot 6H_2O$.

According to Lopatnikova [3], the rate of formation of hexagonal hydroaluminates and their conversion into the cubic form greatly depend on the ratio of solid and liquid phases. The less water in the aluminate–water system, the longer do the hexagonal platelets persist. They may exist from 1 day to 4-5 months, in accordance with the amount of water.

Evidently the strength of hydrated C_3A depends on the content of hexagonal platelets. The cubic hydroaluminate has weaker binding properties, and this accounts for the usual decrease of the C_3A strength at later stages.

The increase of the C_3A strength was somewhat retarded in our experiments. This may be due to the fact that the specimens for the strength tests were not made from a plastic paste, but were molded with very small amounts of water. As was noted above, the life of the hexagonal platelets is greater in presence of smaller amounts of water; probably if the amount of water is less, the rate of formation of the hexagonal platelets is retarded, and the strength increase of the hydrating C_3A is delayed accordingly.

Our results showed that added electrolytes at first retard hydration of C_3A, i.e., they slow down the rate of formation of the hexagonal platelets. It seems likely that the water needed for hydration of C_3A first interacts with the added electrolytes (with dissociation of the water molecules), and hydration of C_3A is therefore retarded. The dissociated water molecules, which have higher kinetic energy than associated molecules (present when electrolytes are not added), act more intensively on C_3A, with accelerated formation of hexagonal platelets and conversion of these platelets into the cubic form.

This conclusion is consistent with the adverse effect of electrolytes on the strength increase of C_3A.

To confirm this conclusion, we used Yung's method [4] of microstructural analysis for studying the hydration of C_3A in presence of these additives.

The specimens for investigation were prepared from C_3A powder passed through a sieve with 10,000 holes per cm^2, mixed with water in 1:100 ratio. The investigation was carried out for the first hydration period (7 days).

Microstructural analysis gave the following results.

Hexagonal platelets and a microgranular mass are formed during hydration of C_3A. In determinations of the refractive index of the hexagonal platelets it was found that $N_{av} = 1.520$; they can therefore be regarded as a hydroaluminate of the type $3CaO \cdot Al_2O_3 \cdot 8H_2O$. The specimens also contained strongly birefringent small crystals of $N_{av} = 1.574$; these were $Ca(OH)_2$ crystals.

Fig. 1 is a micrograph of hydrated C_3A (7 days) in ordinary light. Hexagonal platelets and a microgranular mass are clearly seen.

Fig. 2 is a micrograph of hydrated C_3A (7 days) in polarized light. Fine crystals of $Ca(OH)_2$ can be clearly seen.

In a study of the hydration of C_3A in presence of 0.5% $CaCl_2$, it was found after 7 days that the specimen contains more strongly-polarizing $Ca(OH)_2$ crystals than pure C_3A. The microgranular mass is much finer in this specimen than in pure hydrated C_3A, and resembles an amorphous mass. The hexagonal platelets are somewhat less numerous.

Fig. 3 is a micrograph of hydrated C_3A (after 7 days) with addition of 0.5% $CaCl_2$.

It may be concluded from these results that during the first hardening period of C_3A, added $CaCl_2$ retards formation of hexagonal hydroaluminates and intensifies separation of $Ca(OH)_2$ from C_3A.

In a study of the hydration of C_3A in presence of 0.5% K_2SO_4, the same effects were found after 7 days as with addition of $CaCl_2$, but they were less pronounced; this means that added K_2SO_4 also favors hydrolysis of C_3A and greater liberation of $Ca(OH)_2$, and also retards formation of hexagonal platelets, but to a lesser degree than $CaCl_2$ does.

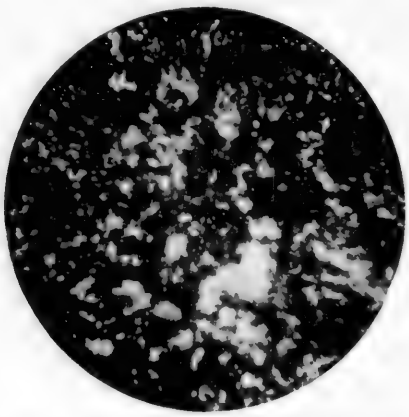

Fig. 3. Hydrated C_3A with addition of 0.5% $CaCl_2$.

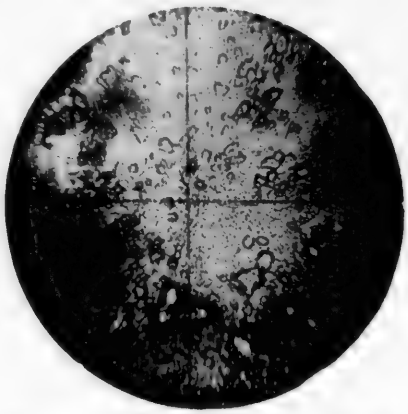

Fig. 4. Hydrated C_3A with addition of 0.5% K_2SO_4.

Fig. 4 is a micrograph (in ordinary light) of hydrated C_3A with 0.5% K_2SO_4. Hexagonal platelets and a large amount of a microgranular mass, amorphous in appearance, can be seen.

In hydration of C_3A with addition of 0.5% $CaCO_3$ there is a very large amount of a gel-like mass, covering the hexagonal plates of calcium hydroaluminate with newly-formed $C_3A \cdot CaCO_3 \cdot 18H_2O$ [5]. The crystals of $Ca(OH)_2$ are not numerous, and they are very small. A microgranular mass is seen. The hydration process is clearly retarded.

These results of microstructrual analysis confirm the earlier conclusion that small amounts of salts of alkali and alkaline-earth metals retard hydration of C_3A during the early stages of hardening (up to 28 days). This retardation is due to changes in the conditions of interaction of the water added during mixing with the C_3A grains in presence of these additives.

Changes in the conditions of interaction of the mixing water with C_3A grains influence the crystallization of the hydrated formations – the size of the crystals formed and the degree of crystallization.

SUMMARY

Additions of 0.1 and 0.5% of electrolytes to C_3A have an adverse effect on its strength increase. The adverse effect of small amounts of electrolytes on the strengthening of C_3A may be attributed to the fact that they

change the conditions of interaction of the mixing water with C_3A grains, retarding this interaction during the first stages of hardening.

LITERATURE CITED

[1] V. F. Zhigalkovich, Coll. Sci. Trans. Sci. Res. Inst. Constructional Materials, Ministry of the Building Materials Industry of the Belorussian SSR, No. 4 (Minsk, 1955).

[2] U. Ayapov, J. Acad. Sci. Kazakh SSR 12 (1956).

[3] L. Ya. Lopatnikov, Proceedings of Conference on Cement Technology [In Russian] (Industrial Construction Press, 1956).

[4] V. N. Yung, Introduction to Cement Technology [In Russian] (1938).

[5] R. Turriziani and G. Schippa, La Ricerca Scientifica 26, 9, 2792 (1956).

Received October 20, 1958

INTERACTION OF SILICA WITH THE HYDROXIDES OF CALCIUM AND MAGNESIUM UNDER HYDROTHERMAL CONDITIONS

Yu. M. Butt and L. N. Rashkovich

There are three possible variants of the interaction of silica with calcium and magnesium hydroxides under conditions of hydrothermal treatment.

1. Both components dissolve in the liquid phase, and then interact to form sparingly-soluble hydrated compounds which are precipitated.

2. On passing into solution, each component attacks the surface of the particles of the other (the component which is the more soluble under the given conditions evidently plays the more active role); here the new compounds are formed and then become detached from the "parent" particles, thereby creating conditions for continuation of the reaction.

3. A solid-phase reaction involving water takes place at the surfaces of contacting particles of the two components. In addition, water acts as a catalyst for the reaction, lowering the surface energy of the particles and thereby facilitating their interaction.

The object of the present work was to elucidate the nature of the processes which take place in the hydrothermal interaction of silica with calcium and magnesium hydroxides; this is of considerable practical as well as theoretical interest.

EXPERIMENTAL

Depth of attack of the quartz particles. Molded specimens of equal density were prepared, containing magnesium oxide and three different sand fractions, with particles of 10–20, 40–60 and 105–150 μ. The specimens were subjected to hydrothermal treatment at 175° under the corresponding saturated steam pressure.

Let us assume that during hydrothermal treatment the components interacted according to the third variant (in the solid phase). It seems likely that in this case the thickness of the layer of new formations around the more active small quartz particles is greater than around the larger particles, or, if the difference between the sizes of the quartz particles is not large enough to have a significant influence on their activity (surface energy),

TABLE 1

Effect of the Size of Quartz Particles on Depth of Attack

Composition of mixture	Time of treatment at 175° (hours)	D_{av} (in μ)	$\frac{SiO_{2\,bound}}{SiO_{2\,total}}$ (k)	x (in μ)
15% MgO + quartz (fraction 10–20μ)	8	15	0.147	0.38
15% MgO + quartz (fraction 20–40μ)	8	30	0.125	0.61
20% MgO + quartz (fraction 10–20μ)	120	15	0.265	0.77
20% MgO + quartz (fraction 105–150μ)	120	128	0.154	3.46

the thickness of the newly formed layer would be independent of the size of the original particles. In a solid-phase reaction it is the thickness of the newly formed layer which prevents interdiffusion and therefore interaction of the starting substances. Therefore, for a given treatment time, the thickness of the newly formed layers around the individual quartz particles is determined only by the mobility (activity) of the molecules present on the particle surfaces and able to diffuse through the layer toward the second component.

It is a very complicated matter to determine the thickness of the newly formed layer directly under the microscope, but it can be calculated, as it is proportional to the depth of attack of the quartz, i.e., the decrease in the size of the original particle. If we assume that the particles are spherical of average diameter D, we can find the depth of attack (x) from the following expression:

$$\frac{1}{3}\pi D^3 n\gamma - \frac{1}{3}\pi (D - 2x)^3 n\gamma = k \cdot \frac{1}{3}\pi D^3 n\gamma,$$

where k is the fraction of quartz reacted, n is the number of quartz particles, and γ is the density of quartz.

Solving this equation for x, we have

$$x = \frac{D}{2}(1 - \sqrt[3]{1-k}).$$

Values of x calculated from experimental data are given in Table 1.

It is clear from Table 1 that the depth of attack (x) of the quartz particles under the given treatment conditions increases with particle size. It was noted earlier that if the reaction took place in the solid phase the reverse effect should be observed, or else the depth of attack should be constant.

These results can be explained if we accept the hypothesis that the reaction takes place in solution. Indeed, since the bulk density (and hence the porosity) of the specimens was the same, the amounts of water present in them were also equal. If we assume that quartz–water equilibrium had been reached and that solubility differences between particles of different sizes are not large, then equal amounts of SiO_2 must have passed into the liquid phase in all the specimens (k = constant). In that case, as the equation shows, the depth of attack must be directly proportional to the diameter.

There is no direct proportionality in our results, and deviations from it increase with increasing differences of particle size. The explanation is that equilibrium concentration of silica was not attained, and since quartz is dissolved at the surface, more SiO_2 passed into solution from the small particles (with a greater total surface) than from the large. Nevertheless, it is quite clear that the results do not support the solid-phase reaction hypothesis, and can be explained only if the reaction takes place in solution (Variants I and II).

TABLE 2

Effect of the Amount of Liquid Phase on the Rate of Formation of Calcium Hydrosilicates

Treatment time (hours)	S/L	$\frac{SiO_2 bound}{SiO_2 total}$ (%)	$\frac{CaO bound}{CaO total}$ (%)	Hydrosilicate content (%)	Notes
1*	1/3	17.0	23.6	18.3	Sand with S_{sp} = 0.3 m^2/g (by Carman's method)
	1/10	20.4	30.2	26.8	
2	1/3	66.4	88.6	77.2	Sand with S_{sp} = m^2/g (by nitrogen adsorption)
	1/10	78.9	92.1	86.8	
3	1/3	75.4	94.5	84.8	Sand with S_{sp} = m^2/g (by Carman's method)
	1/10	87.5	100.0	93.7	

* The temperature reached 130°; 1.5 hours required to raise the temperature to 175°.

Effect of the amount of liquid phase on the reaction rate. If the reaction takes place in solution (Variant I), then the greater the amount of solution, the more new substance is formed in unit time, as larger amounts of the components interact simultaneously. If the reaction proceeds at the component surfaces (Variant II), increase of the amount of liquid phase should not have much influence on the reaction rate, as it does not extend the reaction zone, but merely makes "peeling" of the particles somewhat easier. In absence of stirring this influence of the amount of liquid phase is slight.

Experiments were performed with suspensions of $Ca(OH)_2$ and SiO_2 with different solid–liquid ratios (S/L).

The experiments were carried out in hydrothermal bombs (100 cc in volume) at 175°. The molar ratio of CaO to SiO_2 was 0.8. The results of the experiments are given in Table 2.

The results in Table 2 show that the reaction rate increases with increase in the amount of liquid phase, and more new substance is formed in a given time of hydrothermal treatment.

TABLE 3

Effect of Specimen Density on the Rate of Formation of Calcium Hydrosilicates

Specimen type	Density (g/cc)	$\frac{SiO_2 bound}{SiO_2 total}$ (%)	$\frac{CaO bound}{CaO total}$ (%)	Hydrosilicate content (%)
Suspension	S/L = 1/3.5	89.6	100.0	94.18
Plastic	0.96	79.4	96.4	87.55
Molded**	1.16	64.2	96.0	80.06
Molded	1.54	52.5	93.0	72.60

** Specimens treated in water.

TABLE 4

Effect of Stirring on the Rate of Reaction of Lime with Silica

Conditions	$\frac{SiO_2 bound}{SiO_2 total}$ (%)	$\frac{CaO bound}{CaO total}$ (%)	Contents of new substance (%)
Not stirred	89.0	87.2	86.96
Stirred	93.0	99.3	95.95

It is interesting to compare the reaction rate of the components in specimens of different densities. The corresponding data are presented in Table 3. The CaO/SiO_2 molar ratio was 0.8 for all the specimens. The hydrothermal treatment was performed at 175°, for 14 hours. The results in Table 3 show that with increase of density (which is equivalent to decrease of the amount of liquid phase present) the rate of formation of calcium hydrosilicates decreases. It may be noted that this result may have practical applications in certain cases.

The experimental results thus refute also Variant II, according to which the reaction takes place at the particle surfaces, and confirm that lime interacts with silica in solution.

Formation of a colloidal structure during the reaction of calcium hydroxide with silica. We examined the contents of some hundreds of bombs in which calcium hydrosilicates had been synthesized. These observations showed that even at the earliest stages of the treatment a colloidal structure, retaining large amounts of water, is formed in the reaction mixture. It was found in special experiments that a separated liquid phase is present above the paste only if the weight ratio of water to mixture of CaO(C) and SiO_2(S) (here S_{sp} of sand = 4.6 m^2/g, C/S = 0.8) used is greater than 7; otherwise all the water which does not enter the composition of the hydrosilicate

TABLE 5

Effect of the Density of Molded Specimens on the Course of Interaction of Lime with Silica

Treatment time (hours)	Density (g/cc)	$\frac{SiO_2 \text{ bound}}{SiO_2 \text{ total}}$ (%)	$\frac{CaO \text{ bound}}{CaO \text{ total}}$ (%)	Contents of new substance (%)
0	1.19	11.3	22.4	18.8
	1.44	17.7	28.6	24.3
6	1.19	24.0	73.9	53.2
	1.44	44.7	79.7	61.8
12	1.19	50.4	82.5	66.4
	1.44	50.6	79.5	65.2
48	1.19	77.0	96.7	86.3
	1.44	59.7	96.0	77.8

TABLE 6

Effect of the Medium on the Rate of Formation of Calcium Hydrosilicates

Density of specimens (g/cc)	Medium	$\frac{SiO_2 \text{ bound}}{SiO_2 \text{ total}}$ (%)	$\frac{CaO \text{ bound}}{CaO \text{ total}}$ (%)	Contents of hydrosilicates (%)
1.16	Steam	49.5	90.6	69.8
	Water	64.2	96.0	80.1
1.54	Steam	49.5	90.8	70.2
	Water	52.5	93.0	72.6

is retained within the formed structure. By the time 175° is reached the original suspension acquires a thick creamy consistency, and after one hour of treatment at this temperature a gelatinous mass is formed. After three hours of treatment the substance has a dense structure the volume of which is 4-5 times that of the dry mixture. This mass dries very slowly (even under vacuum) with considerable shrinkage.

Such a structure should be formed not only in suspensions but also in molded specimens.

The structure so formed has a dual effect on the component interaction. On the one hand, it hinders further reaction because dissolution of new portions of the starting materials is obstructed by the surrounding colloidal phase, but, on the other hand, it may have a positive influence on the strength of the product because of the more intimate bonding of the forming and recrystallizing new substances.

Experiments were carried out in which the contents of the bombs were stirred during the experiment by means of a magnetic stirrer. A 2.1 g sample of mixture with C/S = 0.8 was covered with 50 ml of water and steamed for 5 hours at 175° (Table 4).

These experiments showed that stirring accelerates interaction of the components. In such experiments the original suspension acquired the consistency of a slurry but water did not separate out, so that although a colloidal system was formed it did not give rise to a compact structure. It follows that the formation of a colloidal structure does retard interaction of the components and gives rise to peculiarities in the course of reaction in molded specimens of different densities (Table 5). Lime–sand specimens with C/S = 0.8 were treated at 175°.

It follows from these results that at the initial stages of hydrothermal treatment the reaction is more rapid in specimens of higher density, but after a certain time (about 12 hours in our experiments) the contents of newly-formed substances in specimens of both densities become equal, and after that more new substance is formed in the less dense specimens.

This result can be explained as follows. In the denser specimens there is a higher content of the reactants per unit volume. So long as there is enough liquid in the specimen the components are dissolved more rapidly in the denser specimens (as the dissolution surface is greater), and the reaction therefore proceeds at a higher rate. Subsequently the forming colloidal structure prevents penetration of fresh portions of water (penetrating as the result of capillary condensation) into the specimen, and the reaction slows down. Water penetrates more easily into the less dense specimens, and the reaction rate in them increases for a longer time than in the denser specimens. This is confirmed by results of chemical analysis of molded specimens (C/S = 0.8) of different densities, treated in water and in steam at 175° for 13.5 hours (Table 6).

It follows from Table 6 that specimens of different density treated in steam have approximately equal contents of newly-formed substance (even somewhat higher in the denser specimens), but corresponding specimens treated in water show a significant difference; more new substance is formed in the less dense specimens. When a specimen is treated in water, access of water into the specimen is considerably easier than it is in steaming, and the mechanism discussed earlier is more clearly revealed.

Effect of the specific surface of lime on its reaction with silica. The rate of reaction can be raised if the solubilities of the starting substances are increased. This is valid if the reaction takes place in solution.

In view of the fact that at 175-200° the solubility of $Ca(OH)_2$ becomes less than the solubility of quartz, it is better to try to increase the solubility of lime in the first instance. It may be noted that this fact is often disregarded by technologists in practice.

The simplest way of increasing the solubility of lime is to increase its specific surface. We prepared $Ca(OH)_2$ of S_{sp} = 17.5 m^2/g (determined by nitrogen adsorption) by hydration of calcium oxide in water vapor at room temperature (during 40 days), and $Ca(OH)_2$ of S_{sp} = 10.4 m^2/g by hydration of the same calcium oxide in boiling water. Each type of slaked lime was mixed with quartz sand (10-20 μ fraction) in the ratio CaO/SiO_2 = 0.8, and 7 g samples of the mixtures were mixed with 50 ml of water and steamed in the bomb for 3 hours. The results of chemical analyses are given in Table 7.

The data in Table 7 show that the reaction is accelerated if the dispersity of the lime is increased; this confirms the hypothesis that the reaction takes place in solution.

Thermograms of the specimens characterized in Table 7 are shown in the figure. The curves for both specimens shown an endothermal effect of $Ca(OH)_2$ dissociation (at 540°) which, in agreement with the foregoing, is less for the specimen with the relatively higher specific surface of lime. This specimen also gives an exothermal effect at 865° which, according to Kalousek [1], corresponds to a hydrosilicate of the composition $C_{1.25}SH_n$. The specimen in which lime

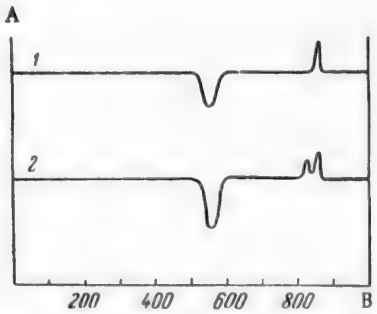

Thermograms of specimens steamed in suspension form at S/L = 1/7 at 175° for 3 hours; $CaO:SiO_2$ = 0.8. Sand fraction 10-20μ; A) heat effect of reaction; B) temperature (°C); specific surface of $Ca(OH)_2$ (m^2/g): 1) 17.5, 2) 10.4.

TABLE 7

Effect of the Specific Surface of Lime on the Rate of its Interaction with Silica

S_{sp} of $Ca(OH)_2$ (m^2/g)	$\frac{SiO_2 \text{ bound}}{SiO_2 \text{ total}}$ (%)	$\frac{CaO \text{ bound}}{CaO \text{ total}}$ (%)	Hydrosilicate content (%)
17.5	41.0	76.4	57.53
10.4	37.2	65.5	50.28

has the relatively lower specific surface gives two exothermal effects: at 865°, corresponding to $C_{1.25}SH_n$, and at 835°, corresponding to CSH_n.

In 1955 Kalousek [1] showed that hydrothermal treatment of a mixture of lime and quartz with C/S = 0.8 at 175° leads first to formation of a hydrosilicate of the composition $C_{1.25}SH_n$ which then passes into CSH_n, and the latter is subsequently converted into a hydrosilicate of the composition $C_{0.8}SH$ (tobermorite), which is the most valuable product in lime–sand mortars. In our view, the lifetime of each of these hydrosilicates is determined by the concentration range of their constituents in the solution surrounding the hydrosilicate. Variation of the composition of the liquid phase, namely, increase of the SiO_2 concentration in solution, leads to consecutive conversions of the solid phases, each of which is stable only over a definite concentration range.

In our experiments the reaction went further, in this sense, in the specimen of lower specific surface of lime than in the specimen in which the specific surface of lime was relatively greater (with higher solubility) as in the first specimen part of the $C_{1.25}SH_n$ was already converted into CSH_n. We attribute this to decrease of the SiO_2 concentration in solution as the result of higher solubility of the lime.

Thus, increase of the dispersity of the lime (in specimens with C/S = 0.8) has a dual effect. On the one hand, it accelerates binding of the components to form hydrosilicate, and on the other, it retards the attainment of equilibrium by hindering the formation of the stable phase (tobermorite) which, moreover, is of great practical significance (the binding material in high-quality lime–sand mortars is tobermorite).

In practice lime may be hydrated in different ways, in accordance with the process conditions: it may or may not be previously powdered, steam or water may be used, it may be treated in silos, drums, or other hydration equipment, or it may be hydrated in the formed products (if ground quicklime is used). The dispersity of lime must vary with the hydration conditions and with the properties of the lime itself, and this must undoubtedly influence the formation rate and phase composition of calcium hydrosilicates formed in autoclave treatment of lime–sand products.

SUMMARY

Results of experimental studies of the interaction of silica with calcium and magnesium hydroxides under conditions of hydrothermal treatment show that hydrosilicates are formed as the result of dissolution of the components and their subsequent interaction in the liquid phase. Because of this the reaction rate is greatly influenced by the amount of liquid phase present in the specimens; the latter is directly related to the density of the specimens. The crystals of newly formed substances deposited from solution tend to form a colloidal structure which hinders access of water to the reacting components and thereby retards the reaction.

Increase of the solubility of the original components (in particular, of lime) accelerates the reaction on the one hand, and has a significant influence on the phase composition of the products on the other.

LITERATURE CITED

[1] G. L. Kalousek, ACJ Journal, 26, 989 (1955).

Received March 21, 1958

STUDY OF THE FORMATION CONDITIONS, COMPOSITION, AND PROPERTIES OF SODIUM ALUMINOCARBONATE

M. N. Smirnov

Carbonation of aluminate solutions yields not only aluminum hydroxide but also, in a number of cases, the compound $Na_2O \cdot Al_2O_3 \cdot 2CO_2 \cdot nH_2O$, which we have named sodium aluminocarbonate [1]. Sodium aluminocarbonate, in the form of the mineral dawsonite of the composition $Na_2O \cdot Al_2O_3 \cdot 2CO_2 \cdot 2H_2O$, is found in nature, and information on this compound is given in a paper by Harrington, Friedel, and Chaper [4]. Another mineral of the dawsonite group, a hydrated aluminocalcite of the composition $CaO \cdot Al_2O_3 \cdot 2CO_2 \cdot 5H_2O$, is also found in nature.

The literature contains data on the preparation of various aluminocarbonates of sodium, potassium, and ammonium. In particular, Löwig [5] described the conditions for preparation of sodium and potassium aluminocarbonates of the composition $(Na_2O, K_2O) \cdot Al_2O_3 \cdot 2CO_2 \cdot 5H_2O$ (by slow addition of aluminate solutions to carbonated solutions of sodium and potassium carbonates). According to Löwig, sodium and potassium aluminocarbonates have a well-defined crystalline structure and are not decomposed by water.

In carbonation of aluminate solutions of industrial concentrations, alkali aluminocarbonates are formed at the final stage of the process, when the alumina content reaches several grams per liter. Contamination of aluminum hydroxides by aluminocarbonates is inadmissible, and therefore in the production of alumina from bauxites by the calcination process the carbonation of aluminate solutions is not taken to completion. When the technological process conditions make it necessary to continue carbonation of the aluminate solutions to complete liberation of the alumina, as in the production of alumina from nephelines, a two-stage carbonation method is used. Aluminum hydroxide is separated in the first carbonation stage, and alkali aluminocarbonates in the second.

However, the formation of aluminocarbonates in carbonation of aluminate solutions of relatively high concentrations was observed in some cases [6]. We also obtained sodium aluminocarbonate by the interaction of aluminum hydroxide with sodium carbonate–bicarbonate solutions, when the extent of reaction increased with increasing dispersity of the aluminum hydroxide.

These results [6] demonstrate the significance of alkali aluminocarbonate formation in the carbonation of aluminate solutions, and shed new light on the mechanism of the process. The formation conditions of alkali aluminosilicates and aluminocarbonates have much in common; thus, the composition of the corresponding compounds is analogous (for example $Na_2O \cdot Al_2O_3 \cdot 2CO_2 \cdot 2H_2O$ and $Na_2O \cdot Al_2O_3 \cdot 2SiO_2 \cdot 2H_2O$).

EXPERIMENTAL

Method of investigation and starting materials. Sodium carbonate (chemically pure) and aluminate solutions made from aluminum hydroxide and caustic soda (chemically pure) were used for the experiments.

The liquid phases were analyzed by the usual volumetric and in some instances gravimetric methods adopted in the alumina industry. The alkali and alumina contents of the precipitates were determined gravimetrically, and CO_2 was determined volumetrically by the well-known direct method.

The apparatus used for carbonation of the solutions is shown schematically in Fig. 1. It consisted of a steel carbonation vessel 1 immersed in a water thermostat 2. The carbonation vessel was 250 mm high and

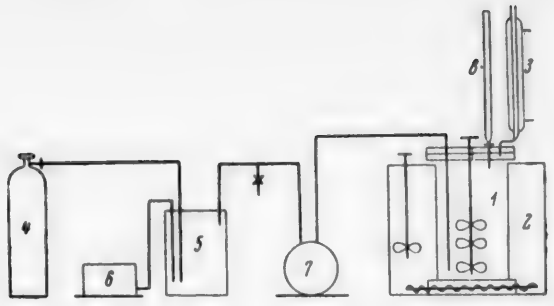

Fig. 1. Scheme of carbonation unit.

130 mm in diameter. The carbonated solution was stirred by means of a blade stirrer the rotation speed of which could be varied by changes of pulleys. Evaporation of the carbonated solution was prevented by means of a glass condenser 3 fitted in the vessel lid; this also served as an outlet for the gas phase. The lid of the vessel contained openings for the solution feed, sampling, and introduction of carbon dioxide through a bubbler. When dilute carbon dioxide was used for carbonation, gas from the cylinder 4 was mixed with air in the large mixer 5. The feed rates of air, by the blower 6, and carbon dioxide into the mixer were regulated by a system of valves. The amount of carbon dioxide supplied to the carbonation vessel was recorded by the meter 7, and the gas concentration was maintained to within ±1% (absolute). The temperature in the thermostat was regulated automatically to within ±0.5°. Aluminate solution was fed continously into the carbonation vessel from the buret 8, fitted with a stopcock and mounted in the lid of the vessel; the temperature of the solution inside the buret was kept constant by circulation of water through the surrounding jacket.

Influence of temperature conditions on formation of sodium aluminocarbonate in carbonation of aluminate solutions. The effect of temperature on formation of sodium aluminate in carbonation of aluminate solutions is shown by the data in Table 1.

TABLE 1

Influence of Temperature Conditions on Formation of Sodium Aluminocarbonate

Temperature (°C)	Content of Al_2O_3 (%) in precip. in the form of		Molar comp. of sodium aluminocarbonate dried at 80°			
	aluminum hydroxide	sodium aluminocarbonate	Na_2O	Al_2O_3	CO_2	H_2O
20	72.0	28.0	1.03	1.0	2.05	5.12
40	41.0	59.0	0.98	1.0	2.04	5.01
60	19.0	81.0	1.05	1.0	1.97	5.09
80	3.0	97.0	0.98	1.0	2.03	5.07
90	0.0	100.0	1.04	1.0	2.06	2.11

The sodium aluminate solution used for carbonation contained (in g/liter): Al_2O_3 9.4; Na_2O_k 10.6; Na_2O_y 85.6. While this solution was being carbonated by pure carbon dioxide, another aluminate solution containing (in g/liter): Al_2O_3 109.4 and Na_2O_k 102.5 was slowly added to it. At a carbon dioxide rate of 12-16 liters/hour, and Al_2O_3 concentration of about 2 g/liter and $NaHCO_3$ concentration of about 5 g/liter (as bicarbonate Na_2O) was maintained in the carbonated solution.

The data in Table 1 show that the amount of sodium aluminocarbonate formed in carbonation of aluminate solutions increases with temperature. This is completely analogous to the formation of sodium aluminosilicate in the removal of silica from aluminate solutions.

It may be seen that the composition of the sodium aluminocarbonate corresponds to the formula $Na_2O \cdot Al_2O_3 \cdot 2CO_2 \cdot nH_2O$, the amount of combined water being 5 molecules up to 80°, and 2 molecules at 90°.

Effect of the sodium bicarbonate content of the carbonated solution on formation of sodium aluminocarbonate. It is known that rapid precipitation of sodium aluminosilicate from aluminate solutions at low temperatures occurs only when the silica content exceeds the limit of metastable solubility.

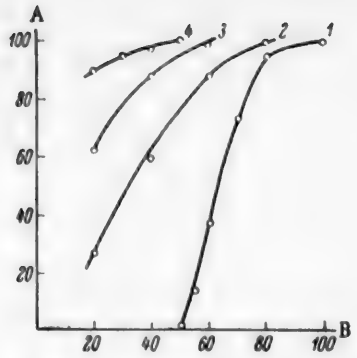

Fig. 2. Effect of sodium bicarbonate content on the amount of sodium aluminocarbonate formed: Na_2O contents corresponding to the bicarbonate present (g/liter): 1) 0; 2) 2-5; 3) 5-10; 4) 10-20. A) Al_2O_3 (%) combined as sodium aluminocarbonate; B) temperature (°C).

On the assumption that exactly the same applies in the formation of sodium aluminocarbonate, the sodium bicarbonate content of the carbonated solution should have a strong influence on the degree of formation of sodium aluminocarbonate.

Fig. 2 shows the dependence of the amount of alumina bound in the form of sodium aluminocarbonate on the sodium bicarbonate content of the carbonated aluminate solution.

Solutions of the composition indicated above were used for these experiments. The feed rates of carbon dioxide and aluminate solutions were such as to a relatively constant, but different in each experiment, content of sodium carbonate.

The data in Table 2 show that the formation of sodium aluminocarbonate greatly depends on the content of sodium bicarbonate in the carbonated solution. The higher the sodium bicarbonate content, the lower the temperature at which sodium aluminocarbonate is formed. However, sodium aluminocarbonate may be formed even if there is no sodium bicarbonate in the carbonated solution. Thus, Curve 1 represents the results of experiments in which aluminate solution was carbonated under conditions such that sodium bicarbonate could not be present in the solution volume. In this series of experiments the caustic soda content of the carbonated solutions was maintained at 2-5 g/liter.

It may be concluded from these results that in some instances sodium aluminocarbonate may be formed in absence of sodium bicarbonate in the volume of the carbonated solution. However, this does not exclude the presence of sodium bicarbonate at the regions of contact between the carbon dioxide and the carbonated solution.

The above data show that the rate of formation of sodium aluminocarbonate under otherwise constant conditions is determined by the temperature of the carbonated solution.

Influence of the composition of the carbonated aluminate solution on formation of sodium aluminocarbonate. The experimental results in Table 2 illustrate the influence of the composition of carbonated solutions containing considerable amounts of caustic soda on the formation of sodium aluminocarbonate at 90°. Pure carbon dioxide was used for the carbonation.

TABLE 2

Effect of Composition of the Aluminate Solution on Formation of Sodium Aluminocarbonate at 90°

Composition of original aluminate solution (g/liter)			Carbonation time (min)	Al_2O_3 (%) present in the solid phase as	
Al_2O_3	Na_2O_k	Na_2O_y		aluminum hydroxide	sodium aluminocarbonate
53.8	60.7	85.6	90	88.0	12.0
25.4	29.2	85.6	40	14.0	86.0
17.2	18.6	85.6	30	4.0	96.0
9.4	10.6	85.6	15	0.0	100.0
53.8	60.7	61.9	90	92.0	8.0
25.4	29.2	61.7	40	18.5	81.5
17.2	18.6	61.9	30	10.0	90.0
25.4	29.2	38.7	40	66.0	34.0
17.2	18.6	18.9	30	67.0	33.0
9.4	10.6	12.7	15	73.0	27.0

TABLE 3

Effect of Seeding with Aluminum Hydroxide on Formation of Sodium Aluminocarbonate

Composition of original solution (g/liter)			Carbonation time (min)	Amount of $Al(OH)_3$ introduced (g/liter)	Amt. of Al_2O_3 (%) passing from solution into the solid phase as	
Al_2O_3	Na_2O_k	Na_2O_y			aluminum hydroxide	sodium aluminocarbonate
25.4	29.2	85.6	40.0	0.0	14.0	86.0
				10.0	72.0	28.0
				50.0	78.0	22.0
17.2	18.6	85.6	30.0	0.0	4.0	96.0
				10.0	56.0	44.0
				50.0	64.0	36.0
25.4	29.2	38.7	40.0	0.0	66.0	34.0
				10.0	83.0	17.0
				50.0	91.0	9.0
9.4	10.6	12.7	15.0	0.0	73.0	27.0
				10.0	93.0	7.0
				50.0	96.0	4.0

TABLE 4

Effect of the Feed Rate of Pure Carbon Dioxide at 90° on the Amount of Sodium Aluminocarbonate Formed During Carbonation

Composition of original solution (g/liter)			Feed rate of carbon dioxide (liters/minute)	Carbonation time (min)	Contents of Al_2O_3 (%) in solid phase as	
Al_2O_3	Na_2O_k	Na_2O titr.			aluminum hydroxide	sodium aluminocarbonate
25.4	29.2	85.6	1.3	40	14.0	86.0
			0.57	90	42.0	58.0
			0.15	360	67.0	33.0
17.2	18.6	85.6	1.0	30	4.0	96.0
			0.5	60	28.0	72.0
			0.15	360	44.0	56.0
9.4	10.6	12.7	1.0	15	73.0	27.0
			0.5	60	91.0	9.0
			0.25	120	97.0	3.0

The experimental results show that at 90° sodium aluminocarbonate can be formed at relatively high contents of caustic soda in carbonation of aluminate solutions. The higher the sodium carbonate content and the lower the sodium aluminate content, the more alumina in the carbonated aluminate solution is combined in sodium aluminocarbonate.

Effect of seeding with aluminum hydroxide on the extent of binding of alumina in the carbonated solution in the form of sodium aluminocarbonate. Comparison of the experimental results in Table 2 shows that for a given total alkali content in the carbonated solution the amount of sodium aluminocarbonate formed increases with decreasing alumina content of the original solution. From this and from industrial data it may be concluded that the presence of aluminum hydroxide in the carbonation zone has a significant influence on the course of sodium aluminocarbonate formation. The possibility of sodium aluminocarbonate formation decreases in presence of aluminum hydroxide.

To determine the influence of seeding with aluminum hydroxide on the extent of formation of sodium aluminum carbonate, data are presented in Table 3 on the carbonation of a series of aluminate solutions by pure carbon dioxide at 90°.

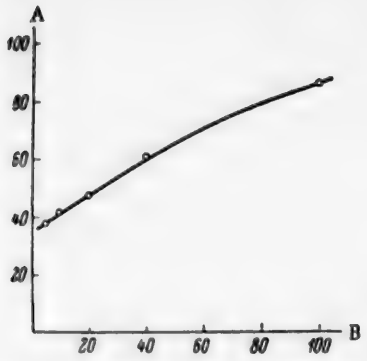

Fig. 3. Effect of the CO_2 content of the gas on the amount of sodium aluminocarbonate formed.

The experimental results in Table 3 show that seeding with aluminum hydroxide has a considerable influence on the course of formation of sodium aluminocarbonate. The possibility of its formation in the carbonation of aluminate solutions decreases with increases of the amount of aluminum hydroxide in the reaction zone.

The composition of the solid phase formed depends in a definite manner on the presence of aluminum hydroxide in the carbonation zone; aluminum hydroxide has a certain directing effect on the process, causing separation of more aluminum hydroxide.

Effect of the rate of carbonation of aluminate solutions at 90° on the composition of the solid phase formed. The data in Table 4 illustrate the influence of the feed rate of carbon dioxide in carbonation, and Fig.3 shows the influence of carbon dioxide concentration.

TABLE 5

Effect of the Stirring Rate of Aluminate Solutions in Carbonation at 90° on the Composition of the Solid Phase Formed

Composition of original solution (g/liter)			Stirrer speed (r.p.m.)	Al_2O_3 (%) present in solid phase as	
Al_2O_3	Na_2O_k	Na_2O titr.		aluminum hydroxide	sodium aluminocarbonate
25.4	29.2	85.6	12	14.0	86.0
			148	28.0	72.0
			250	37.0	63.0
17.2	18.6	85.6	12	4.0	96.0
			148	12.0	88.0
			250	19.0	81.0

These results show that the formation of sodium aluminocarbonate is determined to a considerable extent by the rate at which carbon dioxide is fed into the carbonated solution. It is evident that the more carbon dioxide enters the carbonated solution and the higher its concentration, the greater is the possibility of local formation of sodium bicarbonate which is necessary for formation of sodium aluminocarbonate at the point of contact between the gas and solution.

In this connection it was of interest to examine the influence of the rate of stirring of the aluminate solution on the amount of sodium aluminocarbonate formed.

In the experiments described above, the stirrer speed was 12 rpm (peripheral speed 5 meters per minute). The influence of stirrer speed is shown in Table 5.

Increase of stirrer speed apparently decreases the possibility of local overcarbonation of the solutions with formation of sodium bicarbonate, and the amount of sodium aluminocarbonate formed is therefore less.

SUMMARY

1. Sodium aluminocarbonate of the composition $Na_2O \cdot Al_2O_3 \cdot 2CO_2 \cdot nH_2O$, is formed during carbonation of aluminate solutions under certain conditions.

2. Formation of sodium aluminocarbonate is favored by low contents of caustic alkali in the medium, presence of large amounts of sodium carbonate, high temperature, and absence of aluminum hydroxide seed in the carbonated aluminate solution.

3. When the solution is seeded with aluminum hydroxide, sodium aluminocarbonate is formed at a relatively low alumina content, which decreases with increase of the amount of aluminum hydroxide in contact with the carbonated aluminate solution.

4. Sodium aluminocarbonate is formed in the form of the pentahydrate at temperatures below 90°, and as the dihydrate above 90°.

LITERATURE CITED

[1] M. N. Smirnov, Trans. All-Union Aluminum and Magnesium Inst. 22, 92 (1940).

[2] B. I. Harrington, Canadian Nat. 7, 305 (1874).

[3] G. Friedel, Bull. Soc. Min. 4, 28 (1881).

[4] M. Chaper, Bull Soc. Min. 4, 155 (1881).

[5] C. Löwig, German Patents 19784 (1882) and 70175 (1892).

[6] M. N. Smirnov, Dissertation [In Russian] (All-Union Aluminum and Magnesium Inst., Leningrad, 1954).

Received October 8, 1958

ACTION OF ACID SOLUTIONS ON GLASSY LITHIUM ALUMINOSILICATES

S. K. Dubrovo

The chemical durability of glassy lithium aluminosilicates has been studied little. Nevertheless, all-round investigations of lithium aluminosilicate glasses are now becoming very important in connection with the use of such glasses in the production of especially strong materials.

In our earlier investigations we studied the breakdown of glassy sodium aluminosilicates in acid solutions in relation to the degree of depolymerization of the silicon–oxygen framework of the glass (rupture of Si–O–Si linkages) with increasing contents of sodium oxide and alumina [1, 2]. It was found that the resistance to acids decreases with replacement of silica by alumina in sodium aluminosilicates, at a constant molar percentage of sodium oxide. When the sodium oxide content is decreased to 12.5 molar %, the acid resistance is almost independent of the silica–alumina ratio. It was of great interest to determine whether this relationship holds if the sodium ion is replaced by the lithium ion, which has the greater field of force.

The present investigation was accordingly undertaken in order to study the effect of silica–alumina ratio in glassy lithium aluminosilicates on their chemical breakdown in acid solutions.

EXPERIMENTAL

Two series of glassy lithium aluminosilicates were made. The composition of one series corresponded to lithium bisilicate with additions of 0.05 to 1 mole of alumina. The second series consisted of glasses of the type $Li_2O \cdot yAl_2O_3 \cdot xSiO_2$, where x is 2, 3, 4, and 6; in some of them part of the alumina was replaced by silica at a constant molar content of lithium oxide. This was accompanied by increase of the oxygen number, defined as the ratio of the number of gram atoms of oxygen to the sum of the numbers of gram atoms of silicon and aluminum [2].

The methods used for making the glasses and preparing the specimens were described earlier [3]. The experimental conditions and apparatus were the same as in the experiments with glassy lithium silicates [4]. Chemical durability in 0.1 and 1 N hydrochloric acid solutions was studied by determination of the amounts of components dissolved out of the glass, expressed in moles per square centimeter of glass surface.

The breakdown process was also characterized in terms of the quantities α and β, which are the respective fractions of silica and alumina dissolved out of the glass layer subjected to the action of the acid [1].

In addition to the above-mentioned glassy lithium aluminosilicates, native α-spodumene was also used in experiments under the same conditions. The β-spodumene modification, which differs from α-spodumene in physical properties [3], was prepared by the action of heat on the latter for 2 hours at 1000°. In this conversion the coordination number of aluminum changes from six to four. Spodumene glass was also prepared by fusion of β-spodumene. Both β-spodumene and spodumene glass were investigated as described above.

The results are given in Tables 1 and 2 and Fig. 1 and 2. These results show that the first additions of alumina to lithium bisilicate decrease the amounts of glass components dissolved out by the action of acids. With 0.3 mole of alumina and over, the chemical durability of glassy lithium aluminosilicates decreases: the values of n_{Li_2O}, $n_{Al_2O_3}$, and n_{SiO_2} increase. The process consists of predominant leaching of lithium and aluminum ions, with formation of a silica-rich residual layer on the glass surface. From the composition 1 : 0.5 : 2 onward the relative proportions of all the dissolved components are virtually the same as they are in the

TABLE 1

Breakdown of Glassy Lithium Aluminosilicates in 0.1 N Hydrochloric Acid Solution

Molar proportions			Components (α – fraction of SiO_2, β – fraction of Al_2O_3)	$n \cdot 10^6$ (moles/cm^2) during time (hours)			
Li_2O	Al_2O_3	SiO_2		1	2	4	6
1	0.05	2	Li_2O	0.85	1.1	1.4	1.6
			Al_2O_3	0.006	0.008	0.01	0.01
			SiO_2	0.016	0.018	0.018	0.018
			β	0.14	0,14	0.14	0.13
			α	0.009	0.008	0.001	0.006
1	0.15	2	Li_2O	0.20	0.23	0.27	0.33
			Al_2O_3	0.006	0.006	0.006	0.006
			SiO_2	0.013	0.013	0.013	0.013
			β	0.020	0.017	0.015	0.013
			α	0.030	0.028	0.024	0.020
1	0.30	2	Li_2O	0.40	0.43	0.46	0.58
			Al_2O_3	0.17	0.21	0.22	0.23
			SiO_2	0.12	0.15	0.17	0.21
			β	1.4	1.7	1.6	1.3
			α	0.15	0.17	0.18	0.18
1	0.50	2	Li_2O	10.5	14.9	25.0	27.2
			Al_2O_3	3.9	6.7	9.3	11.9
			SiO_2	17.5	32.3	41.1	51.0
			β	0.74	0.90	0.73	0.88
			α	0.83	1.08	0.80	0.93
1	1	2	Li_2O	3.6	6.3	8.3	11.5
			Al_2O_3	2.2	5.5	8.8	9.0
			SiO_2	6.6	12.5	16.5	21.0
			β	0.61	0.87	1.06	0.80
			α	0.91	0.99	0.99	0.91
1	0.8	2.2	Li_2O	8.3	11.2	18	22.7
			Al_2O_3	5.2	9.0	14.8	16.0
			SiO_2	13.4	24.5	36.6	56.2
			β	0.80	1.0	0.99	0.90
			α	0.73	0.99	0.92	1.1
1	0.6	2.4	Li_2O	6.6	8.8	11.2	19.8
			Al_2O_3	3.7	6.4	10.4	12.0
			SiO_2	10.2	18.2	26.5	30.0
			β	0.93	1.20	1.50	1.0
			α	0.66	0.86	1.0	0.63
1	1	3	Li_2O	2.5	4.8	8.2	9.0
			Al_2O_3	2.3	4.2	7.2	7.9
			SiO_2	7.5	12.6	21.9	24.8
			β	0.99	0.90	0.90	0.89
			α	1.03	0.91	0.92	0.95
1	0.75	3.25	Li_2O	0.31	0.51	1.1	1.2
			Al_2O_3	0.29	0.44	0.70	0.82
			SiO_2	0.47	0.64	0.65	0.68
			β	1.20	1.1	0.85	0.90
			α	0.47	0.39	0.18	0.18
1	0.5	3.50	Li_2O	—	0.03	0.04	0.08
			Al_2O_3	0.01	0.01	0.01	0.01
			SiO_2	0.01	0.01	0.01	0.01
			β	—	0.66	0.50	0.25
			α	—	0.10	0.07	0.035

TABLE 1 (continued)

Molar proportions			Components (α – fraction of SiO_2, β – fraction of Al_2O_3)	$n \cdot 10^6$ (moles/cm^2) during time (hours)			
Li_2O	Al_2O_3	SiO_2		1	2	4	6
1	1	4	Li_2O	—	—	—	0.056
			Al_2O_3	0.03	0.04	0.05	0.05
			SiO_2	0.03	0.05	0.08	0.08
	α-Spodumene		Li_2O	0.04	0.06	0.06	0.06
			Al_2O_3	0.02	0.02	0.02	0.03
			SiO_2	0.02	0.02	0.02	0.02
	β-Spodumene		Li_2O	0.15	0.29	0.36	0.40
			Al_2O_3	0.18	0.21	0.23	0.25
			SiO_2	0.17	0.18	0.20	0.20
	Spodumene glass		Li_2O	0.04	0.05	0.06	0.06
			Al_2O_3	0.03	0.03	0.05	0.05
			SiO_2	0.02	0.02	0.02	0.02
1	1	6	Li_2O	0.021	0.031	0.050	0.05
			Al_2O_3	0.013	0.015	0.018	0.018
			SiO_2	0.04	0.07	0.09	0.09

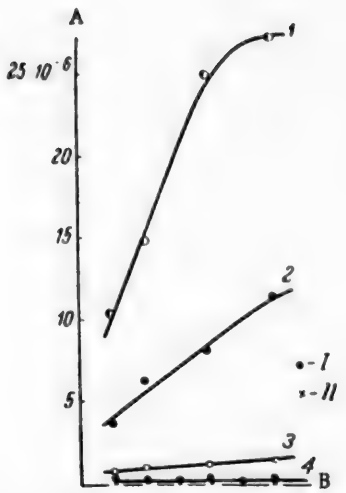

Fig. 1. Action of 0.1 N hydrochloric acid solution at 40° on glassy lithium aluminosilicates: A) values of $n_{Li_2O} \cdot 10^{-6}$; B) time (hours); molar proportions of $Li_2O : Al_2O_3 : SiO_2$: 1) 1 : 05 : 2, 2) 1 : 1 : 2, 3) 1 : 0.05 : 2, 4) 1 : 0.3 : : 2 (I) and 1 : 0.15 : 2 (II).

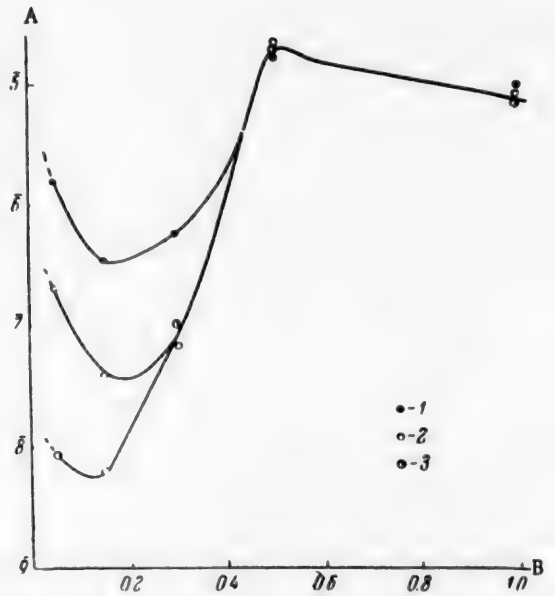

Fig. 2. Effect of alumina contents of lithium aluminosilicates on their chemical durability in 0.1 N hydrochloric acid solution: A) values of: $\log n_{Li_2O}, \frac{Al_2O_3}{a}, \frac{SiO_2}{b}$, B) amounts of Al_2O_3 (moles) added to lithium bisilicate; 1) n_{Li_2O}, 2) $n_{Al_2O_3}$, 3) n_{SiO_2}.

original glass, i.e, the whole glass is, in a sense, dissolved. On addition of 1 mole of alumina to lithium bisilicate the glass formed is also virtually soluble in acids, although the rate of the solution process is considerably lower than for the 1 : 0.5 : 2 composition. Less than half the amounts of lithium oxide and silica are dissolved out in a given time in the former case. The rate of loss of alumina from the glass is the same for both glasses, but if these amounts are calculated relative to the alumina contents of the original glasses, the same proportions are found as for lithium oxide and silica. A similar result was obtained for sodium aluminosilicates when the action of different acids on glasses of the compositions 1:0.5:2 and 1:1:2 was compared.

TABLE 2

Breakdown of Glassy Lithium Aluminosilicates in 1 N Hydrochloric Acid Solution

Molar proportions			Components (β = fraction of Al_2O_3, α = = fraction of SiO_2)	$n \cdot 10^{-6}$ (moles/cm^2) during time (hours)			
Li_2O	Al_2O_3	SiO_2		1	2	4	8
1	0.30	2	Li_2O	4.60	5.30	5.70	6.06
			Al_2O_3	1.44	1.79	2.30	2.60
			SiO_2	0.54	0.82	1.09	1.15
			β	1.0	1.1	1.3	1.4
			α	0.06	0.08	0.09	0.09
1	0.50	2	Li_2O	44	104	202	295
			Al_2O_3	27	50	93	142
			SiO_2	101	191	392	548
			β	1.2	0.97	0.92	0.96
			α	1.1	0.91	0.87	0.93
1	1	3	Li_2O	18.1	28	38	57
			Al_2O_3	15.2	50	60	79
			SiO_2	21	45	83	110
			β	0.84	0.8	1.6	1.4
			α	0.38	0.53	0.72	0.64
1	0.5	3.5	Li_2O	—	—	0.07	0.07
			Al_2O_3	0.01	0.01	0.01	0.01
			SiO_2	0.01	0.02	0.02	0.02
			β	—	—	0.28	0.28
			α	—	—	0.08	0.08

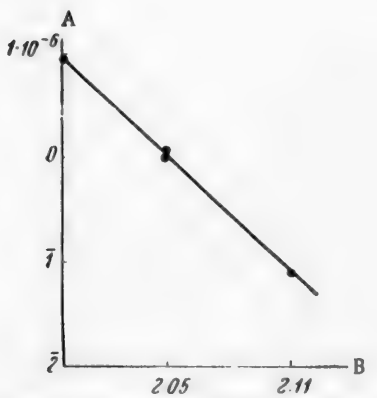

Fig. 3. Variation of the acid resistance of lithium aluminosilicates (of the 1:1:3 type) with the oxygen number: A) values of log $n_{Li_2O} \cdot 10^{-6}$ B) oxygen number (O/Al + Si).

When the action of acid solutions on glassy lithium aluminosilicates of the second series (of the $Li_2O \cdot yAl_2O_3 \cdot xSiO_2$ type) is considered, the following relationships may be noted. With increase of oxygen number at a constant molar content of lithium oxide, i.e., with decrease of the relative content of alumina, the chemical durability of glasses in the 1:1:3 series increases (Fig. 3). In glasses of the 1:1:2 type the rates at which all the components pass into solution evidently also decrease with increase of oxygen number; this can be seen by comparing the behavior of the 1: 0.8:2.2 and 1:0.6:2.4 glasses. The glass of the composition 1:1:2 in this series is an exception; its breakdown rate is less than the breakdown rates of the above-mentioned glasses, but its oxygen number is smaller.

It follows from the data in Table 1 that the chemical durability of glassy lithium aluminosilicates increases with their silica content (up to a definite limit).

Beyond 66.7 molar % (composition 1:1:4) the chemical durability is almost constant. The same table also shows that α-spodumene is more resistant to acids than β-spodumene, and spodumene glass is similar to α-spodumene in this respect.

With increase of the hydrochloric acid concentration from 0.1 N to 1 N the breakdown rate of the relatively unstable lithium aluminosilicate glasses increases 5 to 10-fold (the compositions 1:0.5:2, 1:1:3 etc.). With the chemically durable aluminosilicate glasses, such as that of the composition 1:0.5:3.5, the rates at which the components are dissolved out of the glass remain almost unchanged with change of the acid concentration; the same was found for sodium aluminosilicates.

Experiments were carried out under the same conditions with lithium and sodium glasses to compare their durabilities in hydrochloric acid solutions. The comparative data, presented in Table 3, indicate that glassy lithium aluminosilicates (like the silicates) are more resistant than the corresponding sodium aluminosilicates.

However, introduction of a third component—aluminum oxide—reduces the difference in the acid resistance of lithium and sodium glasses. This is revealed especially clearly by comparison of silicates and aluminosilicates of equal molar R_2O contents. For example, in presence of 25 molar % R_2O the amount of sodium oxide dissolved out of sodium trisilicate is 24 times the amount of lithium oxide dissolved out of lithium trisilicate. At the same time, the amounts of the components dissolved out of aluminosilicates of the same R_2O content differ by a factor of less than 2.

It also follows from Table 3 that the difference in acid resistance between lithium and sodium aluminosilicates decreases with increase of the $SiO_2:Al_2O_3$, i.e., with increase of the oxygen number.

DISCUSSION OF RESULTS

With increase of the relative proportion of alumina in lithium glasses the aluminum—silicon—oxygen framework is broken down more rapidly, as is the case with sodium glasses. This is found not only when part of the silica is replaced by alumina at a constant (molar) content of R_2O, but in a number of cases replacement of R_2O by equimolecular amounts of alumina at a constant SiO_2 content also results in decreased resistance to acids, as is evident from the data in Table 4. The breakdown of glassy lithium aluminosilicates in acid solutions depends mainly on their $SiO_2:Al_2O_3$ ratio. The higher this ratio, the less is the acid resistance influenced by variations of their lithium oxide contents in the range of 16-30 molar %. At higher and lower contents of lithium oxide the acid resistance depends less on the silica—alumina ratio (Fig. 4).

A similar situation is found for sodium aluminosilicates. The only difference is that the curves for chemical durability as a function of the sodium oxide content are shifted in the direction of lower contents (in molar %). These results demonstrate the weakening of the silicon—oxygen framework in lithium aluminosilicates,

TABLE 3

Comparative Durability of Glassy Lithium and Sodium Aluminosilicates in Hydrochloric Acid Solutions

Composition (molar %)				Amounts dissolved, $n \cdot 10^6$ (moles/cm²) in 6 hours			HCl concentration (normality)
Li_2O	Na_2H	Al_2O_3	SiO_2	R_2O	Al_2O_3	SiO_2	
30.3	—	9.1	60.6	0.58	0.23	0.21	0.1
—	30.3	9.1	60.6	1.20	0.20	0.13	
28.6	—	14.3	57.1	295	142	548	1
—	28.6	14.3	57.1	573	255	962	
25	—	25	50	18.7	18.7	35	0.1
—	25	25	50	34	34	66	
20	—	10	70	0.08	0.01	0.01	
—	20	10	70	0.07	0.01	0.03	
16.66	—	16.66	66.66	0.06	0.05	0.08	
—	16.66	16.66	66.66	0.86	0.64	0.27	

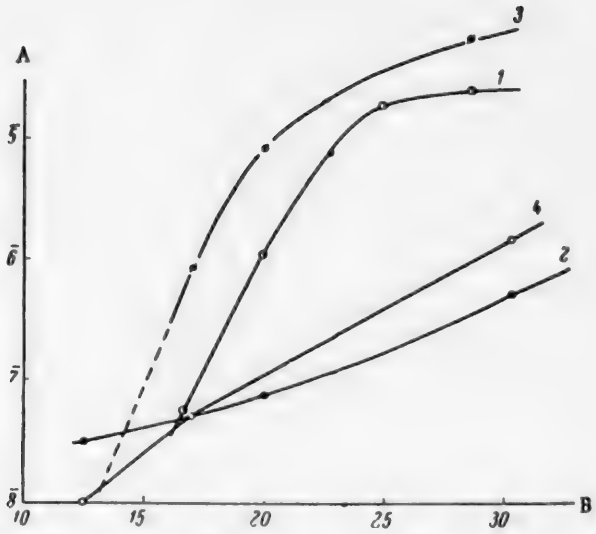

Fig. 4. Variations of the acid resistance of glassy lithium and sodium aluminosilicates with the $\frac{SiO_2}{Al_2O_3}$ ratio: A) values of log n_{R_2O}, B) R_2O (molar %); $\frac{SiO_2}{Al_2O_3}$ ratios for lithium glasses; 1) 4, 2) 6-7; for sodium glasses: 3) 4, 4) 6-6.6.

TABLE 4

Variations of the Acid Resistance of Glassy Lithium and Sodium Aluminosilicates on Replacement of R_2O by Al_2O_3

Composition (molar %)				$\frac{SiO_2}{Al_2O_3}$	Amounts dissolved, $n \cdot 10^8$ (moles/cm²) in 6 hours		
Li_2O	Na_2O	Al_2O_3	SiO_2		R_2O	Al_2O_3	SiO_2
30.3	—	9.1	60.6	6.6	0.58	0.23	0.21
25	—	15	60	4	19.8	12	30
20	—	20	60	3	9.0	7.9	24.8
—	30.3	9.1	60.6	6.6	1.2	0.20	0.13
—	19.7	19.10	61.2	3.2	9.6	7.0	21.0
—	31.7	4.8	63.5	13.2	4.2	0.03	0.008
—	20.4	16.2	63.4	3.9	9.0	5.6	3.12
32.8	—	1.6	65.6	41	1.6	0.01	0.02
20.0	—	15	65.0	4.3	1.2	0.82	0.68
—	32.8	1.6	65.6	41	32	0.01	0.02
—	16.7	18.3	65.0	3.5	6.9	6.3	5.8

with regard to acid resistance, as the result of depolymerization by aluminum oxide. This probably also accounts for the lower acid resistance of β-spodumene as compared with α-spodumene. Change of the coordination number of aluminum from six to four, when aluminum enters the silicon–oxygen framework, should diminish resistance to the corrosive action of acids.

SUMMARY

1. It was found in a study of the chemical durability of lithium aluminosilicate glasses in hydrochloric acid solutions that the action of acids on these glasses is characterized by preferential removal of lithum and aluminum ions with formation of a silica-rich surface layer.

2. The breakdown rate of glassy lithium aluminosilicates depends mainly on their silica–alumina ratio. The higher the relative silica content, the less is the influence of changes in the amount of lithium oxide in the glasses on the acid resistance.

3. Glassy lithium aluminosilicates have higher chemical durability than sodium glasses of the corresponding molecular compositions. This difference diminishes with increasing contents of silica and alumina in the glasses.

LITERATURE CITED

[1] S. K. Dubrovo, Bull. Acad. Sci. USSR, Div. Chem. Sci. 2, 244 (1954).*

[2] S. K. Dubrovo, Bull. Acad. Sci. USSR, Div. Chem. Sci. 10, 1157 (1958).*

[3] S. K. Dubrovo and Yu. A. Shmidt, J. Appl. Chem. 32, No. 4, 742 (1959).*

[4] S. K. Dubrovo, J. Appl. Chem. 32, No. 5, 979 (1959).*

Received July 4, 1958

*Original Russian pagination. See C. B. Translation.

INVESTIGATION OF THE OPTICAL PROPERTIES OF LITHIUM ALUMINOBOROSILICATE GLASSES•

A. A. Appen and Gan' Fu-si (Kan Fu-si)

Lithium borosilicate, aluminosilicate, and aluminoborosilicate glasses have been studied little as yet. Papers have recently been published by Bezborodov and Ulazovskii [1] and by Moore and McMillan [2], but the optical properties of these glasses have not been studied systematically. Having obtained the corresponding data for soda [3] and potash [4] glasses, we were naturally interested in the influence of lithium ions on these properties.

The methods used for preparation of the specimens and for measurement of the optical properties are described in the preceding communication [3].

Lithium borosilicate glasses containing from 10 to 30% Li_2O crystallize during cooling. To prepare transparent glasses, the glass melts were poured into water. Crystallization is retarded appreciably by addition of alumina, and glasses containing up to 8% alumina do not crystallize on annealing. The correction for the lowering of the refractive index of chilled glasses as compared with annealed was determined by special experiments. The refractive indices of the chilled glasses were measured by the immersion method [5].

The compositions of the glasses studied were the same as those of the soda and potash glasses, namely: Series I) $16Li_2O \cdot yB_2O_3 \cdot xAl_2O_3 \cdot (84-x-y)SiO_2$, Series II) $(32-y)Li_2O \cdot yB_2O_3 \cdot xAl_2O_3 \cdot (68-x)SiO_2$, where x is 0, 4, 8 and 12 molar %; y is 0, 4, 8, 12, 16, 24, 32 molar %. The properties of the original glasses are given in Table 1.

To compare the effects of alkali oxides on optical properties, we first consider 3-component systems.

The systems $Me_2O \cdot Al_2O_3 \cdot SiO_2$. The refractive indices of lithium glasses are much higher than those of sodium and potassium glasses, while the values of n_D are somewhat higher for sodium than for potassium glasses.

TABLE 1

Refractive Indices and Densities of the Original Glasses

Series I			Series II		
glass composition	n_D	d	glass composition	n_D	d
$16Li_2O \cdot 84SiO_2$	1.495	2.263	$32Li_2O \cdot 68SiO_2$	1.534	2.344
$16Li_2O \cdot 8B_2O_3 \cdot 76SiO_2$	1.505	2.287	$24Li_2O \cdot 8B_2O_3 \cdot 68SiO_2$	1.524	2.348
$16Li_2O \cdot 12B_2O_3 \cdot 72SiO_2$	1.507	2.290	$20Li_2O \cdot 12B_2O_3 \cdot 68SiO_2$	1.518	2.321
$16Li_2O \cdot 16B_2O_3 \cdot 68SiO_2$	1.509	2.294	$12Li_2O \cdot 20B_2O_3 \cdot 68SiO_2$	1.497	2.254
$16Li_2O \cdot 24B_2O_3 \cdot 60SiO_3$	1.511	2.283	$8Li_2O \cdot 24B_2O_3 \cdot 68SiO_2$	1.482	2.167
$16Li_2O \cdot 32B_2O_3 \cdot 52SiO_2$	1.513	2.265			

• Communication III in the series on the aluminoborate anomaly of properties of silicate glasses.

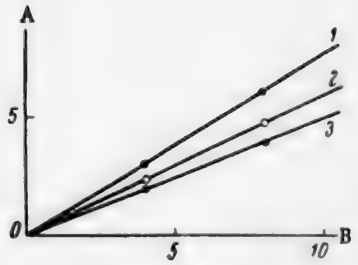

Fig. 1. Variations of the refractive-index difference with chemical composition of glasses in the system $32\,Me_2O \cdot xAl_2O_3 \cdot (68-x)\,SiO_2$ on replacement of SiO_2 by Al_2O_3: A) values of $\Delta n_D \cdot 10^3$, B) values of x (molar % Al_2O_3); glasses: 1) lithium; 2) sodium; 3) potassium.

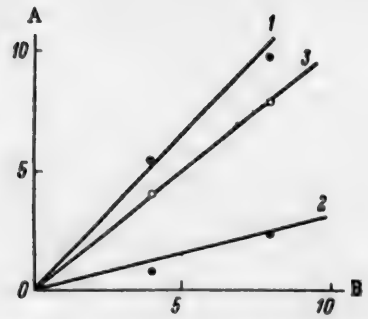

Fig. 2. Variations of the density difference with chemical composition of glasses in the system $32\,Me_2O \cdot xAl_2O_3 \cdot (68-x)\,SiO_2$ on replacement of SiO_2 by Al_2O_3: A) values of $\Delta d \cdot 10^2$, B) values of x (molar % Al_2O_3); glasses: 1) lithium; 2) sodium; 3) potassium.

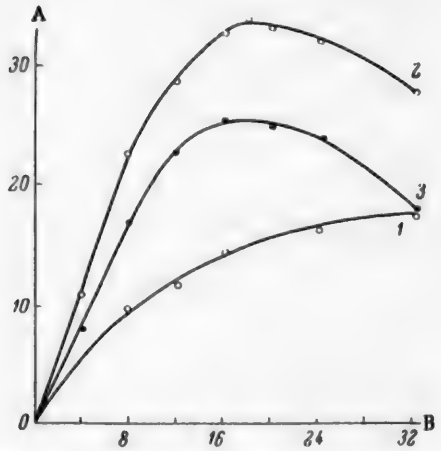

Fig. 3. Variations of the refractive-index difference with chemical composition of glasses in the system $16\,Me_2O \cdot yB_2O_3 \cdot (84-y)\,SiO_2$ on replacement of SiO_2 by B_2O_3: A) values of $\Delta n_D \cdot 10^3$; B) values of y (molar % B_2O_3); glasses: 1) lithium; 2) sodium; 3) potassium.

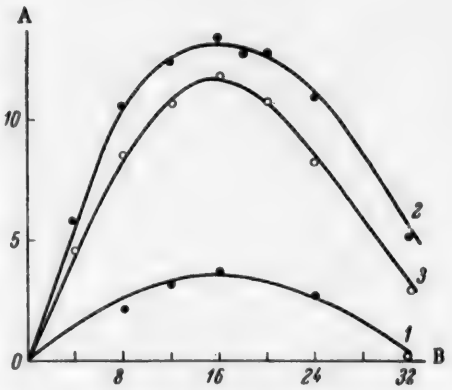

Fig. 4. Variations of the density difference with chemical composition of glasses in the system $16\,Me_2O \cdot y\,B_2O_3 \cdot (84-y)\,SiO_2$ on replacement of SiO_2 by B_2O_3: A) values of $\Delta d \cdot 10^2$; B) values of y (molar % B_2O_3); glasses: 1) lithium; 2) sodium; 3) potassium.

Sodium glasses have higher densities than potassium glasses, and somewhat higher than lithium glasses. The same is found for other silicate systems with high alkali contents [6].

On replacement of silica by alumina the refractive index increases most rapidly in lithium glasses, which are followed by sodium and potassium glasses (Fig. 1). The greatest density increase is also found in lithium glasses, but sodium and potassium glasses change places (Fig. 2). Molecular refraction of the glasses conforms to the following sequence: potassium > sodium > lithium.

The systems $Me_2O \cdot B_2O_3 \cdot SiO_2$. Fig. 3 and 4 show that in the case of sodium and potassium glasses the curves for the refractive-index and density changes on replacement of silica by boric anhydride generally have

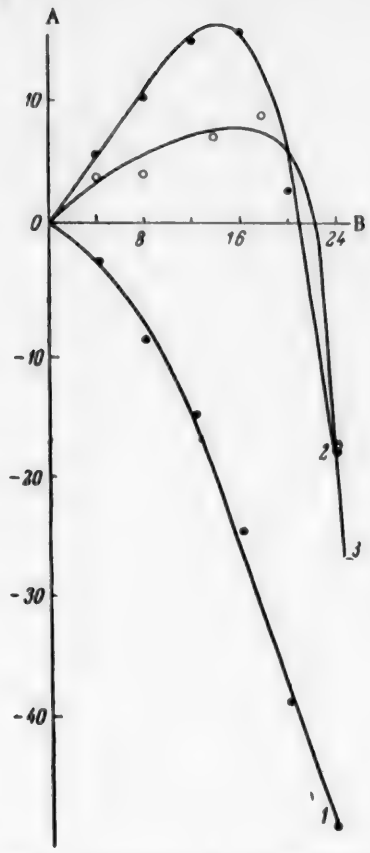

Fig. 5. Variations of the refractive-index difference with chemical composition of glasses in the system (32−y) $Me_2O \cdot yB_2O_3 \cdot 68SiO_2$ on replacement of Me_2O by B_2O_3: A) values of $\Delta n_D \cdot 10^3$; B) values of y (molar % B_2O_3); glasses: 1) lithium; 2) sodium; 3) potassium.

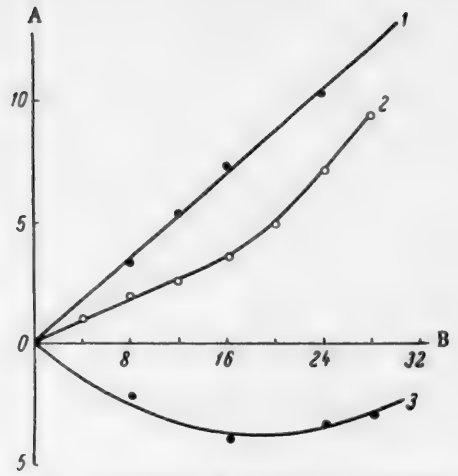

Fig. 6. Variations of molecular-refraction difference with chemical composition of glasses in the system (32−y) $Me_2O \cdot yB_2O_3 \cdot 68(SiO_2)$ on replacement of Me_2O by B_2O_3: A) values of MR; B) values of y (molar % B_2O_3); glasses: 1) lithium; 2) sodium; 3) potassium.

maxima. The behavior of lithium glasses is different. The refractive index of lithium glasses increases continously, whereas the density remains almost constant. The refractive indices and densities are greatest for sodium glasses and least for lithium glasses, while potassium glasses occupy an intermediate position. The molecular refraction changes in the same sequence as for aluminosilicate glasses.

Fig. 5 shows that when alkali oxides are replaced by boric anhydride the curves for the refractive-index differences of sodium and potassium glasses have distinct maxima, whereas n_D of lithium glasses decreases steadily.

It follows from Fig.6 that changes of molecular refraction do not always conform satisfactorily to the additivity rule; for example, Curve 3 has a weak minimum.

The system $Li_2O \cdot B_2O_3 \cdot Al_2O_3 \cdot SiO_2$. Whereas the character of the variations of the optical properties and density is approximately the same for potassium as for sodium aluminoborosilicate glasses, the behavior of lithium aluminoborosilicate glasses is distinctive. Fig. 7 shows that in the first series of glasses the refractive index increases on replacement of silica by alumina over a wide range of Li_2O/B_2O_3 ratios (from ∞ to 1/2), and n_D and d tend to decrease only at high Al_2O_3 contents. The aluminoborate anomaly is almost entirely lacking in curves for the properties of lithium glasses. The only hint of it is the appearance of weak maxima on the curves. In no instance did replacement of the first portions of SiO_2 by Al_2O_3 result in decreases of n_D or d.

The molecular refraction increases linearly at all Li_2O/B_2O_3 ratios.

Fig. 8 shows that on replacement of silica by boric anhydride in presence of Al_2O_3, the refractive-index difference curves exhibit maxima, and addition of Al_2O_3 does not make the maxima diffuse, as in the case of sodium and potassium glasses, but, on the contrary, intensified them.

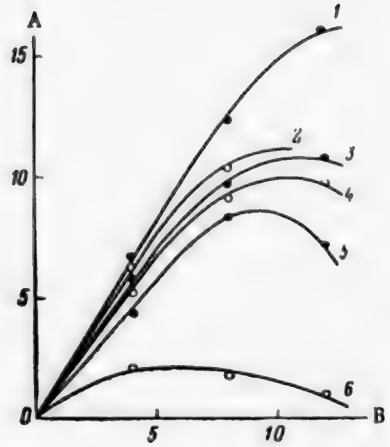

Fig. 7. Variations of the refractive-index difference with chemical composition of glasses of the first series, 16 $Li_2O \cdot y\ B_2O_3 \cdot x\ Al_2O_3 \cdot (84 - x - y)$. SiO_2, on replacement of SiO_2 by Al_2O_3: A) values of $\Delta n_D \cdot 10^3$, B) values of x (molar % Al_2O_3); curves: 1) y = 0, 2) y = 8, 3) y = 12, 4) y = 16, 5) y = = 24, 6) y = 32.

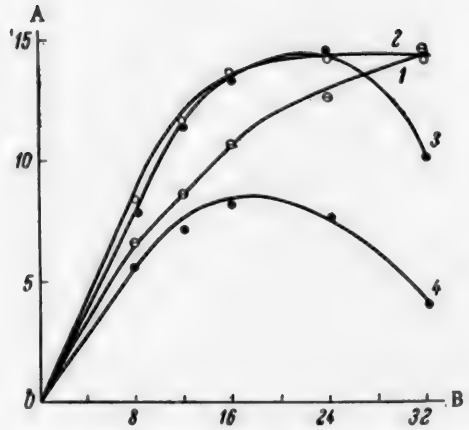

Fig. 8. Variations of the refractive-index difference with chemical composition of glasses of the first series, 16 $Li_2O \cdot y \cdot y \cdot B_2O_3 \cdot x\ Al_2O_3 \cdot (84-x-y)\ SiO_2$ on replacement of SiO_2 by B_2O_3: A) values of $\Delta n_D \cdot 10^3$, B) values of y (molar % B_2O_3); curves: 1) x = 0, 2) x = 4, 3) x = 8, 4) x = 12.

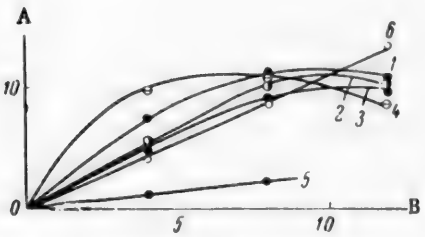

Fig. 9. Variations of the refractive-index difference with chemical composition of glasses of the second series, $(32-y)\ Li_2O \cdot y B_2O_3 \cdot x\ Al_2O_3 \cdot (68-x)\ SiO_2$, on replacement of SiO_2 by Al_2O_3: A) values of $\Delta n_D \cdot 10^3$; B) values of x (molar % Al_2O_3); curves 1) y = 0, 2) y = 8, 3) y = 12, 4) y = 16, 5) y = 20, 6) y = 24.

The density changes of lithium glasses resemble the refractive-index changes, but the positions of the maxima on the n_D and d curves do not coincide (Table 2).

Experimental results for the second series of glasses are plotted in Fig. 9. On replacement of silica by alumina the refractive index and density increase in all cases. The Li_2O/B_2O_3 ratio influences only the form of the curves: at Li_2O/B_2O_3 ratios from 3 to 1 there are faint maxima, while at lower Li_2O/B_2O_3 ratios n_D increases linearly.

Variations of molecular refraction conform satisfactorily to the additivity rule in this series.

DISCUSSION OF RESULTS

The experimental results show that the strength of the electric field of the alkali-metal cation has a strong influence on the nature of the composition–property curves.

Since the radius of the lithium ion is small, the structure of the glass remains compact on introduction of Li_2O, and the Li^+ ions fill the voids in the framework. As the radii of sodium and especially of potassium ions are greater than those of lithium ions, the glass structure is loosened on introduction of Na_2O and K_2O into the glass. This explains why the molecular volume of lithium glasses is much smaller than that of sodium or potassium glasses.

The strength of the Na–O and K–O bonds is low, and sodium and potassium ions readily give up oxygen to aluminum and boron ions for formation of tetrahedrons. Therefore variations of optical properties and density follow a similar course in potassium and sodium glasses. Lithium not only has a small ionic radius,

TABLE 2

Positions of Maxima on the n_D and d Curves on Replacement of SiO_2 by B_2O_3 at Different Al_2O_3 Contents

Properties	n_D				d			
Al_2O_3 content of glass (%)	0	4	8	12	0	4	8	12
Position of maximum (% B_2O_3)	None	> 32	22	16	16	11	10	2

but its bond strength with oxygen is considerably greater. This cannot fail to influence changes in the coordination of Al^{3+} and B^{3+} ions.

It follows from Fig. 3 that on replacement of silica by boric anhydride in the system $Li_2O \cdot B_2O_3 \cdot SiO_2$ the effect of n_D increase is weaker by a factor of 2 or 3 than in the corresponding sodium and potassium systems. The density of lithium borosilicate glasses remains almost unchanged on replacement of SiO_2 by B_2O_3, whereas the density of sodium and potassium glasses rises sharply (Fig. 4). These facts indicate that change of the coordination number of boron to four proceeds with much more difficulty in lithium than in sodium or potassium glasses. In other words, there are fewer (BO_4) tetrahedrons in lithium glasses for a given molar alkali content, while the proportion of oxygen not linked to boron in the form of (BO_4) tetrahedrons is greater in them. It follows that (AlO_4) tetrahedrons may be formed in lithium aluminosilicate glasses without removal of oxygen from the (BO_4) tetrahedrons and destruction of the latter. The oxygen linked to silicon and lithium is sufficient for the formation of (AlO_4) tetrahedrons. It follows from this that introduction of Al_2O_3 into lithium glasses should not be accompanied by decreases of n_D and d. On replacement of silica by alumina n_D and d of lithium aluminoborosilicate glasses increase at all Li_2O/B_2O_3 ratios.

Change of the coordination number of Al^{3+} ions in lithium glasses to four is apparently also hindered somewhat, as the difference between the bond strength of oxygen with Li^+ and Al^{3+} of coordination number six is not large. A small proportion of the Al^{3+} ions possibly retain a coordination number of six. This hypothesis is indirectly supported by the fact that on replacement of SiO_2 by Al_2O_3 the refractive index and density of boronless lithium glasses increase more rapidly than in the case of corresponding sodium and potassium glasses.

Difficulties in changing the coordination number of B^{3+} ions, and to some extent of Al^{3+} ions, to four, explain, in our opinion, the almost total absence of aluminoborate anomaly of properties in lithium glasses.

SUMMARY

1. The variations of the optical properties of lithium aluminoborosilicate glasses have certain distinguishing peculiarities, and therefore lithium glasses cannot be regarded as similar to potassium or sodium glasses. The aluminoborate anomaly of properties is almost nonexistent in lithium glasses.

2. Structural changes in the glass account for the observed results. It appears that in lithium glasses change of the coordination number of boron to four is hindered.

LITERATURE CITED

[1] M. A. Bezborodov and V. A. Ulazovskii, Investigation of $Li_2O-B_2O_3-Al_2O_3-SiO_2$ Systems in the Glassy State [In Russian] (Belorussian Polytechnic Institute, 1957).

[2] H. Moore and P. W. McMillan, J. Soc. Glass. Techn. 40, 66 (1956).*

[3] A. A. Appen and Kan Fu-Si, J. Appl. Chem. 32, No. 5, 983 (1959).*

[4] A. A. Appen and Kan Fu-Si, J. Appl. Chem. 32, No. 5, 991 (1959).*

*Original Russian pagination. See C. B. Translation.

[5] G. B. Bokii, The Immersion Method [In Russian] (Izd. MGU, 1948).

[6] A. A. Appen, J. Appl. Chem. 24, 1001 (1951).*

[7] K. H. Sun, J. Am. Ceram. Soc. 30, 277 (1947).*

Received September 29, 1958

*Original Russian pagination. See C. B. Translation.

PRODUCTION OF CARBON DISULFIDE BY "NONEQUILIBRIUM" REDUCTION OF SULFUR DIOXIDE BY METHANE

Ya. P. Berkman and S. V. Kushnir

The L'vov Polytechnic Institute

The expansion of artificial-fiber production planned for the near future involves a considerable increase in the demand for carbon disulfide. Studies of new and more rational methods of its production are therefore of interest.

This paper presents the results of a laboratory investigation of the reduction of sulfur dioxide by natural methane under conditions such that carbon disulfide is the main reaction product. We believe that this procedure merits serious attention in the development of a technical process for the manufacture of carbon disulfide.

According to literature data, the reaction between sulfur dioxide and methane at temperatures up to 1000° is heterogeneously catalytic. When this system reaches thermodynamic equilibrium, the reaction products should be sulfur or carbon disulfide [1]. This direction of the reaction was studied fairly fully by Yushkevich [2] and Walker [1]. They showed that the reaction takes this course in presence of active catalysts (CaS, bauxites) at $t > 700°$. The component ratio $N = SO_2 / CH_4$ has the main influence on the course of this process. At low values of N, reduction of SO_2 proceeds as far as formation of H_2S:

$$SO_2 + CH_4 = H_2S + CO + H_2O, \quad (1)$$

and at high temperatures elemental sulfur is formed:

$$2SO_2 + CH_4 = 2S + CO_2 + 2H_2O. \quad (2)$$

In 1938 Zawadzki [3] discovered another direction of the reaction of SO_2 with CH_4 in presence of quartz catalyst. He showed that in presence of quartz the reaction proceeds only at $t > 800°$ and results in the formation of carbon–sulfur compounds (COS and CS_2) and appreciable amounts of elemental sulfur. This course of the reaction, leading to the formation of products which do not correspond to equilibrium in the SO_2–CH_4 system, may for brevity be named the "nonequilibrium" course. Zawadzki put forward the hypothesis that reduction in the presence of quartz is halted at an intermediate stage. In his opinion, the main product at this stage is carbonyl sulfide, which is relatively unstable and can decompose further in two ways:

$$COS \rightleftarrows CO + S, \quad (3)$$

$$2COS \rightleftarrows CS_2 + CO_2. \quad (4)$$

Increase of temperature accelerates Reaction (3), with a considerable increase of the proportion of S and a decrease of the proportion of COS in the products. At 800-900° the over-all equation for the process (according to Zawadzki) is

$$3SO_2 + 2CH_4 = 2COS + S + 4H_2O. \quad (5)$$

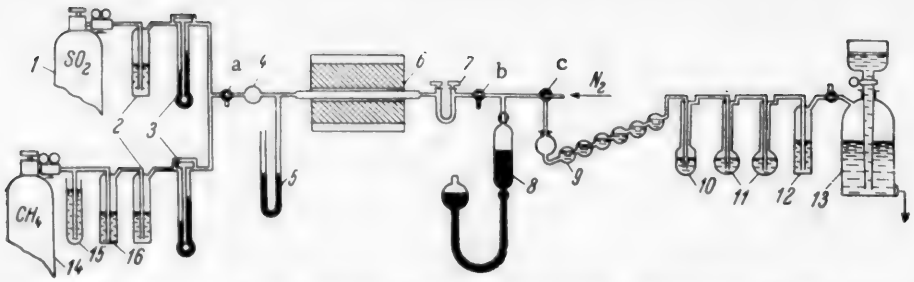

Scheme of apparatus: 1) SO_2 cylinder; 2) wash bottles with concentrated H_2SO_4; 3) capillary flowmeter; 4) calcium chloride tube; 5) manometer; 6) tubular electric furnace; 7) U tube with $CaCl_2$; 8) mercury pipet; 9) bulb absorber with 0.1 N I_2; 10) wash bottle with KI solution; 11) absorbers for COS; 12) wash bottle with H_2SO_4; 13) aspirator gas holder; 14) methane cylinder; 15) hydraulic seal; 16) wash bottle with KOH solution, a, b, c) three-way cocks.

In contrast to equilibrium reduction, the nonequilibrium process has not been studied in detail, and much of it needs clarification. Zawadzki's views on the reaction mechanism also seemed to us to be unconvincing. It was therefore decided to study the nonequilibrium reduction of SO_2 by methane, with special reference to the following problems: 1) the contents of carbonyl sulfide and carbon disulfide in the reduction products, 2) effect of the methane–sulfur dioxide ratio, 3) effect of temperature in presence of large amounts of methane, 4) activity of the quartz catalyst.

Experimental procedure. The apparatus used for investigation of the reaction is shown in the figure. It consisted of a quartz reaction tube heated in an electric furnace, sulfur dioxide and methane supply lines, absorption line for the gaseous reduction products, and a pipet with a mercury seal for sampling the gas. The temperature inside the reaction tube was measured by means of a TP-5 thermocouple (with an MP-1 galvanometer) calibrated against the boiling point of sulfur and the melting point of potassium chloride. Sulfur dioxide and natural methane in cylinders were used for the experiments•. The SO_2 was dried before use in a wash bottle containing concentrated sulfuric acid, while traces of mercaptans were removed from methane in a wash bottle containing concentrated KOH, and the gas was then dried by means of concentrated H_2SO_4. The gas rates were measured by means of oil-filled capillary flowmeters, carefully calibrated for the corresponding gases.

TABLE 1

Analysis of Reduction Products

t(°C)	N	Distribution of reduced S (%)			
		H_2S	S	CS_2	COS
800	0.42	6.9	26.4	65.7	1.0
900	0.40	14.0	26.0	59.2	0.8
800	2.0	0.8	31.1	66.9	1.2

Before the start of an experiment a uniform flow of dry gaseous SO_2–CH_4 mixture of known composition was established at a definite rate by means of the flowmeters. The composition of the mixture was checked by direct determinations of SO_2 in a Hempel pipet with a mercury seal.

• The composition of natural methane gas (from Dashava) was (%): CH_4–97.83, C_2H_6–0.44, C_3H_8–0.18, C_4H_{10}–0.05, C_5H_{12} and higher –0.11, N_2–1.1.

After the furnace had been heated to the required temperature the mixture was introduced into the reaction tube. The reaction products were passed through a filter to trap sulfur, then through a calcium chloride tube, and drawn out through the three-way cock c. When 10-15 minutes had elapsed from the start of the reaction (the blow-through period) the cock c was turned and the aspirator connected so that the exit gases were drawn into the absorption system for analysis (atmospheric pressure being maintained in the reaction tube). Hydrogen sulfide and sulfur dioxide were absorbed in the wash bottle containing 0.1 N I_2, iodine vapor in the wash bottle with 10% KI, carbonyl sulfide in the wash bottle with ammoniacal $CaCl_2$ solution, and ammonia vapor in strong sulfuric acid. The residual gas was collected over a saturated solution of common salt in the aspirator. After a definite time the gas leaving the furnace was connected to the draft by means of the cock b, while nitrogen from a cylinder was admitted through the right-hand branch of cock c to rinse out the absorption system. During rinsing of the absorption system a reserve gas sample was collected in the mercury buret. The sampling time was noted accurately, as this is necessary in calculations of the amount of sulfur dioxide entering the furnace.

TABLE 2

Effect of Component Ratio $N = SO_2/CH_4$ on the Reduction of SO_2 by Methane over Quartz

SO_2 (%)	N	Distribution of reduced S (%) (B %)			$\frac{CO_2}{SO_2 red}$	$\frac{CO}{SO_2 red}$
		CS_2	S	H_2S		
10	0.11	72.5	3.0	24.5	0.075	0.268
30	0.43	71.9	26.7	1.43	0.082	0.209
50	1.0	67.7	31.4	0.86	0.118	0.230
60	1.5	67.1	32.0	0.88	—	—
70	2.3	68.3	31.7	Traces	0.182	0.166
75	3.0	66.1	33.2	0.7	0.088(?)	0.201

The iodometric–acidimetric method was used for determination of SO_2 and H_2S. The absorbed COS was oxidized by hydrogen peroxide to $SO_4^{=}$ and determined gravimetrically as $BaSO_4$. The CS_2 content of the residual gas was determined by the combustion method [4]. As direct determination of elemental sulfur was impossible, it was found from the difference between the sulfur in the original SO_2 and the sulfur found as SO_2, H_2S, CS_2 and COS. The analytical results were expressed as molar yields on the converted sulfur dioxide.

Contents of carbonyl sulfide and carbon disulfide in the reduction products. Zawadzki's data on the relative proportions of CS_2 and COS in the reaction products appeared to us to be unreliable. For separate determinations of these gases, Zawadzki condensed CS_2 at −78° and absorbed COS in alcoholic KOH solution. If the volume of the rinsing gas is large and the amounts of CS_2 formed are relatively small, a considerable proportion of the latter must inevitably be carried out of the condenser and absorbed together with COS. As a result, Zawadzki would have obtained high results for COS and low for CS_2. Therefore only his values for the sum of $COS + CS_2$, may be regarded as reliable.

Our experiments (with another method for separate determinations of CS_2 and COS) were performed with a hollow tube of clear quartz at a gas rate v = 20 ml/minute. The results of experiments under different conditions are given in Table 1.

These results show that the main sulfur compound of carbon is not COS, as Zawadzki believed, but CS_2. Only small amounts of carbonyl sulfide are formed.

Zawadzki's view that carbon disulfide is a secondary product formed by decomposition of the oxysulfide is at variance with the results of thermodynamic calculations performed by Siller [5]*. According to Siller,

*Lepsoe's thermodynamic data [6], calculated from Stock's experimental results [7], are untrustworthy, as Stock's data do not reflect true equilibrium for the reaction [8].

TABLE 3

Effect of Temperature on Reduction of SO_2 by Methane over Quartz

Expt. No.	t (в °C)	N	Degree of reduction of SO_2 (%)	Distribution of reduced S (%)			$\frac{CO_2}{SO_2 red}$	$\frac{CO}{SO_2 red}$
				CS_2	S	H_2S		
				Series I				
1	800	0.45	62.9	72.3	22.5	5.25	0.162	0.209
2	850	0.43	82.3	65.5	23.3	11.2	0.165	0.265
3	900	0.39	88.5	60.0	26.0	14.0	0.150	0.271
4	950	0.37	92.2	56.6	24.5	19.8	0.158	0.332
				Series II				
5	800	0.77	38.0	69.5	26.0	4.5	0.072	0.204
6	850	0.85	66.8	70.8	23.0	6.2	0.118	0.230
7	900	0.86	92.2	65.6	23.0	11.4	0.128	0.307
8	950	0.89	100.0	51.2	11.0	37.8	0.132	0.482
				Zawadzki's experiments				
9	810	3.0	35.4	78.9	21.1	Traces	—	0.217
10	875	2.2	42.4	67.7	31.5	0.7	0.127	0.240
11	950	2.8	74.0	29.3	69.4	1.3	0.168	0.020
12	1000	2.8	71.3	14.6	85.4	Traces	0.349	0.005

COS cannot decompose with formation of CS_2 at all. Therefore carbon disulfide must be not only the main but also the primary product of nonequilibrium reduction of SO_2 by methane.

In subsequent experiments CS_2 and COS were not determined separately, but only their sum, which was taken as CS_2. The COS absorbers were removed from the absorption line, and the sum of CS_2 + COS was determined in the gas contained in the aspirator by the combustion method. This made it also possible to determine CO_2 and CO in the residual gas.

Effect of component ratio $N = SO_2 / CH_4$. Zawadzki's experiments were performed only with relatively small amounts of reducing agent, at $N > 2$. He did not investigate the region of $N < 2$. Our experiments with low values of N were carried out at 800° and gas rate v = 20 ml/minute. The required value of N for the mixture was adjusted by appropriate regulation of the feed rates of the two gases. The results of the experiments are given in Table 2. The results of one of Zawadzki's experiments at N = 3 are also given.

The results show that carbon disulfide is the principal reduction product of SO_2 in all cases; its yield is almost independent of the component ratio and corresponds to about 2/3 of all the reduced sulfur. The sum of $H_2S + S$ is therefore also virtually constant; over a wide range of N (from 0.4 upward) mainly S is formed, and H_2S predominates only at very high concentrations of methane in the gas ($N < 0.4$). The oxidation products of methane, CO and CO_2, are present in a molar ratio of about 2:1.

Therefore the over-all reduction reaction at 800° may be represented by the approximate equation:

$$8SO_2 + 6CH_4 = 3CS_2 + 2S + 2CO + CO_2 + 12H_2O. \quad (6)$$

Effect of temperature. Zawadzki's experiments were performed only with high sulfur dioxide–methane ratios ($2 < N < 3$). However, such conditions are of little practical significance, as the deficiency of methane makes the percentage reduction of SO_2 low. It was therefore thought desirable to study the effects of temperature also at high contents of the reducing agent in the reaction mixture.

The experiments were performed in a quartz tube at a constant gas rate (v = 22 ml/minute). The results of these experiments are given in Table 3, which also contains, for comparison, results of Zawadzki's experiments at $N > 2$. Zawadzki's data for CO_2 and CO are calculated as molar yields on the converted SO_2.

TABLE 4

Activity of Quartz Catalysts

Expt. No.	Catalyst	Degree of reduction of SO_2(%)	Distribution of reduced S (%)		
			CS_2	S	H_2S
1	Clear quartz tube	30.5	67.7	31.4	0.86
2	Clear quartz tube+ lumps of clear quartz	38.4	72.8	27.2	Traces
3	Clear quartz tube+ lumps of opaque quartz	81.4	67.6	31.5	0.9

Table 3 shows that increase of temperature increases the degree of reduction of sulfur dioxide but lowers the yield of carbon disulfide. The CS_2 yield decreases especially sharply with increase of temperature at high values of N (in Zawadzki's experiments), i.e., at low concentrations of the reducing agent. It follows that the best conditions for high yields of carbon disulfide are moderate temperatures (800-850°) and excess of reducing agent in the reaction mixture (low N).

The decrease of the CS_2 yield at low values of N leads to increase of hydrogen sulfide yield at constant sulfur yield. Experiment No. 8 is noteworthy; this differs from the rest of the experiments by having a very much lower sulfur yield and a high yield of hydrogen sulfide. This is easily explained on the assumption that sulfur is a secondary reaction product, formed by the interaction of SO_2 and H_2S in presence of water vapor. In Experiment No. 8 the reduction of sulfur dioxide was 100% complete and there was evidently not enough oxidizing agent for most of the hydrogen sulfur dioxide. At high values of N a decrease of the yield of carbon disulfide is accompanied by an increase of the sulfur yield, while hydrogen sulfide is almost absent.

The oxidation products of methane are CO and CO_2; in our experiments ($N < 1$) increase of temperature led to a considerable increase of the CO yield, whereas in Zawadzki's experiments, ($N>2$), on the contrary, the CO_2 yield increased.

According to Walker [1], the reaction products in equilibrium reduction of SO_2 by methane at $N < 1$ are H_2S and CO, and at $N > 2$, S and CO_2. Therefore the increased yields of H_2S and CO (in our experiments) or of S and CO_2 (in Zawadzki's experiments), with simultaneous decreases of the CS_2 yields, on increase of temperature may be interpreted as representing an approach from the nonequilibrium to the equilibrium state. If all three series of experiments are compared, it is easy to see that the higher the methane concentration in the gas mixture (the lower the value of N), the slower is this shift in the direction of equilibrium. It follows that excess of reducing agent favors the nonequilibrium course of the process.

Our experimental results indicate that the shift of the nonequilibrium system SO_2-CH_4 in the equilibrium direction proceeds by way of the heterogeneous catalytic reaction of carbon disulfide hydrolysis:

$$CS_2 + 2H_2O = 2H_2S + CO_2. \quad (7)$$

According to Bacon [9], quartz is a very ineffective catalyst for this reaction, which is therefore far from quantitative even at high temperature. The above reaction accounts very satisfactorily for the increase of H_2S yield (at $N < 1$) with increase of temperature, owing to decrease of the CS_2 yield at constant S yield. On the other hand, at $N > 2$, decrease of the CS_2 yield results in an increased yield of elemental sulfur as the result of secondary interaction of H_2S with excess SO_2.

Catalytic activity of quartz. Zawadzki noted that different types of quartz differ in their catalytic activity in the reaction between sulfur dioxide and methane. However, his paper does not contain any quantitative data.

TABLE 5

Effect of Contact Time

v (ml/min)	Degree of reduction of SO_2 (%)	Distribution of reduced S (%)		
		CS_2	S	H_2S
10	51.4	71.1	28.7	0.2
20	38.4	72.8	27.2	Traces

TABLE 6

Effect of the Degree of Reduction

Degree of reduction of SO_2 (%)	Distribution of reduced S (%)		
	CS_2	S	H_2
44.7	72.5	3.0	24.5
20.5	73.6	2.4	24.0

For elucidation of the question of the activity of quartz catalysts, we carried out several experiments at 800°, component ratio N = 1.0, and gas rate (v) 20 ml/minute, in an empty quartz tube and in a tube filled with lumps of clear or opaque quartz (Table 4).

It follows from Table 4 that clear quartz has low catalytic activity in the nonequilibrium reduction of SO_2 by methane. Increase of its surface produces only a slight increase in the degree of reduction of SO_2. The activity of opaque quartz is considerably higher. Opaque quartz does not differ from clear in the character of its effect, as it gives the same distribution of sulfur between the reduction products.

As the system is not in equilibrium, the influence of contact time on the course of reaction is of particular interest. To investigate this question, we performed another experiment in a tube filled with lumps of clear quartz (as in Experiment No. 2, Table 4), at a gas rate reduced by a half but otherwise under the same conditions. These experiments are compared in Table 5.

It can be seen that increase of contact time increases the extent of reaction, but has no influence at all on the character of the process, i.e., on the distribution of sulfur between the products. This shows that quartz is a strictly selective catalyst for nonequilibrium reduction of sulfur dioxide by methane.

Even in the preliminary experiments it was noticed that the catalytic activity of the quartz tube fell as the result of repeated use. For example, in experiments with an original mixture of the same composition (50% SO_2) performed in the same tube under the same conditions but after definite time intervals*, the degree of reduction was 78.4, 56.1, 41.5, 30.5%. The fall of activity gradually slowed down. Its lower limit corresponded to 20-25% reduction. However, the fall of catalytic activity of the quartz and decrease of the degree of reduction was not reflected in any way in the nature of the process, i.e., in the proportions of the reaction products. This is evident from the results of two experiments performed under the same conditions (t = 800°, v = 20 ml/minute, N = 0.11), given in Table 6.

Our experiments showed that neither heating of the tube in a current of oxygen nor treatment with hot acids increased the catalytic activity of deactivated quartz.

It may be concluded from the foregoing that pure quartz is not a suitable catalyst for nonequilibrium reduction of SO_2 by methane. However, the results obtained with opaque quartz indicate that the quartz catalyst may be activated.

It should be pointed out in conclusion that nonequilibrium reduction of SO_2 by methane, which gives CS_2 in yields of up to 75%, certainly merits further study as a possible practical method for production of carbon disulfide.

SUMMARY

1. In a study of the reduction of sulfur dioxide by methane over quartz catalyst at various temperatures (800-950°) and component ratios ($N = SO_2/CH_4 = 0.5-3.0$) it was shown that in presence of quartz the process is a nonequilibrium one, and occurs with formation of carbon disulfide as the main product:

*Every 8-10 experiments, i.e, 20-30 hours of heating of the tube.

$$8SO_2 + 6CH_4 = 3CS_2 + 2S + 2CO + CO_2 + 12H_2O.$$

2. The process is insensitive to variations of contact time and component ratio, i.e., it is pseudoequilibrium in character. However, increase of temperature brings the system closer to a state of true equilibrium and lowers the yield of carbon disulfide considerably. The optimum conditions for high yields of carbon disulfide are: low component ratios (N ~ 1) and moderate temperature (800-850°).

3. The activity of the quartz catalyst is relatively low, and decreases during use. A search must therefore be started for other and more efficient catalysts for the nonequilibrium reduction of SO_2 by methane.

LITERATURE CITED

[1] C. W. Walker, Ind. Eng. Ch. 38, 906 (1946).

[2] N. F. Yushkevich et al., J. Chem. Ind. 11, No. 2, 33 (1934).

[3] J. Zawadzki, Przem. chem. 22, 558 (1938).

[4] A. A. Il'inskaya and L. M. Kontorovich, Industrial Lab. 13, No. 1, 29 (1947).

[5] C. W. Siller, Ind. Eng. Ch. 40, 1327 (1948).

[6] R. Lepsoe, Ind. Eng. Ch. 30, 92 (1938).

[7] A. Stock and P. Seeling, Ber. 52, 681 (1919).

[8] A. Klemenc, Z. anorg. Ch., 254, 265 (1947).

[9] R. F. Bacon and E. S. Boy, Ind. Eng. Ch. 37, 469 (1945).

Received February 20, 1958

SOLUBILITY OF THE CHLORIDES OF LEAD, ARSENIC, AND IRON IN THE PRESENCE OF STANNOUS CHLORIDE

D. M. Chizhikov and B. Ya. Tratsevitskaya

In the conversion of poor tin concentrates by the calcium chloride process [1], the sublimate contains, in addition to stannous chloride, chlorides of certain metals present with tin in the ore. These include iron, lead, arsenic, copper, antimony, bismuth, and others. Tin is extracted from the chloride sublimate by a hydrometallurgical process.

When the chloride sublimate is leached by dilute hydrochloric acid, certain impurities enter the solution together with stannous chloride.

Qualitative spectrum analysis of the leached extract showed that the metallic impurities may be divided into three groups: 1) metals which predominantly pass into solution (iron, zinc, manganese); 2) metals which predominantly remain in the insoluble residue (copper, arsenic, antimony); and 3) metals which are distributed between the solution and the residue (lead, magnesium, aluminum).

Metallic impurities which are more electropositive than tin, such as copper, bismuth, antimony, and arsenic, may be removed from solution by precipitation on tin [2].

In this investigation we studied the behavior of lead, arsenic, and iron chlorides when dissolved in presence of stannous chloride.

Solubility of lead chloride in stannous chloride solutions. The solubility of lead chloride is influenced by the presence of compounds which yield chloride ions in solution. The solubility of lead chloride decreases with increase of hydrochloric acid concentration from 0 to 9.1% [3]. On further increase of the hydrochloric acid concentration the concentration of lead chloride in solution begins to increase (Fig. 1).

The existence of the complex chloride anions $[PbCl_4]^{2-}$ and $[PbCl_3]^{-}$ has been reported in the literature.

When the acid content of the solution is above 3 moles per liter, $[PbCl_4]^{2-}$ ions predominate. In the acidity range of 0.8-2.5 moles/liter, $[PbCl_3]^{-}$ ions predominate in solution. Both these complex anions are readily soluble in water, but they are decomposed when the acidity falls below 0.8 mole/liter [4].

Minima indicative of complex formation in the ascending regions of the curves have been found for the systems $PbCl_2-ZnCl_2-HCl-H_2O$ and $PbCl_2-CaCl_2-HCl-H_2O$ [5]. Our experiments on the solubility of lead chloride in solutions of stannous chloride were carried out at 20°. To prevent hydrolysis of stannous chloride, a saturated solution of lead chloride containing 20 g of hydrochloric acid per liter was prepared. This solution contained 1.30 g of lead chloride per liter in equilibrium with solid $PbCl_2$. To this solution, stannous chloride was added in amounts corresponding to stannous chloride contents from 0 to 350 g per liter of solution. Equilibrium was reached after 12 hours. The results of these experiments are plotted in Fig. 2.

The data in Table 2 show that as the stannous chloride concentration is increased from 0 to 38.5 g/liter the lead chloride content falls from 1.30 to 1.04 g/liter. On further increase of the stannous chloride concentration to 352 g/liter the lead chloride content of the solution rises to 2.37 g/liter. Evidently, at stannous chloride concentrations above 38.5 g/liter, soluble complex salts are formed from stannous chloride and lead chloride.

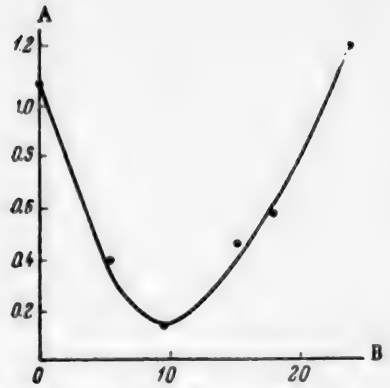

Fig. 1. Effect of hydrochloric acid concentration on the solubility of lead chloride: A) $PbCl_2$ concentration (%); B) HCl concentration (%).

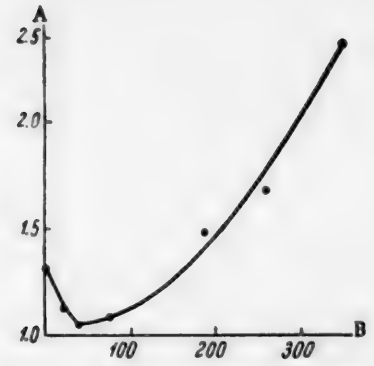

Fig. 2. Effect of stannous chloride concentration on the solubility of lead chloride: A) $PbCl_2$ concentration (%); B) $SnCl_2$ concentration (%).

Study of the behavior of arsenious chloride in stannous chloride solution. It is known [6] that in an acid medium the following reaction takes place:

$$2As^{3+} + 3Sn^{2+} \rightleftarrows As^{0} \downarrow + 3Sn^{4+}, \quad (1)$$

in this reaction stannous chloride reduces arsenic to the metal and is itself oxidized to stannic chloride. Since Reaction (1) is accompanied by the reaction

$$As^{3+} + 3H_2O \rightleftarrows AsO_3^{3-} + 6H^+, \quad (2)$$

the acidity must be increased to suppress formation of AsO_3^{3-} ions.

We studied the quantitative relationship between precipitation of elemental arsenic and acidity of the leaching solution.

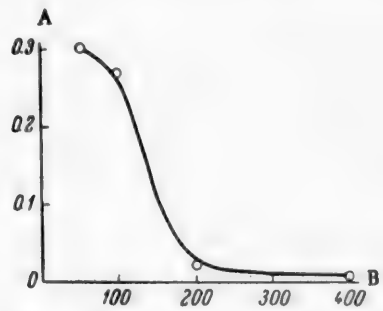

Fig. 3. Effect of acid content of the leaching solution on precipitation of elemental arsenic: A) As concentration (g/liter); B) HCl concentration (g/liter).

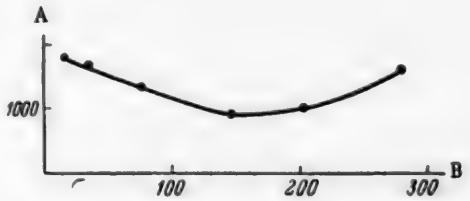

Fig. 4. Effect of ferrous chloride concentration on the solubility of stannous chloride: A) $SnCl_2$ concentration (g/liter); B) $FeCl_2$ concentration (g/liter).

The experiments were performed at 20°. The stannous chloride content of the solutions was 50 g/liter. The acid contents of the solutions were 50, 100, 300 and 400 g HCl per liter. Arsenic was added to these solutions to give a concentration of 0.3 g per liter. When equilibrium had been established, the arsenic and tin contents were determined.

The results of these experiments are given in Fig. 3.

It follows from Fig. 3 that an acid content of 410 g HCl per liter is not enough for complete precipitation of arsenic. The amount of arsenic remaining in solution is 0.0096 g As per liter, or 3.19% of the amount of As added. On decrease of the hydrochloric acid concentration to 205 g/liter the amount of arsenic in solution increases to 0.0206 g/liter, or 6.84% of the amount added.

Decrease of the acid content to 100 g/liter weakens the reaction considerably; 90% of the added arsenic remains in solution.

When the acid content is 50 g HCl per liter, there is virtually no reduction of arsenious chloride to the element by stannous chloride.

Study of the effect of ferrous chloride on the solubility of stannous chloride. Experiments on the solubility of stannous chloride were carried out at 20°.

Solutions containing from 15 to 300 g of ferrous chloride per liter and 20 g of hydrochloric acid per liter were prepared. Stannous chloride was added in excess to these solutions.

At equilibrium, which was reached in 12 hours, the iron and tin contents of the solutions were determined.

The results of these experiments are given in Fig. 4.

Fig. 4 shows that in presence of 16 g of ferrous chloride per liter the solution contains 1150 g of stannous chloride per liter. On increase of the ferrous chloride concentration to 148 g/liter the solubility of stannous chloride falls to 984 g/liter. On further increase of the ferrous chloride concentration the solubility of stannous chloride begins to rise, and reaches 1118 g $SnCl_2$ per liter when the $FeCl_2$ concentration is 281 g/liter. The existence of a minimum and the subsequent ascent of the curve can be attributed to formation of complex compounds between the ferrous and stannous chlorides. It follows that the presence of over 148 g of ferrous chloride per liter should assist dissolution of stannous chloride. However, if stannous chloride crystallizes from solution, an excess of ferrous chloride should be avoided, as at ratios of $FeCl_2 : SnCl_2 \geq 15 : 100$ ferrous chloride would crystallize out first.

SUMMARY

1. In a study of the behavior of lead, arsenious, and ferrous chlorides in presence of stannous chloride solutions it was found that the solubility of lead chloride increases when the stannous chloride content of the solution is raised above 38.5 g/liter. Accordingly, to prevent dissolution of considerable amounts of lead, the stannous chloride content of the solution during leaching of the sublimate should not exceed 200 g/liter.

2. Increase of the acid content to 410 g HCl per liter is not enough to prevent dissolution of arsenic. It follows that increase of the acidity of the leaching liquor cannot in practice be used as a means of preventing passage of arsenic from the chloride condensate into solution. Ferrous chloride is mainly dissolved during the leaching process. The presence of over 138 g of ferrous chloride per liter in the solution favors more complete dissolution of stannous chloride. When stannous chloride crystallizes out, ferrous chloride is precipitated with it. The stannous chloride crystals are therefore contaminated with iron.

LITERATURE CITED

[1] D. M. Chizhikov and G. S. Frents, The Chloride Method for Conversion of Tin Ores and Concentrates [In Russian] (1941).

[2] D. M. Chizhikov and B. Ya. Tratsevitskaya, Bull. Acad. Sci. USSR, Div. Tech. Sci. 12 (1947).

[3] Volkov, Trans. Inst. Phys.-Chem. Analysis, 3.

[4] I. A. Korshunov and Z. V. Kresnyakova, J. Gen. Chem. 22, 11, 1962 (1950).

[5] D. M. Chizhikov and A. S. Shakhov, J. Phys. Chem. 8, 4 (1936).

[6] G. Shoiher, Wiener Monatshefte 42, 411 (1921).

Received April 12, 1958

SUBLIMATION OF ZINC SULFIDE

D. B. Averbukh, E. A. Vetrenko
and G. I. Chufarov

This paper contains data on the sublimation of zinc sulfide under vacuum and in a reducing atmosphere.

EXPERIMENTAL

Starting material and method of investigation. The starting material was zinc sulfide prepared by the action of hydrogen sulfide on zinc oxide (reactive, chemically-pure grade) at 850°. The sulfide contained 65.7% zinc and 32.4% sulfur by chemical analysis.

The experiments were performed in a vacuum apparatus with gas circulation, the gaseous reaction products being frozen in a trap immersed in liquid nitrogen. The rate of sublimation of zinc sulfide under vacuum was estimated from the weight loss of the original sample per unit time. The sublimation rate in presence of carbon monoxide and hydrogen was found from the difference between the weight loss of the original sample and the amount of carbonyl sulfide or hydrogen sulfide formed.

RESULTS AND DISCUSSION

Sublimation of zinc sulfide was studied over the 900-1200° temperature range. In experiments in presence of carbon monoxide or hydrogen, the initial gas pressure was maintained in the range of 50-500 mm.

The results of a series of experiments performed under vacuum at 10^{-4} mm are given in Table 1. The degree of volatilization of zinc sulfide, expressed as the % weight loss relative to the original weight of the sample, is given in this table.

The condensate contained zinc sulfide only. Dissociation products of the sulfide were not detected.

Table 2 contains the results of a series of experiments on volatilization of zinc sulfide in an atmosphere of carbon monoxide at 1100°. The table gives the amount of volatilized sulfide, found from the weight loss, and the amount of reduced sulfide calculated from the volume of carbonyl sulfide formed. The difference between these two values is equal to the amount of sulfide sublimed. All the results are given as percentages on the initial weight of sulfide.

TABLE 1

Volatilization of Zinc Sulfide Under Vacuum

Temperature (°C)	Duration of expt. (hours)	Degree of volatilization (%)
900	1	22.89
925	1	32.63
950	1	56.86
975	1	78.05
1000	0.5	63.78

The experiments showed that two processes take place in a reducing medium—sublimation and reduction of sulfide. Their rates are additive, and together they constitute the observed total rate of volatilization. Table 2 shows that the rate of sublimation decreases with increasing carbon monoxide pressure, whereas the reverse is true of the rate of reduction.

The pressure in the system has a very strong influence on the total volatilization rate of zinc sulfide. Thus, whereas 1 g of zinc sulfide was 100% volatilized in 1 hour under high vacuum, under a carbon monoxide pressure of 5 mm it was only 52% volatilized. This is of great practical significance in vacuum distillation of sulfides.

TABLE 2

Volatilization of Zinc Sulfide in Carbon Monoxide at 1100°

Initial CO pressure (mm)	Duration of experiment (hours)	Rate of (% of original sample)		
		volatilization, total	reduction	sublimation
50	5	82.5	16.5	66.0
250	1	14.5	10.5	4.0
250	2.5	32.02	23.6	8.42
250	5.5	65.12	38.5	26.62
250	9.0	97.78	59.8	37.98
500	5.0	56.6	43.2	13.40

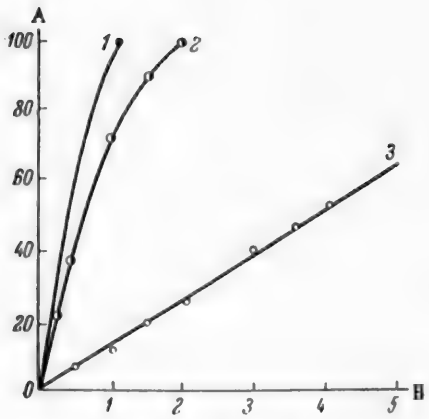

Fig. 1. Comparison of the volatilization rates of ZnS under vacuum and in presence of carbon monoxide and hydrogen at 1100° and initial H_2 or CO pressures of 500 mm: A) degree of volatilization (%); B) time from start of experiment (hours); 1) vacuum; 2) H_2; 3) CO.

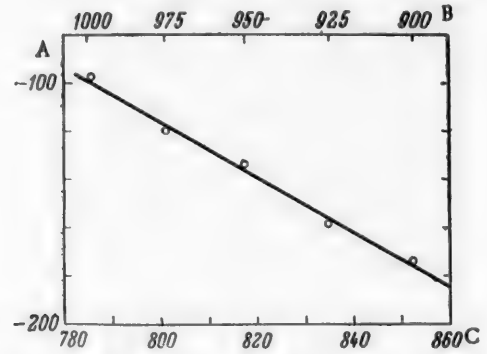

Fig. 2. Effect of temperature on the saturated vapor pressure of ZnS: A) values of $(\log P) \cdot 10^2$; B) temperature (°C), C) values of $(1/T) \cdot 10^6$.

The sublimation rate of zinc sulfide is considerably higher in a hydrogen atmosphere than in carbon monoxide.

The volatilization rates of zinc sulfide at 1100° under vacuum, in hydrogen, and in carbon monoxide are compared in Fig. 1. It follows from Fig. 1 that zinc sulfide volatilizes at the highest rate under vacuum. Thus, for a given time (1 hour), the degree of volatilization is 100% under vacuum, 72% in hydrogen, and only 14% in carbon monoxide.

The experimental results show that both the reduction rate and the sublimation rate are higher in hydrogen than in carbon monoxide. The increase of the sublimation rate is due to the higher rate of diffusion of sulfide molecules from the solid surface into the gas.

In all the experiments the sublimation rate remained constant for a long time, although the amount of solid phase decreased. This shows that a saturated vapor is formed over the surface of the finely-divided sulfide.

As is known, the rate of volatilization depends on the saturated vapor pressure, but in presence of a gaseous medium it also depends on the nature of the gas into which the volatilizing molecules diffuse.

According to the literature [1, 2], in the interdiffusion of gases the coefficient of diffusion in hydrogen is 4-5 times as great as in carbon monoxide. In our experiments the rate of volatilization of zinc sulfide at 1100° was likewise 4-5 times as high in hydrogen as in carbon monoxide.

TABLE 3

Saturated Vapor Pressure of Zinc Sulfide

Temperature (°C)	Saturated vapor pressure of ZnS (mm Hg)				
	our data	Pogorelyi [4]	Veselovskii [5]	McCabe [6]	Lumsden [7]
900	0.0181	0.081	0.0207 •	0.0578	0.0240
925	0.0261	–	–	–	–
950	0.0457	–	–	–	–
975	0.0637	–	0.123	–	–
1000	0.1052	0.328	–	0.520	0.188

•Corresponds to 892.9°.

The results of experiments on vacuum volatilization can be used to find the relationship between the ZnS saturated vapor pressure and temperature with the aid of the Langmuir equation [3]:

$$P = \frac{17.14m}{S\tau K}\sqrt{\frac{T}{M}}, \qquad (1)$$

where P is the saturated vapor pressure (mm Hg), m is the amount of substance volatilized (in g), S is the cross section of the condensation tube (in cm^2), τ is the time of volatilization (in seconds), K is Clausing's factor [3], T is the absolute temperature, and M is the molecular weight of the vapor.

Table 3 contains values for the saturated vapor pressure of ZnS calculated from our experimental data and from the results of other workers [4-7].

The values are of the same order of magnitude in all cases.

The results are plotted in $\log P - \frac{1}{T}$ coordinates in Fig. 2.

The relationship between the saturated vapor pressure and temperature is represented by the equation:

$$\lg P = -\frac{11\,300}{T} + 7.9 \text{ (mm Hg)}.$$

Hence the equation for the isobaric potential becomes

$$\Delta Z^\circ = 51\,600 - 22.8T,$$

which corresponds to the following values for the heat and entropy of sublimation:

$$\Delta H^\circ = 51\,600 \text{ cal/mole}, \quad \Delta S^\circ = 22.8 \text{ cal/degree} \cdot \text{mole}.$$

SUMMARY

1. In a study of the sublimation of zinc sulfide under vacuum and in presence of carbon monoxide and hydrogen at temperatures of 900-1200° it was found that in a reducing atmosphere two processes take place – sublimation and reduction; the sublimation rate of zinc sulfide is higher in hydrogen than in carbon monoxide, because of the greater rate of diffusion of the vapor molecules from the solid surface into the gas.

2. The volatilization rate of zinc sulfide under the investigated conditions was highest under vacuum.

3. The relationship between the saturated vapor pressure of ZnS and temperature is represented by the equation $\lg P = -\frac{11\,300}{T} + 7.9$.

LITERATURE CITED

[1] Technical Encyclopedia. Physcial, Chemical, and Technological Data [In Russian] (1931) p.247.

[2] V. A. Pazukhin and A. Ya. Fisher, Vacuum in Metallurgy [In Russian] (GONTI, Moscow, 1956) p.26.

[3] S. Dushman, Scientific Foundations of Vacuum Technique (IL, Moscow, 1950) p. 23, 82 [Russian translation].

[4] A. D. Pogorelyi, J. Phys. Chem. 22, 731 (1948).

[5] B. K. Veselovskii, J. Appl. Chem. 15, 422 (1942).

[6] McCabe, J. of Metals, 6, 9, 969 (1954).

[7] J. Lumsden, Discussions Faraday Soc. 4, 239 (1948).

Received April 7, 1958

DETERMINATION OF THE AMOUNTS OF COMMON SALT IN HEAPS

E. I. Akhumov and L. A. Bakk

The preceding paper [1] dealt with natural losses of Baskunchak salt during storage in heaps. The present paper is concerned with the important practical question of the determination of the amount G of evaporated or rock salt stored in a heap:

$$G = \delta V, \tag{1}$$

where V is the volume of the heap and δ is the average bulk density of common salt.

The problem in this form reduces to determination of heap volume from measurement data and estimation of the most probable average bulk density of salt of different degrees of subdivision in the heap.

Measurement of the Heap

Common salt is stacked in heaps of various sizes and shapes, in accordance with the area and configuration of the available space, the amount of salt unloaded, and nature of the conveying devices, but usually the heaps are in the shape of an obelisk—a section of height h, of a four-sided pyramid cut off by a horizontal plane, based on a rectangle of width a and length b; the dimensions of the top surface are a_1 and b_1 respectively (Fig. 1). The slope of the heap sides is determined by the natural angle of rest (φ), which depends on the type of salt (evaporated, rock, etc.), its fineness, granulometric composition, and mosture content when the heap is made. In the case of ground salt φ increases with particle size and moisture content of the salt. For Baskunchak salt φ varies between 40 and 50°. For dry salt of moderate fineness φ is close to 45° [2, 3]. For given values of a, b, and h the angle φ determines the dimensions of the top surface of the obelisk (Fig. 2):

$$\left.\begin{aligned} a_1 &= a - \frac{2h}{\tan\varphi} \\ b_1 &= b - \frac{2h}{\tan\varphi} \end{aligned}\right\} \tag{2}$$

The volume of the heap is found from the formula for the volume of an obelisk:

$$V = \frac{h}{6}[ab + (a + a_1)(b + b_1) + a_1 b_1]. \tag{3}$$

In practice, the base (a and b) and top (a_1 and b_1) of the heap are carefully measured and the dimensions of the side faces l_a and l_b are found for different cross sections; the results are used for calculating the heights of the heap in these sections (Fig. 2):

$$\left.\begin{aligned} h &= \sqrt{l_a^2 - \left(\frac{b - b_1}{2}\right)^2} \\ h &= \sqrt{l_b^2 - \left(\frac{a - a_1}{2}\right)^2} \end{aligned}\right\} \tag{4}$$

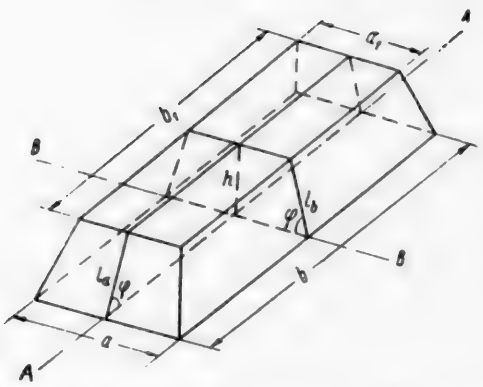

Fig. 1. Shape and dimensions of the heap.

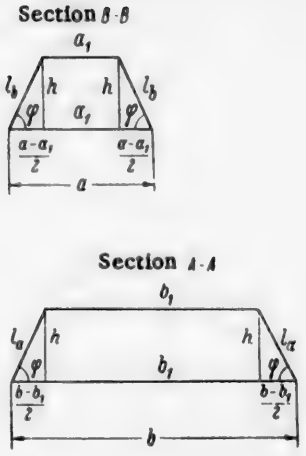

Fig. 2. Cross section of the heap.

The arithmetic mean of these heights is taken for the calculations. If the heap contains dents or air pockets, their volume is subtracted from the volume of the heap calculated by Equation (3).

Bulk Density of Common Salt

The bulk density of common salt was determined by Lüning and Hautag [4], Drukker and Gakichko [5], and Telentyuk [6], and of other salts by Pestov [2]. They found that the bulk density of a salt is a complex function of a number of factors, of which the most important are the fineness and granulometric composition of the salt, its moisture content, and the pressure of the top layer in the heap.

We shall consider the influence of each of these factors and the empirical relationships established by Akhumov, in relation to evaporated and rock salt.

Granulometric composition (size distribution). Observations have shown [6, 2] that the larger the individual crystals in the whole salt mass, the higher is its bulk density. At the limit, when the crystals are very large, the bulk density of the salt is equal to its specific gravity. The dependence of bulk density δ_r on crystal size r is represented by the general equation

$$\delta_r = \frac{K_r \cdot (r - r_0) \cdot d}{1 + (r - r_0) \cdot K_r}, \tag{5}$$

where r_0 is the linear size of the smallest possible salt crystal, d is its density, and K_r is a constant.

Since $r \gg r_0$, Equation (5) may be written in the form

$$\frac{1}{\delta_r} = \frac{1}{d} + \frac{1}{K_r \cdot d \cdot r}. \tag{6}$$

Equation (6) shows that a linear relationship exists between the reciprocals of the bulk density and crystal size.

If the size distribution of the salt particles is known, the average linear dimensions of the crystals in the mixture can be found from the formula

$$r = \frac{100}{\sum_{i=1}^{i=n} \frac{x_i}{r_i}}, \tag{7}$$

where r_i and x_i are the average linear size of the crystals in a given fraction and the content of this fraction (in wt. %) in the mixture, and n is the number of such fractions [7].

TABLE 1

Effect of Size Distribution on the Bulk Density of Baskunchak Salt [6]

Samples	W (wt. %)	Contents x_i (in wt. %) of fractions of particle size r_i (mm)						$\sum \frac{x_i}{r_i}$	r (in mm)	$\frac{1}{r}$	δ_r, (tons/m³)	$\frac{1}{\delta_r}$
		<0.5	0.5–1	1–2	2–3	3–5	>5					
Grinding No. 1:												
"golubaya granatka"	0.30	49.6	43.6	6.0	0.6	0.2	—	260.8	0.38	2.61	1.18	0.847
"novosadka"	0.133	23.4	57.8	18.4	0.4	—	—	183.1	0.55	1.83	1.20	0.833
"mechanical grain"	0.207	36.0	56.4	7.4	0.2	—	—	224.2	0.45	2.24	1.17	0.855
Grinding No. 2												
"novosadka"	0.12	9.2	21.2	52.4	15.2	2.0	—	108.6	0.92	1.09	1.23	0.813
"mechanical grain"	0.093	6.0	14.0	44.0	28.6	7.0	0.4	85.3	1.17	0.85	1.30	0.769
Grinding No. 3												
"golubaya granatka"	0.23	2.8	8.4	20.4	31.2	33.6	3.6	57.6	1.74	0.58	1.27	0.787
"novosadka"	0.17	5.0	10.8	25.8	36.0	21.6	0.8	71.6	1.40	0.72	1.27	0.787
"mechanical grain"	0.13	3.0	8.0	16.4	24.9	40.2	3.0	56.0	1.79	0.56	1.28	0.781

Table 1 contains Telentyuk's data [6] for the bulk densities of Baskunchak salt of different grindings and of approximately constant moisture content (from 0.1 to 0.3%); these results confirm the relationship represented by Equation (6).

Moisture content. It has been shown experimentally [2] that the bulk density δ_W of any salt decreases with its moisture content W. Telentyuk's data [6] for Baskunchak salt of No. 1 grinding, presented in Table 2, illustrate the nature of this variation.

The relationship between the bulk density and moisture content of a salt is represented by the equation

$$\delta_W = \frac{\delta_0}{1 + K_W \delta_0 \cdot W}, \qquad (8)$$

where δ_0 is the bulk density of the salt with zero moisture content (W = 0), and K_W is a constant.

Equation (8) may be written in the form

$$\frac{1}{\delta_W} = \frac{1}{\delta_0} + K_W \cdot W; \qquad (9)$$

it follows that a linear relationship exists between the reciprocal bulk density and the moisture content of the salt.

The data in Table 2 confirm the validity of Equation (9).

Pressure. The pressure of the overlying layer packs the salt down, especially during prolonged storage in the heap, thereby increasing its bulk density.

The relationship between the bulk density δ_h of the salt and the height h of the layer above it in the heap is represented by the equation

$$\delta_h = \frac{\delta_0}{1 - K_h \cdot \delta_0 \cdot h}, \qquad (10)$$

where δ_0 is the bulk density of the salt on the surface of the heap (h = 0), and K_h is a constant.

Equation (10) may be written in the form

$$\frac{1}{\delta_h} = \frac{1}{\delta_0} - K_h \cdot h. \qquad (11)$$

TABLE 2

Effect of Moisture Content on the Bulk Density of Baskunchak Salt [6]. No. 1 Grinding

W (wt. %)	δ_W (tons/m³)	$\frac{1}{\delta_W}$
0.02	1.21	0.83
0.5	1.18	0.85
0.8	1.18	0.85
1.25	1.13	0.88
2.5	1.11	0.90
3.04	1.09	0.92

Equation (11) is confirmed by Telentyuk's data for Artemovsk rock salt in Table 3.

The foregoing examples show how the individual influence of each of the determining factors on the bulk density of common salt can be taken into account. However, these considerations are valid only before the salt has caked, i.e, has become converted into a continuous solid mass as the result of complex physicochemical processes which occur under the continuous action of meteorological factors: atmospheric precipitation, action of air of different humidities, temperature, wind, and others. It should also be noted that these factors vary in the course of a day and more so over longer time intervals. As the result of caking, common salt stored in a heap has a somewhat higher bulk density than it would have if caking did not occur.

TABLE 3

Effect of the Pressure of the Overlying Layer on the Bulk Density of Artemovsk Rock Salt [6]. Moisture content 1.7%

h (in m)	Pressure (kg/cm²)	Duration of storage in heap (days)									
		1		6		20		53		110	
		δ_h (tons/m³)	$\frac{1}{\delta_h}$	δ_h (tons/m³)	$\frac{1}{\delta_h}$	δ_h (tons/m³)	$\frac{1}{\delta_h}$	δ_h (tons/m³)	$\frac{1}{\delta_h}$	δ_h (tons/m³)	$\frac{1}{\delta_h}$
1	0.135	1.142	0.876	1.163	0.860	1.173	0.853	1.175	0.851	1.193	0.838
2	0.27	1.161	0.861	1.169	0.855	1.178	0.849	1.181	0.847	1.193	0.838
3	0.54	1.161	0.860	1.186	0.843	1.197	0.835	1.209	0.827	1.229	0.814

To obtain the most reliable values for the average bulk density of caked common salt in a heap, it must be determined experimentally by the known method [2]; the samples must be taken from different parts of the heap, as the bulk density is different at different points in the heap.

The average bulk density of common salt is determined as follows from the heap measurements. When a known amount of salt has been piled in a heap, the heap is measured as exactly as possible as described above, and its volume is calculated by Equation (3). Equation (1) is then used to find the average bulk density δ_1 corresponding to the given heap volume V_1. After some time the salt contracts owing to mechanical and physicochemical causes, and the volume of the heap decreases to V_2. These results are used to find the average bulk density δ_2 of the caked salt by means of Equation (1):

$$\delta_2 = \delta_1 \frac{V_1}{V_2}. \qquad (12)$$

It should be noted that the bulk density of the salt in the heap then remains virtually unchanged after one year of storage for salt of No. 1 grinding, and after three years in the heap for salt of No. 2 and No. 3 grindings.

However, in practice this determination of the bulk density of the salt is complicated and sometimes impossible, and therefore purely empirical data must be used.

On the basis of numerous determinations performed over a number of years we may recommend the following empirical data for the average bulk density of common salt (evaporated and rock) in relation to its degree of grinding and state (caked or noncaked) (Table 4). It is evident from the data in Table 4 that the bulk densities of rock salt are somewhat higher than those of evaporated salt of the corresponding degrees of grinding. Experience has shown that these empirical data (Table 4)are in good agreement with the true bulk densities both of evaporated and of rock salt stored in heaps.

TABLE 4

Empirical Data on the Average Bulk Density (in tons/m^3) of Common Salt Stored in Heaps

Salt	Grinding					
	No. 1		No. 2		No. 3	
	not caked	caked	not caked	caked	not caked	caked
Evaporated (lake) . .	1.18	1.23	1.23	1.28	1.28	1.42
Rock	1.20	1.25	1.25	1.31	1.30	1.46

There are exceptions, which depend both on climatic conditions and on the dimensions of the heap. Corrections must be applied in each individual case, with the use of the data in this paper as a guide.

LITERATURE CITED

[1] E. I. Akhumov, J. Appl. Chem. 30, 1246 (1957).*

[2] N. E. Pestov, Physicochemical Properties of Granular and Powdered Chemical Products [in Russian] (Izd. AN SSSR, 1947) p. 196.

[3] B. F. V'yunov, Trans. All-Union Salt Research Institute 1 (9), 72 (1954).

[4] O. Lüning and H. Hautag, Z. Untersuch. Nahrungs u. Genussmittel, 49, 1/2, 1 (1925).

[5] G. Drukker and S. Gakichko, Bull. Fish Ind. (Organ of the Supreme Council of the National Economy and People's Commissariat of Agriculture) 11, 35 (1925); Trans. Sci. Res. Inst. Fish Ind. 2, 52 (1927).

[6] E. S. Telentyuk, Bull Central Sci. Res. Salt Lab. GUSP, People's Commissariat of the Food Industry USSR, 2, 78 (1939).

[7] E. I. Akhumov and E. I. Nikolaeva, J. Appl. Chem. 27, 48 (1954).*

Received October 2, 1958

*Original Russian pagination. See C. B. Translation.

THE USE OF SULFURIC ACID FOR REGENERATION OF CATION-EXCHANGER BEDS IN THOROUGH DEMINERALIZATION OF WATER

V. P. Meleshko, O. V. Chervinskaya,
N. S. Anpilova, and R. I. Zolotareva

The Voronezh State University and the Voronezh
Radio Component Factory

This paper contains the results of a study of the regeneration conditions of cation-exchanger beds in an industrial unit for thorough demineralization of water. These investigations were necessary because the available literature data refer mainly to incomplete demineralization of water, in which some residual hardness is permitted in the treated water [1]. Moreover, the theory of this problem is not discussed adequately in the literature.

The following methods for regeneration of the cation exchanger were studied: by means of dilute sulfuric acid solutions (0.3-0.4 N), by means of stronger sulfuric acid with additions of sodium hexametaphosphate (HMP), and double regeneration—displacement of the calcium by means of sodium chloride, followed by treatment of the resin with sulfuric acid.

Regeneration of the Cation Exchanger by Dilute Sulfuric Acid

Solutions of sulfuric or hydrochloric acid are used for regeneration of cation-exchanger beds in demineralization of water. The latter acid is the preferable reagent. It does not form sparingly-soluble compounds with the calcium ions displaced from the resin. It may be used in the form of 1-2 N solutions, which are the most advantageous from the point of view of chemical and water consumption. Nevertheless, the use of hydrochloric acid is undesirable. This is because of difficulties in conveying, volatility, and the low percentage content of hydrogen chloride in the concentrated acid.

Sulfuric acid is free from these disadvantages. However, it must be used under conditions which exclude clogging of the bed with calcium sulfate. Generally 0.3-0.4 N solutions of sulfuric acid are used in water treatment. Although these concentrations are higher than 0.016 N, which is the concentration corresponding to the solubility products of $CaSO_4$, such solutions are nevertheless not very effective desorbents for strongly acidic cation exchangers. Moreover, more water is consumed in their preparation. The time needed for treatment of the resin is also greater. It is possible to use 0.3-0.4 N H_2SO_4 solution because of the ability of $CaSO_4$ to form supersaturated solutions which can exist for some time. This time determines the applicability conditions of sulfuric acid.

The following experiments were performed in order to determine the effect of the contents of $Ca^{"}$ and $SO_4^{"}$ ions on the time of existence of these supersaturated solutions. Equal volumes (10 ml each) of $CaCl_2$ and H_2SO_4 solutions at concentrations from 0.1 to 1.0 N were mixed, and the course of precipitation was observed• (Table 1).

• It is evident that because of the different conditions the time of existence of supersaturated solutions determined by this method corresponds only approximately to the time of their existence in the resin bed.

TABLE 1

Time of Existence of Supersaturated Solutions in Relation to the Concentrations of $CaCl_2$ and H_2SO_4

Concentration of $Ca^{\cdot\cdot}$ and $SO_4^{\cdot\cdot}$ ions (meq/ml)	Ionic product $IP = [Ca^{\cdot\cdot}] \times [SO_4^{\cdot\cdot}]$	Observed effect
0.1	0.003	Slight precipitate after 20 hours
0.2	0.010	Solution turbid after 20 minutes
0.3	0.023	Solution turbid after 10 minutes
0.4	0.040	Instantaneous precipitation

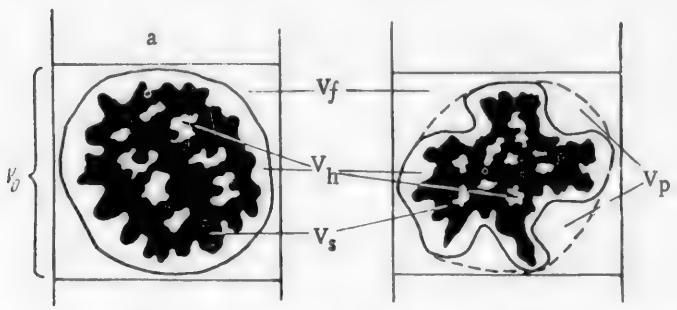

Fig. 1. Schematic representation of the filtering layer in a cation-exchange column: a) with rigid resin particles of ideally streamlined form; b) with porous resin.

It follows from the table that the Ca resin can be regenerated by sulfuric acid if the product of the molar concentrations of the precipitate-forming ions ($IP = [Ca^{\cdot\cdot}][SO_4^{\cdot\cdot}]$) is not greater than 0.023, and if portions of solution with this value of the IP do not remain in the resin bed for more than 10-15 minutes.

We used the consecutive-layer method [2-4] to calculate the maximum concentration of calcium ions in the resin bed during regeneration by sulfuric acid. It was assumed that the particles of cation-exchange resins (KU-1, SBS, sulfonated coal) are of irregular shape and have numerous cracks and pores both on the surface and throughout their volume. The distribution of liquid and solid phases in a filtering layer in relation to porosity may be represented in simplified form as shown in Fig. 1. Here a represents a column with ideally streamlined particles; b, a column with a porous resin. In case a, the total volume V_0 of the filtering layer is the sum of the volume V_s of the solid phase, the volume V_h of water hydrating the polar groups, and the so-called free-flowing volume V_f between the resin grains. With a porous sorbent (b) the total volume of the layer includes the volume V_p of the resin pores filled with the solution. The exchanging ions move along the column with the liquid flowing through the volume V_f, whereas the solution in V_p is retained by forces of capillary attraction. The redistribution of ions between V_f and V_p is similar to the redistribution of substance between the motile and stationary solvents in partition chromatography. Therefore in ion-exchanger beds the regenerating solution becomes diluted with the water remaining in V_p after the resin has become loosened.

In calculations relating to beds with porous resin we assume that the processes occur in the following sequence. As an elementary volume of the regenerating solution (v_e) enters an elementary layer of the bed (v_0), the solution concentrations in v_e and v_p, i.e., in the pore liquid of the elementary layer of the resin (v_s), become equalized. Simultaneously, ion exchange takes place between v_s and the aggregate volume $v_e + v_p$. The volume v_e then pass to the lower elementary layers, where the process is repeated in the same sequence.

We then use the balance equations (1a) and (1b), the ion-exchange isotherm (2) and the conditions of exchange equivalence (3) and (4):*

$$gS^{H}_{i,n} + v_n C^{H}_{i,n} + v_e C^{H}_{i,n} = gS^{H}_{i,n-1} + v_p C^{H}_{i,n-1} + v_e C^{H}_{i-1,n}, \tag{1a}$$

$$gS^{Ca}_{i,n} + v_p C^{Ca}_{i,n} + v_e C^{Ca}_{i,n} = gS^{Ca}_{i,n-1} + v_p C^{Ca}_{i,n-1} + v_e C^{H}_{i-1,n}, \tag{1b}$$

$$\frac{S^{H}_{i,n}}{S^{Ca}_{i,n}} = K \frac{C^{H}_{i,n}}{C^{Ca}_{i,n}}, \tag{2}$$

$$(v_p + v_e) C^{H}_{i,n} + (v_p + v_e) C^{Ca}_{i,n} = v_p (C^{H}_{i,n-1} + C^{Ca}_{i,n-1}) + v_e (C^{H}_{i-1,n} + C^{Ca}_{i-1,n}), \tag{3}$$

$$S^{H}_{i,n} + S^{Ca}_{i,n} = S^0, \tag{4}$$

and find the basic calculation formula

$$C^{Ca}_{i,n} = -\frac{1}{2(v_p + v_e)}\left(\frac{K}{1-K} M - N + \frac{S^0}{1-K}\right) \pm$$

$$\pm \sqrt{\left[\frac{1}{2(v_p + v_e)}\left(\frac{K}{1-K} M - N + \frac{S^0}{1-K}\right)\right]^2 + \frac{K}{1-K} \cdot \frac{1}{(v_p + v_e)^2} \cdot M \cdot N}, \tag{5}$$

where

$$M = [v_p (C^{H}_{i,n-1} + C^{Ca}_{i,n-1}) + v_e (C^{H}_{i-1,n} + C^{Ca}_{i-1,n})],$$

$$N = (v_p C^{Ca}_{i,n-1} + v_e C^{Ca}_{i-1,n} + gS^{Ca}_{i,n-1}].$$

When K < 1 there is a plus sign before the root, and when K > 1, the sign is minus.

It is easy to see that for columns with nonporous resins Equation (5) is simplified, as $v_p = 0$.

Equation (5) was used to calculate the course of variation in the concentrations of Ca^{++} and SO_4^{--} ions in the filtering layers during regeneration of nonporous and porous resins. It was assumed that the acid is 0.3, 0.5, and 1.0 N in the former case, and 1 N in the latter. The calculations were based on experimental data for KU-1 resin: the exchange constant K = 0.45 was calculated from Equation (2); V_f per gram of the air-dry resin was 0.95 ml; V_p was 0.62 ml/g, and the exchange capacity of the resin S^0 = 1.7 meq/g. The initial values were $C^{Ca}_{i,0} = C^{H}_{i,0} = C^{Ca}_{0,n} = 0$. The resin weight (g) in an elementary layer was taken as unity. The other associated values were: $v_p = 0.62$, $v_e = 0.95$, $S^{Ca}_{i,0} = S^0 = 1.7$ and $S^{H}_{i,0} = 0$. In the interaction of the resin with 0.3, 0.5, and 1.0 N acid solutions, $C^{H}_{0,n}$ was taken to be 0.3, 0.5, and 1.0, respectively.

Values of V_f were determined by measurement of the volume of liquid flowing out freely from the column. For determination of V_p a standard 0.5 N H_2SO_4 solution was passed through the column until the concentrations

* Here S^0 is the exchange capacity of the resin (in meq/ g); g is the weight of resin in the elementary layer (g); v_p is the volume of liquid in the pores of an elementary layer of resin (ml); v_e is the elementary volume of the regenerating solution, equal to the volume of liquid between the resin grains in the elementary layer (ml); $S^{H}_{i,n}$ and $S^{Ca}_{i,n}$ are, respectively, the hydrogen and calcium ion contents in the i-th elementary layer of resin after the passage of the n-th volume v_e through it (meq/g); $C^{H}_{i,n}$ and $C^{Ca}_{i,n}$ are the concentrations of H^+ and Ca^{++} ions in the n-th volumes v_p and v_e after the passage of the n-th volume v_e through the i-th layer (meq/ml).

of the eluate and the original solution became equal. The acid remaining in the bed was then rinsed out with water and titrated by alkali. The number of milliliters of 0.5 N acid in the wash water corresponded to $V_f + V_p$.

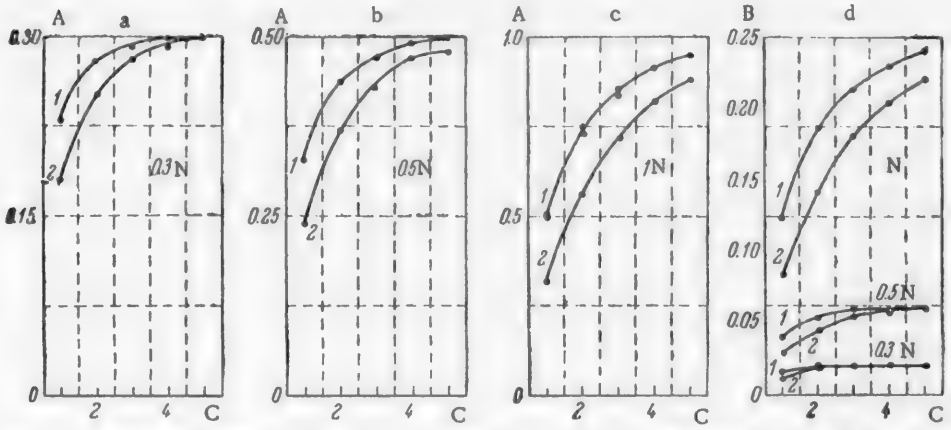

Fig. 2. Variations of the calcium-ion concentration (a,b,c) and IP (d) in the first and second elementary volumes of the regenerating solution: A) concentration of calcium ions (meq/ml); B) values of IP; C) number of consecutive elementary layers in the column; 0.3 N, 0.5 N, and 1 N are the acid normalities; the numbers on the curves are the numbers of the elementary volumes.

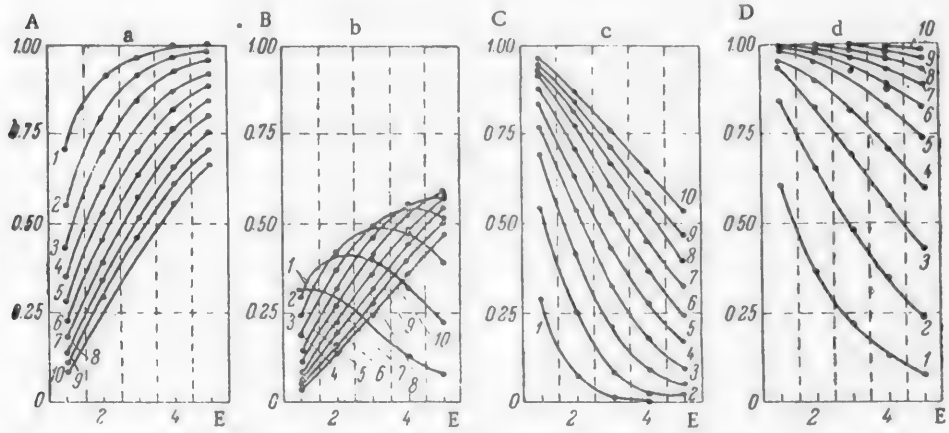

Fig. 3. Changes in the concentrations of the exchanging ions in the filtering layer of an ion-exchange column with passage of elementary volumes of regenerating solution through it: A) values of $\frac{S^{Ca}}{S^0}$, B) values of $\frac{C^{Ca}}{C^H_{0\,n}}$, C) values of $\frac{C^H}{C^H_{0,n}}$, D) values of $\frac{C^{SO''_4}}{C^H_{0,n}}$, E) numbers of consecutive elementary layers in the column; $C^H_{0,\,n}$ is the original concentration of the regenerating solution; the numbers on the curves are the numbers of the elementary volumes.

For a column with a nonporous resin it was sufficient to calculate the interaction of two elementary volumes of solution with five elementary layers in the column (Fig. 2). It was found that the concentration of $Ca^{\cdot\cdot}$ ions in the bed rapidly reaches a maximum value, equal to the initial acid concentration (Fig. 2, a, b, c). When the resin is treated with 0.3 N acid, IP does not exceed the maximum permissible value of 0.023 (Fig. 2, d). At higher acid concentrations IP exceeds the permissible maximum, even in the upper layers of the bed.

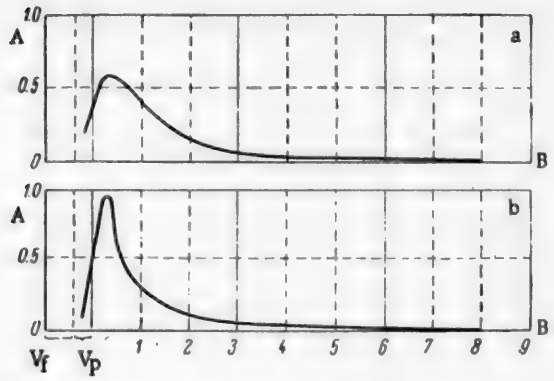

Fig. 4. Regeneration of Ca resin by 1 N acid: A) values of $C_{Ca}^{-}/C_{0,n}^{H}$, B) numbers of equivalent volumes of the regenerating solution.

Calculations relating to a column with a porous resin (Fig. 3) lead to the following conclusions. Dilution of the regenerating solution by the water contained in V_p slows down the extraction of calcium (Fig. 3, b) but it has little influence on the increase of $SO_4^{"}$ concentration (Fig. 3,d). The greatest dilution occurs in the first v_e. Its $Ca^{"}$ content decreases as it passes from the first to the succeeding layers. In the following v_e the $Ca^{"}$ concentration increases. However, its highest value is reached only at some distance from the top level of the resin. Therefore a solution with the maximum permissible IP flows through only a part of the bed, which is equivalent to a shorter residence time in the column. This is confirmed by theoretical and experimental curves (Fig. 4). The initial portion of Curve 4, a is plotted from calculated data (Fig.3,b). The second half of its descending portion is extrapolated from experimental data (Fig. 4,b, and Fig. 5). Curve 4,b was obtained for regeneration of a thick layer of resin (1500 mm) by 1 N HCl at a percolation rate of 3.3 m/hour. Fig. 4,b shows that the highest concentration of calcium in the eluate reaches 0.8-0.9 N, and that a solution of this concentration flows through about a half of the resin layer, contained in the lower part of the column.

Therefore with porous resins and especially with resins of low exchange capacity it is possible to use sulfuric acid solutions of somewhat higher concentrations than indicated in Table 1. This also explains why 0.4 N sulfuric acid solutions may be used in water-treatment practice.

Regeneration of Resin by Sulfuric Acid in Presence of Sodium Hexametaphosphate

Sodium hexametaphosphate raises the stability of supersaturated $CaSO_4$ solutions owing to formation of soluble $Na_2Ca_2P_6O_{18}$ or $Na_4CaP_6O_{18}$ complexes [5]. It follows that, if HMP is added to sulfuric acid, solutions of higher concentrations, up to 1 N, may be used for regeneration [6]. It must be taken into account that HMP gradually decomposes and is converted into orthophosphate. Its half life in 1 N H_2SO_4 in 28 hours [6].

Two series of experiments were carried out in order to determine the effects of H_2SO_4 concentration and of the amount of HMP added on the time of existence of supersaturated $CaSO_4$ solutions. The first series of experiments was analogous to those described above. In the second series the relative proportions of the $Ca^{"}$ and $SO_4^{"}$ contents were varied in such a way that IP remained constant. The sulfuric acid used in the experiments contained various amounts of HMP. It was found that either in absence of HMP or in presence of 25 mg of HMP per liter a precipitate was formed instantaneously at $Ca^{"}$ and $SO_4^{"}$ concentrations of 0.4 N. The time before formation of the precipitate increased with increasing contents of HMP, but not proportionately. At $Ca^{"}$ and $SO_4^{"}$ concentrations of 0.5 N and over, there were no noticeable differences in the stabilizing effects of HMP additions of 200-400 mg/liter.

The time of existence of supersaturated solutions is a function of IP, irrespectively of the absolute concentrations of the ions which give rise to this value. No precipitate is formed for 24-48 hours when the HMP content is 100 mg/liter and over and IP is 0.010-0.023. When the ionic product is 0.040-0.123 a precipitate is formed in a time which varies from several hours to 15 minutes. With further increase of IP the time before precipitate formation decreases sharply.

The following conclusions are drawn from the results of these experiments. If an H_2SO_4 solution containing 200-400 HMP per liter is passed through the column at a rate such that a given portion of it does not remain in the bed for more than 15 minutes, then 0.123 may be taken as a safe value of IP. This means that the total $Ca^{"} + SO_4^{"}$ ion concentration may be approximately 1.4 N (Fig. 6). It follows that Ca resins can be regenerated by means of 0.7-0.8 N H_2SO_4 solutions containing 200-400 ml of HMP per liter. If the resin layer is thin or the percolation rate high, the H_2SO_4 concentration may be raised still further. Thus, it follows from Fig.4,b that a

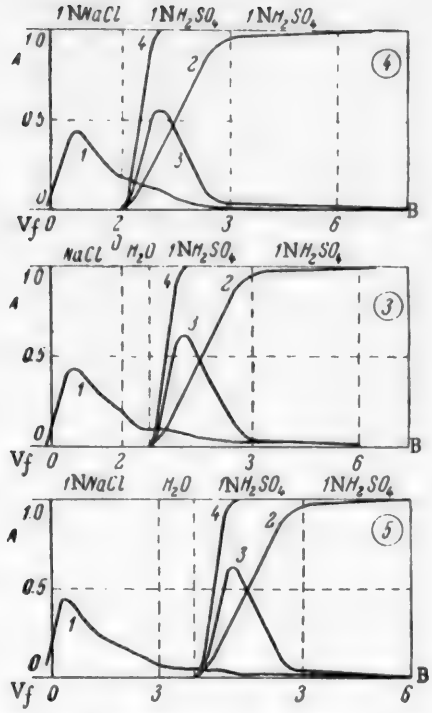

Fig. 5. Regeneration of Ca resin by 1 N NaCl and H_2SO_4 solutions: A) C/C_0, B) numbers of equivalent volumes of regenerating solution; 1) extraction of Ca ions, 2) amount of residual acid in eluate, 3) contents of sodium ions in eluate, 4) contents of sulfate ions in eluate; the numbers in the corners of the graphs correspond to the experiment numbers (Table 2).

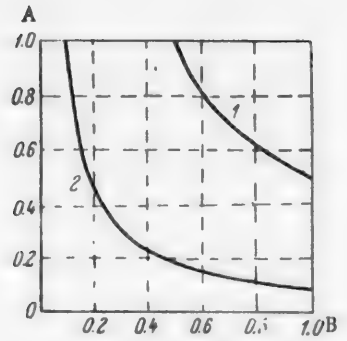

Fig. 6. Variations of IP with normalities of Ca^{++} (A) and SO_4^{--} (B) ions: values of IP: 1) > 0.123; 2) > 0.023.

solution in which the average Ca^{++} ion concentration is 0.8 N is in contact with not more than one half of the filtering layer. Then with a layer 1.0 m thick and at a percolation rate of 10 m/hour a solution with the maximum permissible IP is present in the column for about 3 minutes. This time is at the limit of precipitate formation from 0.9 N solutions of calcium chloride and sulfuric acid.

Double-Regeneration Method

There is hardly any information in the literature on consecutive regeneration of cation exchangers by means of NaCl and H_2SO_4 solutions. This type of regeneration essentially consists of removal of most of the calcium from the resin by NaCl solution, with subsequent displacement of sodium ions by H_2SO_4 solution [7]. The effectiveness of double regeneration was confirmed by three series of experiments. In the first series the resin was regenerated by 3 equivalent volumes* of 1 N NaCl, 3 equivalent volumes of 0.5 N H_2SO_4, and 3 equivalent volumes of 1 N H_2SO_4. The second series of experiments was concerned with the possibility of decreasing the amount of NaCl, and therefore 2 or 3 equivalent volumes of NaCl solution and 6 equivalent volumes of 1 N H_2SO_4 were taken. In the third series of experiments the possibility of repeated use (recycling) of H_2SO_4 solution was investigated. The resin was regenerated by 3 equivalent volumes of NaCl, 3 equivalent volumes of recycled acid, and 3 equivalent volumes of fresh H_2SO_4 solution. The results of these experiments are given in Table 2 and Fig. 5.

In each of these experiments 6 g of the resin was taken in the H form, put into the column, and saturated with 0.05 N $CaCl_2$ solution. Calcium was determined by means of Trilon B in the combined effluent and wash waters. The amount of calcium taken up by resin was found by difference. The regenerating solutions were passed through the column at a rate of 5 m/hour. Consecutive 2.5 ml samples of effluent were first analyzed. The total calcium content was determined in the last portion of effluent, corresponding to three equivalent volumes of acid. Curves 3 and 4 in Fig. 5 correspond to independent experiments. The increase of the SO_4^{--} concentration in the effluent was found by passing 1 N H_2SO_4 solution through the column with the resin in the H form, washed out with water. The curve for Na^+ extraction was determined during regeneration of the Na resin.

* The equivalent volume is the volume of solution containing dissolved electrolyte in an amount equivalent to the exchange capacity of the resin in the column.

TABLE 2

Results of Experiments on Double Regeneration of Ca Resin

Expt. No.	Calcium taken up (meq)	Calcium extracted (in meq) by solutions and water							Total Ca^{++} extracted (meq)	Amount of water for intermediate rinsing (ml)
		1 N NaCl		H_2O	0.5 N H_2SO_4	recycled H_2SO_4	1N. H_2SO_4			
		2 ev.	3 ev.		3 ev	3 ev	3 ev	3 ev		
1	9.37	—	7.95	0.23	0.78	—	0.35	—	9.31	6.5
2	9.27	—	7.78	0.37	0.82	—	0.36	—	9.33	6.5
3	9.48	6.17	—	0.78	—	—	1.72	0.73	9.40	6.5
4	9.23	6.31	—	—	—	—	2.39	0.50	9.20	0
5	8.82	—	7.53	0.17	—	—	1.03	0.21	8.94	6.5
6	8.82	—	7.63	0.04	—	—	0.89	0.36	8.92	10.0
7	9.98	—	7.93	0.39	—	0.84	0.45	—	9.64	10.0
8	9.68	—	8.24	0.44	—	0.36	0.36	—	9.60	10.0
9	9.88	—	8.12	0.46	—	0.76	0.48	—	9.82	10.0

Note. e.v. = equivalent volume

The use of 2 equivalent volumes of NaCl, even if the resin in subsequently washed out with water, does not prevent clogging with calcium sulfate when 1 N H_2SO_4 is used. If the resin is regenerated by 3 equivalent volumes of NaCl and then washed out with water, then the Ca^{++} ion concentration falls to a value such that a precipitate is not formed even when the SO_4^{--} concentration is 1 N.

DISCUSSION OF RESULTS

A laboratory unit was used for preparation of demineralized water, for determination of the water quality in relation to the method used to regenerate the resin. The second-stage exchanger columns were regenerated by 9 equivalent volumes of acid. Each column was regenerated 4 times during the tests. The specific resistance of the water obtained was $2-7 \cdot 10^6 \Omega \cdot cm$. Its quality did not deteriorate after introduction of newly regenerated columns into the cycle. The amount of water required to wash out excess acid did not increase in subsequent regenerations. This also confirmed that the resin was not clogged by calcium sulfate.

It follows that each of the regeneration methods considered above ensures the production of highly demineralized water. Therefore the choice of one of them depends on technological or economic advantages. The technological characteristics of each method are clear from the foregoing description. For an economic comparison, we calculated the costs of the chemicals required. It was found that the most expensive method is double regeneration, which moreover requires complicated equipment. However, its advantage is that it completely prevents clogging of the resin with calcium sulfate. The costs of regeneration by H_2SO_4 with added HMP and by 1 N hydrochloric acid (taken for comparison) are the same. The cost of reagents in regeneration by dilute H_2SO_4 is somewhat higher. The total costs in this process are increased still more because of the 3-fold increase of the amount of water required for making the solution. The technological process with the use of 0.3 N H_2SO_4 may be simplified if the concentrated acid is introduced into the water pipe by means of an injector. However, in that case the consumption of acid and water increases still further.

Costs may be lowered by repeated use of the regenerating solutions. The whole amount of solution used to treat the resin should be divided into 3 equal portions of 2-3 equivalent volumes each. In all the variants of regeneration by means of H_2SO_4 the first portion of effluent, containing most of the desorbed calcium, is discarded. If 0.3 N acid is used, and in double regeneration, the second portion of effluent should also be discarded, and only the last should be recycled. The second and third portions may be recycled if HMP is used. The technological process is then the same as in regeneration by means of hydrochloric acid [8]. Because of the tendency of HMP to decompose it is also necessary to adjust the recycled solution accordingly.

SUMMARY

1. An equation was derived for layer-by-layer calculations relating to the operation of a cation-exchange column, with dilution of the regenerating solution by the liquid in the resin pores taken into account; this equation shows that Ca resin may be regenerated by 0.3-0.4 N sulfuric acid solutions because of the ability of $CaSO_4$ to form supersaturated solution and also owing to dilution of the regenerating solution by water present in the resin pores.

2. In a study of the stabilizing action of sodium hexametaphosphate on mixed solutions of calcium chloride and sulfuric acid it was shown that in presence of 200-400 mg of hexametaphosphate per liter, Ca resin can be regenerated by 0.8-1.0 N H_2SO_4 solutions.

3. It is shown that clogging of the resin bed by calcium sulfate is prevented completely by double regeneration of Ca resin by consecutive treatment with 1 N NaCl and H_2SO_4 solutions.

LITERATURE CITED

[1] F. G. Prokhorov, Boiler Feed-Water Treatment by the H–Na Cation Exchange Method [in Russian] (Institute of Technical and Economic Information, Moscow, 1946) p. 14, 27.

[2] E. N. Gapon and T. B. Gapon, in the book: Chromatographic Method of Ion Separation [in Russian] (IL, Moscow, 1949) p. 9.

[3] V. V. Rachinskii, Proc. Acad. Sci. USSR 88, 883 (1953).

[4] V. P. Meleshko and V. B. Voitovich, Proc. Acad. Sci. USSR 102, 965 (1955).

[5] C. Calmon, in the book: Ion Exchange (IL, Moscow, 1951) p. 107 [Russian translation].

[6] A. B. Atterberry, Ind. Eng. Ch. 37, 100 (1945).

[7] R. Kunin and R. Myers, Ion Exchange Resins (IL, Moscow, 1952) p. 98 [Russian translation].

[8] V. P. Meleshko, Bull. Council of National Economy, Voronezh, 10-11, 42 (1958).

Received April 14, 1958

ADVANTAGES OF THE SUSPENSION POLYMERIZATION AND POLYCONDENSATION METHODS AND EQUIPMENT FOR PRODUCTION OF ION-EXCHANGE RESINS BY THESE METHODS*

F. T. Shostak, M. V. Vittikh and I. V. Samborskii

For many years we have been concerned with the production of ion-exchange resins by methods of suspension (pearl) polymerization and polycondensation. As the result of these investigations, individual laws governing the formation of ion exchangers in pearl (spherical) form have been established and standard equipment has been proposed for production of ion exchangers of good sorptional properties and narrow fractional composition. The production of ion exchangers by suspension polymerization and condensation has attracted the attention of both Soviet and foreign workers.

Ion-exchange polymers are now made predominantly by methods of suspension polymerization. However, resins of the condensation type are made almost exclusively by methods of block condensation (the American IR-4B anion exchanger, the German Wofatits, the Soviet resins AN-1, KU-1, etc.). This situation is caused by differences in the properties of the original monomers used.

In the production of polymerization ion-exchange resins the starting substances are insoluble or sparingly soluble in water or aqueous salt solutions. Therefore water may be successfully used as the medium for suspension polymerization. On the other hand, the starting materials in the production of condensation ion-exchange resins are generally soluble in water. Therefore water cannot be used in practice as the dispersion medium. The use of hydrophobic organic liquids for this purpose involves considerable difficulties (necessity for complete removal of the nonsolvent, difficulties in size classification, cracking of the granules on wetting, the "covering effect," etc.).

These questions have been considered little in the literature, and then only in relation to suspension polymerization. There are no literature data on the production of ion exchangers by suspension polycondensation. The only exceptions are a few patents [1].

Conditions for preparation of both polymerization and condensation ion-exchange resins have been worked out in our laboratory. The present authors and other co-workers have obtained the following ion exchangers in globular form by means of suspension condensation: the cation exchangers KU-1G, KU-20, KU-5MG; the anion exchangers AN-2FG, AN-9G, AV-16, ÉDÉ-10P. Suspension polymerization was used in the production of KB-4PA and SG-1 cation exchangers, AV-15 anion exchangers, and many others.

Characteristic Features of Ion Exchangers Made by the Suspension Method

In the suspension method the resin particles are obtained in the form of globules (beads) of regular shape and the required size during the hardening stage; in block polymerization or polycondensation the resin hardens in the form of relatively large blocks which are then broken up by crushing equipment. It is obvious that particles of resins made by block polymerization are of irregular shapes. Ion exchangers in globular (bead) form have a number of advantages over these [2].

* Communication I in the series on preparation of ion-exchange resins by suspension polymerization and polycondensation methods.

1. Spherical particles are packed more uniformly and closely in the column. This, on the one hand, somewhat increases the capacity of the column and, on the other, decreases the possibility of channeling in the resin layer. It is known that channeling greatly lowers the efficiency of ion-exchange columns.

2. Spherical particles are less subject to abrasion. Decrease of abrasion lengthens the service life of the resin and diminishes the amount of dust formed.

3. Spherical particles are less subject to disintegration. Granules made by crushing contain cracks and internal stresses (caused by the action of the crushing equipment) and therefore they disintegrate more readily in use.

4. The presence of considerable amounts of dust and fines, found when crushed resin is used, may increase the resistance of the column and cause channeling.

5. Resins made by suspension polymerization (or polycondensation) usually have better chemical and physical properties, as local overheating of the reaction mass which occurs during block polymerization is avoided in their production.

6. As a rule, resins made by the suspension method are not subjected to the very long heat treatment required in the block method.

7. Resin particles in bead form are more convenient for use in mixed beds and in beds used for continuous operation.

8. Resins in bead form differ from crushed resins classified on the same sieves in having a narrower size range owing to the absence of needle-shaped particles.

It should also be noted that the suspension method of resin production is more convenient and simple. If this method is adopted there is no need for drying equipment often of very complex design (such as the so-called "cross condenser" in the production of KU-1 resin), or for crushing and grinding equipment. In some cases sifting, which is inevitable in the production of resins by block condensation, may be eliminated. The amount of waste dust is appreciably diminished.

Because of these reasons, and because of the use of the recommended standard equipment, the method of suspension polymerization is more economical for this purpose.

Among the special features of the suspension method is the need to obtain the final product of a definite and narrow size range. The grain size of different ion-exchange resins in the USSR varies in the 0.3-2.0 mm range. In the United States of America the usual commercial brands intended for use in ion-exchange columns are generally made in granule sizes from 16-20 to 50-60 mesh (~1.0−0.25 mm) [3].

The efficiency of the resin decreases if larger granules are used. Because the diffusion process is lengthened, the flow rate through the bed is lowered, and this has a very appreciable influence on output.

The bed resistance increases if finer granules are used. If the range of granule size is wide the sorptional capacity is incompletely utilized and there is excessive consumption of regenerating materials.

The granule sizes indicated above are most commonly used for water treatment. Resins of other particle sizes are often needed for other purposes (isolation of individual metals, separation of radioactive decay products, analytical purposes). Therefore in development of methods of suspension polymerization it is necessary to allow for a wide range of particle sizes, each in predetermined narrow limits.

The equipment used for the process is significant in this respect [4].

Equipment. In principle, different types of equipment may be used for suspension polymerization or polymerization or polycondensation. However, even the earliest investigations showed that the design of the reactor is important in the production of ion exchangers. The most important parameters in this case are the size and shape of the reactor and the design of the stirrer.

There are two possible approaches to the design of equipment for the process: 1) a mixture of organic nonsolvents may be used with its density chosen to be close to the density of the condensation mass; the equipment demands become less stringent (stirrers of different designs may be used), but emulsifiers must be added and

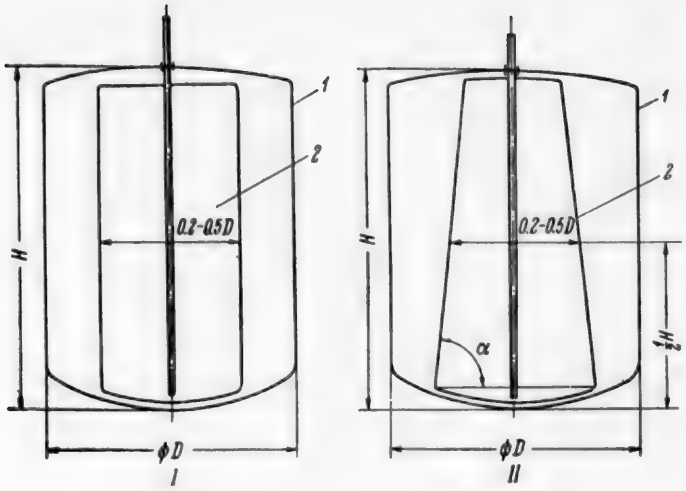

Sheet stirrer: 1) reactor; 2) stirrer.

TABLE 1

Particle Size Distribution of Ion-Exchanger Resins Made with the Use of Different Stirrers

Characteristics	Contents of fraction (%)		
	anchor stirrer, AN-2F	trapeziform sheet stirrer	
		AN-2F	KU-5M
Particle size (mm)			
up to 0.3*	5.5	0.9	3.95
0.3–0.5	8.6	7.5	11.6
0.5–1.0	79.3	78.8	80.65
1.0–1.3	3.2	9.0	3.8
1.3–2.0	2.6	3.8	0.0
over 2.0*	0.8	0.0	0.0
Mean granule diameter** (mm)	0.73	0.76	–
Heterogeneity coefficient**	2.55	1.94	–
Suitability coefficient**	93.70	99.10	–

*Wastes.

**The following terminology [5] is adopted: "mean diameter" is the aperture diameter of a screen through which 50% (by weight) of the granules passes; "heterogeneity coefficient" is the ratio of aperture diameters of a screen through which 80% of the granules passes and a screen through which 10% passes; "suitability coefficient" is the % content of particles corresponding to technical requirements with respect to size (from 0.3 to 2 mm).

mixtures of definite density have to be prepared; 2) a mineral oil, such as transformer oil, which has good stabilizing power and is chemically almost inert toward all condensation materials may be used.

The second approach is considered in the present communication.

Up to 1956 a stirrer of the anchor type and a cylindrical reactor were used in our laboratory for suspension polymerization and condensation processes. The shape of the reactor was determined by its height–diameter ratio. This ratio was usually in the range of 5:1 to 4:1. This type of reactor was developed for reactions of

suspension polymerization. These reactors were used for the production of KU-2, KB-4 and other ion exchangers. The disadvantages of this design became apparent in the transition from laboratory to pilot-scale tests, and especially in the planning of a granulator (reactor) of the industrial type.

TABLE 2

Effect of Granulator Height (Trapeziform Sheet Stirrer) on Size Distribution

Characteristics	Contents of fractions (%) at height–diameter ratio	
	3:1	1.5:1
Particle size (mm)		
up to 0.3	0.9	0.5
0.3–0.5	7.5	3.0
0.5–1.0	78.8	89.4
1.0–1.3	9.0	2.7
1.3–2.0	3.8	3.4
over 2.0	0.0	1.0
Mean granule diameter	0.76	0.77
Heterogeneity coefficient	1.94	1.74
Suitability coefficient	99.10	98.5

In development work on production of new types of cation exchangers (KU-5M, KU-20) by suspension polycondensation, carried out in 1956, the adopted reactor design proved unsuitable in practice: the resin particles were irregularly shaped with large variations in individual grain size; the formulation used in block polycondensation proved unacceptable; the reaction mass settled on the bottom of the reactor.

Work on improvement of the reactor design was initiated in order to eliminate these defects. A new design of stirrer and reactor was developed as a result. The proposed stirrer was in the shape of a rectangular (I) or trapeziform (II) sheet (see diagram). In contrast to the type used previously, the reactor was of the standard type generally used in the chemical industry: it was cylindrical with an oval bottom, the ratio of height to diameter was about 1-2:1, while the ratio of the width of the stirrer sheet to the reactor diameter varied over a wide range, usually between 1:2 and 1:5.

Comparative efficiency trials were carried out on the previously recommended anchor stirrer, propeller and other types of stirrer, and our sheet stirrer. The sheet stirrer was found to give a narrower range of granule size than the anchor and especially the propeller type. This is illustrated by the results obtained in the production of KU-5M cation exchanger and AN-2F anion exchanger.

The amount of granules above the maximum size of 2 mm was 0.8% in AN-2F anion exchanger made in a 6-liter reactor with an anchor stirrer, 0.6% in a 6-liter reactor with a sheet stirrer, and 0.3% in a 50-liter reactor. The content of dust wastes (particles smaller than 0.3 mm in diameter) was, with the use of the sheet stirrer, 0.3-1.7% for AN-2F anion exchanger and 4.0% for KU-5M cation exchanger; with the anchor stirrer it was 5.5% for AN-2F and 15% for KU-5M.

The particle-size composition of products made under laboratory conditions with different types of stirrers is given in Table 1.

Table 1 shows that the particle-size composition is better if a sheet stirrer is used.

The difference between the efficiencies of these stirrers becomes more pronounced on the pilot-plant scale. With an anchor stirrer the linear velocities of the particles at the reactor periphery and at the shaft are different. Their concentrations in different regions of the reactor also differ (as found by visual observations). This explains the large deviations in the limiting particle sizes, the wide spread of size distribution, and the presence

of a considerable amount of waste (dust). It is evident that the difference between the particle velocities at the center of the reactor and the periphery increases with increase of reactor size, and the size distribution of the product therefore becomes less satisfactory. This forced designers to construct granulators of inconvenient design, difficult to put into practice: long reactors of small cross section, fitted with long unsupported stirrers.

However, even this did not provide a complete solution to the problem of obtaining products of uniform particle size. With the use of sheet stirrers virtually the same results are obtained with short as with tall reactors (Table 2).

When a sheet stirrer is used the linear velocities of individual granules differ little from each other. The sheet blades, which occupy almost the entire height of the reactor, throw the granules uniformly against the reactor walls along its entire height. This confers a uniform circular motion to the particles. With the use of a sheet stirrer the particles move almost entirely in the annular space between the stirrer edges and the reactor wall. This eliminates the sharp variations between the velocities of individual particles, characteristic of anchor and other types of stirrers. By means of this type of granulator it proved possible to obtain a product of acceptable size distribution without the need for screening.

A rectangular sheet stirrer is generally used. However, if the density of the mass appreciably exceeds the density of the medium and the mass tends to settle out on the bottom of the reactor, it is better to use a trapeziform rather than a rectangular stirrer. The stirrer angle (see diagram) depends on the difference between the densities of the reaction mass and dispersion medium, and to some extent on the size of the vortex formed by rotation of the stirrer in the nonsolvent. The angle decreases with increase of the density difference between the reaction mass and the nonsolvent.

The granule size can be varied to some extent by variations of the parameters of the sheet stirrer or of the ratio between reactor diameter and the width of the stirrer sheet. The granule size decreases with increasing width of the stirrer sheet or with decrease of the ratio between reactor diameter and stirrer width. This is because these changes increase the linear velocity of the granules.

The new reactor design was tested in the production of various types of ion exchangers (mainly KU-5M and AN-2F). The trials showed that this type of reactor is universally applicable, and can be used in practice for the production of any type of ion exchanger by the suspension method. This makes it possible to use the same plant for the production of different types of resins. This is very important, because different grades of resins are generally made in small lots, and the plant used for their production does not work to full capacity or else must be planned to a very low output, which is uneconomic. This is confirmed by foreign practice. For example, in the United States, the country with the most extensively developed ion-exchanger industry (the output is 5000-6000 tons per year[6]), a few factories produce dozens of different industrial types.

In the Soviet Union a separate plant of individual type is still planned for each new type of resin.

SUMMARY

Ion exchangers made in the form of globular particles by suspension polymerization or polycondensation are shown to be advantageous. A new granulator design has been worked out. This design gives products of a narrow particle-size range with a low percentage of wastes, and makes it possible to vary the globule size by changes of the stirrer parameters. This design can be used for the production of different types of ion exchangers. The question of standard equipment for the production of ion exchangers is thereby solved.

LITERATURE CITED

[1] Japanese Patent 6869 (1951); U. S. Patents 2518420 (1950); 2610170 (1952).

[2] H. Ohlinger, Polystyrol. Berlin, 104 (1955).

[3] G. Osborn. Synthetic Ion Exchanger, London, 15 (1955).

[4] W. Hohenstein and H. Mark, J. Polymer Sci. 1, 127 (1946); H. Ohlinger, Polystyrol (Berlin, 1955) p.105.

[5] I. E. Apel'tsin et al., Ion Exchangers and Their Applications [in Russian] (State Standards Press, 1949) p. 105.

[6] F. Nachod and J. Schubert, Ion Exchange Technology, N.Y. (1956).

Received April 11, 1959

DETERMINATION OF THE ISOTOPE COMPOSITION OF CERTAIN NATURAL SOURCES OF WATER

L. M. Yakimenko, É. D. Kuznets, M. A. Rabinovich, and M. A. Vitashkina

There have been numerous investigations of the isotope composition of hydrogen and oxygen in various waters.

Literature data on the contents of the heavy hydrogen isotope (deuterium) and heavy oxygen isotopes (O^{17} and O^{18}) vary considerably for different samples of natural waters. This can be attributed to a considerable extent to the great experimental difficulties in determining the true isotopic composition of natural waters.

In recent years interest in determinations of the isotopic composition of natural waters has increased in connection with the growing production of heavy water. Accordingly, a method of complete isotopic analysis has been developed and a number of samples of natural waters have been investigated.

Data on two water samples are presented below.

Samples were obtained for the investigation from the Moscow water supply (Mytishchi source), taken May 8, 1952, and from a mountain river in the Caucasus, taken March 15, 1952, during the spring floods.

The investigated samples were normalized against hydrogen free from deuterium, and the densities of the original samples were compared with the densities after normalization. A correction was introduced for changes in the isotopic composition of oxygen during normalization.

The densities of the samples were determined by the flotation method [1]. Fractionation of the hydrogen and oxygen isotopes during purification of the samples by distillation was taken into account. The error due to fractionation of the isotopes during distillation by the method used for purification is estimated at 0.1 γ •

The isotopic composition of the hydrogen in the test sample was normalized by means of the isotope-exchange reaction between water vapor and deuterium-free hydrogen:

$$HDO + H_2 \rightleftarrows H_2O + HD. \quad (1)$$

Deuterium-free hydrogen was made in an apparatus consisting of one electrolysis stage and a cascade of ten isotope exchange stages [2]. The electrolysis cell was fed with natural water. The electrolytic hydrogen passed through the cascade of isotope-exchange stages, and the liquid formed after combustion entered the cascade countercurrent to the hydrogen. Before the combustion burner 5-10% of hydrogen containing not more than 0.05 γ of deuterium was collected for normalization of the sample. The normalization was effected by a continous process in a unit of thirteen consecutive isotope-exchange stages in presence of oxygen-free nickel catalyst.

A block diagram of the unit is shown in Fig. 1, and details are represented in Fig. 2.

Each isotope-exchange stage consisted of a contact apparatus 1, the lower portion of which served as the evaporator 2, and a condenser 3. The catalyst 4 was placed on the grid 5 in the contact apparatus. All the

• $\gamma = 1 \cdot 10^{-6}$ g/cc.

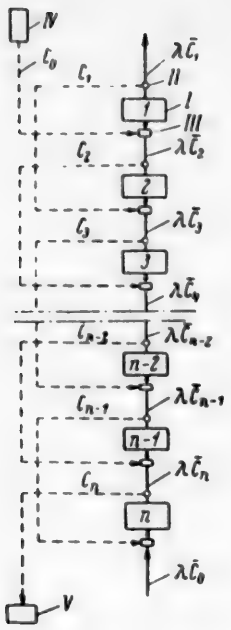

Fig. 1. Block diagram of unit: I) contact apparatus; II) condenser; III) evaporator; IV) header; V) receiver for normalized liquid.

contact reactors of the unit together with their evaporators were contained in an aluminum block 6 fitted with an electric heater 7 and thermal insulation 8.

Deuterium-free hydrogen passed through the flow meter 9 into the silica gel columns 10 cooled by water, and passed consecutively through all the isotope-exchange stages. After the first stage the hydrogen enriched with deuterium was discarded.

The test sample of water was fed from the header flask 11 by means of the clip 12 and dropper 13. Water normalized against deuterium-free hydrogen was collected from the condenser of the thirteenth exchange stage in a receiving flask. The amount of Raney nickel catalyst used was in large excess, by a factor of 1.05, over the amount necessary to ensure approach to equilibrium at each of the exchange stages. A large margin was provided in the heat-transfer areas in the evaporator, the tubes of supply of hydrogen in the contact apparatus, and the condensers. Therefore the temperature in the contact apparatus was virtually the same as that of the aluminum block, which was kept constant at 400 ± 10°. Artesian water at 8° was used for cooling. The gases were cooled in the condenser to 9-10°.

Determination of The Principal Cascade Parameters

The following notation is used: C_0 and $\bar{C}_0$ are the deuterium concentrations in the original sample and in the deuterium-free hydrogen; C_n, C_{n-1}, . . . C_2, C_1 and $\bar{C}_n$, $\bar{C}_{n-1}$, . . . $\bar{C}_2$, $\bar{C}_1$ – are the deuterium concentrations in the condensate and hydrogen after a given exchange stage; α is the coefficient of distribution of deuterium between water and hydrogen after any isotope-exchange stage; λ is the ratio of the gas and vapor flow rates; β is the ratio of the deuterium concentrations in the hydrogen at the entry and exit of the last stage.

The deuterium balance for each stage is determined by the equation

$$\lambda\bar{C}_{i+1} + C_{i-1} = \lambda\bar{C}_i + C_i. \tag{2}$$

For low deuterium concentrations the distribution coefficient can be represented by the equation

$$\alpha = \frac{C_i}{\bar{C}_i}. \tag{3}$$

Since $\beta = \bar{C}_0/\bar{C}_n$, we have from Equation (3) for the last exchange stage

$$C_n = \bar{C}_0 \frac{\alpha}{\beta}. \tag{4}$$

From Equation (2), with Equation (4) taken into account, we can derive an equation for the change ΔC in the deuterium concentration in the liquid in its passage through the last (n-th) stage

$$\Delta C_n = \bar{C}_0 \lambda \left(\frac{1}{\beta} - 1\right). \tag{5}$$

For any stage, we also have

$$\Delta C_i = \lambda (\bar{C}_i - \bar{C}_{i+1}). \tag{6}$$

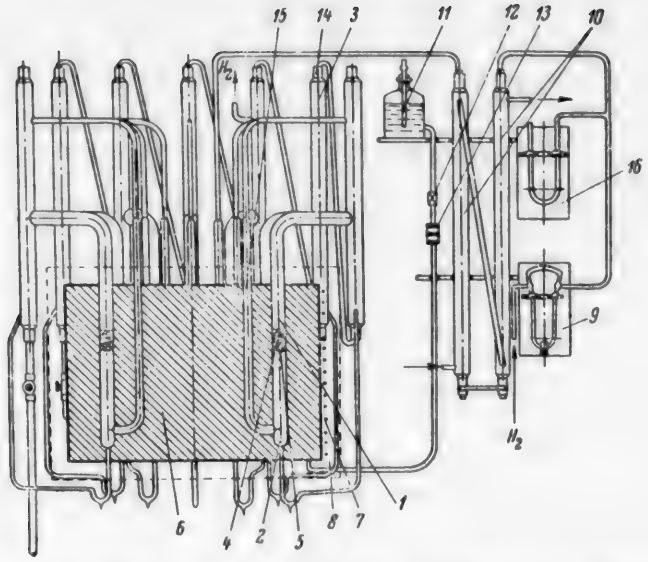

Fig. 2. General view of unit: 1) contact apparatus; 2) evaporator; 3) condenser; 4) catalyst; 5) grid; 6) aluminum block for temperature regulation; 7) electric heater; 8) heat insulation for block; 9) flow meter; 10) silica gel column; 11) header flask; 12) clip; 13) dropper; 14) condenser cooling tube; 15) tube for supply of hydrogen from the condenser to the contact apparatus of the previous stage; 16) manometer.

Since $C_i = C_{i+1} + \Delta C_{i+1}$, and correspondingly $\bar{C}_i = \bar{C}_{i+1} + \Delta C_{i+1}/\alpha$, we have from Equation (6)

$$\Delta C_i = \frac{\lambda}{\alpha} \Delta C_{i+1}. \tag{7}$$

From Equations (5) and (7) we obtain an expression for the change of the deuterium concentration in the liquid at any (i-th) stage of a cascade consisting of n stages

$$\Delta C_i = \bar{C}_0 \lambda \left(\frac{1}{\beta} - 1\right)\left(\frac{\lambda}{\alpha}\right)^{n-1}. \tag{8}$$

The deuterium concentration in a sample after normalization may be represented by the equation

$$C_n = C_0 - (\Delta C_n + \Delta C_{n-1} + \ldots + \Delta C_2 + \Delta C_1). \tag{9}$$

Substituting into Equation (9) values of ΔC_i from Equation (8), we have

$$C_n = C_0 - \bar{C}_0 \lambda \left(\frac{1}{\beta} - 1\right)\left[1 + \frac{\lambda}{\alpha} + \left(\frac{\lambda}{\alpha}\right)^2 + \ldots + \left(\frac{\lambda}{\alpha}\right)^{n-2} + \left(\frac{\lambda}{\alpha}\right)^{n-1}\right], \tag{10}$$

and hence

$$C_n = C_0 - \lambda_0 \bar{C}_0 \left(\frac{1}{\beta} - 1\right) \frac{\left(\frac{\lambda}{\alpha}\right)^n - 1}{\frac{\lambda}{\alpha} - 1}, \tag{11}$$

$$n = \frac{\log\left[\frac{\frac{C_0}{\bar{C}_0}\left(\frac{\lambda}{\alpha}-1\right)+\frac{\alpha}{\beta}-\lambda}{\lambda\left(\frac{1}{\beta}-1\right)}\right]}{\log\frac{\lambda}{\alpha}}. \quad (12)$$

The required number of stages in the isotope-exchange cascade is determined by the values of the coef - ficients α, λ and β. To reduce the number of exchange stages needed, in view of the increasing role of fractionation of oxygen isotopes in the cascade with increase of λ, the following values were taken for the coefficients: $\alpha = 1.6$, $\lambda = 3.0$ and $\beta = 0.8$.

For $C_0 = 16\ \gamma$ and $\bar{C}_0 = 0.05\ \gamma$ the number of stages needed is about 10, and the deuterium concentration in the liquid after normalization is $0.1\ \gamma$. In view of the fact that there is some degree of irregularity in the gas and vapor flow rates, 13 exchange stages were used.

To ensure that $\alpha = 1.6$, the isotope exchange was effected at 400°.

Fractionation of Oxygen Isotopes

Because of incomplete condensation of water vapor, oxygen isotopes undergo fractionation in the condensers of the isotope-exchange stages. The condensate becomes richer and the uncondensed water vapor poorer in heavy oxygen isotopes.

The following notation is used: C_i', C_i'', C_i''' are the concentrations of heavy oxygen isotope in the water vapor entering the condenser, in the condensate, and uncondensed vapor respectively at the i-th stage; a is the amount of uncondensed vapor (as % of the total inflow of liquid).

The equation for the material balance of the heavy oxygen isotope at any stage (Fig. 1) is

$$100C''_{i-1} + aC'''_{i+1} = (100 + a)\,C'_i = 100C''_i + aC'''_i. \quad (13)$$

The ratio between the concentrations C_i'' and C_i''' can be found from the modified Rayleigh equation:

$$\frac{C'''_i}{C''_i} = \left(\frac{100+a}{a}\right)^{1-\alpha} = K, \quad (14)$$

where α is the separation factor of oxygen isotopes in evaporation, determined from Equation (3):

$$\lg \alpha = \frac{a}{T} + b, \quad (15)$$

where a = 3.20, b = −0.0068.

For the last stage (n), which is entered by dry hydrogen, Equations (13) and (14) become

$$100C''_{n-1} = 100C'_n = (100 - a)\,C''_n + aC'''_n, \quad (13a)$$

$$\frac{C'''_n}{C''_n} = \left(\frac{100}{a}\right)^{1-\alpha} = K_n. \quad (14a)$$

Under the experimental conditions used, the change of the isotopic composition of oxygen in the sample tested, determined by means of Equation (13), (14), and (15), was $0.191\ \gamma$ at a final gas temperature of 5° in the condensers, and $0.196\ \gamma$ at 10°.

A correction of $0.2\ \gamma$ for the change in the isotope composition of the oxygen in the sample during normalization was subsequently applied to the analytical results.

Test of the unit. To test the general operation of the unit, experiments were performed on normalization of water with a high deuterium content. The deuterium concentration was 2.0% in the original liquid and 0.0075% in the hydrogen used for normalization; the block temperature was 400°, the hydrogen rate was 75 liters/hour and the liquid rate was 18-20 ml/hour. Intermediate sampling vessels were introduced after the condensers of stages 1, 3, 5, 7, 9, and 11. The samples were analyzed by the flotation method.

The stage-by-stage distribution of the deuterium concentration in the condensate is given in Table 1. Values calculated from Equation (11) are also given.

TABLE 1

Distribution of Deuterium Concentration in the Condensate

Expt. No.	Deuterium concentration (in $\% \cdot 10^{-3}$) at stages						
	1	3	5	7	9	11	13
1	997	273	84	44	10	14	14
2	1034	292	85	36	20	14	14
Calculated	1075	314.2	97.7	36.2	18.7	13.7	12.3

The actual distribution of the deuterium concentration in the liquid at different cascade stages is in satisfactory agreement with the calculated data.

After this, water samples were normalized against hydrogen free from deuterium.

Investigation of Moscow water samples. The results of the first series of experiments are given in Table 2. The mean deviations in individual determinations are also given. The liquid rate was 20 ml/hour, and the feed rate of deuterium-free hydrogen was 75 liters/hour, which corresponded to removal of 10% hydrogen from the apparatus for production of deuterium-free hydrogen.

TABLE 2

Results of the First Series of Experiments

Expt. No.	Number of determinations	$-\Delta d$ in comparison with standard (in γ)
3	5	15.8 ± 0.2
4	3	15.4 ± 0.1
5	2	15.5 ± 0.0
6	4	15.7 ± 0.3
7	2	15.6 ± 0.2
	Mean	15.6 ± 0.2

TABLE 3

Results of the Second Series of Experiments

Expt. No.	Number of determinations	$-\Delta d$ in comparison with standard (in γ)
8	6	15.4 ± 0.2
9	10	15.3 ± 0.3
10	8	15.6 ± 0.2
11	5	15.3 ± 0.1
12	3	15.5 ± 0.1
	Mean	15.4 ± 0.2

A sample of the same water before normalization was used as the reference standard.

In a second series of experiments the liquid and gas rates were halved and samples were taken. Each sample was analyzed several times.

The results of the second series of experiments are given in Table 3.

The average value of Δd for all the determinations is $-15.5 \pm 0.2\gamma$. With a correction of 0.2 γ for fractionation of heavy oxygen isotopes, and 0.1 γ for the residual deuterium content of the sample, the Moscow water contained 15.8 ± 0.2 γ of deuterium.

TABLE 4

Analytical Results for Water from a Caucasian Mountain River

Expt. No.	$-\Delta d$ in comparison with standard (γ)			
	standard – mountain-river water		standard – Moscow water	
	no. of determinations	results	no. of determinations	results
13	2	14.9 ± 0.1	4	15.5 ± 0.2
14	5	14.7 ± 0.1	5	15.0 ± 0.2
	Mean	14.7 ± 0.1	–	15.3 ± 0.2

Investigation of a sample of water from a Caucasian mountain river. The samples were normalized at a water rate of 10 ml/hour and $\lambda = 3$.

The densities of samples after normalization were compared with the density of the same water before normalization and of Moscow water.

The results are given in Table 4.

The true deuterium content of the mountain-river water, after corrections for the residual deuterium content in the normalized sample (0.1 γ) and for fractionation of oxygen isotopes (0.2 γ) is 15.0 ± 0.1 γ, which is lower than that of Moscow water by 0.8 γ.

The density difference between a normalized sample of mountain-river water and Moscow main water, with the same corrections applied, is 15.6 ± 0.2 γ. Comparison of this value with the difference of densities between normalized and ordinary Moscow water (15.8 ± 0.2 γ) leads to the conclusion that the isotope composition of oxygen in the two water samples differs by not more than 0.2 γ.

SUMMARY

1. A method and apparatus have been devised for continuous normalization of water samples against deuterium-free hydrogen.

2. Two samples of natural water were investigated. It was found that the deuterium content of Moscow main water (from the Mytishchi source) is 15.8 ± 0.2 γ, and that of water from a Caucasian mountain river during the flood period, 15.0 ± 0.2 γ.

3. The isotope composition of the oxygen in the samples differs by not more than 0.2 γ.

LITERATURE CITED

[1] A. I. Shatenshtein et al., Isotope Analysis of Water [in Russian] (Izd. AN SSSR, 1954).

[2] L. M. Yakimenko, A. I. Shatenshtein, M. A. Rabinovich, E. A. Yakovleva, and Z. M. Borisova, J. Inorg. Chem. 2, 2507 (1957).

[3] I. Kirschenbaum, Heavy Water (IL, 1953) [Russian translation).

Received August 16, 1957

DETERMINATION OF THE ISOTOPE COMPOSITION OF MOSCOW TOWN WATER

L. M. Yakimenko, M. A. Rabinovich,
M. A. Vitashkina, and E. D. Kuznets

The electrolytic method at constant electrolyte volume was used for determination of the deuterium content of a sample of Moscow town water (Mytishchi source) and for determination of differences in the contents of heavy oxygen isotopes in the oxygen of the atmosphere and water.

Isotope equilibrium between the water, fed into the electrolytic cell, and the electrolysis gases was attained by prolonged electrolysis without removal of fractions enriched with heavy hydrogen and oxygen isotopes.

EXPERIMENTAL

The true deuterium content of the sample and the correction for different contents of heavy oxygen isotopes in the water and atmospheric oxygen were determined by comparison of densities of water samples formed by combustion of hydrogen and oxygen from the electrolytic unit; the combustions were carried out in a number of variants, with standard hydrogen, deuterium-free hydrogen, atmospheric oxygen, and the two electrolytic gases together.

The apparatus is shown schematically in Fig. 1.

The water to be investigated was fed continuously from the header vessels 2 into the electrolyzer 1 consisting of four cells. The hydrogen and oxygen passed through the separating columns and pressure regulators 3, were cooled in the condensers 4, and passed through the isotope phase-exchange columns 5, sprayed with the water under investigation, to equalize the isotope composition of the hydrogen and oxygen in the water vapor carried over with the gas with the isotope composition of the sample under investigation. In this manner the unit could be operated without collection of the enriched fraction.

Gas samples passed through the precombustion columns 6, the condensers 7, the drying columns 8, and flow meters 9; after additional drying in the silica gel columns 10 they passed to the burners 11 for combustion. Liquid samples were collected in the receivers 12.

Calculations showed that under the experimental conditions used, the maximum error due to fractionation of hydrogen and oxygen isotopes during purification by means of catalysts did not exceed 0.08–0.10 γ.

To attain isotope equilibrium, the electrolysis was continued for a long time under constant conditions – volume of liquid in the electrolyzer, electrolyte temperature, load, and other characteristics.

The isotope composition of the liquid charged into the electrolyzer was close to equilibrium in order to shorten the time required to reach equilibrium.

In the first group of experiments the liquid in the system was completely changed twice in 24 hours, and the separation factor was maintained at the level of $\alpha = 4$ by suitable adjustment.

In the second group of experiments 0.33 of the total amount of liquid was changed in 24 hours and $\alpha = 6.5$.

The following notation is used: C_0, C, $\bar{C}$, C_p, $\bar{C}_p$ are the concentrations of the heavy hydrogen (or oxygen) isotope in the sample, in the electrolyte, and in the gas at a given instant and after isotope equilibrium has been established; V_0 and V are the volumes of the liquid in the unit and of the water decomposed by electrolysis; β is the degree of approach to equilibrium.

For electrolysis at constant volume, the material-balance equation may be written in the form

$$V_0 dC = C_0 dV - \frac{C}{\alpha} dV. \tag{1}$$

Rearrangement of Equation (1) and integration from 0 to V and from C_0 to C gives

$$\frac{V}{V_0} = \alpha \ln \frac{\alpha - 1}{\alpha - \frac{C}{C_0}}. \tag{2}$$

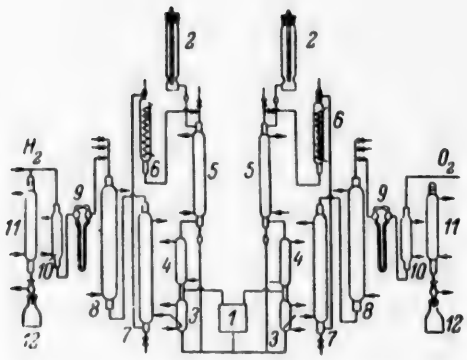

Fig. 1. Diagram of unit: 1) electrolyzer; 2) header vessels; 3) separating columns and pressure regulators; 4) condensers; 5) isotope phase-exchange columns; 6) precombustion columns; 7) condensers; 8) drying columns; 9) flow meters; 10) silica gel columns; 11) burners; 12) receivers.

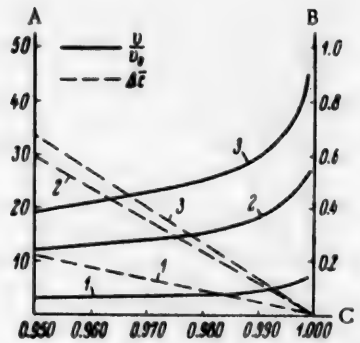

Fig. 2. Values of V/V_0 and $\Delta\bar{C}$ calculated from Equations (6) and (7): A) values of V/V_0 B) values of $\Delta\bar{C}$ (in γ); C) values of β; values of α: 1) 1.023, 2) 4, 3) 6.5.

Since $\epsilon = \alpha - 1$, we have

$$C_p = C_0 + \varepsilon C_0, \tag{3}$$

$$C = C_0 + \beta\varepsilon C_0, \tag{4}$$

$$\bar{C} = \frac{C_0 + \beta\varepsilon C_0}{\alpha}. \tag{5}$$

From Equations (2) and (4) we have

$$\frac{V}{V_0} = \alpha \ln \frac{1}{1 - \beta}. \tag{6}$$

The difference between the actual and equilibrium contents of the heavy isotopes in the gases is given by the equation:

$$\Delta\bar{C} = \bar{C}_p - \bar{C} = \frac{C_0 \varepsilon}{\alpha}(1-\beta). \qquad (7)$$

Values of V/V_0 and $\Delta\bar{C}$, calculated from Equations (6) and (7), are plotted in Fig. 2. The values α = 1.023 and C_0 = 200 γ are taken for the oxygen isotopes, and α = 4 or 6.5 (in accordance with the conditions of the first and second series of experiments respectively) and C_0 = 16 γ for the hydrogen isotopes.

The concentration of heavy isotopes in the gas differs by values not exceeding 0.1 γ for oxygen at $V/V_0 \approx$ $\approx$ 4, and for hydrogen at α = 4 and 6.5 at V/V_0 = 20 and 32 respectively.

TABLE 1

Results of Determinations of Density Differences Between P_5 Samples and the Standard

Apparatus No.	Expt. No.	Duration of expt. (days)	Number of determinations	$-\Delta d$ in comparison with standard (γ)
1	1	25	3	15.0 ± 0.4
	2	26	3	15.4 ± 0.1
	3	27	3	15.3 ± 0.1
	4	29	2	15.2 ± 0.1
2	5	45	4	15.8 ± 0.2
	6	47	4	16.0 ± 0.4
	7	48	4	15.3 ± 0.4
			Mean	15.4 ± 0.3

TABLE 2

Results of Experimental Determinations of P_1-P_2 and P_3-P_4

Apparatus No.	Expt. No.	Duration of expt. (days)	P_1-P_2		P_3-P_4	
			no. of determinations	Δd (in γ)	no. of determinations	Δd (in γ)
1	1	5	3	8.3	3	7.7
	2	10	4	8.4	–	–
	3	14	4	7.3	3	7.9
	4	23	3	8.0	3	8.0
	5	27	–	–	3	7.8
	6	29	3	8.1	–	–
	7	31	3	8.5	4	7.2
	8	34	3	7.5	3	8.0
2	9	45	–	–	4	8.1
	10	47	–	–	4	7.4
	11	50	–	–	2	7.8
			Mean	8.0	–	7.8

In the first group of experiments, isotope equilibrium was attained to within 0.1 γ after 2 days of oxygen and after 10 days for hydrogen. In the second group of experiments the times were 12 and 96 days respectively.

After oxygen isotope equilibrium had been established, the following combustion samples were taken: P_1, hydrogen from the system with air; P_2, hydrogen from the system with oxygen from the system; P_3, standard hydrogen with air; P_4, standard hydrogen with oxygen from the system; P_5, deuterium-free hydrogen with oxygen from the system.

Deuterium-free hydrogen was prepared in a special unit. Its deuterium content did not exceed 0.05 γ [1].

Excess oxygen was used in combustion of samples P_1-P_4, and excess hydrogen in combustion of sample P_5.

The fact that the densities of samples P_1, P_2, and P_4 remained constant with time indicated that oxygen and hydrogen isotope equilibrium had been reached. The comparison standard was the Moscow water used for feeding the system. Densities of the samples were determined by the flotation method [2].

Table 1 contains the results of determinations of the density differences between P_5 samples and the standard, which give the deuterium content of Moscow water, and the average deviations in individual determinations.

With a correction of 0.1 γ for incomplete oxygen isotope equilibrium, the deuterium content of the water is 15.5 ± 0.3 γ, which is in good agreement with the value obtained by another method (15.8 ± 0.2 γ) [3].

Table 2 contains values of P_1-P_2 and P_3-P_4, which represent differences in the contents of heavy oxygen isotopes in water and in the sample of Moscow water investigated. The value of P_3, from the results of repeated determinations, was taken as 1.3 ± 0.2 γ.

The average correction for the difference in the contents of heavy oxygen isotopes in air and in Moscow town water, with an allowance for incomplete oxygen isotope equilibrium in the electrolyzer, is 8.0 γ.

The value found [1] for the density of zero standard water free from deuterium and containing oxygen with the isotope composition of atmospheric oxygen (in comparison with the Moscow standard) was 7.3 γ.

The density of the water samples (sample P_5) free from deuterium and with oxygen of the same isotope composition as in Moscow water, obtained in our experiments, was 15.5 γ, in comparison with the same standard. The density difference 15.5 γ − 7.3 γ = 8.2 γ gives the correction for excess content of the heavy oxygen isotopes in air as compared with water; this is in good agreement with the above data.

SUMMARY

1. Isotope analysis of water from the Mytishchi source (Moscow town supply) was carried out by decomposition of the water with formation of hydrogen and oxygen of the same isotopic composition as in the original water.

2. The deuterium content of the water from the source was found to be 15.5 γ, and the correction for the difference in the contents of heavy oxygen isotopes in atmospheric oxygen and in the sample was 8.0 γ.

LITERATURE CITED

[1] L. M. Yakimenko, A. I. Shatenshtein, M. A. Rabinovich, E. A. Yakovleva, Z. M. Borisova, and E. N. Zvyagintseva, J. Inorg. Chem. 2, 2507 (1957).

[2] A. I. Shatenshtein et al., Isotope Analysis of Water [in Russian] (Izd. AN SSSR, 1954).

[3] L. M. Yakimenko, É. D. Kuznets, M. A. Rabinovich, and M. A. Vitashkina, J. Appl. Chem. 32, No. 6, 1244 (1959).*

Received August 16, 1957

*Original Russian pagination. See C. B. Translation.

RADIOMETRIC INVESTIGATION OF THE ADSORPTION OF CERTAIN IONS IN RELATION TO METAL CORROSION IN SALT SOLUTIONS

N. G. Chen

Adsorption of ions on the surface of a metal during corrosion has been studied little, although this problem is worthy of attention both from the theoretical and the practical aspects. Investigations of adsorption of ions in relation to metal corrosion in electrolyte solutions should shed light on the corrosive effects of certain salt ions.

We studied the corrosion of carbon steel in relation to the adsorption of ions on its surface. The degree of corrosion was determined by the well-known gravimetric method, and adsorption by means of radioactive isotopes. The radioactive tracers were the S^{35}, Ca^{45}, and P^{32} isotopes as the compounds $Na_2S^{35}O_4$, $Ca^{45}Cl_2$, $Na_3P^{32}O_4$ and $Na_2HP^{32}O_4$.

The experiments were conducted as follows. The calculated amount of the corresponding radioactive isotope was added to a solution of stable salt in distilled water, with a concentration of 5 g/liter. Experimental solutions of different concentrations were then prepared from this by dilution. The solution was poured into the experimental apparatus, the bottom of which was a detachable specimen of the steel 3 under investigation, 65 × 65 × 2 mm in size. The apparatus was heated electrically; during the experiment the specimen was in contact with the corrosive medium on the one side, and with the heater on the other, and at the end it was washed with tap water until its activity became constant (see diagram). The specimen was then dried, weighed on an analytical balance, and the activity of the surface which had been in contact with the boiling solution was determined. The corrosion products were then removed by treatment with inhibited hydrochloric acid, the specimen was washed, dried, and weighed again, and the weight of the corrosion products was found by difference.

After removal of the corrosion products the activity of the specimens never exceeded the background activity. Adsorption was calculated from the equation

$$\Gamma = \frac{A \cdot C \cdot 100}{B\,(P_2 - P_1)},$$

where Γ is the adsorption (%), A is the activity of the specimen (pulses/second), C is the concentration of the solution (mg/ml), B is the specific activity of the solution (pulses/ml·second), P_2 is the weight of the specimen with the layer of corrosion products (mg), and P_1 is the weight of the specimen after removal of the corrosion products (mg).

All the experiments were performed to an accuracy of 3.3% at pH = 9.

Before each experiment the specimen was cleaned thoroughly with emery and washed in alcohol.

The results of the experiments are given in Table 1, which presents the relationship between the amount of substance adsorbed and its concentration, i.e., $\Gamma = f(C)$.

It may be seen that positively charged ions (Ca^{2+}) are adsorbed by the metal surface during corrosion several times as rapidly as negatively charged ions (SO_4^{2-}); moreover, the corroding metal surface adsorbs both positive and negative ions from boiling electrolyte solutions. Our explanation of this fact is that iron has a negatively charged surface in electrolyte solutions [1], as the difference between the potential corresponding to the system iron–medium and the zero-charge potential is less than zero, i.e., $E - E_{q=0} < 0$.

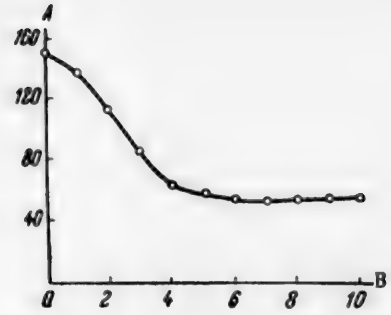

Variation of the activity of a specimen with the number of washings in water: A) activity (pulses/second), B) number of washings.

Therefore the double layer at the iron surface will contain mainly positive ions on the solution side. This means that the iron surface, which is negatively charged in electrolyte solutions, should adsorb mainly cations. However, the experiments show that adsorption of anions, in particular SO_4^{2-}, is also possible. This indicates that the surface of the corroding iron is heterogeneous in the electrical sense, i.e., the fact that both cations and anions are adsorbed indicates that both negative and positive charges are present.

In our opinion, the presence of positive charges on the surface of a corroding metal may be explained as follows: the iron surface becomes covered with corrosion products consisting of iron oxides and hydroxides; under certain conditions the latter release hydroxyl groups into the solution, and a positive charge results.

The adsorption of $Na_3P^{32}O_4$ and $Na_2HP^{32}O_4$ (Table 1) is of considerable interest, as both these substances are used as inhibitors of boiler corrosion. The experimental results show that sodium phosphates have very high adsorbability; they are adsorbed in much greater amounts than sodium sulfate and calcium chloride by the metal surface during corrosion (Table 1). The ions of these salts form the following series in order of decreasing adsorption: $PO_4^{3-} > HPO_4^{2-} > Ca^{2+} > SO_4^{2-}$; at higher concentration, the series is $HPO_4^{2-} > PO_4^{3-} > Ca^{2+} > SO_4^{2-}$.

TABLE 1

Adsorption of Ions on the Surface of a Corroding Metal

$Na_2S^{35}O_4$		$Ca^{45}Cl_2$		$Na_3P^{32}O_4$		$Na_2HP^{32}O_4$	
equilibrium concentration (g/liter)	adsorption (%)	equilibrium concentration (g/liter)	adsorption (%)	equilibrium concentration (g/liter)	adsorption (%)	equilibrium concentration (g/liter)	adsorption (%)
0.0752	7.41	0.0311	81.8	0.0030	150.0	0.0120	200
0.1147	22.2	0.1049	161.2	0.0047	638.0	0.0332	341.4
0.2347	12.2	0.2336	174.7	0.0312	747.0	0.0517	570.4
0.3668	25.0	0.5137	158.0	0.0565	644.4	0.1378	852.8
0.5862	38.0	0.8277	155.3	0.1241	750.0	0.2011	1200.0
0.7936	29.44	1.0734	183.8	0.4579	752.0	0.4104	1757.0
0.9195	37.2	2.5048	128.0	0.800	575.0	0.5155	1518.3
2.2060	38.7	3.1842	108.0	—	—	1.3319	1494.5
4.0920	32.1	5.000	145.4	—	—	2.500	1695.6

Effect of ion adsorption on metal corrosion. The effect of ion adsorption on metal corrosion was studied in relation to two factors: time and solution concentration. In the former case the experiments were carried out with distilled water and sodium sulfate solution at a concentration of 0.50 g/liter containing radioactive S^{35}; the durations of the experiments were 6, 12, 24, 48, and 72 hours. In the second series of experiments the duration was constant at 10 hours, while the solution concentrations were varied in the range of 0.025; 0.05; 0.1; 0.2; 0.4; 0.6; 0.8; 1; 2.5 and 5 g/liter. These experiments were carried out with solutions of Na_2SO_4, $CaCl_2$, Na_3PO_4 and Na_2HPO_4 containing the corresponding radioactive tracers (S^{35} and P^{32}).

The experimental data showing the effect of duration of the experiments on adsorption and corrosion are presented in Table 2.

It is clear from Table 2 that the corrosion rate of the metal falls with increased duration both in distilled water and in sodium sulfate solution; the rate of sulfate corrosion falls sharply in the region of increasing adsorption of SO_4^{2-} ions. Subsequently, the decreases of adsorption and of the corrosion rate are almost parallel. Sodium sulfate is the more corrosive medium; the corrosion rate in our experiments was roughly trebled in presence of the SO_4^{2-} ion as compared with distilled water. The fact that the corrosion rate is higher in Na_2SO_4

solutions indicates that adsorption of SO_4^{2-} must have an influence on corrosion of the metal. The adsorbed SO_4^{2-} anions may primarily influence the course of electrochemical processes.

In the present instance adsorption of SO_4^{2-} ions facilitates the anode process. This is possibly because the anions adsorbed on the surface of the corroding metal, being negatively charged, accelerate the passage of positively charged ions from the metal into solution, thereby intensifying the anode process. Our experiments support the theoretical views advanced earlier by Antropov [2] in this respect. Moreover, it follows from the experimental data that adsorption of anions, and in particular of SO_4^{2-}, in the 30-70% range does not inhibit corrosion either by electrophoretic shielding of the anodic regions, or by the shielding effect of the adsorbed SO_4^{2-} layer. Finally, the decrease of the corrosion rate with duration of the experiment is evidently due to the protective action of the layer of corrosion products formed on the metal. It should be noted that the positively charged Ca^{2+} ions are adsorbed to a much greater extent than SO_4^{2-} ions by the corroding metal surface. This is quite understandable, as the iron surface carries a negative charge [2] which cannot fail to favor cation adsorption, and the cations adsorbed on the metal surface should generally tend to retard corrosion for the following reasons: 1) the cation layer on the surface of the corroding metal, because of the same sign of its charge, prevents passage of iron ions through the double layer out of the metal into the solution, and ionization of the metal is therefore retarded [2, 3]; 2) the adsorbed cations, being positively charged, may retard corrosion under certain conditions by electrophoretic shielding of the cathodic regions [4]; 3) finally, the adsorption layer may have a shielding effect on the corrosion process.

In fact, our experiments show that there is less corrosion when calcium cations are adsorbed than in the adsorption of SO_4^{2-} anions (Table 3). However, if a large amount of anions is adsorbed the corrosion is greatly retarded; this is the case with sodium phosphates. Table 3 shows that the corrosion rates in phosphate solutions

TABLE 2

Effect of Duration of the Experiments on Adsorption and Corrosion

Duration of expt. (hours)	Distilled water	Na_2SO_4 solution		
	corrosion rate (k) in g/m² · hour	concentration (g/liter)	adsorption (%)	corrosion rate (k) in g/m² · · hour
6	0.4305	5.000	73.2	1.2777
12	0.3388	4.8614	99.8	0.5555
24	0.2256	4.8727	22.1	0.3645
48	0.1347	4.8727	41.3	0.2604
72	0.0995	4.5181	23.6	0.2314

are low in comparison with the rates in Na_2SO_4 and $CaCl_2$ solutions, and considerably lower than in distilled water; this indicates that sodium phosphates exert a protective action. However, the adsorption of Na_3PO_4 and Na_2HPO_4 is enormous, 20-30 times the adsorption of Na_2SO_4. There is no doubt that PO_4^{3-} and HPO_4^{2-} anions

TABLE 3

Effect of Ionic Concentrations on Corrosion Rate

Substance	Corrosion rate (in g/m² · hour) at solution concentrations (g/liter)										
	0	0.025	0.05	0.10	0.20	0.40	0.60	0.80	1.00	2.50	5.00
H_2O	0.3833	—	—	—	—	—	—	—	—	—	—
Na_2SO_4 . .	0.3833	0.4750	0.5417	0.8583	0.8333	0.6500	0.7083	0.6917	0.6917	0.6083	0.6250
$CaCl_2$ . . .	0.3833	0.3333	—	0.4167	0.3417	0.4167	0.4917	0.5167	0.4417	0.6500	0.6833
Na_3PO_4 . .	0.3833	0.2042	0.2583	0.2500	0.3083	0.3333	0.3083	0.2917	0.3250	0.2083	0.2833
Na_2HPO_4 .	0.3833	0.0833	0.1250	0.1667	0.1833	0.2083	0.2708	0.3250	0.2750	0.2830	0.3085

adsorbed in such large amounts must have a strong influence on the anode and cathode processes. This influence is probably due to: first, formation of a stable protective film consisting of the reaction products of phosphate ions and metal ions; second, to electrophoretic shielding of anodic regions on the metal surface; third, by acceleration of ionization of the metal by the action of the adsorbed anion layer, which accelerates the motion of positively charged particles.

Of these three factors, the predominant role in the present instance is played by the first two, and these determine the inhibiting action of sodium phosphates.

SUMMARY

1. The adsorption of SO_4^{2-}, PO_4^{3-}, HPO_4^{2-} and Ca^{2+} ions was studied, in relation to metal corrosion in boiling solutions containing these ions, by the radioactive-tracer methods; it was found that iron surfaces adsorb both positive and negative ions during corrosion in salt solutions. An explanation is put forward to account for the influence of ion adsorption on the course of adsorption.

2. Of the salts studied, the corrosion inhibitors Na_3PO_4 and Na_2HPO_4 are adsorbed to the greatest extent, and sodium sulfate, which has a strong corrosive effect, is adsorbed the least.

3. It was found that the ions form the following series in order of decreasing corrosiveness (a) and adsorbability (b):

$$SO_4^{2-} > Ca^{2+} > PO_4^{3-} > HPO_4^{2-}, \quad (a)$$

$$HPO_4^{2-} > PO_4^{3-} > Ca^{2+} > SO_4^{2-}. \quad (b)$$

LITERATURE CITED

[1] I. L. Rozenfel'd, Inhibitors of Corrosion in Neutral Media [in Russian] (Izd. AN SSSR, 1953).

[2] L. I. Antropov, Influence of Additives on Corrosion of Metals in Acid Media. Problems of Corrosion and Metal Protection [in Russian] (Izd. AN SSSR, 1956).

[3] V. A. Kuznetsov and Z. A. Iofa, J. Phys. Chem. 21, 2 (1947).

[4] L. K. Lepin', The Role of Colloidochemical Phenomena in Corrosion in Salt Solutions. Problems of Corrosion and Metal Protection [in Russian] (Izd. AN SSSR, 1956).

Received June 27, 1957

DETERMINATION OF THE SOLUTION-RATE CONSTANTS OF POWDERED CRYSTALS

A. B. Zdanovskii and N. A. Karazhanov

In kinetic studies of the dissolution of powdered crystals, some workers [1-4] restricted themselves to determinations of changes in solution composition with the time of dissolution, and others [5, 6] to determinations of the solution rates of small crystals of equal sizes.

The present paper contains a description of a method for determination of the solution-rate constants of powdered crystals, based on sieve-analysis data and variations of solution composition during dissolution of definite amounts of any fractions of a powdered material. This method is based in principle on a new variant of the relationship between sieve-analysis data, solution rates, and variations of solution composition during the dissolution process, considered in Zdanovskii's monograph [7].

Fig. 1 shows the general scheme of graphical constructions for determination of linear rates of solution. First, sieve-analysis data are used to plot the cumulative curve I showing the distribution of the amounts (M in % by weight) of fractions from 0 to a definite crystal size, l_{Σ}. Differential curves II are then plotted, showing the relative quantitative distribution $(dM/dl)_{\Delta l}$ of the fractions according to their initial linear dimensions l_0 for different decreases Δl of the linear dimensions of the crystals. The relative amounts of the fractions in Graph II are calculated from the equation

$$\left(\frac{dM}{dl}\right)_{\Delta l} = \left(\frac{dM}{dl}\right)_{l_0}\left(1 - 2\frac{\Delta l}{l_0}\right)^3, \tag{1}$$

where $(dM/dl)_{l_0}$ are the derivatives of M with respect to l when $\Delta l = 0$, determined from the cumulative curve.

To plot Graph III, the amounts M of salt at different Δl are found from the formula

$$M = \int_0^{l_{max}} \left(\frac{dM}{dl}\right)_{\Delta l} dl \tag{2}$$

by graphical (weight) determination of the areas of the curves of $(dM/dl)_{\Delta l}$ against l_0 in Graph II at Δl. Hence, Graph III represents variations of the amounts M of the salt for different decreases of the linear dimensions Δl of the crystals, irrespective of the properties or amount of solvent. The curvature of the lines depends only on the original particle sizes taken.*

Graphs IV and V, which respectively represent variations of the concentration C_x and amount M of the salt with the dissolution time τ, are plotted from experimental data.

The values of M are found from the following relationships:

* Curves 1 and 2 in Graphs III-V (Fig. 1) correspond to fine and coarse fractions respectively.

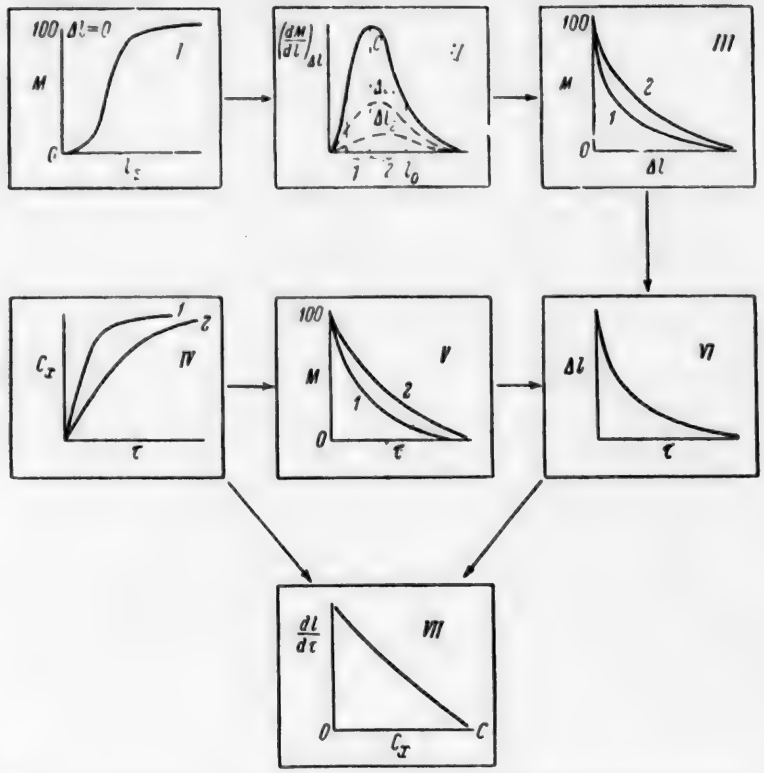

Fig. 1. Construction of graphs for determination of the linear rates of solution of powdered crystals; explanation in text.

$$M = 100\,\frac{G_x}{G_0}, \tag{3}$$

$$C_x = \frac{P_{x-1}C_{x-1} + 100\,(G_{x-1} - G_x)}{P_{x-1} + (G_{x-1} - G_x)}, \tag{4}$$

where G_0 is the initial weight of the crystals; G_{X-1} and G_X are the weights of the crystals and C_{X-1} and C_X are the solution concentrations at times τ_{X-1}, τ_X; P_{X-1} is the weight of original solution involved in the dissolution process (with the sample of solution previously withdrawn taken into account) in the time interval $\tau_X - \tau_{X-1}$.

It follows from Equation (4) that

$$G_x = G_{x-1} - \frac{G_x - C_{x-1}}{100 - C_x} P_{x-1}. \tag{5}$$

Graph VI, which represents the relationship between the decrease Δl of the linear crystal size and the dissolution time τ, is plotted from data of Graphs III and V for comparable values of M. Graph VI is used for finding the derivatives $dl/d\tau$ (linear dissolution rates) which, together with the results of Graph IV, give the final result (Graph VII) – the linear solution rates at different concentrations C_X. In practice, Graphs IV, V, and VII need not be plotted, and appropriate tabulated data may be used instead. The solution-rate constants (K_V) can be found from the linear rates ($dl/d\tau$) by means of the formula

$$\frac{dl}{d\tau} = \frac{K_v \cdot (C - C_x)}{\rho_s} \quad \text{or} \quad K_v = \frac{\rho_s}{C - C_x} \cdot \frac{dl}{d\tau}, \tag{6}$$

TABLE 1

Results of Sieve Analysis of Washed Kieserite

Fraction size (mm)	Amount of salt M (weight %)	
	in fraction	total
0.25	16.2	16.2
0.25–0.5	32.8	49.0
0.5 –0.1	40.1	89.1
1 –2	10.9	100.0

where ρ_s is the density of the solute crystals.

The method described above was used for determination of the solution-rate constants of native microcrystalline kieserite ($MgSO_4 \cdot H_2O$) in water and in its own solutions at various temperatures.

There are relatively few publications in the literature on the rate of solution of kieserite in water and in its own solutions. The first information on this subject was given by Krull [3], who studied the solution of contaminated kieserite samples in water at 25-90°. He obtained approximate results showing that the rate of solution increased rapidly with temperature. Fuller data are contained in Karsten's paper [6]. He dissolved small (< 1 mg) homogeneous kieserite crystals at various temperatures until they disappeared completely. The solution-rate coefficients calculated from his data alter by a factor of 10.5 in the 45-96° range. Zdanovskii's monograph [7] contains relative solution-rate constants for highly disperse synthetic kieserite; the values increased 30-fold in the 25-75° range. Theoretical analysis showed that the dissolution process is nondiffusional in character.

The purpose of the present experimental investigation was to demonstrate the new method for determination of solution rates and to obtain new and more accurate values of K_V for kieserite at various temperatures.

Before the experiments, native conglomerates of kieserite and halite (from the mine of the K. Marx and F. Angels works in East Germany) were crushed in a mortar. The liberated fine salt crystals were washed repeatedly with water (to a negative reaction for chloride) and rinsed with alcohol.

The results of sieve analysis of kieserite crystals washed free from halite are given in Table 1.

TABLE 2

Values of $(dM/dl)_{\Delta l}$, Calculated from Equation (1)

Δl (mm)	l_0 (mm)	$\left(\frac{dM}{dl}\right)_{l_0}$	$\left(\frac{dM}{dl}\right)_{\Delta l}$	Δl (mm)	l_0 (mm)	$\left(\frac{dM}{dl}\right)_{l_0}$	$\left(\frac{dM}{dl}\right)_{\Delta l}$
1/32	0.062	0.1	0	1/16	0.9	5.5	3.51
	0.2	6.7	2.18		1.0	4.0	2.68
	0.3	9.8	4.86	1/8	0.25	8.3	0
	0.4	13.2	7.93		0.3	9.8	0.05
	0.5	16.0	10.72		0.4	13.2	0.69
	0.6	16.5	11.86		0.5	16.0	2.00
	0.7	12.0	9.06		0.6	16.5	3.28
	0.8	8.0	6.27		0.75	9.8	2.92
	0.9	5.5	4.43		0.9	5.5	2.07
	1.0	4.0	3.29		1.0	4.0	1.69
1/16	0.125	2.65	0	1/4	0.5	16.0	0
	0.3	9.8	1.95		0.6	16.5	0.08
	0.4	13.2	4.29		0.7	12.0	0.28
	0.5	16.0	6.75		0.8	8.0	0.42
	0.6	16.5	8.19		0.9	5.5	0.48
	0.7	12.0	6.65		1.0	4.0	0.50
	0.8	8.0	4.80				

These data were used to find the derivatives $(dM/dl)_{l_0}$ for different linear dimensions l_0 of the crystals, shown in Fig. 2. Table 2 gives values of $(dM/dl)_{\Delta l}$, calculated from Equation (1) for different decreases in the linear crystal dimensions.

Subsequent graphical integration of the values of dM/dl with respect to l_0 (Fig. 2) gave the amounts M of kieserite crystals for different values of Δl for two fractions: these values were 0.25-0.5 mm and 0.5-1 mm.

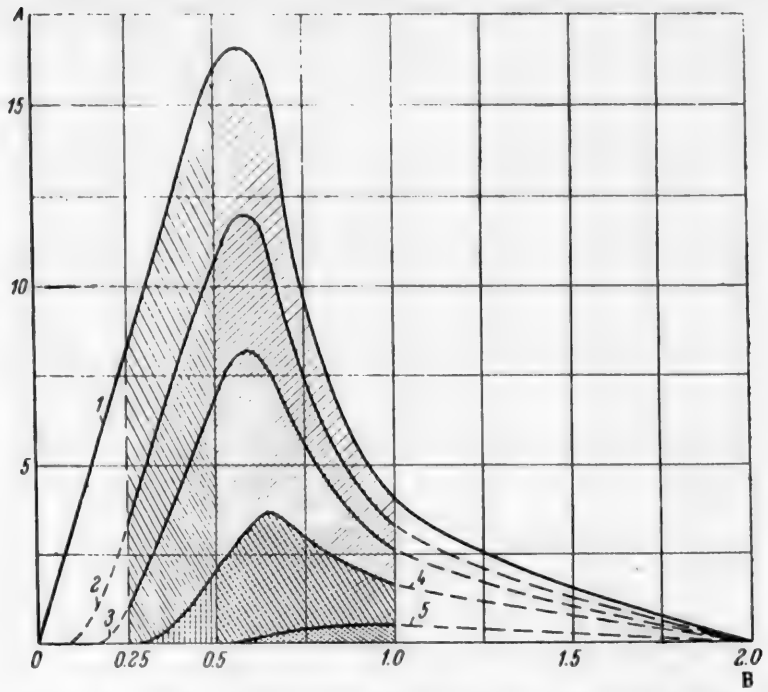

Fig. 2. Relative size distribution of kieserite crystal fractions for different decreases of their linear dimensions: A) values of dM/dl ; B) values of l_0 (mm); values of Δl : 1) 0, 2) 1/32, 3) 1/16, 4) 1/8, 5) 1/4.

TABLE 3

Variations of the Amount of Kieserite with Decrease of Linear Crystal Dimensions

Δl (mm)	Amount of salt (M) for fractions			
	0.5–1 mm		0.25–0.5 mm	
	in g	in wt. %	in g	in wt. %
0	1.4452	100.00	0.8704	100.0
0.0313	1.0681	73.91	0.6316	72.4
0.0625	0.7767	53.74	0.3393	39.0
0.1250	0.3723	25.76	0.0870	10.0
0.2500	0.0455	3.15	—	—

The required areas enclosed by the $(dM/dl) - l_0$ curves were found by weighing of the corresponding regions of graph (millimeter) paper on an analytical balance. The results of these determinations are given in Table 3 and Fig. 3.

Variations of the concentration C_x of the solution during dissolution of kieserite were determined experimentally. The experiments were performed in a 500 ml flask with inlets for a stirrer, thermometer, condenser, and sampling (fuller details in [7], p. 46). A definite amount (400-500 g) of solvent was put in the flask, and 10 g of the chosen fraction of kieserite was quickly added. Samples were taken by means of a pipet (with a cotton-wool plug) and analyzed for magnesium by the Trilon method.

Table 4 contains the results of experiments on the dissolution of two kieserite fractions in water at 25 °C. The curves in Fig. 3 were used to find the decrease Δl of linear crystal size and the derivatives $dl/d\tau$ corresponding to the amounts M of kieserite found. It was found that the average rates of linear dissolution

$(dl/d\tau)$ of kieserite are almost the same (0.0033 and 0.0031) for the 0.25–0.5 mm and 0.5 - 1 mm fractions. This result demonstrates the suitability of our method for determination of the rates of solution of powdered materials and shows that the experimental and calculation errors are relatively small.

All the remaining experiments were performed with the 0.5-1 mm kieserite fraction only.

Table 5 contains the results of determinations of the dissolution rates of kieserite in water at 50, 75, and 96°. Solubility data are required for calculation of the solution-rate constants K_v from our values for the linear dissolution rate $(dl/d\tau)$ by means of Equation (6). The solubility of kieserite at 25 and 50° lies in the metastable region. Its values were therefore determined at four temperatures by Karazhanov [8] by the kinetic method, with the use of fused crystals of anhydrous $MgSO_4$. The latter was very rapidly hydrated on the surface and its subsequent behavior was the same as that of kieserite (compare the solubilites given in Table 6 and in tables [10] at 75 and 95-96°).

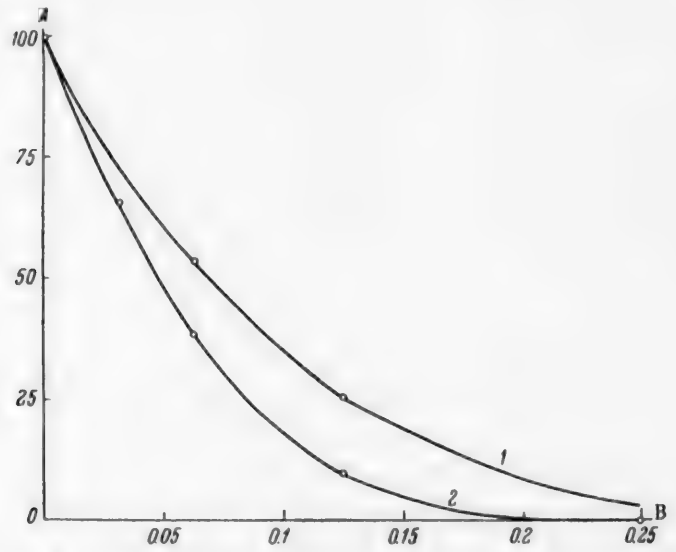

Fig. 3. Variations of the amount of kieserite with decrease of the linear dimensions of crystals of two fractions: A) M (wt. %); B) Δl (mm); fractions (mm): 1) 0.5–1; 2) 0.25–0.5

Table 6 contains the results of experimental determinations of the solution rate of kieserite in water at 25-96° and in its own solutions at 25°, and also calculated values of K_v for different temperatures. These results show that K_v decreases with increase of the $MgSO_4$ concentration; this generally indicates that the dissolution is nondiffusional in character [7]. The nondiffusional character of kieserite dissolution is revealed more clearly by the relationship between the solution-rate constant (K_v) and temperature.

It was shown earlier [7] that the following relationship is valid for salts dissolving by a diffusional mechanism:

$$K_v = \alpha_1 \left(\frac{\Delta\rho D^2}{\mu}\right)^{1/3} = \alpha_1 \frac{\Delta\rho^{1/3}}{\mu} (D\mu)^{2/3}, \qquad (7)$$

where $\Delta\rho$ is the density difference between the salt crystals and the solvent; D and μ are the coefficient of diffusion of the salt and the coefficient of kinematic viscosity of the solution at the experimental temperature, respectively; α_1 is a constant for all salts dissolving by a diffusional mechanism (it value is 15 in the cgs system). The values of μ for the solutions were calculated from Ezrokhi's empirical equation [11] and D was found by extrapolation of literature data [7] from the empirical linear relationship between log D and concentration (in g-equiv/liter) [8], with dependence of $(D\mu)$ on temperature taken into account in accordance with the Einstein-Smoluchowski equation. Our calculated values of α_1 and the diffusion function $(\Delta\rho D^2/\mu)^{1/3}$ are given in Table 6.

TABLE 4

Rate of Solution of 10 g of Kieserite in 400 g of Water at 25°

τ (in hours)	P (in g)	c_x (in % $MgSO_4 \cdot H_2O$)	G_X (in g)	M (in wt. %)	Δl (in mm) from graph, Fig. 3	$dl/d\tau$ (mm/hr)
			0.5-1 mm Fraction			
1.0	400	0.0793	9.682	96.82	0.0032	0.0032
2.0	394	0.1464	9.422	94.22	0.0066	0.0034
2.7	388	0.2062	9.198	91.98	0.0086	0.0029
3.7	383	0.2830	8.913	89.13	0.0119	0.0033
4.67	377	0.3608	8.636	86.36	0.0150	0.0032
5.77	371	0.4552	8.308	83.08	0.0190	0.0036
7.33	365	0.5928	7.835	78.35	0.0248	0.0037
				Mean		0.0033
			0.25-0.5 mm Fraction			
1.0	400	0.0887	9.645	96.45	0.0031	0.0031
2.0	395	0.1666	9.338	93.38	0.0062	0.0031
3.38	390	0.2866	8.874	88.74	0.0105	0.0031
6.0	384	0.5177	7.996	79.96	0.0180	0.0029
				Mean		0.0031

TABLE 5

Solution Rates of 0.5-1 mm Kieserite Fraction (G_0 = 10 g) in Water at Three Different Temperatures

τ (hours	P (g)	c_x (in % $MgSO_4 \cdot H_2O$)	G_X (g)	M (wt. %)	Δl (mm) from Fig. 3	$dl/d\tau$ (mm/hr)
			$t = 50°$			
0.5	400	0.207	9.172	91.72	0.0089	0.0178
1.0	394	0.380	8.489	84.89	0.0172	0.0166
2.0	388	0.691	7.297	72.97	0.0326	0.0154
3.5	382	1.133	5.632	56.32	0.0586	0.0173
5.35	376	1.582	3.993	39.93	0.0886	0.0162
7.07	370	1.878	2.971	29.71	0.1130	0.0142
					Mean . . .	0.0163
			$t = 75°$			
0.33	400	0.407	8.372	83.72	0.018	0.055
0.75	394	0.894	6.454	64.54	0.044	0.062
1.33	388	1.500	4.135	41.35	0.086	0.072
2.33	382	2.038	2.154	21.54	0.138	0.052
					Mean	0.060
			$t = 96°$			
0.181	400	0.539	7.822	78.22	0.026	0.144
0.50	394	1.348	4.657	46.57	0.076	0.152
0.75	389	1.825	2.835	28.35	0.117	0.164
1.00	383	2.060	2.002	20.02	0.143	0.104
					Mean	0.143

TABLE 6

Relationship Between K_V for Kieserite and Certain Properties of its Saturated Solutions

t (°C)	Original solution		Saturated solution		$d\tau/d\tau$ (cm/sec)	$K_V \cdot 10^7$ (cm/sec)	$\frac{\Delta\rho^{1/3} \cdot (D\mu)^{2/3} \cdot 10^6}{\mu}$	α_1
	$MgSO_4$ (wt. %)	$MgSO_4 \cdot H_2O$ (g/ml)	$MgSO_4$ (wt. %)	$MgSO_4 \cdot H_2O$ (g/ml)				
25	0	0	34.9 (1.434)	0.575	0.89	4.0	11.40	0.0035
	10.06 (1.102)*	0.1109			0.46	2.5	—	—
	20.13 (1.220)	0.2454			0.18	1.4	—	—
50	0	0	36.4 (1.450)	0.607	4.52	19.1	25.29	0.0076
75	0	0	36.1 (1.419)	0.589	16.94	73.9	49.79	0.0148
96	0	0	34.0 (1.774)	0.537	39.16	187.4	86.29	0.0217

TABLE 7

Comparison of Values of K for Kieserite, Calculated from Karsten's Data and Determined by Us

t (°C)	c $\left(\frac{g\ MgSO_4 \cdot H_2O}{ml}\right)$	$K_V(C-C_X) \cdot 10^6$ (g/cm² · sec), Karsten	$K_V \cdot 10^6$ (cm/sec)		$\frac{K_I}{K_{II}}$
			I. Karsten	II. Our data	
45	0.607	2.40	3.95	1.4	2.8
60	0.602	6.39	10.61	3.3	3.2
70	0.594	9.41	15.84	5.8	2.8
81	0.579	13.7	23.66	9.6	2.4
87	0.567	16.0	28.21	12.5	2.2
96	0.537	22.22	41.34	18.7	2.2

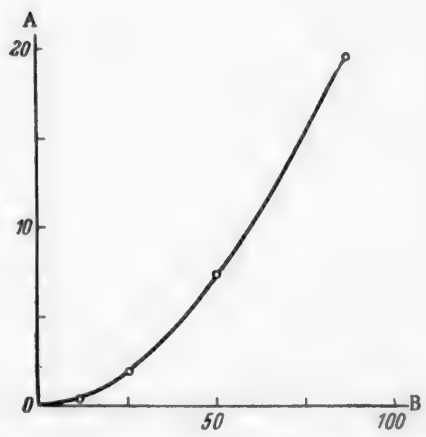

Fig. 4. Variations of K_V for kieserite with the diffusion function $\frac{\Delta\rho^{1/3}(D\mu)^{2/3}}{\mu}$.

A) Values of $K_V \cdot 10^6$, B) values of $\frac{\Delta\rho^{1/3}(D\mu)^{2/3}}{\mu}$.

Fig. 4 represents the dependence of K_V for kieserite on this diffusion function. The relationship is clearly curvilinear, which is characteristic of nondiffusional dissolution. The very small absolute values of α_1 (Table 6) are also evidence of the nondiffusional dissolution of kieserite.

Table 7 contains Karsten's data [6], which also conform to the temperature relationship noted above. However, his absolute values of K_V are 2-3 times higher than ours. Karsten's values for the rates of solution of NaCl and KCl are also double those reported by Zdanovskii [7]. These differences in the rates of solution are evidently due to the very high solvent velocities (70 cm/second) and breakdown of crystals in Karsten's experiments. Therefore our data must be regarded as the more reliable for dissolution of freely suspended salt crystals.

Thus, the method described above for determination of solution rates gives quite reliable results. Strict determination of the true surface area of numerous crystals of different shapes and sizes is unnecessary in this method.

SUMMARY

A new method for determination of the rates of solution of powdered crystals of different shapes and sizes from sieve analysis data and variations of solution composition during the dissolution process has been developed and applied. The new method was used for studying the rate of solution of kieserite in water at 25-96° and in its own solutions at 25°. It was shown by theoretical analysis that the dissolution of kieserite in water is non-diffusional in character.

LITERATURE CITED

[1] P. P. Titov, Trans. Sverdlovsk Mining Inst. 5, 30 (1940).

[2] H. Keitel, Mitteilungen KFA, 32, 95 (1922).

[3] O. Krull, Dissertation (1918); Kali, 18, 33, 70, 168, 187 (1921).

[4] D. Langauer, Przem. Chem. 18, 464 (1934).

[5] W. Jacek, Roczniki chemji. 19, 471 (1929).

[6] O. Karsten, Z. anorg. Ch., 276, 247 (1954).

[7] A. B. Zdanovskii, Trans. All-Union Sci. Res. Inst. Halurgy 33 (1956).

[8] N. A. Karazhanov, Dissertation [in Russian] (All-Union Sci. Res. Inst. Halurgy, Leningrad, 1958).

[9] A. B. Zdanovskii, J. Inorg. Chem. 1, No. 6,1279 (1956).

[10] A. B. Zdanovskii, E. I. Lyakhovskaya, and R. É. Shleimovich, Handbook on Solubilities in Salt Systems, I [in Russian] (Goskhimizdat, 1953).

[11] L. L. Ézrokhi, Trans. All-Union Sci. Res. Inst. Halurgy 27, 132 (1953).

Received December 29, 1958

INVESTIGATION OF THE COMPOSITION OF BINARY SYSTEMS OF ORGANIC SOLVENTS BY PHYSICAL TITRATION WITH WATER WITHOUT THE USE OF TURBIDITY INDICATORS

S. I. Spiridonova

Chair of Inorganic and Analytical Chemistry,
the Saratov Zootechnical and Veterinary Institute

For determination of the quantitative composition of binary systems of various organic solvents, we have proposed a method of physical titration of such mixtures by water in presence of furfural as turbidity indicator [1, 2]. In this method, constant amounts of the turbidity indicator are added to equal volumes of all the investigated mixtures taken for titration. Under these conditions the volume of water added during titration until turbidity appears is a linear function of the concentration of the nonpredominant component of the mixture.

However, binary mixtures of components one of which has low solubility in water are often met in practice. Addition of a special turbidity indicator to the binary mixture then becomes unnecessary, as when such a mixture is titrated by water, turbidity is caused by the sparingly-soluble component of the mixture. Examples of such systems are mixtures of isoamyl alcohol with ethyl alcohol or acetone. The first system was studied about 50 years ago by Fontein [3] in relation to a method for determination of the moisture content of alcohol by titration with isoamyl alcohol, and the second system is used for determination of the moisture content of acetone, also by titration with isoamyl alcohol [4].

In the present investigation we studied the systems ethyl alcohol–isoamyl alcohol and dioxane–isoamyl alcohol in order to develop a method for rapid determination of one of the components in such mixtures by titration with water until the onset of turbidity.

EXPERIMENTAL

The system: ethyl alcohol–isoamyl alcohol. Mixtures of rectified spirit (95.5% ethyl alcohol) and isoamyl alcohol (b.p. 128-130°) containing from 50 to 15% by volume of the latter were taken for the investigation. All the solutions were titrated by water, by the method described by us for the titration of alcoholic solutions of camphor by water [5]. Distilled water was added in small drops (about 100 drops per ml) from a microburet, with shaking of the titrated mixture (in a test tube) in a constant-temperature water bath, until stable turbidity appeared.

The results of physical titration of mixtures of isoamyl and ethyl alcohol by water to the start of turbidity are given in Table 1.

It should be noted that the end point (turbidity threshold) is very sharp, and titration of only two duplicate samples is quite sufficient for a determination; solutions of higher concentrations of isoamyl alcohol are especially easily titrated.

The same results of titration of mixtures of these alcohols by water are plotted in Fig. 1.

The physical titration curve in Fig. 1 may be used as a standard turbidity isotherm for mixtures of isoamyl and ethyl alcohol at the stated temperature. It may be used for graphical determination of the content of a given component if the mixture of unknown quantitative composition is first titrated with water to the appearance of turbidity.

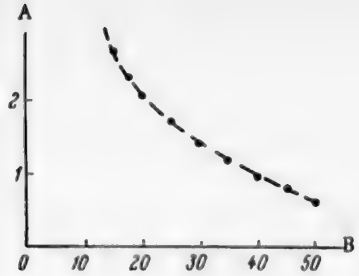

Fig. 1. Isotherm for the onset of turbidity in mixtures of isoamyl and ethyl alcohols during titration with water at 18°: A) volume of water added in titration to turbidity (ml); B) volume concentration of isoamyl alcohol (%).

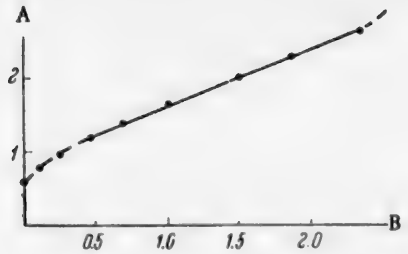

Fig. 2. Isotherm for the onset of turbidity in mixtures of isoamyl and ethyl alcohols during titration with water at 18°: A) volume of water (ml); B) degree of dilution of isoamyl alcohol solutions (n = 1).

TABLE 1

Titration of Mixtures of Ethyl and Amyl Alcohol by Water at 18° to Turbidity

Isoamyl alcohol contents of mixtures (vol. %)	Water added (ml)			
	I	II	III	mean
50	0.615	0.605	0.610	0.610
45	0.780	0.775	0.780	0.778
40	0.990	0.980	0.985	0.985
35	1.200	1.205	1.205	1.203
30	1.420	1.420	1.425	1.423
25	1.690	1.715	1.705	1.703
20	2.090	2.070	2.080	2.080
17.5	2.340	2.330	2.335	2.335
15	2.710	2.690	2.700	2.700

However, it is well known that the use of calibration curves has a number of disadvantages. If such curves are to be accepted as standard, it is necessary in their determination to use components of the highest possible purity and to test numerous control mixtures prepared by precise gravimetric or volumetric methods. Exact temperature control is also necessary. The accuracy of the graph readings largely depends on the scale used. It is therefore convenient for practical purposes and interesting from the theoretical aspect to find a linear relationship between the concentration of a particular component of a given binary mixture and the volume of water added in titration.

It is known that a hyperbola is converted into a straight line if reciprocal concentrations are taken along the concentration axis [6]. If any region of the experimental curve is a hyperbola, then, as Nikitin [7] showed, if the concentration of the substance being determined is replaced by the degree of dilution of the initial (more highly concentrated) solution, a new curve is obtained in which the section in question is linear. The analytical expression of a linear relationship, in all its simplicity, is applicable to this range of dilution (or concentration).

Suppose that the concentration of isoamyl alcohol in the original mixture of isoamyl and ethyl alcohols is c. Let it be diluted with ethyl alcohol to concentration x. Then the degree of dilution n of the original solution is

$$n = \frac{c}{x} . \qquad (1)$$

TABLE 2

Degree of Dilution of an Original (50%) Solution of Isoamyl Alcohol in Ethyl Alcohol

Volume concentration of isoamyl alcohol (%)	50	45	40	35	30	25	20	17.5	15
Degree of dilution of solution $\left(n = \frac{c}{x}\right)$ . . .	1.00	1.11	1.25	1.43	1.67	2.00	2.5	2.86	3.3

Values of the degree of dilution n for the solutions detailed in Table 1 are given in Table 2.

In Fig. 2 the data of Table 1 are represented by a new titration curve; here the degrees of dilution of the original solution, for which n = 1, are taken along the concentration axis.

Fig. 2 shows that there is a linear relationship between the volume of water added and the degree of dilution of a 50% solution for n between 1.25 and 3.33, which, according to Table 2, corresponds to isoamyl alcohol concentrations between 40 and 15%. Therefore a simple linear (first-order) equation can be used to calculate concentrations of isoamyl alcohol in its mixtures with ethyl alcohol.

TABLE 3

Comparison of True and Calculated Concentrations of Isoamyl Alcohol in Mixtures with Ethyl Alcohol

Actual concentrations of isoamyl alcohol (vol. %) in mixtures (c)	Degree of dilution, n	Water added, V (ml)	Calculated alcohol concentration, x (ml)	Relative error (%)
30.000	1.00	1.423	30.000	I standard
28.125	1.067	1.525	27.790	—1.2
26.2500	1.140	1.610	26.090	—0.6
24.375	1.230	1.692	24.560	+0.7
22.500	1.333	1.834	22.680	+0.8
20.625	1.450	2.008	20.440	—0.9
18.750	1.600	2.143	18.720	—0.1
16.875	1.780	2.405	16.960	+0.5
15.000	2.000	2.700	15.000	II standard

The equation of a straight line passing through two fixed points the coordinates of which are (n_1, V_1) and (n_2, V_2) is

$$\frac{V - V_1}{V_2 - V_1} = \frac{n - n_1}{n_2 - n_1}. \tag{2}$$

If $n_1 = 1$ and $n = 2$, then

$$\frac{V - V_1}{V_2 - V_1} = n - 1, \tag{3}$$

and hence

$$n = 1 + \frac{V - V_1}{V_2 - V_1}. \tag{4}$$

Substituting the value of n from this last equation into Equation (1), we find the equation for calculating the required concentration x of the given component

$$x = \frac{c}{1 + \frac{V - V_1}{V_2 - V_1}} \tag{5}$$

or

$$x = c\,\frac{V_2 - V_1}{V_2 + V - 2V_1}. \tag{5a}$$

TABLE 4

Determination of Isoamyl Alcohol in Dilute Solutions in Ethyl Alcohol by Titration with Water (at 18°)

Actual concentration of isoamyl alcohol in solution (vol. %)	Water added in titration (ml)	Isoamyl alcohol found (%)	Relative error (%)
30.0	0.212	30.0	I standard
12.0	0.490	11.78	−1.8
10.0	0.527	10.15	+1.5
8.0	0.586	7.82	−2.2
6.0	0.633	6.14	+2.4
15.0	0.850	15.0	II standard

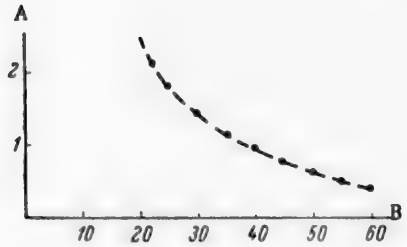

Fig. 3. Isotherm for the onset of turbidity in mixtures of isoamyl alcohol and dioxane during titration with water at 20°: A) volume of water (ml); B) volume concentration of isoamyl alcohol (%).

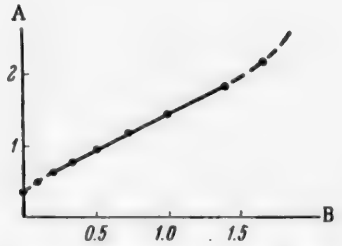

Fig. 4. Isotherm for the onset of turbidity in mixtures of isoamyl alcohol and dioxane during titration with water at 20° : A) volume of water (ml); B) degree of dilution of isoamyl alcohol solutions (n=1).

Therefore in order to calculate the concentration of isoamyl alcohol in such a mixture it is sufficient to have two standard solutions of this alcohol in ethyl alcohol; these solutions together with the unknown solution are titrated with water until turbidity appears (all at the same temperature).

If a 30% solution (by volume) of isoamyl alcohol in ethyl alcohol is taken as standard solution I (n_1, V_1), and a 15% solution is taken as standard solution II, Equation (5a) can be used for easy calculation of the concentrations of all intermediate mixtures, with a very low error relative to the true concentrations of each. The results of such calculations are given in Table 3, based on the results of water titration of solutions of isoamyl in ethyl alcohol in the range of concentrations intermediate between those of the two standard mixtures.

TABLE 5

Titration of Mixtures of Isoamyl Alcohol and Dioxane with Water to Turbidity at 20°

Comp. of titration mixtures (vol. %)		Water added in titration (ml)			
isoamyl alcohol	dioxane	I	II	III	mean
60	40	0.385	0.380	0.383	0.383
55	45	0.490	0.485	0.493	0.493
50	50	0.640	0.640	0.640	0.640
45	55	0.790	0.790	0.785	0.788
40	60	0.960	0.960	0.965	0.962
35	65	1.160	1.165	1.160	1.162
30	70	1.440	1.450	1.450	1.447
25	75	1.815	1.820	1.825	1.820
22.5	77.5	2.160	2.135	2.145	2.147

In practice the determination of isoamyl alcohol (or n-amyl alcohol, which has equally low solubility in water) in mixtures with ethyl alcohol by titration with water to turbidity is carried out as follows. First, a standard mixture of the alcohol to be determined and ethyl alcohol (rectified spirit) is prepared, and the concentration is calculated accurately (about 30% by volume). The second standard mixture is prepared by dilution of a part of standard solution I with an equal volume of ethyl alcohol. 2 ml of each solution is then mixed in a test tube with 2 ml of water and shaken, and 2-3 samples of 1 ml each are taken for titration with water. The solution of unknown concentration of isoamyl alcohol in ethyl alcohol is treated similarly. The required concentration is calculated from Equation (5a).

If the calculated concentration $\underline{x}$ indicates that the amyl alcohol content is above 30%, the unknown mixture should be diluted with an equal volume of ethyl alcohol and the amyl alcohol content determined again. If the content is below 15% (5-10%), it can be determined with some modification of the method [5]. In such a case an equal volume of standard mixture I (30%) is equal to a sample of the unknown mixture, and the resultant mixture is tested as before (diluted with an equal volume of water, and 1 ml of the mixture is titrated with water). The concentration is then calculated from the equation

$$\frac{x+c}{2} = c\,\frac{V_2 - V_1}{V_2 + V - 2V_1}\,, \tag{6}$$

and hence

$$x = c\,\frac{V_2 - V}{V_2 + V - 2V_1}\,. \tag{7}$$

TABLE 6

Degree of Dilution of an Original (60%) Solution of Isoamyl Alcohol in Dioxane

Volume concentration of isoamyl alcohol (%)	60	55	50	45	40	35	30	25	22.5
Degree of dilution, $\underline{n}$	1.00	1.09	1.2	1.3	1.5	1.7	1.0	1.4	1.67

Table 4 contains the results of determinations of isoamyl alcohol in mixtures with ethyl alcohol containing from 5 to 15% of the former.

It can be seen that isoamyl alcohol can be determined satisfactorily in ethyl alcohol even at low concentrations.

After determination of the isoamyl alcohol, the amount of ethyl alcohol (rectified spirit) is found by difference.

The system: dioxane–isoamyl alcohol. Mixtures of dioxane (b.p. 101-102°) and isoamyl alcohol were prepared from different volumes of the two components. Samples of 1 ml each were taken from each mixture and titrated to turbidity. The titration results are given in Table 5 and Fig. 3.

Table 6 contains data on the degree of dilution n of 60% isoamyl alcohol solution by dioxane (from the data of Table 5), and Fig. 4 contains the titration results (from the same data) when the alcohol concentration is replaced by its reciprocal, i.e., the degree of dilution of the original solution.

It is clear from Fig. 4 that a linear relationship between the volumes of water added to turbidity and the degree of dilution holds for n from 1.20 to 2.40, which corresponds to alcohol concentrations from 50 to 25%.

TABLE 7

Comparison of Calculated and True Concentrations of Isoamyl Alcohol in Dioxane Solutions. (From the data of Tables 5 and 6)

True concentration of isoamyl alcohol, c (vol. %)	n	Water added, V (ml)	Calculated alcohol concentration, x (%)	Relative error
50	1.00	0.640	I standard solution	
45	1.11	0.788	44.48	—1.27
40	1.25	0.962	39.28	—1.80
35	1.43	1.163	34.65	—1.00
30	1.67	1.447	29.55	—1.00
25	2.00	1.820	25.00	II standard

Therefore if a 50% solution (by volume) of isoamyl alcohol in dioxane is taken as a standard solution, and a portion of it is diluted with an equal volume of dioxane, two standard mixtures are obtained which serve as the concentration limits within which any intermediate solutions conform to a linear relationship between dilution and the volume of water added to turbidity. In Table 7 the concentrations of isoamyl alcohol in such solutions calculated from Equation (5a) are compared with the true concentrations.

This last table shows that isoamyl alcohol can be easily determined in dioxane solutions by titration with water to turbidity.

Determination of isoamyl alcohol in dilute solutions in dioxane should not present any difficulties if the method described for determination of small amounts of isoamyl alcohol in ethyl alcohol is used.

Our method for determination of isoamyl alcohol in mixtures with ethyl alcohol or dioxane by physical titration with water to turbidity can be applied in all cases when one of the components of a binary mixture is sparingly soluble in water and the other is miscible with water in all proportions.

SUMMARY

1. Binary systems containing isoamyl alcohol and ethyl alcohol or dioxane in various proportions were studied by the method of physical titration to turbidity.

2. Conditions for the existence of a linear relationship between the volume of water added to cause turbidity and the concentration of the minor component in these binary systems have been studied.

3. It is possible to calculate the contents of isoamyl alcohol in mixtures with ethyl alcohol or dioxane from the results of physical titration of the unknown solution and a standard mixture with water; the lengthy construction of a calibration curve is thereby avoided.

4. The proposed method can be extended to any binary mixture containing one component miscible with water in all proportions.

LITERATURE CITED

[1] S. I. Spiridonova, J. Anal. Chem. 4, 169 (1949).

[2] S. I. Spiridonova, J. Phys. Chem. 26, 1827 (1952).

[3] F. Fontein, Z. f. Phys. Chem. 73, 212 (1910).

[4] G. Tammann, Heterogeneous Equilibria (1935) p. 189 [Russian translation].

[5] S. I. Spiridonova, J. Gen. Chem. 7, 1071 (1937).

[6] V. Ya. Anosov and S. A. Pogodin, Fundamental Principles of Physicochemical Analysis [in Russian] (1947) p. 98.

[7] E. K. Nikitin, J. Appl. Chem. 9, 950 (1936).

Received March 25, 1958

LIQUID – VAPOR EQUILIBRIA IN THE SYSTEM METHYLCYCLOHEXANE–2,2,4-TRIMETHYLPENTANE*

I. N. Bushmakin, S. P. Versen,
and N. P. Kuznetsova

The Leningrad (Order of Lenin) State University

The system methylcyclohexane–2, 2, 4-trimethylpentane was proposed in 1946 by Willingham and Rossini [1] for determination of the efficiency of fractionating columns.

The number of theoretical plates for this system is calculated from the average value of α (relative volatility) for the middle of the still–condenser concentration range, the system being assumed ideal.

These authors determined the values of α at 0 and 100%, and these values are regarded as especially accurate.

In using the data of Willingham and Rossini for determinations of column efficiency, we found that the efficiency greatly depends on the concentration of the solution being fractionated. According to our rule, column efficiency should be independent of the concentration of the solution [2]. The failure of this rule indicates, from our viewpoint, that the liquid–vapor equilibrium data (on which the efficiency calculations are based) are inaccurate.

The data of Willingham and Rossini originated as follows: Harrison and Berg [3] studied liquid–vapor equilibria in this system at 741 mm. The values of α calculated by us from their data are indicated by crosses in the diagram. Apparently, Willingham and Rossini decided that Harrison and Berg's data for the extreme concentrations are incorrect, while the data for intermediate concentrations indicate that the behavior of the system is almost ideal. They therefore assumed ideal behavior for the system. On this basis they performed careful measurements of the vapor pressures of the pure components at their boiling points (at 760 mm) and used the ratio p_2^0/p_1^0 to calculate α at 0 and 100%, the values being given to an accuracy of $\pm 1.10^{-5}\alpha$.

Therefore, Willingham and Rossini's data are based on the ill-founded assumption that the system is ideal. Therefore, despite the great accuracy with which the vapor pressures of the pure components were determined, the validity of these data is doubtful. The fact that the column efficiency calculated from these data depends on the concentration of the fractionated solution shows that they must be incorrect.

Accurate data were required for determinations of column efficiencies by means of this system in the course of our investigations of rectification processes. The present investigation of liquid–vapor equilibria in this system was therefore undertaken.

Methylcyclohexane was shaken with concentrated sulfuric acid to a negative formolite reaction in order to remove aromatic compounds, washed with sodium carbonate solution and water, and then distilled repeatedly through columns of 120 theoretical plates (determined for the system benzene–carbon tetrachloride). Similarly, 2,2,4-trimethylpentane was carefully fractionated through columns of 120 theoretical plates. The purified substances were tested for purity by means of columns of 120 theoretical plates [2]. The purified methylcyclohexane

* Communication X.

had n_D^{20} = 1.42307, and 2,2,4-trimethylpentane had n_D^{20} = 1.39146. According to Forziati et al. [4] (U. S. Bureau of Standards), methylcyclohexane (purity 99.9 molar %) has n_D^{20} = 1.42305, and 2,2,4-trimethylpentane (purity 99.8 molar %) has n_D^{20} = 1.39145. •

Two single-evaporation stills of the same (old) design but of different dimensions, and also fractionating columns, were used for investigation of liquid–vapor equilibria. The stills are described in Communication IX [5]. The volume of the still in apparatus I was 130 ml, and in apparatus II, 200 ml. The apparatus was connected to a manostat during the determinations.

The liquid and vapor compositions were determined by differential readings on the scale of a Pulfrich refractometer. For this, scale reading–concentration graphs were first plotted for the concentration ranges to be studied. The error of the scale readings was ±0.1, which corresponds to an error of ±0.04 molar % in the concentration determinations. In each experiment, 8-20 scale readings were taken for each liquid (condensate and liquid in the still); the mean error in determination of the liquid composition was in the region of ±0.01 molar % in the worst cases.

TABLE 1

Liquid–Vapor Equilibrium Data for the System Methylcyclohexane–2,2,4-Trimethylpentane, Determined by the Single-Evaporation Apparatus. P = 760 mm

Apparatus	Contents of 2,2,4-trimethyl pentane (molar %)		α
	liquid	vapor	
I	8.30	8.83	1.070
I	14.93	15.77	1.067
I	27.54	28.71	1.060
II	36.43	37.68	1.055
II	61.52	62.54	1.044
I	83.00	83.48	1.035
I	92.70	92.89	1.029
I	95.06	95.18	1.026

The results of investigations of liquid–vapor equilibria in the single-evaporation apparatus are given in Table 1 and are marked by circles on the diagram.

To confirm the validity of the results obtained in the single-evaporation apparatus at the extreme concentrations, α was also determined at these concentrations with the aid of columns [2]. A column of 6.1 theoretical plates was used for determination of α with 9 molar % of 2,2,4-trimethylpentane, and a column of 30 theoretical plates for determinations of α with 98 molar %. The efficiencies of these columns were determined in experiments in the 30-65 molar % range. The concentrations in experiments with the columns were determined by differential readings on the Pulfrich refractometer scale.

The results obtained for α with the columns are summarized in Table 2 and are marked on the diagram by triangles.

The linear function $\alpha = f(x)$ found by means of the single-evaporation apparatus and confirmed by determinations of α with columns can be represented by the equation

$$\alpha = 1.074 - 0.00050\,x. \qquad (1)$$

This equation was used for calculation of interpolated liquid–vapor equilibrium data. The results are given in Table 3. Table 4 contains our calculated data for construction of diagrams showing the number of theoretical plates as a function of concentration.

The method used for exact calculation of the number of theoretical plates is described in detail in Communication II [6]. The principle of the method is that the concentration range of 0.01–99.99 molar % is broken up into concentration regions. The equation $n = \log[y'(100-x')/x'(100-y')]/\log\alpha$ is used to calculate the number $\underline{n}$ of theoretical plates for each region; the value of α is taken for the middle of the region, and x' and y', the concentrations of the more volatile component, for the beginning and end of the region. The values of $\underline{n}$

• The fact that our liquids had refractive indices close to the standard values is not in itself a conclusive criterion of their purity. Such liquids may still contain considerable amounts of impurities. The purity must be checked by means of fractionating columns in order to ensure a degree of purity adequate for investigations of liquid–vapor equilibria in single-evaporation apparatus and especially for investigations with the use of fractionating columns.

TABLE 2

Values of α for the System Methylcyclohexane–2,2,4-Trimethylpentane, Determined with the Use of Columns
P = 760 mm

Contents of 2,2,4-trimethylpentane (molar %)			α
in still	in condenser	middle of range	
Column of 6.1 theoretical plates			
7.25	10.57	8.91	1.070
7.54	10.86	9.20	1.068
7.60	11.00	9.30	1.069
7.62	11.00	9.31	1.069
Column of 30.0 theoretical plates			
96.73	98.56	97.7	1.028
98.00	99.00	98.5	1.024

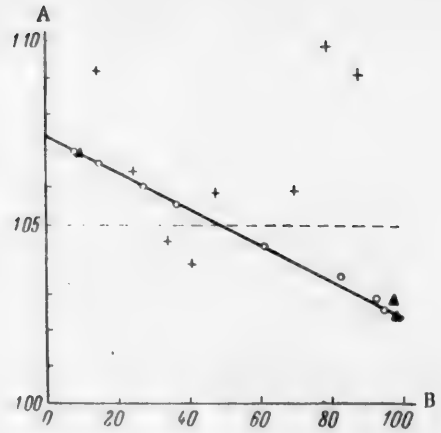

Variation of relative volatility α for the system methylcyclohexane – 2,2,4-trimethylpentane with the concentration of trimethylpentane in the liquid (x): A) relative volatility, B) contents of 2,2,4-trimethylpentane in liquid (molar %); explanations in text.

calculated for the region are added. For precise calculations, the extent of a region should not exceed a certain maximum. This maximum depends on the value of α and on the position of the region; the regions should be narrower as 0 and 100% is approached. The magnitude of a region is determined by trial. A region is regarded as acceptable if the value of $\underline{n}$ calculated for it differs by less than 0.05 of a theoretical plate from the sum of the values of $\underline{n}$ of its constituent regions. The method is very time-consuming in this form. It was therefore modified. Two tables were compiled for calculation of the number of theoretical plates fitting in the range of 0.01–99.99 molar %. The table contains all the auxiliary data for calculation of the number of theoretical plates for the concentration regions. Values of α corresponding to the middles of the concentration regions found, for example, from the diagram) are substituted in them, and $\log [y'(100-x)/x'(100-y')]$ (these are already calculated) is then divided by log α. The magnitudes of the concentration regions (specially chosen) differ in the two tables. Both tables are used for the calculation. Agreement of the numbers of theoretical plates fitting into the 0.01–99.99% range calculated from the tables indicates that the magnitude of the concentration regions is appropriate for the given system and that the calculation is correct.

TABLE 3

The System Methylcyclohexane–2,2,4-Trimethylpentane Liquid–Vapor Equilibrium Data Interpolated from the Linear Function $\alpha = f(x)$ P = 760 mm

Contents of 2,2,4-trimethylpentane (molar %)		α	Contents of 2,2,4-trimethylpentane (molar %)		α
liquid	vapor		liquid	vapor	
3.00	3.21	1.073	60.00	61.03	1.044
5.00	5.34	1.072	70.00	70.80	1.039
10.00	10.62	1.069	80.00	80.53	1.034
15.00	15.84	1.067	85.00	85.39	1.032
20.00	21.01	1.064	90.00	90.25	1.029
30.00	31.22	1.059	92.00	92.20	1.028
40.00	41.27	1.054	94.00	94.15	1.027
50.00	51.20	1.049	98.00	98.05	1.025

TABLE 4

The System Methylcyclohexane – 2,2,4-Trimethylpentane Data for Construction of Diagrams (Number of Theoretical Plates, Concentration). Concentration of 2,2,4-Trimethylpentane in Still = 0.01 Molar %. P = 760 mm

Concentration of 2,2,4-trimethylpentane in condenser reflux (molar %)	No. of plates	Concentration of 2,2,4-trimethylpentane in condenser reflux (molar %)	No. of plates	Concentration of 2,2,4-trimethylpentane in condenser reflux (molar %)	No. of plates
0.01	0	35	125.0	94	218.6
0.1	32	45	133.0	95	225.9
0.3	48	55	141.4	96	234.9
0.5	55	60	145.9	97	247
0.8	62	65	151.1	98	263
1.0	65	70	156.8	98.4	273
1.5	70.5	75	163.6	98.8	285
2.0	74.7	78	168.8	99.0	292
4.0	84.9	81	174.2	99.5	321
6.0	91.1	84	180.5	99.8	360
8.0	95.6	85	182.7	99.9	389
12.0	102.4	88	191.4	99.94	410
16.0	107.5	90	198.5	99.96	428
20.0	111.8	92	207.2	99.98	457
25.0	116.7	93	212.0	99.99	486

TABLE 5

Effect of Concentration on the Refractive Index of Mixtures of Methylcyclohexane – 2,2,4-trimethylpentane

Conc. of 2,2,4-trimethylpentane (molar %)	n_D^{20}	Conc. of 2,2,4-trimethylpentane (molar %)	n_D^{20}
0.0	1.4231	55	1.4041
5	1.4212	60	1.4026
10	1.4194	65	1.4011
15	1.4175	70	1.3996
20	1.4157	75	1.3981
25	1.4139	80	1.3968
30	1.4122	85	1.3954
35	1.4105	90	1.3941
40	1.4088	95	1.3928
45	1.4072	100	1.3915
50	1.4056		

TABLE 6

Check of Liquid–Vapor Equilibrium Data for the System Methylcyclohexane–2,2,4-Trimethylpentane by Means of a Column. P = 760 mm

Region	Concentration of 2,2,4-trimethylpentane (molar %)		Number of plates	
	still	condenser	from α of Willingham and Rossini	from our α
I	10.1	40.4	37.6	29.7
II	36.8	69.4	28.4	29.6
III	68.7	86.1	21.6	30.6
IV	86.4	93.7	17.7	30.1

Usually such tables are much too detailed for full publication, and therefore the table given here was derived as follows: a diagram for the number of theoretical plates as a function of concentration is plotted from the most detailed table, and the diagram is then used to compile a new table, less detailed, but such that the curve of the diagram can be reproduced exactly with its aid.

For accurate determinations of column efficiency by means of the diagram based on Table 4, the concentrations of 2,2,4-trimethylpentane in the condenser and still liquids can be determined in the range of 5-80 molar % by means of a refractometer of the Abbe type (to an accuracy of $\pm 1.10^{-4}$ n_D^{20}). We determined the variations of n_D^{20} with concentration. The results are summarized in Table 5.

For determinations of α with the use of columns, we found the column efficiencies (n) at intermediate concentrations, where the values of α are completely reliable, and then the columns were used at extreme

concentrations, the equilibirum compositions of the liquids in the condenser and the still were found, and, on the assumption that n does not vary with concentration, α was calculated. The fact that the values of α determined with the use of columns fitted on the linear plot of $\alpha = f(x)$ based on data obtained in the single-evaporation apparatus shows that the column efficiency is independent of concentration. To emphasize this fact further and to determine the errors in calculations of efficiency from the data of Willingham and Rossini, we determined the compositions of the liquids in the condenser and still for columns operated over different concentration regions and used these data to calculate the number of theoretical plates using Willingham and Rossini's values of α and our diagrams (Table 4). The results of these determinations are given in Table 6.

It is evident from Table 6 that the data of Willingham and Rossini are quite unsuitable for determinations of column efficiency. The plot of $\alpha = f(x)$, calculated from Willingham and Rossini's data is shown on the diagram in the form of a dash line. For the range of 0.01–99.99 molar % the number of theoretical plates is 385 calculated from the data of Willingham and Rossini, and 486 according to our data.

The above liquid–vapor equilibrium data were subsequently checked by us. The check was carried out with substances of different origin, thoroughly purified, with an apparatus of new design [5], and with the aid of new graphs for refractometer readings against concentration. The results of this check were in exact agreement with the data presented in this paper: for example, with 35.38 molar % of 2,2,4-trimethylpentane the check gave $\alpha = 1.055$, while calculation by Equation (1) gives $\alpha = 1.056$; at 61.83% molar % the check gave $\alpha = 1.043$, and Equation (1) also gives $\alpha = 1.043$.

SUMMARY

1. It is shown that the system methylcyclohexane–2,2,4-trimethylpentane deviates strongly from ideal behavior.

2. The rule established by us earlier, according to which column efficiency is independent of the concentration of the solution being fractionated, is confirmed.

LITERATURE CITED

[1] C. B. Willingham and F. D. Rossini, J. Research. Nat. Bur. St. 37, 15 (1946).

[2] I. N. Bushmakin, R. V. Lyzlova, and P. Ya. Molodenko, J. Appl. Chem. 26, 1258 (1953).*

[3] J. M. Harrison and L. Berg, Ind. Eng. Chem. 38, 117 (1946).

[4] A. F. Forziati, A. R. Glasgow, Jr., C. B. Willingham, and F. D. Rossini, J. Research, Nat. Bur. St. 36, 129 (1946).

[5] I. N. Bushmakin, J. Appl. Chem. 32, No. 4, 812 (1959).*

[6] I. N. Bushmakin, J. Gen. Chem. 21, 1197 (1951).*

Received February 17, 1958

*Original Russian pagination. See C. B. Translation.

MASS TRANSFER ON PERFORATED PLATES WITH DIFFERENT WEIR HEIGHTS

I. N. Kuz'minykh and A. I. Rodionov

The D. I. Mendeleev Institute of Chemical Technology, Moscow

In studies of the operation of perforated plates, attention is always devoted to the hydrodynamics of the bubbling process, and the nature of the gas–liquid interaction on the plate. Numerous investigations have been concerned with these problems [1-8]. It is reported in these papers that at low gas velocities a cellular foam is formed in the plates. The height of this foam first increases and then decreases with increase of the gas rate. The maximum height of the cellular foam layer is found over a fairly wide range of gas velocities, in accordance with the experimental conditions. Decrease of the height of the foam layer is accompanied by a decrease of bubble size, and then by breakdown of the cellular structure. According to our earlier data [7], at gas velocities above 1.2 m/second a new hydrodynamic regime arises on the plate, entirely dissimilar to foaming: streams of gas break through the liquid layer but do not become subdivided into bubbles, and much spray and numerous droplets form above the plate. The gas–liquid layer does not increase in height.

According to other data [6, 9, 10], a semisuspended layer of liquid in the form of rapidly moving films and streams intimately mixed with gas bubbles and streams is formed on the plate. This state was described as the foam regime, and the foam was termed mobile (in contrast to cellular foam, which has low mobility). The layer of mobile foam grows approximately in proportion to the gas velocity in the column. The mobility of the foam also increases, and the foam becomes eddying and streaming. According to the authors cited, the regime is more effective with regard to mass transfer than the cellular-foam regime, irrespectively of the solubility of the gas.

Our experiments [7, 11, 12] and the experiments of other investigators [13] have shown that for sparingly soluble gases the highest mass-transfer coefficients are found at relatively low gas velocities, in the true foaming region, beyond which plate performance is not intensified by increase of gas velocity. These experiments were performed with small amounts of liquid on the plate (h_0) whereas, according to Pozin and Mukhlenov, it is necessary to have both a high gas velocity and a large reserve of liquid on the plate in order to obtain mobile foam. This is is attained by the use of higher liquid rates or of plates with high weirs. Such data were not available, and experiments were therefore carried out to determine mass-transfer coefficients for plates with different weir heights.

The mass-transfer coefficients were determined for two processes carried out on the plates under isothermal conditions: desorption of a sparingly soluble gas (oxygen) from water, and evaporation of water.

The experiments were performed in a unit consisting of two boxes 920 × 90 mm in section, with the plate clamped between them. Atmospheric air preheated in an electric furnace was blown in by means of a blower through a diffuser into the lower box; the air rate was measured by means of a sharp-edged orifice meter with a differential manometer. The plate was sprayed with water previously saturated with oxygen; its flow rate was measured by means of a notch-type meter. The perforated portion of the plate was in the form of a rectangle 700 × 90 mm; at each end there was a container 90 mm wide, one for supplying the liquid to the plate and the other for overflow. The apparatus was provided with manometers for measurement of plate resistance and devices for taking samples of liquid for analysis and for determining the amount falling through the plate perforations.

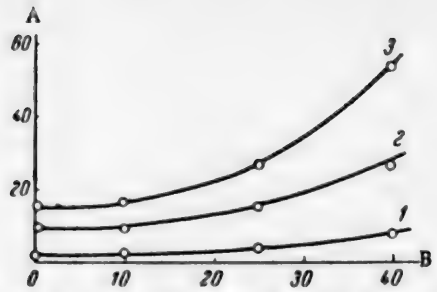

Fig. 1. Leakage at different weir heights: A) leakage (%); B) weir height (mm); gas velocity w_0 (m/second): 1) 7.13, 2) 5.35, 3) 3.58.

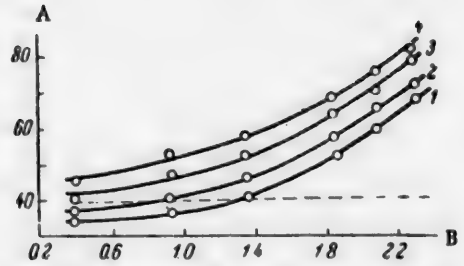

Fig. 2. Variation of plate resistance with gas velocity: A) P (mm H_2O); B) gas velocity (m/second); weir height h (mm): 1) 0, 2) 10, 3) 25, 4) 40.

This unit was used for testing a 4-10 plate (13% open section) made from sheet steel 2 mm thick, both without a weir and with a weir of heights h_w = 10, 25, and 40 mm. The gas velocity w_f calculated for the effective column cross section was varied from 0.32 to 2.3 m/second. The liquid rate was 23.5 m^3/m·hour in all the experiments. The water temperature on the plate was also constant (28 ± 0.3°). The experimental procedure, analysis of the experimental data, and calculation of the mass-transfer coefficients were the same as in our earlier investigations of mass transfer in bubbling [7, 9, 10].

In the course of hydrodynamic tests, the bubbling process was found to occur as follows: at gas velocities up to 1.2-1.4 m/second only part of the plate area was in operation. A foam layer was formed only on the region of the plate near the overflow orifice. At the other end of the plate there was a layer of clear liquid not permeated by streams of gas. The liquid partially fell through the plate perforations in this region. At gas velocities of 1.2-1.4 m/second the bubbling zone spread over the whole plate, on which a gas–liquid layer without a cellular structure was formed. The height of this layer did not change with increase of the gas rate, but more spray and drops were formed, with increasing spray loss.

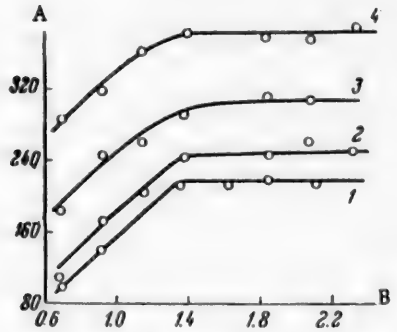

Fig.3. Effect of gas velocity on k_La: A) k_La (m/hour); B) gas velocity (m/second); weir height h (mm): 1) 0, 2) 10, 3) 25, 4) 40.

The minimum gas velocity at which the plate begins to operate without appreciable fall of liquid through the perforations was recorded in the experiments. As is known, this limit is determined by the gas velocity in the perforations, and depends on numerous factors (hole size, liquid rate, weir height, physical properties of the liquid, thickness and material of the grid, etc.). For the plate tested, leakage of liquid ceases when the gas velocity in the perforations reaches 10-12 m/second. This velocity can be determined with sufficient accuracy from the formula

$$w_y = 1000\sqrt{h_0 d},$$

where w_1 is the gas velocity in the perforations at which liquid leakage ceases (m/second), h_0 is the height of the original liquid layer (m), and d is the diameter of a perforation (m).

The amount of liquid leakage as a function of gas velocity at different weir heights was also determined. The results of measurements at three different gas velocities (w_0 = 3.58–5.35–7.13 m/second) are presented in Fig. 1. The proportion of liquid falling through increases with increasing weir height. At a gas rate w_0 = 3.58 m/second and weir height h_w = 40 mm the leakage of liquid through the perforations is over 50% of the total water entering the plate. The plate resistance increases with gas velocity at all values of h_w (Fig. 2). Under constant conditions increase of weir height leads to an increase of plate resistance owing to the increase of the

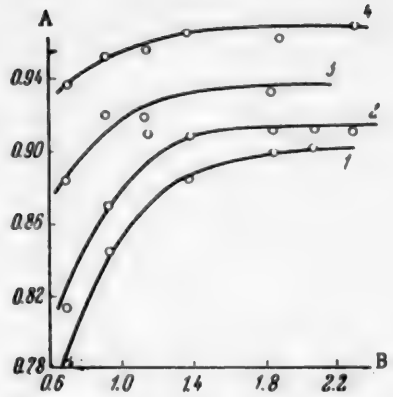

Fig. 4. Effect of gas velocity on plate efficiency: A) η; B) gas velocity (m/second); weir height h (mm): 1) 0, 2) 10, 3) 25, 4) 40.

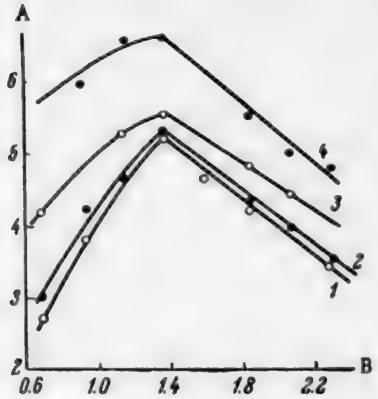

Fig. 5. Effect of gas velocity on k_La/P: A) k_La/P; B) gas velocity (m/second); weir height h (mm): 1) 0, 2) 10, 3) 25, 4) 40.

TABLE

Performance Characteristics of 4-14 and 4-10 Plates

Characteristics	4−14	4−10			
		weir height h_w (mm)			
		0	10	25	40
k_La (m/hour)	324	215	244	290	381
P (mm H_2O)	52	41	46	52	58
k_La/P	6.23	5.25	5.3	5.58	6.57
η	0.928	0.885	0.916	0.916	0.966

liquid layer on the plate. If these data are plotted in logarithmic coordinates, a series of straight lines of the same slope (about 0.13) is obtained; this gives the relationship between plate resistance P and weir height.

$$P = C_1 h_w^{0.13},$$

where C_1 is a proportionality factor which incorporates the influence of all the other factors.

The dash line (Fig. 2) represents the resistance of the gas−liquid layer at h_w = 25 mm. This shows that the resistance of the gas−liquid layer, equal to the difference between the total resistance and the resistance of the dry plate, remains unchanged with increase of the gas velocity. The same is found with other amounts of liquid on the plate.

It has been reported [14] that the efficiency of a perforated plate increases with increase of weir height, but increase of this height above 25 mm is not accompanied by a further increase of the enrichment coefficient. This conclusion was not confirmed by our experiments. As Fig. 3 shows, k_La increased continously with increase of weir height. Curve 1, for the same plate without a weir, is given for comparison in the same graph.

All the curves are similar in character. Up to gas velocities w_f from 1.3 to 1.4 m/second k_La gradually increases with gas velocity. This is because in this range, as was noted earlier, not the whole area of the plate

is operating, clear liquid is present and liquid partially falls through the perforations. With increase of gas velocity the bubbling zone extends over a larger plate area, the leakage diminishes, and $k_L a$ increases accordingly. When the leakage limit has been reached, the mass-transfer coefficient on the plate is no longer influenced by variations of gas velocity in the column, regardless of weir height.

Plots of these data in logarithmic coordinates give two straight lines of different slope; the dependence of $k_L a$ on weir height can therefore be represented by the following equations:

$$k_L a = C_2 h_w^{0.42} \quad (w_f < 1.3 \text{ m/sec}),$$
$$k_L a = C_3 h_w^{0.3} \quad (w_f > 1.3 \text{ m/sec}).$$

Therefore even in these experiments, carried out higher values of h_0, we did not obtain the mobile foam which, according to Pozin, Mukhlenov, et al. [6], is the best mass-transfer medium. Neither did we observe an increase in the height of the gas–liquid layer with increase of the gas rate. Since the mass-transfer coefficient does not change at gas velocities over 1.3 - 1.4 m/second, it follows that under the given conditions there is no increase in the turbulence of this layer. These experiments therefore also confirmed the earlier conclusion [7, 10] that mass transfer through the liquid phase is not intensified by increase of gas velocity if the plate is not operating under the cellular-foam regime.

The differences between the results obtained in experiments on hydrodynamics and mass transfer at high gas velocities in perforated plates can be attributed to certain differences of plate design. The dimensions of the overflow orifice have the greatest influence. In our experiments the plates were provided with overflow orifices which allowed free overflow of the gas–liquid layer. The amount of liquid on them did not change with increase of the gas rate, and therefore there was no increase of the foam layer. The experiments of Pozin, Mukhlenov, et al. were carried out, as was pointed out by one of us [11, 12], with restricted overflow. There was holdup of foam at the overflow orifice, and with increase of the gas velocity this favored accumulation of liquid on the plate, i.e., it led to increases of h_0 and of the foam layer. This is characteristic of plates of the "Turbogrid" type designed without overflow orifices. On these plates the height of the foam layer and therefore the mass-transfer coefficient increases continuously with the gas rate.

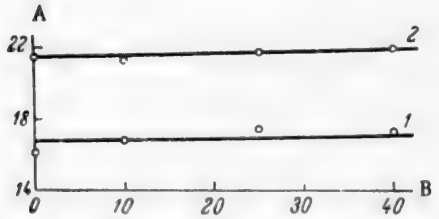

Fig. 6. Effect of weir height on $k_G a$: A) $k_G a$ (kg/m^2 · hr. mm Hg); B) weir height (mm); gas velocity in column, w_f (m/second): 1) 1.38; 2) 2.08.

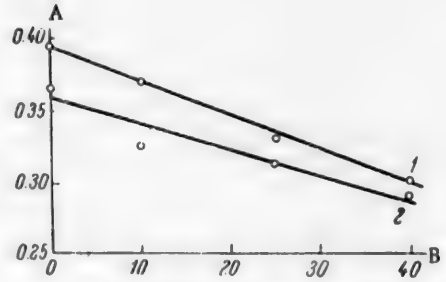

Fig. 7. Effect of weir height on $k_G a/P$: A) $k_G a/P$; B) weir height (mm); gas velocity in column, w_f (m/second): 1) 1.38; 2) 2.08.

In addition to the mass-transfer coefficients $k_L a$ the plate efficiencies were determined experimentally. The efficiency was calculated from the differences between the equilibrium oxygen concentration (c^*, kg/m^3) and the concentration before the plate (c_i, kg/m^3) and after the plate (c_f, kg/m^3) respectively, by means of the formula

$$\eta = \frac{c_i - c_f}{c_i - c^*}.$$

The effect of gas velocity on plate efficiency is shown graphically in Fig. 4. It follows from these results that the plate efficiency varies with the gas rate analogously to k_La., i.e., it increases at first, and at w_f above 1.3 m/second it is independent of the gas velocity. Plate efficiency increases with increase of the wier height (with increase of h_θ). In the region of uniform operation (at gas velocities above 1.3 m/second) the plate efficiency is proportional to the mass-transfer coefficient

$$\eta = Ak_L a.$$

here A is a proportionality factor which depends on h_θ.

It was stated earlier that in desorption of sparingly soluble gases, perforated plates are most effective at gas velocities corresponding to the maximum height of the cellular foam layer. A cellular foam was not formed on the plate tested, and therefore the question of the gas velocity at which the plate operates at the highest efficiency can be examined with reference to the ratio of the mass-transfer coefficient to the plate resistance, k_La/P. Relevant data are presented in Fig. 5. It is seen that the higher the weir, the greater the plate efficiency. The value of k_La/P passes through a maximum with variation of the gas velocity. This maximum is found at a gas velocity close to the limit at which the liquid falls through the plate perforations, for all weir heights. Therefore this gas velocity is the most advantageous with regard to mass transfer.

To determine at what amounts of liquid on the plate the rate of mass transfer is the same in presence of cellular foam as in presence of gas streams and spray, 4-10 and 4-14 plates were compared. A cellular foam is formed on a 4-14 plate (open section 7.4%) but not on a 4-10 plate. The results of the comparison are given in the table. The characteristics for the 4-10 plate were determined with different weir heights, and for the 4-14 plate without a weir. The experimental data for both plates refer to gas velocities at which the maximum effect was obtained. This velocity is 0.92 m/second for the 4-14 plate. At this velocity the cellular foam layer is at a maximum [10]. The characteristics for the 4-10 plate are reduced to $w_f \simeq 1.4$ m/second in all cases. The experimental data were all determined at the same liquid rate L = 23.5 m^3/m·hour.

Comparison of the characteristics of the plates with the same amounts of liquid on them (i.e., at $h_w = 0$) shows that mass transfer is more intensive in presence of cellular foam. Increase of weir height is accompanied by increase of h_θ, which leads to increase of the gas–liquid layer on the plate, and therefore to increase of k_La, P, η, and k_La/P. At $h_w = 40$ mm the amount of liquid on the 4-10 plate is approximately double that on the 4-14 plate. Under these conditions the 4-10 plate is somewhat more effective. This means that with plates on which cellular foam is not formed it is necessary to operate at higher values of h_θ to attain the same efficiency.

Experimental values of k_Ga for the evaporation of water, determined at different baffle heights, are plotted in Fig. 6. The experiments were performed at two gas velocities, 1.38 and 2.08 m/second. It follows from these results that k_Ga is almost independent of weir height, i.e., of the amount of liquid on the plate. Consequently, the ratio k_Ga/P decreases with increasing weir height (with increasing h_θ) (Fig. 7). This means that for processes determined by the resistance of the gas phase it is more advantageous from the economical standpoint to use plates without weirs, i.e., to operate with small amounts of liquid on the plate.

SUMMARY

1. The liquid fall-through limit, leakage, and plate resistance were determined in hydrodynamic tests; the bubbling process is described. No cellular foam was formed at any values of h_w.

At gas velocities up to 1.3-1.4 m/second the plate performs nonuniformly. At $w_f > 1.4$ m/second the height of the gas–liquid layer is independent of the gas rate.

2. At all values of h_w the transfer coefficient k_La increases with the gas rate at first, but at gas velocities above 1.4 m/second it is independent of the gas rate. The plate efficiency varies similarly. It was demonstrated once again that mass transfer in the liquid phase is not intensified by increase of gas velocity if the plate is not operating under cellular-foam conditions.

3. Under conditions of uniform plate operation the coefficient k_La is proportional to the height of the weir raised to the power 0.42. The coefficient k_Ga is independent of weir height.

4. For processes controlled by resistance in the liquid phase, the efficiency is greatest with large amounts of liquid on the plate. For processes controlled by resistance of the gas phase, it is more advantageous economically to use plates without weirs, i.e., to operate with small amounts of liquid.

LITERATURE CITED

[1] V. N. Stabnikov and S. E. Kharin, Theoretical Principles of Alcohol Distillation and Rectification [in Russian] (Food Ind. Press, 1951).

[2] E. Kirschbaum, Destillierund Rektifiziertechnik, Berlin (1950).

[3] N. M. Zhavoronkov and I. É. Furmer, Oxygen 5, 9 (1947).

[4] L. S. Aksel'rod and G. M. Yusova, Oxygen 4, 1 (1950).

[5] L. S. Aksel'rod and V. V. Dil'man, J. Appl. Chem. 1, 28 (1954).*

[6] M. E. Pozin, I. P. Mukhlenov, E. S. Tumarkina, and É. A. Tarat, The Foam Method for Treatment of Gases and Liquids [in Russian] (Goskhimizdat, 1955).

[7] I. N. Kuz'minykh, L. S. Aksel'rod, Zh. A. Koval', and A. I. Rodionov, Chem. Ind. 2, 22 (1954).

[8] I. N. Kuz'minykh and A. I. Rodionov, Trans. MKhTI 18, 109 (1954).

[9] I. P. Mukhlenov, Doctorate Dissertation [in Russian] (Lensoviet Technol. Inst. Leningrad, 1955).

[10] I. P. Mukhlenov, J. Appl. Chem. 31, No. 4, 45 (1958).*

[11] I. N. Kuz'minykh and Zh. A. Koval', J. Appl. Chem. 28, No. 1, 21 (1955).*

[12] I. N. Kuz'minykh and A. I. Rodionov, J. Appl. Chem. 29, No. 9, 1330 (1956).*

[13] Kamei, Takamatsu, and Yamada, Chem. Engng. (Tokyo) 18, 10, 467 (1954).

[14] G. Volland, Chem. Fabrik, 8, 1–2, 6, (1935); Beiheft Verfahrenstechnik, 9 (1935).

Received April 12, 1958

*Original Russian pagination. See C. B. Translation.

NEW CALCULATION METHOD FOR HEAT-TRANSFER EQUIPMENT

I. S. Pavlushenko

The Lensoviet Technological Institute, Leningrad

In an analysis of the free motion of individual particles in a stationary unlimited medium [1], it was shown that the "resistance coefficient" ψ may be eliminated from equations describing the effect, and that the concept of this coefficient is to some extent formal.

Later, in a discussion of methods for determination of frictional losses of pressure in a liquid moving through a pipe [2], it was shown that the "resistance coefficient" λ can also be eliminated from the calculation formulas, and that its use should now be abandoned.

The generalized equations and graphs given in these papers can be used for very simple determinations of sedimentation velocities (and particle diameters) or pressure losses due to friction and are, in our opinion, the most general in character.

There appears to be no objection to the postulate that an equation describing a phenomenon should not contain a coefficient which is a function of the basic quantities which determine the development of the phenomenon as a whole. This principle should prove of practical utility not only in considerations of hydrodynamic effects but also in other cases.

As a further example, we consider the representation of heat transfer and methods of engineering calculations relating to it.

The relationship between the quantity of heat transferred from a medium to a wall (or vice versa), the heat-transfer area and the temperature difference is usually represented by the well-known Newton equation

$$Q = \alpha \cdot \Delta t \cdot F \text{ kcal/hour} \qquad (1)$$

The heat-transfer coefficient α, which is a measure of the rate of heat transfer, depends on the temperature difference and a number of other variables which determine the process as a whole. This coefficient, like all other analogous coefficients, is unnecessary for description of the process. Therefore, it may be eliminated from the calculation formulas and the required quantity (quantity of heat, or heat-transfer area) may be correlated directly with the parameters which determine its value. Such a relationship may easily be established on the following principle: since, for example, the heat-transfer coefficient for geometrically similar systems depends [3] on the temperature of the medium $\underline{t}$, the temperature difference between the medium and the wall, Δt *, the thermal conductivity λ, the heat capacity $\underline{c}$, viscosity μ, and density ρ of the medium, its velocity $\underline{w}$, the determining geometrical dimension $\underline{d}$, and the acceleration due to gravity $\underline{g}$, i.e., $\alpha = f(t, \Delta t, \lambda, c, \mu, \rho, w, d, g)$, it follows that

$$Q = f(F, t, \Delta t, \lambda, c, \mu, \rho, w, d, g). \qquad (2)$$

* For a fixed temperature of the medium, the wall temperature can be defined in terms of the temperature difference, as $t_w = t \pm \Delta t$.

Expansion of the functional relationship (2) by means of dimensional analysis gives

$$\left(\frac{F}{d^2}\right)=C\cdot\left(\frac{Q}{t\cdot\lambda\cdot d}\right)^a\cdot\left(\frac{c\cdot\mu\cdot g}{\lambda}\right)^b\cdot\left(\frac{d^3\cdot\rho^2\cdot g}{\mu^2}\right)^e\cdot\left(\frac{w^2}{g\cdot d}\right)^f\cdot\left(\frac{\Delta t}{t}\right)^h \tag{3}$$

or, in contracted form

$$K_F=C\cdot K_t^a\cdot Pr^b\cdot Ga^e\cdot Fr^f\cdot S_{\Delta t}^h. \tag{3a}$$

To determine the value of the coefficient C and of the indices a, b, e, f, and h in Equation (3), we correlate it with the Newton equation (1) and, for turbulent flow of the medium, with the criterial relationship

$$Nu=0.023\cdot Re^{0.8}\cdot Pr^{0.4}.$$

If these equations are written in similar form

$$F=C\cdot Q^a\cdot t^{-a-h}\cdot\Delta t^h\cdot\lambda^{-a-b}\cdot c^b\cdot\mu^{b-2e}\cdot\rho^{2e}\cdot w^{2f}\cdot d^{2-a+3e-f}\cdot g^{b+e-f}$$

and

$$F=\frac{1}{0.023}\cdot Q\cdot\Delta t^{-1}\cdot\lambda^{-0.8}c^{-0.4}\cdot\mu^{0.4}\cdot\rho^{-0.8}\cdot w^{-0.8}\cdot d^{0.2}\cdot g^{-0.4},$$

it is easily found that C = 43.5, a = 1, h = − 1, b = e = f = − 0.4. Therefore, for turbulent flow of the medium (Re > 10,000)

$$K_F=43.5\cdot K_t\cdot(Pr\cdot Ga\cdot Fr)^{-0.4}S_{\Delta t}^{-1}$$

or

$$K_F=43.5\cdot K_{\Delta t}\cdot(Pr\cdot Re^2)^{-0.4}, \tag{4}$$

where

$$K_{\Delta t}=\frac{Q}{\Delta t\cdot\lambda\cdot d}\cdot$$

Evidently the same result may be obtained directly from the Newton equation and the criterial equation by elimination of α.

Here we have

$$\alpha=\frac{Q}{\Delta t\cdot F}$$

and

$$\alpha=0.023\cdot\frac{\lambda}{d}\cdot(Pr\cdot Re^2)^{0.4},$$

Hence

$$\frac{Q}{\Delta t\cdot F}=0.023\cdot\frac{\lambda}{d}\cdot(Pr\cdot Re^2)^{0.4}$$

or

$$\frac{F}{d^2} = 43.5 \cdot \frac{Q}{\Delta t \cdot \lambda \cdot d} \cdot (Pr \cdot Re^2)^{-0.4},$$

i.e., we obtain Equation (4)*.

For engineering calculations, Equation (4) is more conveniently written in the form

$$F = \frac{43.5 \cdot Q \cdot d}{\lambda} \cdot (Pr \cdot Re^2)^{-0.4} \cdot \frac{1}{\Delta t}. \qquad (4a)$$

Calculation formulas for other typical examples of heat transfer can be derived from the Newton equation in conjunction with the corresponding equations.

For streamline flow of the medium (Re < 2300) along a horizontal duct [4], from the equation

$$Nu = 0.74 \cdot Pr^{0.3} \cdot Re^{0.2} \cdot Gr^{0.1},$$

we have

$$K = 1.35 \cdot K_{\Delta t} \cdot Pr^{-0.3} \cdot Re^{-0.2} \cdot Gr^{-0.1} \qquad (5)$$

or solving for the heat-transfer area,

$$F = \frac{1.07 \cdot Q \cdot d^{0.7}}{\lambda} \cdot \left(\frac{\nu^2}{\beta}\right)^{0.1} \cdot (Pr^{1/3} \cdot Re^{1/3})^{-0.8} \cdot \frac{1}{\Delta t^{1.1}}. \qquad (5a)$$

If the pipe is vertical and the forced and free flows are unidirectional, the numerical coefficient of this equation is 1.27; for counterflow it is 0.955.

$$Nu = k \cdot (Gr \cdot Pr)^m,$$

we have

$$K_F = C \cdot K_{\Delta t} \cdot (Pr \cdot Gr)^n. \qquad (6)$$

The values of the coefficient C and index n depend on the product Pr·Gr:

of	$Pr \cdot Gr < 5.10^2$,	then $C = 0.85$ and	$n = -1/8$;
of	$Pr \cdot Gr = 5.10^2 - 2.10^7$,	then $C = 1.85$ and	$n = -1/4$;
of	$Pr \cdot Gr > 2.10^7$,	then $C = 7.4$ and	$n = -1/3$.

For the boiling of water [3], from the equation

$$\alpha = 39 \cdot \Delta t^{2.33} \cdot p^{0.5},$$

* The temperature ratio is eliminated from Equation (4), as Equation (3) is correlated with an equation in which the ratio of the temperatures of the medium and wall is not taken into account. In general, however, the calculation formula should contain the ratio $(\Delta t / t)$ or (t_w/t) because, according to recent results, the equation for turbulent flow [3] includes the term $(Pr/Pr_w)^{0.25}$, which is numerically little different from $(t_w/t)^{0.25}$.

we have

$$F = \frac{Q}{39 \cdot p^{0.5}} \cdot \frac{1}{\Delta t^{3.33}} . \qquad (7)$$

For condensation of steam [3], from the criterial form of the Nusselt equation

$$Nu = k \cdot (Pr \cdot Ga \cdot Ku)^{1/4},$$

we have

$$K_F = C \cdot K_{\Delta t} \cdot (Pr \cdot Ga \cdot Ku)^{-1/4} \qquad (8)$$

or, solving for the heat-transfer area,

$$F = C \cdot Q \cdot \left(\frac{\mu \cdot l}{\lambda^3 \cdot \gamma^2 \cdot r}\right)^{1/4} \cdot \frac{1}{\Delta t^{3/4}} . \qquad (8a*)$$

For horizontal pipes C = 14 and l = d (pipe diameter); for vertical pipes and plates C = 0.87 and l = h (height of pipe or plate).

All the existing equations for other instances of heat transfer, such as transverse flow around a bundle of pipes, transfer in stirred tanks, etc., can be transformed equally simply.

As an illustration, the proposed and the usual calculation methods may be compared by solution of a problem set by Pavlov, Romankov, and Noskov [4].

" Find . . . the surface area of a vertical tube condenser needed for condensation of 240 kg of saturated benzene vapor per hour at atmospheric pressure. Liquid benzene is removed from the apparatus at the condensation temperature. The condenser is made of steel pipes 38 × 2.5 in diameter. The benzene condenses in the spaces between the pipes, the cooling water passes upward along the pipes at a velocity of 0.011 m/second and is heated from 14 to 35°. The thermal resistance of rust and scale is to be taken into account."

Solution.

1. The temperature conditions can be represented schematically:

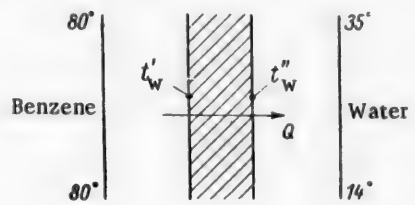

2. The heat flow is

$$Q = G \cdot r = 240 \cdot 94.5 = 2.27 \cdot 10^4 \text{ kcal/hour}$$

3. The average temperature of the water is

$$t_{wt} = \frac{14 + 35}{2} = 24.5°.$$

*The time dimension of viscosity in Equations (8) and (8a) is in hours.

4. The water flow rate is

$$G_{wr} = \frac{Q}{t_f - t_i} = \frac{2.27 \cdot 10^4}{35 - 14} = 1080 \text{ kg/hr} = 1.08 \text{ m}^3/\text{hour}.$$

5. The thermal resistance of the wall is

$$R = r_{rust} + r_w + r_{sc\ k} = 0.0005 + \frac{0.0025}{40} + 0.0003 = 8.6 \cdot 10^{-4} \text{ m}^2 \cdot \text{hr} \cdot {}^\circ\text{C/kcal}.$$

6. The total cross-sectional area of the pipes is

$$S = \frac{V_{sec}}{w} = \frac{1.08}{3600 \cdot 0.011} = 0.027 \text{ m}^2.$$

7. The number of pipes required is

$$n = \frac{S}{0.785 \cdot d^2} = \frac{0.027}{0.785 \cdot 0.033^2} = 32.$$

8. The effective height of the pipes is taken to be (with a subsequent check) h = 0.62 m.

9. The wall temperature on the benzene side is taken (as the result of preliminary trial) to be $t'_w = 72.3°$.

10. The temperature difference and the film temperature on the benzene side are

$$\Delta t_b = 80 - 72.3 = 7.7° \text{ and } t'_{fm} = \frac{80 + 72.3}{2} = 76.15°.$$

11. Calculation Formula (8a) for vapor condensation

$$F = C \cdot Q \cdot \left(\frac{\mu \cdot h}{\lambda^3 \cdot \gamma^2 \cdot r}\right)^{1/4} \cdot \frac{1}{\Delta t^{3/4}},$$

where C = 0.87.

12. The constants of benzene are

$$\lambda = 0.12 \frac{\text{kcal}}{\text{m} \cdot \text{hr} \cdot {}^\circ\text{C}}; \quad \mu = 0.35 \text{ cent.} \quad \gamma = 900 \text{ kg/m}^3.$$

13. $$F_b = 0.87 \cdot 2.27 \cdot 10^4 \cdot \left(\frac{\frac{0.35}{9810 \cdot 3600} \cdot 0.62}{0.125 \cdot 900^2 \cdot 94.5}\right)^{1/4} \cdot \frac{1}{7.7^{3/4}} = 2.02 \text{ m}^2.$$

14. The wall temperature on the water side is

$$t'_w - t''_w = \frac{Q \cdot R}{F} = \frac{2.27 \cdot 10^4 \cdot 8.6 \cdot 10^{-4}}{2.02} = 9.7°,$$

$$t''_w = 72.3 - 9.7 = 62.6°.$$

15. The temperature difference and the film temperature on the water side are

$$\Delta t_{wr} = 62.6 - 24.5 = 38.1°; \quad t''_{fm} = \frac{62.6 + 24.5}{2} = 43.5°.$$

16. The flow of water, since

$$Re = \frac{w \cdot d}{\nu} = \frac{0.011 \cdot 0.033}{6.15 \cdot 10^{-7}} = 590 \text{ — streamline,}$$

where

$$\nu = \frac{\mu \cdot 9.81}{9810 \cdot 1000} = \mu \cdot 10^{-6} = 6.15 \cdot 10^{-7} \text{ m}^2/\text{second.}$$

17. Formula (5a) becomes

$$F = \frac{1.27 \cdot Q \cdot d^{0.7}}{\lambda} \cdot \left(\frac{\nu^2}{\beta}\right)^{0.1} \cdot (Pr^{1/3} \cdot Re^{1/3})^{-0.6} \cdot \frac{1}{\Delta t^{1.1}}.$$

(C = 1.27, as the directions of free and forced flow coincide).

18. The constants of water are

$$\lambda = 0.55 \ \frac{\text{kcal}}{\text{m} \cdot \text{hr.} \cdot {}^\circ\text{C}}: \quad \beta = 4.14 \cdot 10^{-4} \ 1/{}^\circ\text{C}; \quad Pr = 4.05.$$

19.

$$F_{wr} = \frac{1.27 \cdot 2.27 \cdot 10^4 \cdot 0.033^{0.7}}{0.55} \cdot \left[\frac{(6.15 \cdot 10^{-7})^2}{4.14 \cdot 10^{-4}}\right]^{0.1} \cdot$$
$$\cdot (4.05^{1/3} \cdot 590^{1/3})^{-0.6} \cdot \frac{1}{38.1^{1.1}} = 2.02 \text{ m}^2,$$

i.e., $F_b = F_{wr}$, so that the wall temperature was chosen correctly.

20. The pipe height is

$$h = \frac{F}{\pi \cdot d \cdot n} = \frac{2.02}{3.14 \cdot 0.033 \cdot 32} = 0.61 \text{ m},$$

which virtually coincides with the assumed value.

Since there is an established technique for heat-transfer calculations (in particular , various nomograms are used to simplify technical operations), whereas the proposed method for calculation of the heat-transfer area shortens calculations only slightly (the only steps eliminated are determinations of heat loss from values of the Nusselt criterion, the coefficient of heat transfer, and heat flow) the question may arise whether these recommendations are of value.

In this connection it is necessary to emphasize the essential differences of principle between the proposed and the existing method. Elimination of the coefficient (in this instance the heat-transfer coefficient) which is a function of the determining quantities makes it possible to describe the process more rigidly and to approach analysis of different phenomena from a unified standpoint. We consider that on these grounds the new calculation method is preferable.

In conclusion it must be pointed out that the proposed method may prove especially useful for correlation of experimental data and development of calculation methods relating to mass-transfer equipment.

LITERATURE CITED

[1] I. S. Pavlushenko, J. Appl. Chem. 28, 885-898 (1956).*

[2] I. S. Pavlushenko and É. R. Polishchuk, Trans. Lensoviet Technol. Inst. Leningrad, 39 Goskhimizdat, 1957) pp. 204-215.

*Original Russian pagination. See C. B. Translation.

[3] M. A. Mikheev, Fundamentals of Heat Transfer, 3rd edn. [in Russian] Gosenergoizdat, 1956).

[4] K. F. Pavlov, P. G. Romankov, and A. A. Noskov, Examples and Problems for a Course on Processes and Equipment in Chemical Technology, 3rd edn. [in Russian] (Goskhimizdat, 1955) pp.178-181.

Received February 28, 1958

HEAT TRANSFER FROM A FLUIDIZED CATALYST BED TO A HEAT-TRANSFER SURFACE •

I. P. Mukhlenov, D. G. Traber, V. B. Sarkits and T. P. Bondarchuk

The Lensoviet Technological Institute, Leningrad

The use of fluidized beds in heterogeneous conversions is a very effective means of intensifying various technological processes [1].

The use of fluidized catalyst beds for carrying out catalytic processes eliminates the principal factors which restrict the rate of many catalytic conversions and makes it possible to increase considerably the output rate of the equipment used for such processes [2, 3].

Several papers by foreign and Soviet authors deal with heat transfer in fluidized beds of granular materials [4-10].

The data of different authors on the influence of various factors on heat transfer from a fluidized bed to a heat-transfer surface are contradictory, while their proposed empirical formulas are not generally applicable. Their applicability is confined to narrow ranges of experimental conditions.

Further studies are therefore needed in relation to the changes which are introduced by these new hydrodynamic conditions into the mechanism and kinetics of mass and heat transfer.

In contrast to a filtering (quiescent) bed, in which the effective thermal conductivity (λ) and coefficient of heat transfer to the surface (α) are not large (for example, in the contact oxidation of sulfur dioxide over a vanadium catalyst λ = 0.6 kcal/m·hour·degree and α = 6-9 kcal/m^2·hour·degree), the temperature within a fluidized catalyst bed is rapidly equalized owing to the continuous motion of the solid particles, which are the main heat carriers, and heat transfer from the bed to the heat-transfer surface is greatly intensified. According to our data, the coefficient of heat transfer (α) from a fluidized bed of vanadium catalyst with particles 0.38 mm in size increases to 220 kcal/m^2·hour·degree at a gas velocity of 0.3 m/second.

Studies of the mechanism of heat transfer in a fluidized bed and of the influence of the hydrodynamic process conditions on heat transfer between a fluidized bed and a heat-transfer surface enabled us to determine the relationship between α and the gas velocity (w). This relationship is illustrated by a typical curve in Fig. 1. From the instant at which the filtering bed becomes fluidized, increase of gas velocity first causes a relatively slight expansion of the bed and a considerable increase in the pulsation velocities of the catalyst particles, and therefore the heat-transfer coefficient should increase with the gas velocity. However, on further increase of the gas velocity the bed undergoes progressive expansion accompanied, according to O. M. Todes et al. [1], by a decrease of the pulsation velocities of the solid particles. This leads to a decrease of the heat-transfer coefficient. Thus, the resultant influence of various factors during increase of the gas velocity causes α to reach a maximum at a certain gas velocity. When the critical velocity corresponding to the formation of a two-phase stream (transport of solid particles from the apparatus) is reached, the heat-transfer coefficient should fall to a level corresponding to heat transfer from the gas to the heat-transfer surface.

• Communication I.

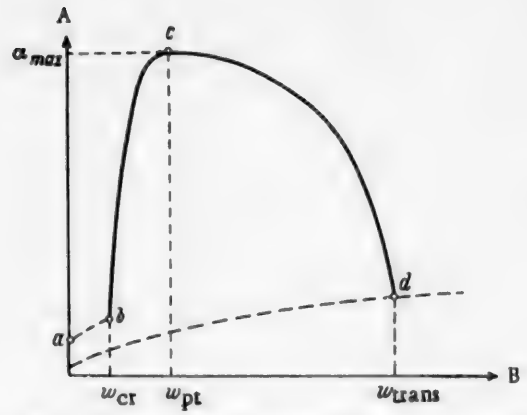

Fig. 1. Effect of gas velocity on the coefficient of heat transfer from a fluidized bed to a heat-transfer surface: A) heat-transfer coefficient α; B) gas velocity $\underline{w}$; heat transfer: ab) in a filtering bed; bcd) in a fluidized bed; me) in equipment without solid phase (without change in the flow regime).

Thus the gas velocity (w) has a decisive influence on the coefficient of heat transfer. It is evident (Fig. 1) that in order to attain maximum heat transfer (α_{max}) the process must be conducted in a fluidized bed at a definite gas velocity (w_{opt}). Moreover, the values of α_{max} and w_{opt} depend on the physical, thermal, and geometrical characteristics of the bed.

Therefore, in the general case:

$$\alpha = \varphi(w, \mu, \rho_g, \lambda_g, c_g, d, f, \rho_s, c_s, \lambda_s, g, D, H_0, t_w, t_b), \quad (1)$$

where: $\underline{w}$, μ, ρ_g, λ_g, c_g are respectively the velocity, viscosity, density, thermal conductivity, and specific heat of the gas; d, f, ρ_s, c_s, λ_s, g are respectively the size, shape and surface factor, density, specific heat, thermal conductivity, and gravitational acceleration of the solid particles; D, H_0, and t_b are, respectively, the diameter, initial height, and temperature of the bed; t_w is the temperature of the heat-transfer surface.

In view of the fact that (according to literature data) the effect of the thermal conductivity of the solid particles is slight, with the aid of dimensional analysis, Equation (1) may be written in the form

$$Nu = c \cdot Re^a \cdot Fr^b \cdot Pr^c \cdot \left(\frac{\rho_s}{\rho_g}\right)^d \cdot \left(\frac{c_s}{c_g}\right)^e \cdot \left(\frac{t_s}{t_w}\right)^f \cdot \left(\frac{D}{d}\right)^g \cdot \left(\frac{H_0}{d}\right)^h \cdot f^i, \quad (2)$$

where $Nu = \alpha \cdot d / \lambda_g$ is the Nusselt group, $Re = w \cdot d \cdot \rho_g / \mu$ is the Reynolds group, $Fr = d \cdot g / w^2$ is the Froude group, $Pr = \mu \cdot c_g \cdot g / \lambda_g$ is the Prandtl group, and f is a dimensionless factor representing the form and state of the surface.

The indices of the groups and ratios in Equation (2) must be determined experimentally. The present communication contains data on the influence of gas velocity and size of the catalyst particles on heat transfer from a fluidized bed to a heat-transfer surface.

EXPERIMENTAL

The apparatus and the temperature measurement scheme are illustrated in Fig. 2 (a and b).

A quartz tube 1, 49 mm in internal diameter and 1 m long, heated by means of the coil 2, contained the catalyst 3. The catalyst bed contained a spiral copper condenser 4, with a tube 4 mm in diameter and a coil diameter of 20 mm. Air was forced by the blower 5 through the catalyst bed and passed into the atmosphere through the trap 6. Water was fed into the condenser from the header 7 through the orifice meter 8 and air-bubble trap 9, and collected during the experiment in the receiver 10 for exact measurement. The average water feed rate was 15 liters/hour. The water temperature at entry into the condenser t_1 and at the exit t_2 was measured by means of the thermocouples 11 connected to the potentiometer 12; it varied from 10-24° to 17-57°, respectively. The bed temperatures T_1 and T_2, near the lower and upper ends of the spiral, respectively, were measured by means of the thermocouples 13, connected to a millivoltmeter 14. In this series of experiments the bed temperature was maintained at about 140°.

The heat-transfer coefficient (K) was calculated from the equation

$$K = \frac{Q}{F \cdot \Delta t} \text{ [kcal/m}^2 \cdot \text{hr. degree]}. \quad (3)$$

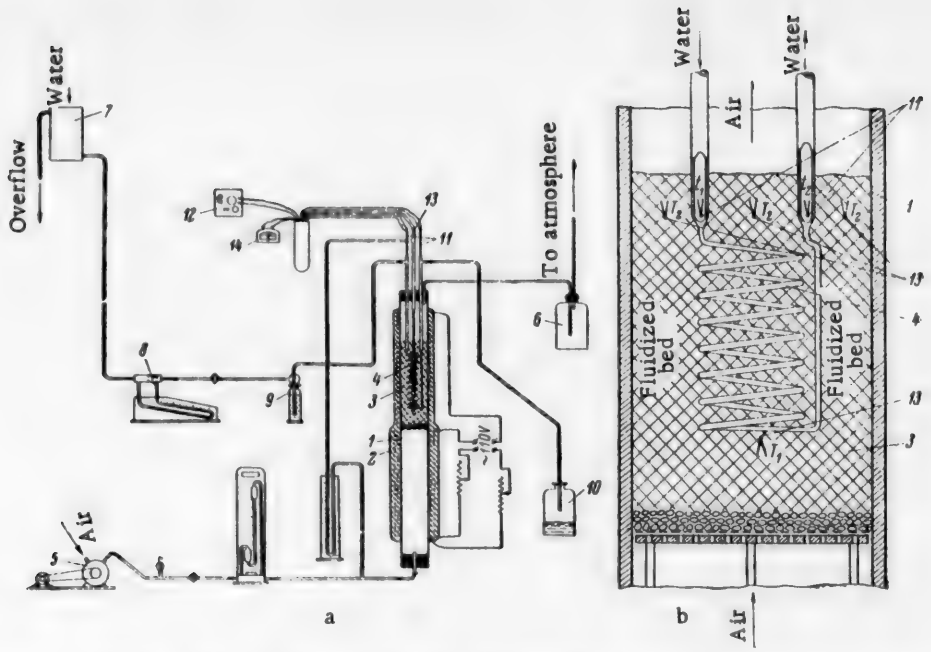

Fig. 2. Apparatus used (a) and temperature measurement scheme (b) for determination of heat-transfer coefficients in a fluidized bed: 1) quartz tube; 2) Nichrome coil; 3) catalyst; 4) condenser; 5) air blower; 6) trap; 7) header; 8) orifice meter; 9) Drechsel flask; 10) water receiver; 11 and 13) thermocouples; 12) potentiometer; 14) millivoltmeter.

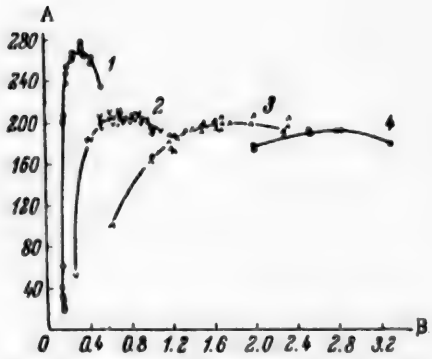

Fig. 3. Dependence of the heat-transfer coefficient on air velocity and particle size of the conversion catalyst: A) heat-transfer coefficient α (kcal/m^2·hour·degree); B) air velocity w (m/second); particle size (mm) 1) 0.38, 2) 0.75, 3) 1.5, 4) 2.5.

The quantity of heat which passed through the heat-transfer surface was determined from the change of the heat content of the water:

$$Q = V \cdot \gamma \cdot c \cdot (t_2 - t_1) \text{ [kcal/hr.]}. \qquad (4)$$

In Equations (3) and (4): F is the heat-transfer surface, equal to the surface area of the copper coil 0.0127 m^2;

$$\Delta t = \frac{(T_2 - t_1) - (T_1 - t_2)}{2.3 \lg \frac{T_2 - t_1}{T_1 - t_2}} \text{ [degrees]};$$

V is the water rate (liters/hour), γ is the density of water, 1 kg/liter; c is the specific heat of water, 1 kcal/kg·degree.

Calculations showed that because of the high thermal conductivity of the condenser walls and the high value of the coefficient of heat transfer from the condenser walls to the water flowing through the coil, the partial coefficients of heat transfer from the fluidized bed to the condenser wall may be assumed equal to the over-all coefficients of heat transfer determined experimentally.

The duration of each experiment was at least 15 minutes. Each experiment was repeated several times and the average results were taken.

The catalyst was prepared by crushing of the industrial catalyst followed by fractionation by sieving. The experiments were performed with BAV vanadium catalyst of average particle size d = 0.38 mm, and with catalyst used for water-gas conversion.

Characteristics of the conversion catalyst are given below.

Fraction on screen (mm)	Average particle size (mm)
−0.5+0.25	0.38
−1 +0.5	0.75
−2 +1	1.5
−3 +2	2.5

Bulk density (g/cc)	Density (g/cc)
0.842	2.84
0.895	2.84
0.948	2.84
0.954	2.84

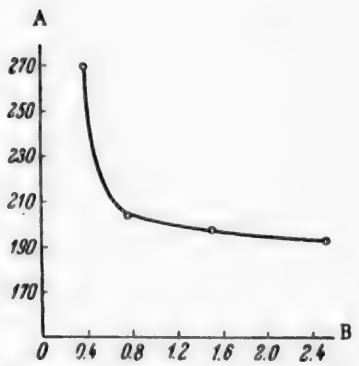

Fig. 4. Effect of particle size of the conversion catalyst on the maximum heat-transfer coefficient: A) heat-transfer coefficient α_{max} (kcal/m²·hour·degree); B) average particle size d_{av} (mm).

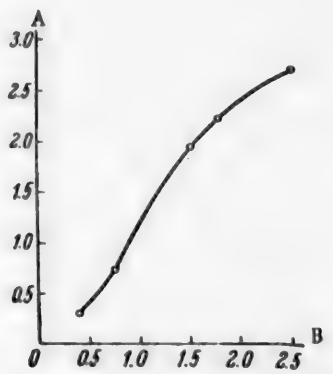

Fig. 5. Variation of the optimum gas velocity with particle size of the conversion catalyst: A) optimum velocity w_{opt} (m/second); B) average particle size d_{av} (mm).

The results of experiments on the effect of the size of the solid particles of the conversion catalyst are shown graphically in Fig. 3. The results are in good agreement with the foregoing considerations on the influence of hydrodynamic conditions on heat transfer in fluidized beds of granular materials. As was to be expected, the character of the relationship $\alpha = \varphi(w)$ is the same in all cases. However, smaller values of α_{max} and less pronounced maxima on the $\alpha = \varphi(w)$ curves are found with larger particles. The values of w_{opt} increase with particle size.

The average results obtained in over 260 experiments for the gas velocities and increases of bed height (represented by the ratio of the height of the fluidized bed H_b to the initial height H_0) corresponding to the maximum values α_{max} for heat transfer from the fluidized bed, for particles of various sizes, are given below.

d	0.38	0.75	1.5	2.5
α_{max}	270	205	198	193
w_{opt}	0.31	0.73	1.92	2.71
H_b/H_0	1.45	1.55	1.61	1.64

It should be noted that especially sharp decreases in the value of α_{max} with increase of particle size are found with the smallest particles ($d < 0.8$ mm). With particles of $d > 0.8$ mm, increase of their size results in only slight decreases of α_{max} (Fig. 4). The graph in Fig. 4 represents the dependence of the optimum gas velocity w_{opt} on particle size; the relationship $w_{opt} = \varphi(d)$ is found to be analogous in character to the relationship $w_f = \varphi(d)$ [3], where w_f is the gas velocity corresponding to fluidization of the bed.

The maximum value of the heat-transfer coefficient (α_{max}) corresponds to a relatively small value of fluidized-bed height, about $1.6 \cdot H_0$.

SUMMARY

1. When a bed of solid particles becomes fluidized the effective thermal conductivity of the bed and rate of heat transfer from the bed to the heat-transfer surface increase sharply.

2. Heat transfer from a fluidized bed to a heat-transfer surface depends on the hydrodynamical, geometrical, and thermal characteristics of the bed; the process may be represented by Equation (2).

3. As the gas velocity is increased, the coefficient of heat transfer from the fluidized bed increases sharply, reaches a maximum, and then decreases with further increase of gas velocity.

4. The values of the maximum heat-transfer coefficient are greater for smaller solid particles. The maximum heat-transfer coefficient decreases sharply on increase of particle size up to 0.8 mm. Further increases in the investigated range result in only slight decreases of the maximum heat-transfer coefficient. The maxima on the $\alpha = \varphi(w)$ curves become less pronounced with increase of particle size.

5. The maximum value of the heat-transfer coefficient corresponds to a fluidized-bed height approximately 1.6 times the height of the original bed.

LITERATURE CITED

[1] Summaries of Papers at the All-Union Technological Conference on Solid-Phase Heterogeneous Processes in Fluidized Beds [in Russian] (State Technology USSR, 1957).

[2] G. K. Boreskov and M. G. Slin'ko, J. Chem. Ind. 6 (1957).

[3] I. P. Mukhlenov, D. G. Traber, and E. S. Rumyantseva, J. Chem. Ind. 8 (1955).

[4] O. P. Agarwal and J. A. Storrow, Chem. and Ind. 69, 17 (1951).

[5] W. Brötz, Chem. Ing. Techn., 24, 2 (1952).

[6] W. M. Dow and M. Jakob, Chem. Eng. Progr. 47, 12 (1951).

[7] M. Leva, Chem. Eng. Progr. 45, 9 (1949); 48, 6 (1952).

[8] H. S. Mickley and C. A. Trilling, Ind. Eng. Chem. 41, 6 (1949).

[9] A. Baerg, J. Klassen and P. E. Gishler, Can. J. Res., 28F, 8 (1950).

[10] J. R. Campbell and F. Rumford, J. Soc. Chem. Ind. 69, 12 (1950).

Received February 14, 1958

ELECTROLYSIS OF SODIUM ZINCATE SOLUTIONS

V. V. Stender and M. D. Zholudev

Electrolysis of zincate solutions is of practical importance not only in the application of protective coatings but also in the production of metallic zinc. With the alkaline process it is possible to use steel equipment, to utilize oxidized zinc-containing materials, and to apply automation to the discharge of the cathodic metal which is obtained in powder form.

Industrial electrolysis of zincate solutions was first effected in a small unit for the production of zinc dust [1, 2], which was used for organic syntheses.

In 1948, after preliminary studies, an alkaline hydroelectrometallurgical process for conversion of oxidized zinc ores and materials was proposed [3].

Pilot-scale trials of the production of spongy zinc by electrolysis of zincate solutions at high current densities were successfully carried out by Morgan [4] and by Baroch et al. [5]. Fedot'ev and Khad'mash [6] and Rutkowski and Winsch [7] developed the technology of the alkaline method for extraction of zinc from wastes. Other workers [8-10] have also studied alkaline leaching of zinc ores and concentrates with subsequent alkaline electrolysis.

The growing interest in alkaline processes in zinc technology prompted us to study certain problems associated with the electrolysis of zincate solutions.

The diffusion coefficients, viscosities, and densities of sodium zincate solutions were determined [11].

In further studies [12] the limits for formation of compact and loose zinc deposits on rotating cathodes were determined. An important peculiarity of the electrolysis of zincate solutions is the formation of spongy deposits on stationary cathodes even at low current densities.

The cause of electrolytic deposition of metals in spongy form still remains a controversial topic. The formation of spongy deposits on the cathode is attributed to the loosening effect of the hydrogen liberated together with the metal [13, 14], or to formation and subsequent decomposition of hydrides [15], or adsorption and precipitation of hydroxides and basic salts on the growing crystals [16-19], or, finally, to discharge of complex ions [20]. Loshkarev et al. [21] demonstrated quantitatively that formation of spongy deposits is associated with decreasing concentration of the discharging ions in the catholyte film on increase of current density up to the limiting diffusion current.

According to Kudryavtsev [22], the formation of spongy zinc on the cathode at low current densities is due to the so-called "ultramicrons" of zinc, which are transferred to the cathode by cataphoresis and deposited on it, giving rise to random crystal growth. Flerov [23] holds a similar opinion, but considers that, in addition to the "ultramicrons," sponge formation is caused also by colloidal zinc oxide particles which are transferred to the cathode by cataphoresis, become embedded in the deposit, and prevent regular growth of the zinc crystals.

We consider that the above concepts are not yet adequately justified, and offer another explanation of the effect: in our view, the cause of sponge formation in electrolysis of zincate solutions lies in the nature of the particles discharging at the cathode.

The nature of the particles discharging from zincate solutions is still under discussion. It is possible that complex ions such as $[Zn_2(OH)_8]^{""}$, $[Zn(OH)_6]^{""}$, $[Zn(OH)_4]^{"}$, $[Zn(OH)_3]^{'}$ are discharged, or that (according

to Gerischer [24] and Dirkse [25]) uncharged zinc hydroxide particles are reduced. Haber [26] considered that complex and not simple ions are discharged from zincate solutions. The nature of the discharging particles in other analogous systems such as indates and plumbates [27] is likewise unsolved.

To find what prevents the electrodeposition of thick and compact zinc deposits on a rotating cathode, we carried out experiments on the influence of aging and dilution of sodium zincate solutions, and on the effect of volumetric current density on the time before formation of a visible spongy deposit begins. It was found that a spongy deposit is formed on a rotating cathode earlier in an electrolyte which had stood for months than in fresh electrolyte.

In experiments on the effect of dilution of zincate solutions on electrolysis it was found that the time before formation of a visible spongy deposit on a rotating cathode increases with the degree of dilution of the zincate solution with water. For example, when a zincate solution containing 50 g of zinc and 120 g of free caustic soda per liter is diluted tenfold, the time required for the appearance of a visible spongy deposit at a current density of 200 amp/m^2 is trebled.

If it is accepted that, as believed by certain authors [28], zincate solutions decompose on dilution with water with formation of zinc hydroxide by way of an intermediate colloidal stage, then the increase of the time before sponge formation in the electrolysis of such solutions could be attributed to the fact that the colloidal particles of zinc hydroxide formed by hydrolysis are involved together with complex ions in direct reduction at the cathode.

This suggests that at low current densities spongy deposits are formed from zincate electrolytes as the result of inadequate access of the discharging particles to the cathode by diffusion. The formation of spongy deposits at individual points on the cathode is associated with a deficiency of zinc hydroxide particles near such points. If the total zinc concentration in an alkaline electrolyte is considerable, spongy deposits are still formed when the zinc hydroxide particles are reduced at the limiting current. A spongy deposit is formed on a rotating cathode earlier at high than at low current densities because of the slower formation of new particles of zinc hydroxide by hydrolysis.

The influence of admixtures and additions in the electrolyte in the alkaline method of zinc production on current efficiency was studied by us earlier [29]; this influence is slight and the current efficiency is generally close to 100%.

In a study of the electrolysis of sodium zincate solutions in relation to the use of this process in metallurgy, we carried out experiments on the formation of compact deposits in a large laboratory unit with a rotating cylindrical cathode 90 mm in diameter. It was found that under the most favorable electrolysis conditions,

TABLE

Specific Surface and Activity in Contact Deposition of Cadmium from Solutions, of Zinc Powders Made by the Thermal and Electrolytic Methods

Preparation conditions				Specific surface of powders (cm^2/g)	Cadmium content of solution (in mg/liter) after contact deposition* during 3 hours in presence of excess of zinc powder (% of theoretical)					
electrolyte composition (g/liter)		temperature (°C)	current density (amp/m^2)		75	160	250	420	770	1260
zinc	caustic soda									
30	200	25	6000	1960	400	28	11	1.5	—	—
30	200	25	4000	1840	420	31	12	1.75	—	—
30	200	25	2000	1680	425	34	14	3.6	1.2	—
30	200	25	700	227	—	50	41	30.0	9.0	1.65
8	140	25	2000	1700	—	33	13	2.9	1.1	—
8	140	25	500	237	—	49	39	30.0	8.0	1.6
Thermal zinc dust				220	520	52	42	34.0	12.0	1.8

*The original solution contained 2000 mg of cadmium per liter.

namely: zinc concentration in the electrolyte 60 g/liter, temperature 75°, and peripheral cathode velocity 80 m/minute, the compact zinc deposits formed at current density 400 amp/m^2 with about 100% current efficiency cannot be obtained over 0.6 mm thick. In other experiments [12, 30], with lower zinc concentrations, electrolyte temperatures, and cathode rotation speeds, the compact deposits obtainable were even thinner.

Electrolytic production of metallic zinc in the form of compact deposits from zincate solutions is not expedient, because these compact deposits are thin, losses in remelting them would be considerable, and considerable force would be required to strip them from the starting sheets. It is better to conduct industrial electrolysis of zincate solutions with formation of spongy deposits; this procedure is preferable because very high current densities may be used and the removal of the metal from the cells can be made completely mechanized and automatic; the spongy zinc can be used as an active precipitation agent in gold and silver metallurgy, in organic synthesis, etc.

Some authors [4, 5] have reported that electrolytic zinc dust is considerably more active than zinc dust made by the thermal process, but they give no quantitative data. We determined the activity of electrolytic zinc dust made from alkaline solutions.

The activity of zinc powders made by the thermal and electrolytic methods was estimated by the degree of removal of cadmium ions from zinc sulfate solution on addition of zinc dust in a definite excess over the stoichiometric quantity. Data on the activities of the zinc powders are presented in the table.

It may be seen that zinc powder made by electrolysis at high current densities is considerably more active than zinc dust made by the thermal process. The activity of electrolytic zinc powder obtained at current densities below the limiting value is the same as that of the thermal zinc dust. The considerably higher activity of zinc powder formed at high current densities can probably be attributed to its large specific surface. To confirm this, the Deryagin method [31] was used to determine the specific surface of zinc powders made by the different methods. It is clear from the data in the table that electrolytic zinc powder made at high current densities has a considerably greater specific surface than the powder made by the thermal method.

SUMMARY

1. It was shown in a study of the influence of structure and dilution of zincate solutions and of current density on the time before the start of formation of a visible spongy deposit of zinc on a rotating cathode that the formation of spongy zinc is undoubtedly associated with inadequate supply of the particles being reduced to the cathode. It is suggested that these particles are zinc hydroxide.

2. In view of the difficulties in obtaining compact zinc deposits of appreciable thickness by electrolysis of zincate solutions, and of the possibility of mechanization of spongy-zinc production, it is recommended to conduct the electrolysis for production of zinc powder, which can be used for contact deposition of metals, in organic synthesis, and for other purposes.

3. The activities and specific surfaces of zinc powders were determined. It is shown that electrolytic zinc powders made from zincate electrolytes at high current densities are three times as active as powders made by the thermal process.

LITERATURE CITED

[1] H. I. Morgan and O. C. Ralston, Trans. Am. Electroch. Soc. 30, 229 (1916).

[2] Gmelins Handbuch d. anorg. Ch. Syst., No. 32, Zink Ergänzungsband 251 (1956).

[3] V. V. Stender, V. G. Sochevanov, T. P. Oleksenko and N. F. Razina, Soviet Authors' Certif. 87734 (1950).

[4] H. I. Morgan, Eng. Min. J. 15, 72 (1950), J. Electroch. Soc. 100, 590 (1953).

[5] C. T. Baroch, R. V. Hilliard and R. S. Lang, J. Electroch. Soc. 100, 165 (1953).

[6] N. P. Fedot'ev and G. G. Khad'mash, J. Appl. Chem. 28, 1104 (1955).

[7] W. Rutkowski and B. Winsch, Prace inst. Min-wa hutn. 8, 163 (1956); cited through Ref. Zhur. Khim. 19991 (1957).

[8] L. V. Favroskaya and E. I. Stolyarova, Bull. Acad. Sci. Kazakh SSR, Mining, Constructional Materials and Metallurgy Series 6, 92 (1956).

[9] S. Sampath, R. Viswanathan, H. Udupa, and B. Dey, J. Scient Industr. Res. 15 (B-c), 11, 669 (1956).

[10] G. Wranglen, J. Electroch. Soc. 97, 353 (1950).

[11] M. D. Zholudev and V. V. Stender, Ukrain. Chem. J. 23, 200 (1957).

[12] M. D. Zholudev and V. V. Stender, Bull. Acad. Sci. Kazakh SSR 7, 30 (1957).

[13] M. Kiliani, Berg.-u. Huttenmännische Ztg., 251 (1883).

[14] Yu. V. Baimakov, Electrolytic Deposition of Metals [in Russian] (LNTI NTO-VSNKh, 1925) p. 163.

[15] V. Engelhardt (editor), Electrometallurgy of Aqueous Solutions (Leningrad, 1937) p. 273 [Russian translation].

[16] F. Foerster and O. Günther, Z. Elektroch. 5, 16 (1888); 6, 301 (1899).

[17] W. Sebborn, Trans. Far. Soc., 29, 285 (1936).

[18] P. S. Titov and E. N. Paleolog, Jubilee Coll. MITsMZ 603 (1940).

[19] P. P. Turov, Dissertation [in Russian] (Moscow, 1949).

[20] O. K. Kudra, J. Phys. Chem. 5, 121 (1935).

[21] M. A. Loshkarev, A. M. Ozerov and N. T. Kudryavtsev, J. Appl. Chem. 22, 294 (1949).

[22] N. T. Kudryavtsev, J. Phys. Chem. 26, 270 (1952); Proc. Conf. on Electrochemistry [in Russian] (Moscow, 1953) p. 258; N. T. Kudryavtsev, R. Yu. Bek, and I. F. Kushevich, J. Appl. Chem. 30, 1093 (1957).*

[23] V. N. Flerov, J. Phys. Chem. 31, 49 (1957).

[24] H. Gerischer, Z. phys. Chem., 202, 3–4, 302 (1953).

[25] T. Dirkse, Z. phys. Chem. (Frankfurt), 5, 1–2, 1 (1955).

[26] F. Haber, Z. Elektrochem. 10, 433 (1904).

[27] N. V. Aksel'rud, Proc. Acad. Sci. USSR 98, 799 (1954); N. V. Aksel'rud and V. B. Spivakivskii, J. Inorg. Chem. 1, 1996 (1956).

[28] S. Banerji, A. Dey and S. Ghosh, Koll. Z. 141, 104 (1955).

[29] M. D. Zholudev and V. V. Stender, J. Appl. Chem. 31, 1036 (1958).*

[30] M. D. Zholudev and V. V. Stender, Ukrain. Chem. J. 24, 570 (1958).

[31] B. V. Deryagin, Industrial Lab. 17, 324 (1951).

Received April 3, 1958

*Original Russian pagination. See C. B. Translation.

CURRENT DISTRIBUTION IN ELECTROLYTIC ZINC COATING OF WIRE

N. V. Sokolov and A. I. Levin

The S. M. Kirov Polytechnic Institute of the Urals

When current distribution over electrodes is considered, it is generally assumed that the cathode potential is approximately the same at all points. However, in zinc coating of wire there are very considerable variations of potential, reaching several volts, along the wire (from the point of contact) owing to the use of especially high current densities and to the motion of the cathode.

These variations of current distribution do not result in irregularities, as with a moving cathode any region of the surface is coated under roughly the same conditions. Nevertheless, higher current densities, sometimes reaching the limiting values, are found on regions of the cathode close to the point of contact.

In some cases relatively high current densities cannot be used for this reason.

According to literature data [1-5], current densities up to 400 amp /dm^2 can be used in electrolytic zinc coating of wire, whereas the current densities used in industrial practice are only 20-150 amp/dm^2.

This paper contains the results of a study of current-density distribution and ohmic losses during electrolytic zinc coating of wire under practical conditions.

Kadner [6] considered the distribution of current on the stationary surface of a circular cylinder (with an infinite plate as anode), and established the following relationship between the minimum and average current densities:

$$D_{av} = D_{min} \sqrt{\frac{a+R}{a-R}}, \qquad (1)$$

where a is the distance between the electrodes and R is the cylinder radius.

Calculations show that if this is so, the ratio ($D_{av} : D_{min}$) is only 1.01-1.07 for wires 0.5-5.0 mm in diameter and interelectrode distances of 25-40 mm; thus, the current density varies little around the periphery.

We consider that it is important to solve another problem, concerned with the current-density distribution along the length of the wire*.

Consider a cylindrical conductor (wire) between two anodes in an electrolyte.

The following symbols are used: I_0 and I_1, the current entering the conductor at the point of contact and at a region under consideration; l, the distance from the point of contact (if the contact is outside the electrolyte, then it is the distance from the point at which the wire enters the electrolyte); S, the area of the region considered; D, the current density at the cathode; V, the voltage drop along the wire; R, the resistance of the region l; ρ, the resistivity.

*This question was first raised by B. N. Kabanov [7].

The decrease of current strength dI over the region dl of the wire per element of the surface dS represents the true current density

$$D = \frac{dI}{dS}, \tag{2}$$

here $I = I_0 - I_1$. Evidently

$$I_1 = I_0 - I = \frac{dV}{dR}. \tag{3}$$

For a conductor of circular section

$$R = \frac{\rho}{\pi r^2} l \text{ and } S = 2\pi r l.$$

Substitution of dS in (2) and dR in (3) gives

$$D = \frac{1}{2\pi r} \cdot \frac{dI}{dl}, \tag{4}$$

$$I = I_0 - \frac{\pi r^2}{\rho} \cdot \frac{dV}{dl}. \tag{5}$$

Differentiating (5) we have

$$\frac{dI}{dl} = -\frac{\pi r^2}{\rho} \cdot \frac{d^2V}{dl^2}.$$

Hence

$$D = -\frac{r}{2\rho} \cdot \frac{d^2V}{dl^2}. \tag{6}$$

With the dimensions: V (in volts), D (amp/dm^2), ρ (ohms $\cdot$ mm$^2 \cdot$ m^{-1}), l (cm), and r (mm), the differential equation for current density becomes

$$D = -\frac{r \cdot 10^5}{2\rho} \cdot \frac{d^2V}{dl^2}. \tag{7}$$

By means of Equation (7) the true current-density distribution can be found from experimentally observed voltage drop in the wire. It is also evident that, conversely, if the current distribution is known, the voltage drop in the wire can be found.

Consequently, if the current in the wires is $I_1 = I_0 = \text{const}$ (when D = 0), the voltage drop is

$$V_0 = I_0 R. \tag{8}$$

For constant D we have

$$V_D = \frac{I_0 R}{2}. \tag{9}$$

If D is a variable quantity, the voltage drop in the wire is given by the expression

$$V = \frac{I_0 R}{n}. \tag{10}$$

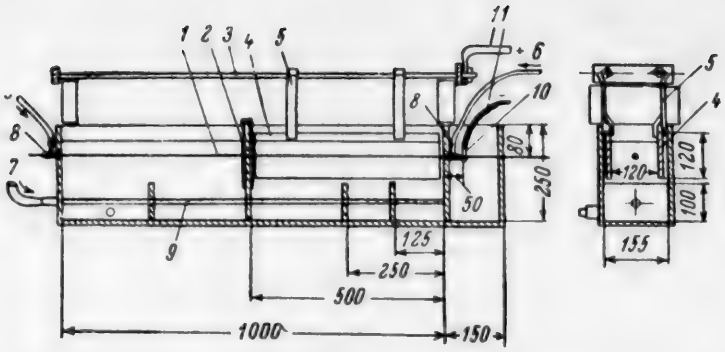

Fig. 1. Experimental cell for electrolytic zinc coating of wire: 1) wire; 2) shield; 3) anode bar; 4) zinc anode; 5) anode suspension; 6) air inlet to T-joint; 7) air inlet for agitation; 8) T-joint; 9) perforated rubber tube; 10) current lead to wire; 11) current leads to cell.

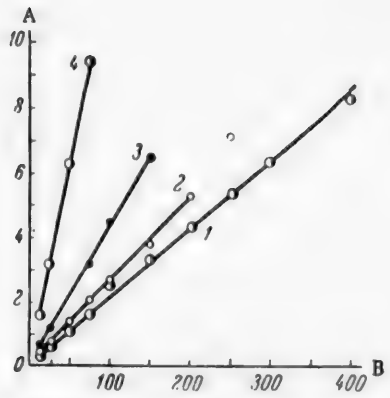

Fig. 2. Variation of cell voltage with current density during zinc coating of wire 0.40 mm in diameter: A) cell voltage (v); B) fixed current density D (amp/dm^2); half-section length l (mm): 1) 125, 2) 250, 3) 500, 4) 1000.

With decreasing current density $n > 2$, the value of $n/2$ can serve as a measure of the irregularity of current distribution over the wire. It can be found from the equation

$$\frac{n}{2} = \frac{I_0 R}{2V}. \qquad (11)$$

An experimental cell with unilateral current leads was designed for experimental study of current-density distribution and of voltage drop in the wire. The cell design is shown in Fig. 1.

A working space (half-section) of variable length could be obtained in the cell, made of vinyl resin, by the positioning of a shield at distances of 125, 250, and 500 mm and in absence of the shield (1000 mm). The wire entered through glass T-joints with air seals. By this means the wire could be introduced into the electrolyte in a straight line without the use of immersion rollers. The current leakage which usually occurs in industrial cells was eliminated by the use of an external contact. The portion of the wire between the contact and entry into the electrolyte was strongly cooled by means of air blown into the T-joint. The wires used for the experiments, 0.40, 0.80, and 1.6 mm in diameter were drawn with the aid of a liquid lubricant, which gave them a particularly clean and bright surface.

Before the experiments the wire was degreased in ethyl alcohol, pickled in 15% sulfuric acid solution, washed in a water spray, and rubbed with felt. The electrolyte was vigorously agitated by means of compressed air.

The electrolyte composition (in g/liter) was: $ZnSO_4 \cdot 7H_2O$ – 670, $KAl(SO_4)_2 \cdot 12H_2O$ – 23.6, $FeSO_4 \cdot 7H_2O$ – 0.26, pH = 2.9–3.1. The temperature was maintained at 39-42°.

The voltage drop along the wire was measured at various current densities from 12.5 to 400 amp/dm^2. The average thickness of the zinc coating was 10 μ in all cases.

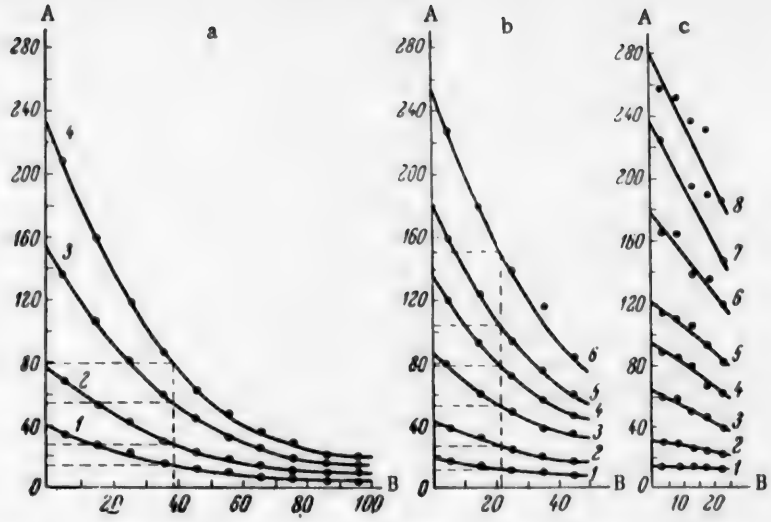

Fig. 3. Variations of current density along a wire 0.40 mm in diameter with the distance from the entry point of the wire into the electrolyte (on the contact side) for different half-section lengths: A) current density D (amp/dm^2); B) length (cm); a) 1–13.6, 2–27.1, 3–53.7, 4–78.8; b) 1–11.7, 2–26.4, 3–52.7, 4–78.8, 5–104, 6–150.5; c) 1–12.6, 2–22.3, 3–50.0, 4–77.2, 5–100.6, 6–145, 7–193, 8–233.

TABLE 1

Current-Density Distribution Along the Wire

Wire diameter (mm)	Half-section length (mm)	Average current density D_{Zn} (amp/dm^2)	$\frac{D_{max}}{D_{min}}$	Coefficient of irregularity $\left(\frac{\pi}{2}\right)$
0.40	250	12.6—233	1.3—1.6	1.05—1.21
0.40	500	11.7—26.4	2.7	1.55—1.75
0.40	500	52.7	2.75	1.53
0.40	500	78.8	3.15	1.57
0.40	—	104	3.4	1.50
0.40	1000	13.6—27.1	10.2—10.5	1.72
0.40	1000	53.7	11.4	1.98
0.40	1000	78.8	12.2	1.91
0.8	250	98.2	1.13	1.0
0.8	500	103.6	1.67	1.23
0.8	1000	105.2	2.93	1.31
1.60	500	99.8	1.25	1.04
	1000	50.8	1.53	1.08

The current was regulated by means of a shunt rheostat and resistors connected in the dynamotor feed circuit. The voltage at the cell terminals, the voltage drop in the wire, and current strength were measured by means of an MVA-47/5 ampere-volt meter and an M-105 millivoltmeter with a 75 mv, 30 amp external shunt (accuracy grade 0.5). Ohmic loss in the wire was determined by means of a special sliding contact.

The current distribution along the wire was investigated gravimetrically with the aid of an analytical balance. The coated wire was cut into pieces, the zinc was dissolved (in sulfuric acid solution containing arsenious oxide as inhibitor), and its weight found by difference. The current density was calculated from the formula

$$D_{Zn} = 3 \cdot 10^5 \cdot \frac{Q}{\tau S}. \qquad (12)$$

TABLE 2

Voltage Drop in a Wire 0.40 mm in Diameter

I_0 (amp)	Constants		Mean I_1 (amp)	Calculated $V = I_1 R$ (in v)	Experimental V (in v)
	A	B			
Half-section length 500 mm					
0.79	1.74	$1.105 \cdot 10^{-2}$	0.37	0.29	0.20
1.57	1.32	$1.12 \cdot 10^{-2}$	0.63	0.49	0.35
3.1	1.05	$0.87 \cdot 10^{-2}$	1.33	1.04	0.79
4.7	0.90	$0.85 \cdot 10^{-2}$	1.9	1.48	1.17
6.3	0.81	$0.84 \cdot 10^{-2}$	2.5	1.95	1.64
9.4	0.72	$0.75 \cdot 10^{-2}$	4.0	3.12	3.1
Half-section length 1000 mm					
1.57	1.37	$1.55 \cdot 10^{-2}$	0.48	0.75	0.71
3.1	1.10	$1.21 \cdot 10^{-2}$	0.95	1.48	1.39
9.4	0.75	$0.94 \cdot 10^{-2}$	2.3	3.6	3.84

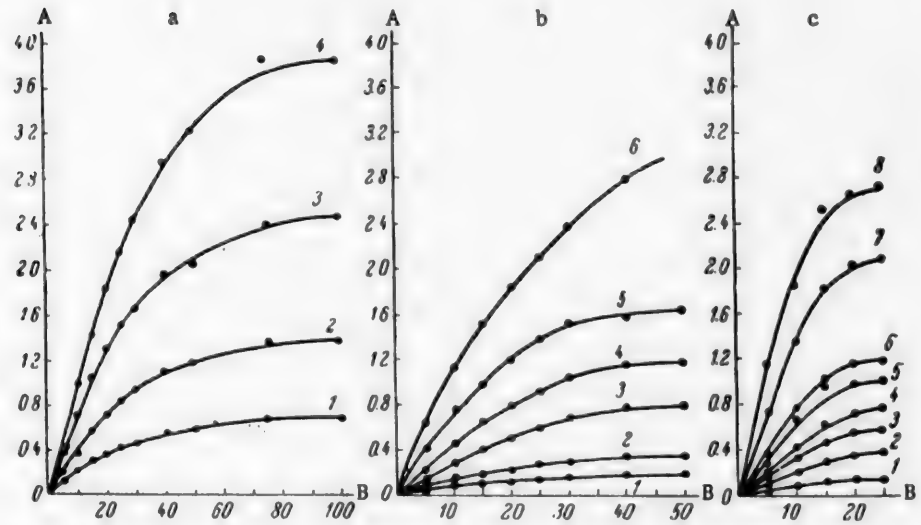

Fig. 4. Voltage drop in a wire 0.40 mm in diameter as a function of the distance from the entry point of the wire into the electrolyte (on the contact side) for different half-section lengths and current densities: A) voltage V (in v); B) length (cm); a) l = 100 cm; D (in amp/dm^2): 1–13.6, 2–27.1, 3–53.7, 4–78.8; b) l = 50 cm; D (in amp/dm^2): 1–11.7, 2–26.4, 3–52.7, 4–78.8, 5–104, 6–150.5; c) l = 25 cm; D (in amp/dm^2): 1–12.6, 2–22.3, 3–50.0, 4–77.2, 5–100.6, 6–145, 7–193, 8–233.

Here D_{Zn} is the current density calculated for zinc (amp/dm^2), Q is the weight of zinc (g), τ is the duration of zinc coating (seconds), and S is the surface area of the specimen (cm^2) (the current efficiency was assumed to be 98 %).

The results of determinations of cell voltage during coating of wire 0.40 mm in diameter at different current densities and half-section lengths are plotted in Fig. 2. It is seen that the voltage at the cell terminals is proportional to the current density.

Experimental values for current density at points on the wire at various distances from the point of entry of the wire into the electrolyte (from the contact side) are plotted in Fig. 3.

Curves for the voltage drop in the wire as a function of the distance from the point of contact (the point of entry of the wire into the electrolyte) for different half-section lengths (1000,500,250 mm) are given in Fig.4.

Irregularities of current distribution could be estimated directly from the ratio of the maximum to the minimum current density, i. e. D_{max}/D_{min}, and indirectly from the results of determinations of voltage drop in the wire (from values of n/2).

The data in Table 1 represent the irregularity of current-density distribution determined for different half-section lengths and average current densities.

It follows from the experimental data (Table 1, Fig. 3) that the irregularity of current-density distribution is very considerable, especially with long half-sections. The irregularity diminishes with increase of the wire diameter (decrease of resistance). It increases with increase of current density.

It can be easily shown from the data in Table 1 that the coefficient of irregularity (n/2) is a satisfactory measure of the current-density distribution. Any deviations in the values of n/2 are apparently caused by errors in determinations of the wire resistance.

It is interesting to note (see Fig. 3) that the straight lines for the average current densities always intersect the $D = f(l)$ curves at points corresponding to the same distance from the entry point of the wire into the electrolyte for a given half-section length. This means that the current distribution remains identical in character for a given half-section length. The curves for the voltage drop in the wire can be represented by an equation of the form

$$V = \frac{l}{a + bl} \tag{13}$$

To determine $D = f(l)$, we find from the second derivative of (13)

$$\frac{d^2V}{dl^2} = -\frac{2ab}{(a + bl)^3}. \tag{14}$$

Substituting (14) into (6) we have

$$D = \frac{r}{2\rho} \cdot \frac{2ab}{(a + bl)^3}. \tag{15}$$

This can be transformed into

$$D = \frac{1}{(A + Bl)^3}. \tag{16}$$

Here A and B are constants the values of which are given in Table 2.

The experimental data fit satisfactorily on straight lines representing the $\frac{1}{\sqrt[3]{D}} - l$ relationship. From (4) and (16) we readily find

$$D = \frac{1}{(A + Bl)^3} = \frac{5}{\pi r} \cdot \frac{dI}{dl}, \tag{17}$$

if D is in amp/cm^2, l is in cm, and r is in mm.

The current strength in the wire is found from (17)

$$I_1 = I_0 - \left[\frac{\pi r}{10BA^2} - \frac{\pi r}{10B} \cdot \frac{1}{(A + Bl)^2}\right]. \tag{18}$$

The method described above was used for calculating the average current strength in the wire ($\overline{I}_1$).

The same relationships were used for finding the values of the voltage drop given in Table 2.

It can be seen that the experimental and calculated (see Table 2) values of the voltage drop in the wire are in satisfactory agreement.

SUMMARY

1. The voltage drop and weight of zinc at different distances from the point of contact along a wire were determined experimentally; equations were derived for the current density as a function of the voltage drop in the wire. It was also demonstrated experimentally that there is a considerable difference between the actual and the average current densities.

2. It is shown that considerable scope for increasing the average current density exists if irregularity of current distribution is diminished by decrease of the length of the cell section (distance between the contacts).

It is shown that the current density in zinc-coating plant can be increased considerably.

LITERATURE CITED

[1] V. I. Lainer and N. T. Kudryavtsev, Fundamentals of Electroplating, 1 [in Russian] (Metallurgy Press, 1953).

[2] M. N. Belyaev, N. T. Kudryavtsev, et al., Technical News, Series on Protective Coatings for Metals, 9, (1934).

[3] G. T. Bakhvalov and A. V. Turkovskaya, Metal Corrosion and Protection [in Russian] (GONTI, 1947).

[4] N. P. Diev, J. Appl. Chem. 22, 361 (1949).

[5] L. K. Gurevich, Bull. Main Admin. Metal Inds. Press, 2, 43-54 (1939).

[6] L. I. Kadaner, J. Phys. Chem. 30, No. 7, 1560 (1956).

[7] B. N. Kabanov, J. Projection Construction Chem. Ind. USSR 1, 41 (1935).

Received April 3, 1958

PERFORMANCE OF NONLAMINATED NICKEL OXIDE PLATES IN ZINCATE SOLUTIONS

V. N. Flerov*

The A. A. Zhdanov Polytechnic Institute, Gor'kii

One of the main obstacles to practical adoption of the nickel–zinc cell Zn $\left|\begin{matrix}\text{KOH}\\ K_2Zn(ON)_4\end{matrix}\right|$ NiOOH has been the strong poisoning action of the zincate electrolyte on the laminated nickel oxide plate. The cell capacity falls severalfold even during the first 20-30 cycles. This difficulty was not overcome in any of the reported investigations concerned with this type of cell, among which special mention must be made of the work of Drumm [1] and Kalaida [2].

The so-called nonlaminated plates, developed and introduced recently [3], represent an essentially new plate design for alkaline cells. These plates are made by impregnation of a highly porous sintered metal (nickel) plaque with active material. The utilization coefficient (K_u) of the active material is considerably higher in nonlaminated plate because of the high conductivity of the plaque and its intimate contact with the active material. Its value usually exceeds 100% (calculated for a change of one unit in the valence of nickel), whereas for laminated plates it is in the 50-55% range. This sharp difference of plate characteristics suggested that there should also be some differences in the action of zincate on laminated and nonlaminated plates respectively. The literature does not contain any reports of investigations into this subject.

The purpose of the present investigation was therefore to study the electrical characteristics of nonlaminated nickel oxide plates in zincate electrolytes, and to determine the influence of various technological and operational factors on them.

EXPERIMENTAL

The nonlaminated nickel oxide plates were made mostly by the procedure developed in Tsygankov's laboratory in the Saratov alkali-battery factory.

The plaques were made from a mixture of powdered nickel (made by the carbonyl process) and NH_4HCO_3 molded onto steel nickel-plated grids. The briquets were sintered in a hydrogen atmosphere, the temperature being raised steadily to 850°. The resultant briquets, 1.7-2.0 mm thick, had 68-78 % porosity. The plaques were then impregnated in nickel nitrate solution with a density of 1.62-1.65 g/cc, heated to 70-90°. After exposure to air for some time (to allow the salt to crystallize) the plates were placed for 2 hours into KOH solution of density 1.20, heated to 60-70°. They were then washed repeatedly in hot water until entirely free from hydroxyl ions. The washed plates were dried at 80-95°.

The impregnation cycle was repeated (or even performed three times).

$Ba(OH)_2$ was introduced into the plaques by impregnation at 60-65° in $Ba(OH)_2$ solution saturated at 40°. The amount of $Ba(OH)_2 \cdot 8H_2O$ introduced into the plaques was 13-17% relative to the $Ni(OH)_2$ present.

To introduce cobalt, the plaques were impregnated in a mixture of $Ni(NO_3)_2$ and $Co(NO_3)_2$ solutions, in which the cobalt content was 5% relative to nickel.

* The experimental work was carried out with the assistance of A. A. Kozhakova.

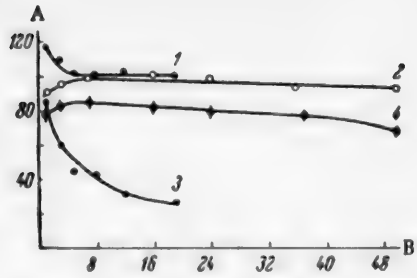

Fig. 1. Variations of the relative capacities of NZ and CN cells with the number of cycles: A) relative capacity (% of the capacity of CN cells after 16-19 cycles); B) cycles; CN cells: 1) laminated; 2) nonlaminated; NZ cells: 3) laminated; 4) nonlaminated.

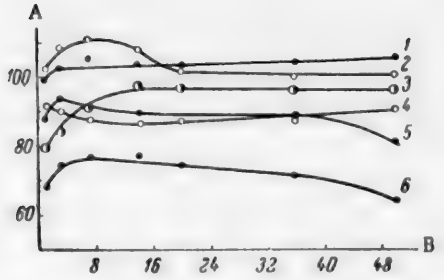

Fig. 2. Variations of the utilization coefficient of nickel oxide plates with the number of cycles, for different numbers of impregnations: A) utilization coefficient (%); B) cycles; CN cells: 1) single impregnation; 2) twofold; 3) threefold; NZ cells: 1) single impregnation; 2) twofold; 3) threefold.

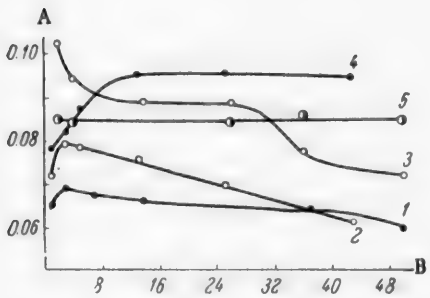

Fig. 3. Variations of the specific capacity of nickel oxide plates in NZ and CN cells with the number of cycles: A) specific capacity (amp-hr/g); B) cycles; NZ cells: 1) nonformed plates after twofold impregnation; 2) nonformed plates after threefold impregnation; 3) formed plates after threefold impregnation; CN cells: 4) plates after threefold impregnation; 5) plates after threefold impregnation, "poisoned" by zincate.

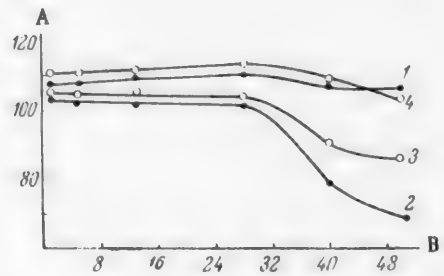

Fig. 4. Effect of additions on variations of the utilization coefficient of the active material with the number of cycles: A) utilization coefficient (%); B) cycles; 1) CN reference cell, without additives; NZ cells: 2) reference; 3) addition of 5% Co; 4) addition of 13-17% $Ba(OH)_2 \cdot 8H_2O$; electrolyte with addition of 15 g $LiOH \cdot H_2O$ per liter.

The negative plates were sintered zinc plates similar in principle to the plates in silver–zinc cells [4]. These plates were made from a mixture of ZnO with 3% starch solution in 40:1 ratio. The plates were molded under a pressure of 150 kg/cm^2, with cadmium-plated copper leads inserted. The finished briquets were dried and wrapped in 3 layers of cellophane, previously soaked in hot water (to remove glycerol) and then treated in $MgCl_2$ solution (to confer greater resistance to alkaline liquors).

The dimensions of the nickel oxide plates were 14 × 34 × 2 mm. The zinc and cadmium electrodes were of similar dimensions.

The nickel–zinc (NZ) cells were assembled from two nickel oxide and one zinc plate each. To facilitate diffusion of electrolyte to the plates, a layer of capron fabric was placed between them. The plates were packed fairly closely in transparent plastic vessels.

The limiting factor with regard to cell capacity was the positive plate. The electrolyte was KOH solution, density 1.30, with or without added LiOH. The choice of electrolyte concentration was determined by its greatest effectiveness at subzero temperatures. In this electrolyte, the zinc concentration becomes established at 43-48 g/liter during operation. The cells were charged at current density 1.60 amp/dm^2 until gas was abundantly evolved on the positive plates. The plate capacity was determined in discharge of the cells at current density 1.05 amp/dm^2 to a final voltage of 1.40 v (to 1.00 v for CN cells). The utilization coefficient of the active material was calculated for a change of the valence of nickel by one unit; it was also taken into account that when dried to 95° the active material in the pores conforms to the formula $Ni(OH)_2$.

Nonlaminated nickel oxide plates differ considerably from laminated plates by the action of zincate on them. Whereas the capacity of laminated plates in NZ batteries is less by a factor of 3.5-4 than the plate capacity of CN (cadmium–nickel) cells after only 19-20 cycles, and there is a tendency to further decrease, different results are obtained with nonlaminated plates. Even if special measures are not taken, the capacity of such plates in zincate electrolyte is only 15-20% lower than the plate capacity in pure alkali (Fig. 1). This capacity remains virtually constant during 30-40 cycles, and then decreases somewhat.

The number of impregnations of the plate has a considerable influence on the variation of plate capacity with the number of cycles. It must be pointed out that enough active material cannot be introduced into the plate by a single impregnation, and the operation must be performed twice or even three times. However, each successive impregnation gives a smaller weight increase (and a lower value of K_u). If the total weight increase in three impregnations is taken as 100%, then the first impregnation introduces 45-50% of the total amount of active material, the second introduces 30-35%, and the third, 15-20%. In two impregnations 30-35% of active material on the weight of the plate can be introduced, and in three impregnations, 35-45%. The plate porosity decreases with the number of impregnations; after a single impregnation the porosity is 50-53%, after two it is 42-45%, and after three, 36-39% (for unused plates).

Zincate has a poisoning effect on the nickel oxide electrode whatever the number of impregnations, but this effect is greater after a larger number of impregnations (Fig. 2)*. The maximum values of K_u for plates in NZ and CN cells, respectively, differ by 12, 17, and 21% after one, two, and three impregnations, respectively.

TABLE

Variations of the Electrical Characteristics of Nickel Oxide Plates in NZ Cells Stored in the Filled State. Electrolyte: KOH, density 1.30, + 15 g $LiOH \cdot H_2O$ per liter of room temperature

Cell No.*	Method of storage	Service time in days, and cycle				
		7/4	23/5	38/6	54/7	71/8
		K_u of active material (%)				
1	In discharged state	114	108	115	119	114
2		116	108	103*	125	123
3		106	103	109	102*	104
4		109	107	114	98*	108
5		113	108	99*	116	115
6	In charged state	113	119	116	113	—
7		119	124	121	125	121
8		113	121	113	115	110
9		105	110	109	109	108
10		114	117	113	113	111

* Cells 1-5 were given an additional charge after storage, with the exception of instances marked by asterisks.

* All the curves are based on average results for a number of cells.

This difference is especially intensified with increase in the number of cycles. The capacity of nickel oxide plates in NZ cells after a single impregnation even increases somewhat with the number of cycles, whereas plates impregnated twice, and especially three times, gradually show a fall of capacity. Because of these changes, the differences between the values of K_u for NZ and CN cells with different numbers of impregnations at the 50th cycle reached 14, 21, and 29% for one, two, and three impregnations, respectively.

Whereas during the first few cycles the third impregnation gave a certain advantage with regard to capacity, at the 50th cycle the absolute capacity of such plates was less than that of plates impregnated twice.

It must be emphasized that these results refer only to impregnation in $Ni(NO_3)_2$ solution of a definite concentration. The influence is actually exerted by the amount of active material deposited in the plate (for a given porosity) rather than by the number of impregnations.

Plates impregnated three times in $Ni(NO_3)_2$ solution of density 1.40 showed approximately the same variations of K_u with the number of cycles as plates impregnated once in $Ni(NO_3)_2$ solution of density 1.65.

Preliminary forming of twice-impregnated plates in pure alkali does not produce any noticeable changes in their characteristics. Any initial capacity increase of such electrodes was lost at the 10th to 15th cycle. Forming has a strong influence on plates impregnated three times (Fig. 3). Throughout all the cycles their capacity was 20-25% greater than the capacity of nonformed plates, although both types showed a decrease of capacity.

The capacity loss of nonlaminated plates caused by the action of zincate is not prevented even by prolonged soaking of the plates in alkali. Such plates, incorporated in CN cells, had K_u 10-12% lower than the reference plates.

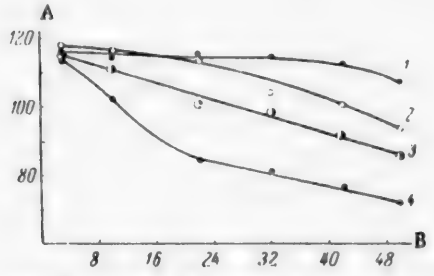

Fig. 5. Effect of K_2CO_3 on the characteristics of nickel oxide plates in NZ cells: A) utilization coefficient (%); B) cycles; initial K_2CO_3 content of electrolyte (g/liter):1) 3, 2) 50, 3) 100, 4) 150 electrolyte : 7 g-equiv/liter of KOH + K_2CO_3.

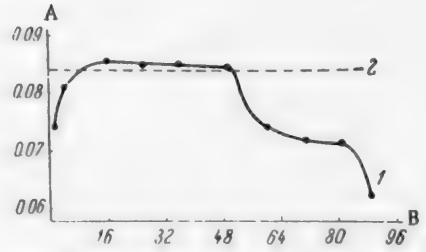

Fig. 6. Effect of the number of cycles on the specific capacity of nickel oxide plates in cells of the NZ-3 type: A) specific capacity (in amp-hr/g); B) cycles; 1) NZ cell; 2) actual specific capacity of plates in cells of the KNB-2 type.

Increase of the drying temperature to 130-150° has some stabilizing effect on plate capacity. With this change of procedure the decrease of K_u for the active material in plates after twofold impregnation generally did not exceed 5% in 50 cycles. With larger amounts of active material the decrease of capacity with the number of cycles was independent of the drying temperature.

The effects of a number of additives introduced to increase K_u of the active material and to prevent its decrease with the number of cycles were investigated. Most of the tests were with additives which had been found to have favorable effects in CN cells with laminated plates; in particular, additions of cobalt [5], barium, and LiOH [6].

Addition of cobalt to nonlaminated plates in NZ cells proved to have little effect (Fig. 4). Impregnation of the plates with $Ba(OH)_2$ solution did not change K_u, but had some stabilizing effect in cycling. The best results were obtained with the use of a composite electrolyte (KOH of density 1.30 + 15 g $LiOH \cdot H_2O$) per liter.

In this electrolyte, the utilization coefficient of the active material rose by 8-12%. The plates retained their increased capacity for 30-40 cycles, after which there was a relatively rapid fall of capacity, so that all the initial advantages of the composite electrolyte were lost. The simultaneous addition of $Ba(OH)_2$ and LiOH had a stronger and more stable effect (Fig. 4).

In this case, K_u of the plates was approximately the same as that of plates in CN cells filled with ordinary electrolyte. In 50 cycles the capacity decreased by only 5-8%.

One of the most harmful impurities in nickel oxide plates used in zincate electrolytes is carbonate, which causes a rapid decrease of electrode capacity with increasing number of cycles. During the initial cycles, K_2CO_3 at concentrations up to 100 g/liter does not produce any appreciable decrease of K_u. During subsequent cycles even smaller amounts of carbonate begin to have a detrimental effect (Fig. 5).

Prolonged static exposure of the plates in zincate electrolyte between operating cycles did not result in any appreciable deterioration of the characteristics if the intervals between the cycles did not exceed two weeks and if the electrolyte was protected against drying and carbonation (see table).

With longer periods of inactivity there was an appreciable deterioration of the characteristics of plates stored in the charged state.

Threefold impregnation, a high drying temperature, preliminary forming of the plates in pure alkali, introduction of $Ba(OH)_2$ as a plate additive, and the use of a composite electrolyte are all measures which, together with protection of the electrolyte against carbonation, make it possible to produce plates of high specific capacity which remains stable for a fairly large number of cycles. Fig. 6 shows the effect of the number of cycles on the specific capacity of plates made in this manner. Plates 27 × 55 mm in size were assembled in batteries of 3-3.5 amp-hr capacity. Average results for four batteries were used for plotting the curve. For comparison, the same diagram shows the specific capacity of plates of the same dimensions, assembled in CN cells of the KNB-2 type, on the assumption that this capacity is 20× in excess of the nominal. The fall in capacity of plates in NZ cells at about the 60th cycle is due partly to the formation of connecting bridges (spongy zinc) between some of the cell plates, and partly to the presence of excess active material. Investigations have shown that the weight of active substance adsorbed during impregnation must not exceed 40-45% of the initial plate weight. None of the measures indicated above could prevent a fall of plate capacity after a large number of cycles if the amount of active substance incorporated in the plate exceeded 45-50%.

DISCUSSION OF RESULTS

The smaller influence of zincate on nonlaminated nickel oxide plates as compared with laminated (Fig. 1) can hardly be ascribed to any special properties of the active material in these plates. The active material was prepared by the same method in both cases: by the interaction of a solution of nickel salt with excess alkali. The observed difference is evidently due to the specific influence of the nickel plaque on the active material in contact with it. More intimate contact between the conducting plaque and the active material favors rapid and deep forming of the active material. This, in turn, prevents extensive poisoning of the activity [2]. The higher tendency to poisoning in plates with higher contents of active material should evidently be attributed to the fact that the active material is further from the conducting plaque, as this retards forming of the plate (Fig. 2).

Examination of the course of the capacity–cycles curves reveals two stages at which the plate capacity decreases in zincate electrolyte. The first stage occurs during the earliest cycles, when the capacity falls by 10-20%. This poisoning is not prevented if the plates are soaked in alkali (Fig. 3). After 30-60 cycles there is a new and greater fall of plate capacity. Whereas the first stage of capacity decrease is poisoning of the active material by zincate in the true sense, probably by the same mechanism as in laminated plates, the second stage, in our opinion, is mechanical rather than chemical in character. This is indicated by the existence of a prolonged region of stable capacity before the second stage of K_u decrease appears. The fact that the plate capacity lost at this stage is restored by a change of electrolyte also supports this view (Fig. 3).

The considerable influence of drying temperature and the absence of a second stage in the case of once-impregnated plates (Fig. 2) show that one of the causes of the second poisoning stage is swelling of the active material. This causes blocking of some of the pores in the plate, so that some of the inner regions are cut off. Zhil'tsov and Kosobryukhov [7] showed that increase of the temperature used for drying nickel hydroxide

reduces the swelling of the active material. The fact that the plate capacity does not decrease in CN cells shows that it is zincate which causes greater swelling of the hydroxide.

One of the main causes of the fall of plate capacity after a large number of cycles is, undoubtedly, aging of the zincate electrolyte [8]. In the discharge of a sintered zinc plate enclosed in cellophane the zinc concentration cannot reach a level at which the solid phase is precipitated from the electrolyte [9]. With increasing number of cycles the equilibrium may break down owing to carbonation of the electrolyte and decomposition of water by electrolysis, and this would lead to deposition of the solid phase from the electrolyte, primarily in the plate pores. In our opinion, the effect of added $Ba(OH)_2$ is to decarbonate the electrolyte rather than to act on the active material.

SUMMARY

1. Nonlaminated nickel oxide plates are much less susceptible to the poisoning action of zincate than laminated plates.

2. The performance of a nonlaminated nickel oxide plate in zincate electrolyte is improved considerably by increase of the drying temperature in impregnation, by introduction of $Ba(OH)_2$ into the plate, and by the use of a composite electrolyte in the cell.

3. The poisoning effect of zincate increases with increase of active material in the plate. Previous forming of the plate in pure alkali has a favorable influence in such cases.

4. One of the main causes of the fall in capacity of nonlaminated plates with increasing number of cycles is carbonation of the electrolyte.

LITERATURE CITED

[1] G. Drumm, The Railway Engineer, Sept., 258, 280 (1933).

[2] T. N. Kalaida, Dissertation [in Russian] (Leningrad, 1939).

[3] G B. Ellis, H. Mandel and D. Linden, J. Electroch. Soc. 99, 9 (1952).

[4] S. Eidensohn, J. Electroch. Soc. 99, 29 (1952).

[5] H. Winkler, Deutsche Elektrotechnik, 8 (1955).

[6] T. A. Edison, German Patent 203284 (1908).

[7] B. A. Kosobryukhov and N. P. Zhil'tsov, Collected Scientific Papers on Chemical Sources of Current [in Russian] (Central Laboratory for Storage Batteries, Leningrad) 4, p. 88.

[8] V. N. Flerov, J. Phys. Chem. 31, 49 (1957).

[9] V. N. Flerov, J. Appl. Chem. 32, No. 1, 132 (1959).*

Received April 19, 1958

*Original Russian pagination. See C. B. Translation.

INFLUENCE OF COLD DEFORMATION AND SURFACE QUALITY ON GASEOUS CORROSION OF AUSTENITIC CHROME–NICKEL STEEL*

A. V. Shreider, E. M. Kontsevaya
and V. G. Trakman

Production of stainless chrome–nickel steel involves the consecutive stages of hot rolling, heat treatment and pickling of the product, cold rolling, heat treatment, and pickling of the cold-rolled sheet. The heat treatment of 1Kh18N9 chrome–nickel steel and of 1Kh18N9T chrome–nickel–titanium steel is carried out with the gaseous medium at 1070-1100° and the metal at 1010-1040°, while the corresponding temperatures for 1Kh13N4G9 chrome–nickel–manganese steel are 1130-1150° and 1070-1100°. The technological process for scale removal includes the following consecutive operations: treatment for 15 ± 5 minutes in a melt of 80% NaOH and 20% $NaNO_3$ at 500 ± 50°, cooling and washing in running water, treatment for 15 minutes in a solution of 19 ± 1% H_2SO_4 and 4 ± 1% NaCl at 75 ± 5°, washing, bleaching, and passivation for 5 minutes in 7 ± 1% HNO_3 at 45 ± 5°.

Considerable losses of metal occur in production as the result of scale formation and subsequent removal of the scale by pickling. The aim of the present investigation was to verify the view, held as the result of practical experience, that there is a connection between the corrosion losses of metal on the one hand, and the shrinkage in cold rolling and the surface quality of the sheet on the other.

EXPERIMENTAL

The metal specimens studied were of the following composition (%): 1) 1Kh18N9–0.10 C, 1.12 Mn, 0.69 Si, 0.015 S, 0.033 P, 10.38 Ni, 18.35 Cr; 2) 1Kh18N9T–0.11 C, 1.37 Mn, 0.54 Si, 0.018 S, 0.034 P, 9.60 Ni, 17.57 Cr, 0.59 Ti; 3) 1Kh13N4G9–0.13 C, 8.97 Mn, 0.42 Si, 0.012 S, 0.022 P, 3.98 Ni, 12.95 Cr.

The following specimens were made from each alloy: hot-rolled–pickled, polished on a felt disk with State Optical Institute paste, sandblasted; cold-rolled with 10, 20, 30 and 40% sheet shrinkage.

The kinetics of high-temperature oxidation was studied by the method of continuous weighing [1] in an oxidizing atmosphere at 900, 1000, and 1100°, with exposure times of up to 60-80 minutes. The kinetic curves were plotted in $\Delta g - \tau$, $\Delta g - \lg\tau$, $\lg\Delta g - \lg\tau$, and Δg **coordinates, where Δg is the weight increase in time τ. It was found from the slopes of the linear logarithmic and semilogarithmic plots for different states of the metal and from the temperatures whether τ the high-temperature oxidation conforms to the logarithmic law $\Delta g = K \lg \tau + a$ or to the parabolic law $\lg g^n = K\tau$, where K is the rate constant and $\underline{a}$ is the weight increase for $\tau = 1$. The plots of $\lg \Delta g = f(1/T)$, where T is the absolute temperature, were used to determine the influence of the composition, state, and quality of the metal surface on the process of high-temperature oxidation in relation to temperature, and the activation energy Q was then calculated.

The surface quality was evaluated by means of the Abbott profilometer [2, 3] both before heat treatment and after removal of the oxide film by pickling.

---

*Communication I on high-temperature oxidation of stainless sheet steel.

** lg≡log. Publisher's note.

Influence of Shrinkage on High-Temperature Oxidation

The results of kinetic experiments on gaseous corrosion of 1Kh18N9T and 1Kh18N9 are plotted in Fig. 1., and the oxidation laws found and the values of Q are given in Table 1.

The curves for 1Kh18N9 and 1Kh18N9T at 900° are logarithmic in character. The protective properties of the oxide films diminish with increase of temperature and the oxidation at 1000° and especially at 1100° conforms very closely to a parabolic law.

At 900° the retarding effect of previous cold rolling on oxidation is revealed—gaseous corrosion diminishes with increasing shrinkage. This effect of shrinkage becomes less pronounced at higher temperatures. The influence of the shrinkage of the metal on the oxidation rate can also be analyzed by comparison of the values of the coefficients K of $\lg \tau$ for the logarithmic law (at 900°) and of the indices $\underline{n}$ of Δg^n for the parabolic law (at 1000 and 1100°)—the rate of gaseous corrosion decreases with decrease of K, while the protective properties of the film increase with increase of $\underline{n}$. Comparison of the values of Q (Table 1) shows that the activation energy of gaseous corrosion is increased considerably (by a factor of 2 or more) by cold deformation.

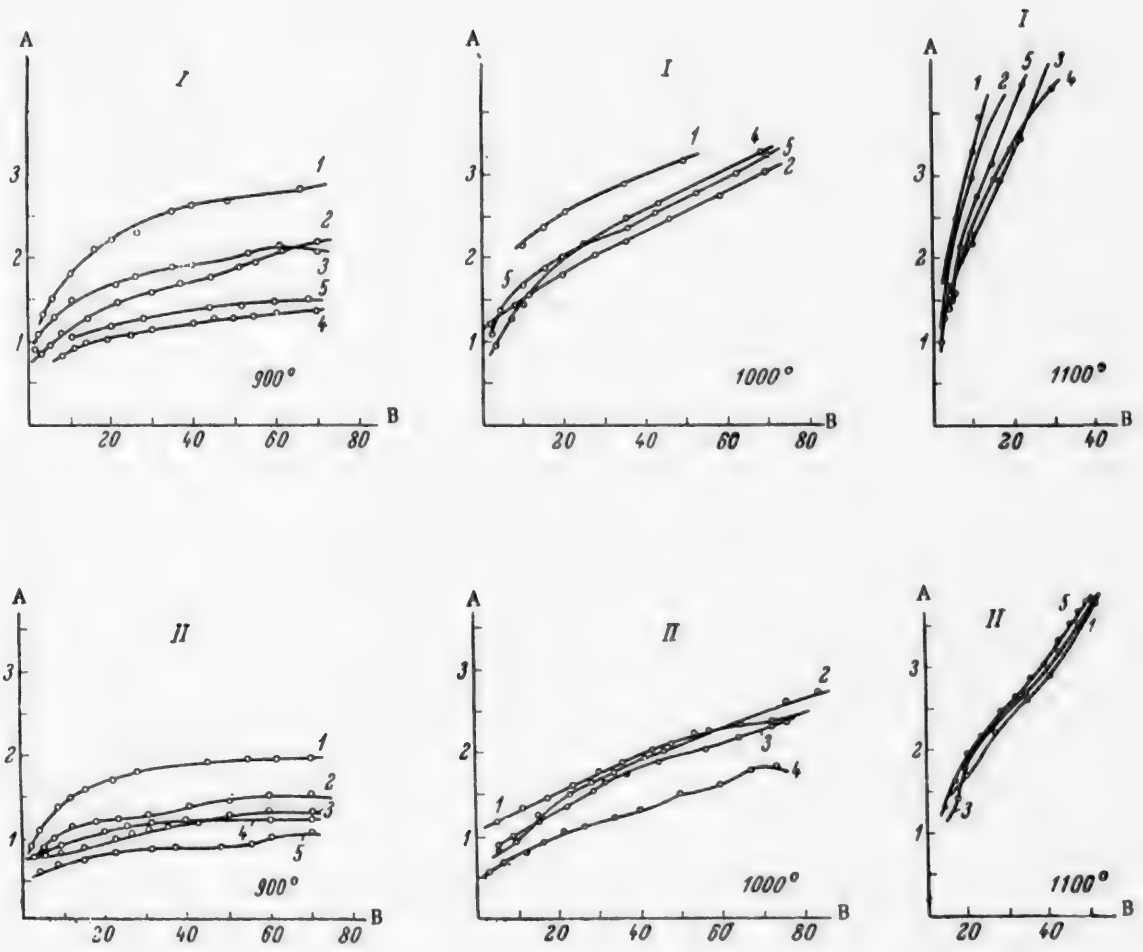

Fig. 1. Kinetics of high-temperature oxidation of 1Kh18N9T and 1Kh18N9 at 900, 1000, and 1100°: A) weight increase Δg (g/m^2); B) time τ (minutes); 1) hot-rolled specimens; cold-rolled with shrinkages (%) 2) 10, 3) 20, 4) 30, 5) 40; steel: I) 1Kh18N9T; II) 1Kh18N9.

TABLE 1

Laws of High-Temperature Oxidation at Various Temperatures and Shrinkages, and Values of the Activation Energy Q for the Investigated Metals Calculated from the Weight Increase During 60 Minutes

Metal	Shrinkage (%)	Oxidation laws at temperatures			Q (in cal.)
		900°	1000°	1100°	
1Kh18N9T	HR*	$\Delta g = 1.26 \lg \tau + 0.67$	$\Delta g^{2.81} = 0.91\tau$	$\Delta g^{1.17} = 0.43\tau$	7300
	10	$\Delta g = 0.95 \lg \tau + 0.28$	$\Delta g^{3.41} = 0.74\tau$	$\Delta g^{1.25} = 0.41\tau$	16000
	20	$\Delta g = 0.80 \lg \tau + 0.68$	$\Delta g^{3.01} = 1.10\tau$	$\Delta g^{1.84} = 0.54\tau$	18300
	30	$\Delta g = 0.59 \lg \tau + 0.30$	$\Delta g^{3.12} = 0.50\tau$	$\Delta g^{1.65} = 0.43\tau$	26400
	40	$\Delta g = 0.60 \lg \tau + 0.40$	$\Delta g^{3.13} = 0.90\tau$	$\Delta g^{2.51} = 0.43\tau$	23400
1Kh18N9	HR*	$\Delta g = 0.84 \lg \tau + 0.60$	$\Delta g^{2.61} = 0.24\tau$	$\Delta g^{1.42} = 0.28\tau$	13700
	10	$\Delta g = 0.44 \lg \tau + 0.62$	$\Delta g^{2.72} = 0.26\tau$	$\Delta g^{1.81} = 0.41\tau$	20000
	20	$\Delta g = 0.51 \lg \tau + 0.34$	$\Delta g^{2.71} = 0.21\tau$	$\Delta g^{1.71} = 0.37\tau$	23000
	30	$\Delta g = 0.40 \lg \tau + 0.52$	$\Delta g^{3.13} = 0.10\tau$	$\Delta g^{2.02} = 0.49\tau$	22000
	40	$\Delta g = 0.31 \lg \tau + 0.40$	$\Delta g^{3.21} = 0.16\tau$	$\Delta g^{2.21} = 0.67\tau$	24000
1Kh13N4G9	HR*	$\Delta g^{1.18} = 0.85\tau$	$\Delta g^{0.91} = 1.50\tau$	$\Delta g^{1.17} = 6.25\tau$	21400
	10	$\Delta g^{1.02} = 0.93\tau$	$\Delta g^{0.90} = 2.12\tau$	$\Delta g^{1.02} = 3.90\tau$	24000
	20	$\Delta g^{0.95} = 0.59\tau$	$\Delta g^{0.96} = 1.95\tau$	$\Delta g^{1.08} = 4.91\tau$	24800
	30	$\Delta g^{0.96} = 0.47\tau$	$\Delta g^{0.82} = 5.47\tau$	$\Delta g^{1.12} = 4.95\tau$	23300
	40	$\Delta g^{0.92} = 0.45\tau$	$\Delta g^{0.86} = 1.10\tau$	$\Delta g^{1.18} = 5.99\tau$	22800

*HR—hot-rolled metal.

The somewhat greater oxidation of 1Kh18N9T in comparison to 1Kh18N9 is due to the presence of easily-oxidized titanium.

Comparison of Fig. 1 and 2 shows that 1Kh13N4G9 is oxidized in air much more rapidly (at 15-25 times the rate) than 1Kh18N9 and 1Kh18N9T; the fact that the indices n are close to 1 and that the curves are nearly linear indicates that the products of high-temperature oxidation have no protective properties. Examination of the graphs and analysis of the mathematical expressions for the oxidation laws shows that the degree of shrinkage has almost no influence on the oxidation rate of 1Kh13N4G9. The values of Q in gaseous corrosion of 1Kh13N4G9 is also almost unaffected by the shrinkage.

The relationship found between high-temperature oxidation and shrinkage in cold rolling might be explained in the light of concepts [4] according to which deformation of metals (for example, in cold rolling) is accompanied by absorption of a part of the energy of deformation. This absorbed part is used in reformation of bonds in the slip regions. Here free electrons are replaced by rigid electronic bridges—the electrons are, in a sense, bound to definite regions of the ionic lattice. Therefore hard, strong regions of low plasticity with transformed bonds are formed in the slip regions during plastic deformation of the metal and the accompanying strengthening. Strengthening of the ionic bond brings it closer in character to the atomic bond, which corresponds to higher bond energies than the metallic bond.

Thus, the observed decrease of oxidation rate and increase of activation energy as the result of shrinkage may be regarded as consequences of strengthening of interionic bonds in the crystal lattice of the metal.* Exposure at 1100° leads to "rest" and recrystallization of 1Kh18N9 and 1Kh18N9T; the retarding influence of strengthening on gas corrosion is thereby eliminated.

*The influence of the partial ferritic transformation in cold rolling is insignificant, as reconversion to austenite should take place in a few minutes at the temperatures studied.

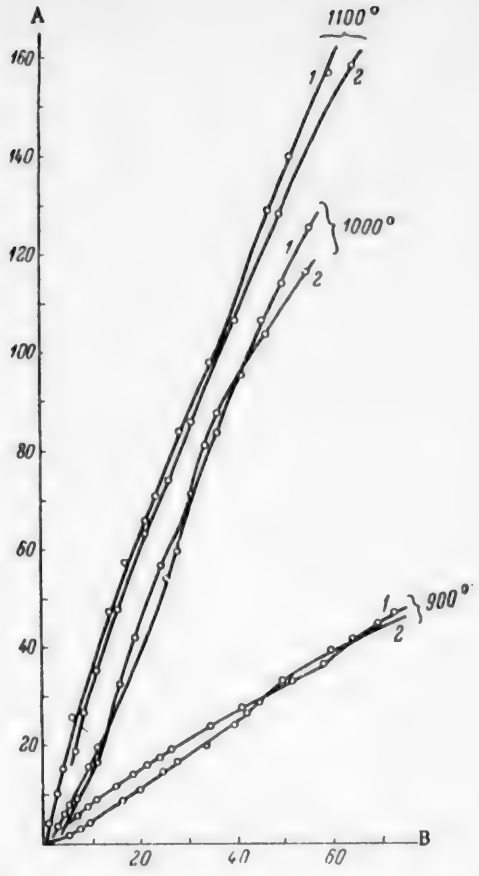

Fig. 2. Kinetics of high-temperature oxidation of 1Kh13N4G9 at 900, 1000, and 1100°: A) weight increase Δg (g/m^2); B) time τ (minutes); 1) hot-rolled specimens; 2) cold-rolled with 40% shrinkage.

The almost linear course of the oxidation curves for 1Kh13N4G9 steel is due to the presence of a large amount of manganese, which leads to formation of loose and easily flaking scale [3]. In addition, the resistance of 1Kh13N4G9 steel in an oxidizing medium is lower because of the lower content (13%) of the alloying metal, chromium, as compared with 1Kh18N9T and 1Kh18N9 (18%). Shrinkage has no influence on Q for this steel because of the high chemical activity of Mn in air at temperatures of 900° and over [6]. Because of the good mutual solubility of Mn and Fe oxides [6], manganese accumulates in the outer layer of the scale [7]. This rapid diffusion of the preferentially oxidized manganese [8] may prevent shrinkage from exerting its influence on the bond strength between the ions (or atoms) in the metal lattice during emergence of ions from the metal into the film in high-temperature oxidation.

The fairly persistent inhibiting effect (lasting for up to 60 minutes from the start of oxidation) of previous cold rolling on high-temperature oxidation may be attributed to difficulties in elimination (by recrystallization) of reinforcement sites with an atomic structure. Another cause may be the increased inhibiting effect on diffusion of gaseous corrosion, found in the layers of the protective film which were formed first on the metal lattice distorted by the cold rolling: such a film reproduces the structure of the deformed steel, while subsequent recrystallization of the metal does not influence the structure and protective properties of this oxide layer.

Connection Between Surface Smoothness and Tendency to Corrosion During High-Temperature Oxidation and Pickling of the Metal

Analysis of the results obtained for 1Kh18N9T and 1Kh18N9 showed that at 1000 and 1100° there is almost no difference between the rates of gaseous corrosion of sandblasted and polished specimens; the indices n of Δg for 1Kh18N9T and 1Kh18N9 do not differ by more than 3%, which is definitely within the error limits of the experiments and graphical constructions. However, in the oxidation of 1Kh18N9T and 1Kh18N9 steels at 900°, which conforms to a logarithmic law, the initial corrosion rate is lower for the polished metal. Thus, the oxidation is represented by the equation $\Delta g = 0.87 \lg\tau + 0.15$ for polished specimens of cold-rolled 1Kh18N9 steel, and by the equation $\Delta g = 0.90 \lg\tau + 0.60$ for sandblasted specimens.

The activation energies found for sandblasted specimens of 1Kh18N9T and 1Kh18N9 were lower (by 18 and 17% respectively) than those found for polished specimens.

In the case of 1Kh13N4G9 steel the surface smoothness has no appreciable influence on the oxidation rate or the energy of activation.

The influence of polishing on the course of gaseous corrosion at the initial stages is explained, on the one hand, by the formation of a reinforced thin surface layer during polishing; this layer is rapidly destroyed during the initial stages of oxidation. On the other hand, sandblasting accelerates oxidation because of the easier cracking of oxide films on surfaces with coarse microrelief [9], and the increase of the true surface area of the metal.

TABLE 2

Effect of Surface Finish of the Original Metal on its Smoothness after Heat Treatment and Pickling by the Works Procedure

Steel grade	H_{rms} * (in μ) for the specimens			
	polished		sandblasted	
	before treatment	after treatment	before treatment	after treatment
1Kh18N9	0.2	1.1	3.4	4.2
1Kh18N9T	0.2	0.7	3.0	4.0
1Kh13N4G9	0.2	4.2	4.0	4.0

*H_{rms} is the root mean square deviation of the peak heights and crevice depths from a certain median line.

TABLE 3

Effect of Cold Deformation with Different Degrees of Shrinkage on Changes in the Surface Finish after Heat Treatment and Pickling by the Works Procedure

Condition of metal	H_{rms} (in μ) for steels					
	1Kh18N9		1Kh18N9T		1Kh13N4G9	
	before treatment	after treatment	before treatment	after treatment	before treatment	after treatment
Original (hot-rolled metal)	3.2	–	2.2	–	2.5	–
After deformation with shrinkage (%):						
10	0.7	1.4	0.9	1.8	0.7	1.3
20	0.6	1.0	0.7	1.4	0.5	1.1
30	0.2	1.0	0.3	1.1	0.4	0.7
40	0.2	0.8	0.5	1.2	0.2	0.6

The surface of 1Kh18N9 and 1Kh18N9T specimens after high-temperature oxidation (during heat treatment) and subsequent pickling is smoother if the metal had previously been polished (Table 2). The increase in surface roughness caused by high-temperature oxidation and pickling is almost the same for 1Kh18N9 and 1Kh18N9T specimens.

Because of the low resistance of 1Kh13N4G9 steel to gaseous corrosion in an oxidizing medium the metal is very strongly attacked to a great depth, and therefore oxidation of polished steel of this grade is accompanied by formation of a very rough film–metal interface, which becomes apparent during scale removal by pickling.

Hot-rolled metal has a considerably rougher original surface than cold-rolled (Table 3); the further increase of roughness resulting from gaseous corrosion and pickling is so serious that the surface formed is beyond the sensitivity limits of the profilometer. On the other hand, in the case of cold-rolled metal the greater the shrinkage the less does the surface smoothness deteriorate. This is due to the general increase of surface smoothness with increased shrinkage as the result of cold rolling (Table 3).

TABLE 4

Effect of Surface Smoothness on Losses of Metal after Heat Treatment and Pickling by the Works Procedure

Metal grade	Surface state	Losses (g/m^2-min)
1Kh18N9	Polished	65
	Sandblasted	103
1Kh18N9T	Polished	56
	Sandblasted	81

Whereas the surface quality has little influence on the course of high-temperature oxidation, during the subsequent descaling the more extensive sandblasted surface leads to greater corrosion of the metal under the oxide film (Table 4).

SUMMARY

1. Cold deformation (shrinkage) of austenitic 1Kh18N9 and 1Kh18N9T stainless steels as the result of cold rolling retards their high-temperature oxidation. This retardation is less at higher temperatures. This effect may be attributed to strengthening of the metallic bonds as the result of cold deformation.

2. This retardation of gaseous corrosion in an oxidizing medium is not found for 1Kh13N4G9 steel because of its high content of rapidly-oxidized manganese.

3. Polished metals are corroded more slowly in the gas phase than metals with very rough surface only during a initial brief period of high-temperature oxidation. During longer exposures, metals with very smooth and very rough surfaces are oxidized at almost the same rate.

4. The smoothness of the metal after heat treatment and subsequent pickling is greater with increased shrinkage.

5. The decrease of metal losses during heat treatment and subsequent pickling with increasing shrinkage is due both to retardation of high-temperature oxidation during heat treatment and to decreased attack on the metal during the subsequent pickling.

LITERATURE CITED

[1] N. P. Zhuk and B. V. Linchevskii, J. Phys. Chem. 28, No. 3, 440 (1954).

[2] P. E. D'yachenko, V. É. Vainshtein, et al., Modern Instruments for Measurement of Surface Roughness of Machine Parts [in Russian] (Izd. AN SSSR, 1950).

[3] G. Schlesinger, Surface Finish (Mashgiz, 1947) [Russian translation].

[4] G. V. Akimov, Proc. Acad. Sci. USSR 47, 8 (1946).

[5] F. F. Khimushin, Stainless, Acid-Resisting, and Heat-Resisting Steels (Metallurgy Press, 1945).

[6] A. B. Kinzel and R. Franks, High-Chromium, Stainless, and Heat-Resisting Steels (Metallurgy Press, 1945) [Russian translation].

[7] V. V. Ipat'ev and V. I. Tikhomirov, Sci. Mem. Leningrad State Univ., Chem. Sci. Ser. 14 (1954).

[8] I.I. Kornilov, A.T. Durnov, and L.I. Pryakhina Proc. Acad. Sci. USSR 58, No.8, 1665 (1947).

[9] A. V. Shreider, J. Phys. Chem. 24, No. 4, 455 (1950).

Received November 10, 1957

FORMATION OF AN ACID SALT OF LEAD IN HYDROCARBON SOLUTIONS OF BUTYRIC ACID

I. N. Putilova and A. R. Myagkova

Moscow Electrotechnical Institute of Communications

When bearing alloys such as leaded bronzes corrode in mineral oils, the lead contained in them enters the hydrocarbon phase in the form of salts of organic acids of relatively low molecular weight (butyric and others). The frictional wear of bearing alloys [1, 2] is very intimately associated with the formation of these salts and their dissolution in lubricating oils. In studies of corrosion processes in hydrocarbon solutions of fatty acids it has been observed repeatedly that different products, dependent on the acid concentration in solution, may be formed by corrosion of the metals. If the acid concentration is low, basic [3] or neutral salts, which are compounds of low solubility, are formed, whereas at high acid concentrations acid salts may be formed, and these are generally more soluble in the nonpolar corrosive media [4, 5]. It is quite obvious that these differences in the solubility of the reaction products greatly influence the rate of corrosion [6]. In recent years increasing attention has been devoted to the composition of corrosion products in corrosion studies [7].

Acid salts of monobasic carboxylic acids differ in many respects from the neutral salts. The peculiarities of acid salts are due to the presence of hydrogen bonds, to which they probably owe their existence [8].

There is relatively little information in the literature on the structure and properties of acid salts of the carboxylic acids. This is to some extent due to the fact that most of the work has been done with aqueous solutions of the salts, and there have been far fewer studies of solutions in nonpolar liquids, where the conditions for formation of acid salts are more favorable. It is no accident that various studies of the properties of acid salts of monobasic carboxylic acids were conducted with the use of nonaqueous solutions [9-11]. An interesting fact is that the number of H^+ ions per univalent metal ion (Na^+, K^+) in a molecule of an acid salt is not randomly variable, and that the formation of acid salts of quite definite types is probable [11].

EXPERIMENTAL

We were able to demonstrate the formation of acid lead butyrates by cryoscopic investigations of benzene and naphthalene solutions of butyric acid. The formation of the acid salt was observed when neutral lead butyrate was dissolved, or lead plates were corroded in solutions of butyric acid in these hydrocarbons. The following materials were used in the experiments: specimens of S-0 grade lead, benzene (d_4^{20} 0.785, b.p. 80.4°) which had been thoroughly dried and distilled over sodium, butyric acid (d_4^{20} 0.9640, b.p. 162° at 765 mm) prepared by repeated rectification of the chemically pure substance, and naphthalene purified by twofold distillation (m.p. 80°).

Neutral lead butyrate was prepared by the action of lead carbonate (chemically pure) on a benzene solution of butyric acid with gentle heating on a water bath. The butyrate was separated from the unchanged carbonate, washed repeatedly with isooctane to remove residual butyric acid, and recrystallized from solution in alcohol. The lead content of the purified product was found to be 54.7%. This corresponds to the neutral butyrate $Pb(C_3H_7COO)_2$. The salt was analyzed gravimetrically, lead being precipitated as $PbSO_4$. $Pb(C_3H_7COO)_2$ melts at 74° to form a thick transparent liquid which crystallizes only after a long interval. $Pb(C_3H_7COO)_2$ is insoluble in melted naphthalene, sparingly soluble in water (0.49 g/100 g H_2O), and slightly more soluble in benzene (1.45 g/100 g C_6H_6).

TABLE 1

Change of Freezing Point of Butyric Acid Solutions in Benzene and Naphthalene on Addition of $Pb(C_3H_7COO)_2$

Expt. No.	Solvent	Solute	m	$-\Delta t$
1	Benzene	Butyric acid	0.2	0.547
2	Benzene	Butyric acid + lead butyrate	0.2 from 0 to 0.0250	0.545
3	Benzene + H_2O to saturation	Butyric acid	0.5	1.305
4	Benzene + H_2O to saturation	Butyric acid + lead butyrate	0.5 0.050	1.270
5	Naphthalene	Butyric acid	0.2	0.705
6	Naphthalene	Butyric acid + lead butyrate	0.2 from 0 to 0.0125	0.707

If butyric acid is first dissolved in the benzene or naphthalene, the solubility of the butyrate greatly increases. For example, 0.1 mole of $Pb(C_3H_7COO)_2$ (38.1 g) dissolves completely in 100 g of benzene or naphthalene containing more than 0.02 mole of butyric acid. It dissolves very slowly in C_6H_6, but the process is accelerated considerably if the acid concentration is increased and the liquid is warmed to 30-35°. Clear solutions of low viscosity are formed, with all the properties of true solutions. The freezing points of solutions of butyric acid in C_6H_6 and $C_{10}H_8$ were determined before and after addition of neutral lead butyrate, by means of the cryoscopic apparatus. The results of the cryoscopic determinations are given in Table 1, where $\underline{m}$ is the number of moles per 1000 g solvent and Δt is the observed change of freezing point relative to that of the pure hydrocarbon (mean of 3 determinations). The minus sign indicates that the freezing point was depressed in all the experiments.

Experiments No. 1 and 2 were carried out with benzene dried as described above, and No. 3 and 4 with C_6H_6 saturated with water at 20°. In Experiments No. 2, 4 and 6, lead butyrate was added by small portions in the total amounts stated—0.0125 or 0.05 mole. The freezing point depression Δt remained constant, varying only by a few thousandths of one degree.

In view of the fact that the acid is present in these solutions mainly as the dimer $(C_3H_7COOH)_2$, the value of Δt and therefore the concentration of the solute molecules would be unchanged if each $Pb(C_3H_7COO)_2$ molecule combines with one dimeric acid molecule to form the salt $Pb(C_3H_7COO)_2(C_3H_7COOH)_2$. The freezing point of the solution might also remain constant if a colloidal solution of the salt was formed. However, as already stated, true solutions were formed, free from the light scattering and other properties characteristic of colloidal systems.

Moreover, the formation of true molecular solutions of lead salts in acidified hydrocarbons was confirmed by the experiments, described below, on the freezing points of hydrocarbon solutions after corrosion of lead specimens in them.

The formation of acid salts of this composition in naphthalene solutions indicates that carboxylic acids which are monobasic in aqueous solutions behave as dibasic in hydrocarbon solutions, retaining one of the hydrogen bonds in the molecule of the acid salt.

The remarkable ability of these salts to dissolve in liquid hydrocarbons with formation of stable solutions must be noted.

Attempts to isolate acid lead butyrate in crystalline form proved unsuccessful; liquid viscous glassy products were obtained in all cases [12]. Similar products were occasionally observed during corrosion of lead in hydrocarbon solutions of butyric acid, when they formed a separate liquid phase, almost free from hydrocarbon, with the water which was simultaneously formed.

TABLE 2

Change of the Freezing Point of Solutions of Butyric Acid in C_6H_6 and C_8H_{10} after Corrosion of Lead in Them

Corrosive medium	Δp		$+\Delta t$		
	in	in moles per 1000 g solvent	experimental	expected on formation of	
				acid salt	acid salt hydrate
Benzene + 0.2 mole butyric acid	0.0300	0.006	0.055	0.030	0.045
	0.0570	0.011	0.080	0.055	0.078
	0.0780	0.015	0.120	0.075	0.112
	0.0936	0.018	0.138	0.090	0.135
	0.1090	0.021	0.195	0.105	0.163
	0.1230	0.024	0.225	0.120	0.180
	0.1410	0.027	0.265	0.135	0.203
Naphthalene + 0.2 mole butyric acid	0.0492	0.009	0.085	0.066	0.099
	0.0834	0.022	0.157	0.157	0.228

Different results are obtained if the benzene is artificially humidified before the cryoscopic determinations by contact with water for several days. It is seen from the results of Experiments No. 3 and 4 (Table 1) that when lead butyrate is added to a solution of butyric acid in benzene humidified in this way the value of Δt does not remain constant as in Experiments No. 1 and 2 but decreases somewhat. This increase of freezing point by the introduction of a new substance indicates that the concentration of the dissolved particles does not increase (as might have been expected) but decreases. This may be the consequence of association of the acid-salt molecules into larger aggregates.

Water molecules are the binding agents, as this effect is observed only in presence of water. The amount of water required to saturate 100 g of benzene is 3.0 millimoles [13].

The water molecules present in benzene solution are associated, so that, as our experiments showed, the freezing point of benzene saturated with water is almost the same as that of dry benzene.

Our value for the freezing point elevation of the solution, 0.035° (Table 1, Experiments No. 3 and 4: 1.305 − 1.270 = 0.035°) can be interpreted on the assumption that all the dissolved water takes part in the association, forming $[Pb(C_3H_7COO)_2(HC_3H_7COO_2)]_2 \cdot 2H_2O$. A hydrate of the same composition was formed during corrosion of lead in benzene solutions of butyric acid (Table 2). It may be noted that the amount of H_2O in water-saturated benzene is sufficient for association of about 28% of the dissolved salt.

Attempted experiments with addition of water to naphthalene solutions did not give reproducible results because of the considerable evaporation of water at t = 80−90°.

The formation of acid butyrates may also be observed by measurements of the freezing points of solutions of butyric acid in benzene and naphthalene after corrosion of lead plates in them. In Table 2 the weight loss Δp of the specimens is correlated with the freezing-point elevation of the solutions $+\Delta t$. The amount of solution used was 25 g (the lead plates were 10 cm^2 in area).

If a neutral salt was formed as the result of corrosion of lead, the number of molecules in solution would remain unchanged and the freezing point would remain at the same level ($\Delta t = 0$). However, it is clear from the data in Table 2 that the freezing point of the solution rises ($\Delta t > 0$). It follows that the number of molecules in solution decreases. If the salt $Pb(C_3H_7COO)_2(C_3H_7COOH)_2$ was formed, a mole of $Pb^{\cdot\cdot}$ ions entering the solution would produce a freezing-point elevation ($+\Delta t$) of 5° in benzene and 6.9° in naphthalene, as this amount of lead (207 g) would additionally bind 1 mole of acid dimer.

Table 2 shows that the freezing-point elevation of benzene solutions is always greater than the value calculated for formation of the acid salt. This is because the water which is inevitably formed in corrosion of lead, in an amount equivalent to the amount of lead converted, causes association of the acid-salt molecules with formation of a hydrate of the same composition, $[Pb(C_3H_7COO)_2(HC_3H_7COO)_2]_2 \cdot 2H_2O$. In contrast to the analogous experiments with benzene saturated with water, in this instance the water concentration is sufficient

for association of all the molecules of the dissolved salt. It must be emphasized, however, that the accuracy of the cryoscopic method is considerably reduced under the experimental conditions used, if only because part of the corrosion products adheres to the specimen and is removed with it before the freezing-point determinations.

This possibly explains why the freezing-point elevations ($+\Delta t$) observed in our experiments are rather greater than the values calculated on the assumption that the hydrate is formed (Table 2, Columns 4 and 6).

Quite different results are obtained with solutions of butyric acid in naphthalene, where hydrate formation is impossible becuase of evaporation of water. In these solutions, corrosion of lead yields an anhydrous acid salt of the same composition $Pb(C_3H_7COO)_2(C_3H_7COOH)_2$ as that formed when $Pb(C_3H_7COO)_2$ is dissolved.

We consider that these results may be of interest, as acid lead butyrates and their hydrates are not described in the literature.

Investigation of these compounds sheds light on the chemical aspects of corrosion processes involving lead in oils and other hydrocarbon media. At the same time we would point out that the cryoscopic method is sometimes useful in studies of corrosion and corrosion products.

SUMMARY

1. Cryoscopic determinations revealed the existence of the acid salt $Pb(C_3H_7COO)_2(C_3H_7COOH)_2$ formed by the reaction of $Pb(C_3H_7COO)_2$ with butyric acid dissolved in benzene or naphthalene. The same salt is formed during corrosion of lead in naphthalene solutions of butyric acid.

2. The same (cryoscopic) method was used to demonstrate the presence of the hydrate $[Pb(C_3H_7COO)_2 \cdot (HC_3H_7COO)_2]_2 \cdot 2H_2O$ after interaction of $Pb(C_3H_7COO)_2$ with a benzene solution of butyric acid, saturated with water. This hydrate is also formed when lead reacts with a benzene solution of the acid.

LITERATURE CITED

[1] K. S. Ramaiya and V. L. Val'dman, Petroleum Economy 11 (1937).

[2] G. M. Nurk and E. É. Verner, Proc. 2nd All-Union Conference on Friction and Wear in Machines [in Russian] (Izd. AN SSSR, 1947) p.318.

[3] D. Turnbull and D. R. Frey, J. Phys. Colloid. Chem. 51, 681 (1947).

[4] L. G. Gindin, T. A. Miskinova and I. N. Putilova, Proc. Acad. Sci. USSR 4, 683 (1956).*

[5] L. G. Gindin and V. A. Kazakova, J. Appl. Chem. 24, 958 (1951).*

[6] L. G. Gindin, V. A. Kazakova and I. N. Putilova, Proc. Acad. Sci. USSR 80, 5, 277 (1951).

[7] Corrosion 13, 2, 111; 9, 567 (1957).

[8] Batuev, Progr. Chem. 4 (1941).

[9] P. Walden, Elektrochemie nichtwasseriger Lösungen, Verlag A. Barth, Leipzig, 30 (1924).

[10] H. P. Kaufmann, Th. Lüssling, Fette u. Seifen, 55, 2, 90 (1953).

[11] T. G. Levi, Gaz. Chim. Ital. 62, 709 (1932).

[12] H. J. Braun, Die Metallseifen, Verlag O. Spamer, 35 (1932).

[13] Technical Encyclopedia Data Book [In Russian] 6, 113.

Received December 11, 1957

*Original Russian pagination. See C. B. Translation.

PRODUCTION OF SULFITE PULP FOR VISCOSE

L. E. Akim, T. G. Badmas, N. A. Mel'chakova
S. L. Talmud and A. N. Tuzhetskaya

The Leningrad Technological Institute of the Pulp and Paper Industry

Koskinen [1] drew attention to the fact that if unbleached sulfite pulp is passed twice through a "Lampensator" there is not only a considerable reduction in the resin content of the pulp, but decrease of lignin and ash contents and an increase of the α-cellulose content; i.e., the pulp is partially refined. It was also noted that the consumption of chlorine in bleaching is reduced owing to the removal of harmful impurities.

Talmud, Derevyagina, and Ioffina [2,3] determined quantitatively the stability of emulsified resin in resin–water and resin–sulfite liquor–water systems and the contents of resin in pulps under various conditions for separation of the liquor from the fibers. It was found that when the temperature of the cooking liquors is lowered large amounts of resin are liberated; this resin is deposited on the fibers and raises the resin content of the pulp. It was noted that as much liquor as possible should be removed from the digesters during discharge of the pulp, and the liquor should be separated from the fibers at about 100°.

Talmud, Ivanyushkina, Popova, and Yanzuvaeva [4] first raised the question of refining unbleached pulp by fractionation with the most thorough removal of fine cellulose fibers. For these trials pulp samples were taken from the digesters. The fibers were separated from the liquor while hot, so that liberation of resin from the liquor and deposition on the fibers was excluded. The fine fibers were separated by prolonged washing on a No. 65 screen. It was shown that the pulp can be almost completely deresinified as the result of such fractionation. Moreover, the α-cellulose content rose considerably.

The advantages of fractionation of cellulose by fiber length were confirmed by Perila [5], who reported that after removal of 12.6 % of short fibers the cellulose reactivity is increased and the filterability of the viscose solutions improved.

In 1954 Talmud, Turzhetskaya, and Kuleshova studied the chemical composition of fine cellulose fibers and fractionated the cellulose present in them by molecular weight. It was found that fine cellulose fibers contain (calculated on the bone-dry substance) 19.0% resins and fats (soluble in ethyl alcohol and acetone), 7.2% lignin, 1.5% ash, and only 72.3% cellulose.

The results of this work confirmed that pulp may be refined by removal of its low-grade component, short fibers.

For reasons beyond the authors' control, this work was not published until 1957 [6].

Independently of this work, Sarten [7] published a paper at the end of 1954, in which the extremely low quality of fine cellulose fibers was noted.

Rogovin [8,9] put forward the view that in order to increase xanthate solubility, improve filterability, and reduce sharply the amounts of impurities present in viscose pulp, fine fibers should be removed as thoroughly as possible.

Talmud and Gracheva [10] purified bleached pulp by fiber fractionation and investigated fine fibers of bleached pulp. It was found that bleached pulp is refined by removal of fine fibers.

The resin content of bleached pulp refined by removal of fine fibers was considerably higher than that of refined unbleached pulp. The explanation was that in the production of bleached pulp the sulfite liquor was separated from the fibers with considerable cooling, so that the resin separated out and was deposited on the fibers. The quality of bleached fine cellulose fibers was also extremely low. Investigation of the morphological composition of these fibers showed that they contain considerable amounts of medullary and parenchyma cells.

Talmud, Aizenshtadt, Ioffina, Kuz'mina, Lavrent ev, and Turzhetskaya [11] repeated earlier work on dissolving pulps and confirmed the earlier findings according to which fractionation of unbleached pulps by fiber length is advisable and necessary.

Very recently the question of pulp fractionation has attracted the attention of numerous foreign workers. Several papers on the subject have appeared [12-14]. The last two of these contain detailed reviews of the literature.

The chemical composition of the fine cellulose fibers from unbleached sulfite pulp shows that it is quite unjustified to leave this fraction in pulp destined for viscose production.

The question of the advisability of fractionation of pulp by fiber length can be also considered from another standpoint. It is known that the losses during bleaching and hot alkaline refining of viscose pulp are very high. In a number of mills producing viscose pulp the losses in these processes reach 25-30%. In addition, the consumption of bleaching agents, caustic soda (about 100 kg per ton of pulp) and power for heating the pulp is very high.

The question arises of the nature of the production losses during bleaching and hot alkaline refining.

We suggest that, after removal of harmful impurities (resins, fats, lignin, and ash) from the fine cellulose fibers during bleaching and hot alkaline refining, these fibers, which have a high cont ent of fractions of low molecular weight, react most vigorously with the alkali, are partially dissolved in it and partially dispersed, and are therefore largely lost with the wastes.

In our opinion, unbleached pulp should be fractionated by fiber length and the fine fibers should be removed from the main stream; this should sharply diminish fiber losses and decrease consumption of bleaching agents, of caustic soda for refining of the viscose pulp, and of heat and power.

The object of the present investigation was a study of chemical losses during bleaching and hot alkaline refining of pulp, with different methods for the preliminary purification of the unbleached pulp, i.e., without previous fractionation and with fractionation by removal of different proportions of fine fibers. It was also intended to investigate the possibility of lowering the consumption of bleaching agents, alkali, heat, and electric power in these processes. We do not regard the separated fine cellulose fibers and the accompanying larger fibers as production losses of cellulose, but rather as fibers which differ sharply in chemical composition from the main bulk of the pulp and which should therefore be used for production of lower grades of pulp than that used for viscose.

EXPERIMENTAL

The experiments were performed with unbleached sulfite pulps taken from the thickeners of the refining section of the Priozerskii pulp mill. Two batches of pulp, differing in bleachability, were taken.

A part of the original unbleached pulp of Batches I and II was not subjected to preliminary treatment. The rest of the pulp was fractionated by fiber length, fine fibers being washed in such a way as to give three samples, differing in the amounts of fine fibers removed, for each batch. The fine fibers were washed out on No. 65 screens. During the forced removal of fine fibers some of the larger fibers were, of course, also washed out. Samples of the original (unfractionated) unbleached pulp, and fractionated pulp were then treated in accordance with the process developed by Akim et al., for production of refined viscose pulp.

The cellulose was chlorinated to bleachability values of 10-12 permanganate units under the following conditions: chlorine consumption for Batch I (lower bleachability), 2.3%; for Batch II (higher bleachability), 2.6%; pulp concentration 2.5%; chlorination time 45 minutes.

The hot alkaline treatment was carried out at 95°, pulp concentration 10%, alkali consumption 7.5% on the fiber weight, duration 2.5 hours.

TABLE 1

Pulp Yields at Different Stages

Pulp batch	Amount of fine fibers removed (%)	Bleachability (permanganate units)	Yield (% on original pulp)			Chemical losses of cellulose (%)	Relative decrease of loss (%)
			after chlorination	after alkaline treatment	after hypochlorite bleach		
I	0	35.0	98.69	80.52	80.16	19.84	—
	5.00	27.8	99.61	83.63	82.90	17.10	13.8
	11.17	27.5	99.27	83.63	83.50	16.70	15.8
	18.46	29.2	99.05	84.33	85.93	15.07	24.04
II	0	46.0	98.87	81.98	81.48	18.52	—
	6.47	40.0	99.47	83.30	83.30	16.70	9.8
	9.13	40.4	99.25	3.30	83.30	16.70	9.8
	17.4	37.6	98.79	83.87	83.87	16.13	12.9

The final bleaching was effected by means of calcium hypochlorite at 38-40°, pulp concentration 7%, consumption of active chlorine 1% on the fiber weight, duration 3 hours.

The fibers were separated from the liquor after each treatment stage by means of a cloth filter. Analyses of the filtrates showed them to be quite free of suspended matter. Therefore the cellulose losses found are truly chemical.

The pulp yields at different stages and the total cellulose losses during treatment of these samples are given in Table 1.

It is clear from the data in Table 1 that preliminary fractionation of unbleached pulp has a significant influence on the pulp yield in bleaching and hot alkaline treatment of the pulp.

All the samples of Batches I and II were analyzed in detail.

The analytical results are given in Table 2.

A number of important conclusions may be drawn from the results (Table 2). Preliminary removal of fine fibers lowers the pentosan content of unbleached pulp. This decrease is most pronounced on removal of 18.46 and 17.40% of fine fibers. The contents of resins and fats in unbleached pulp, as shown by the results of extraction with dichloroethane, decrease with progressive removal of fine fibers and reach 0.48 and 0.51% respectively. The resin content of unbleached pulp cannot be reduced further in practice until the separation of sulfite liquor from the fiber has been improved (by the use of temperatures of about 100°).

The resin and fat contents, as found by dichloroethane extraction, of unfractionated bleached cellulose Batches I and II were 0.45 and 0.32% respectively (the GOST 5982-51 specifications are 0.7% for grade II and 0.55% for grade I); this shows that the conditions chosen for bleaching and hot alkaline refining give a cellulose with a low resin content, despite the fact that the original unbleached pulps contained 1.70 and 1.31% resin. Bleaching and hot alkaline refining of previously fractionated cellulose lowered the resin and fat contents still further (down to 0.28 and 0.26%). The lignin content of the unbleached pulp was reduced 6-fold by preliminary removal of fine fibers. The chosen conditions for bleaching and hot alkaline refining made it possible to obtain a bleached pulp with low lignin contents —0.25 and 0.23% (the GOST specifications are 0.75% for grade II and 0.65% for grade I) — despite the fact that the original unfractionated pulps contained 3.07 and 3.32% lignin respectively. As the result of fractionation, the α-cellulose contents of unbleached pulp rose to 89.16 and 89.45%, the standard specifications for refined viscose pulp being 89% for grade II and 91.5% for grade I. The adopted procedure of bleaching and hot alkaline refining gave high contents of α-cellulose —93.94% and 95.01%— in bleached pulps, unfractionated and previously fractionated, respectively. The average degree of polymerization of unbleached pulp first increases and then decreases somewhat as the result of fractionation. Data on the average degree of polymerization after hot alkaline refining and bleaching are less significant, as the effects of the treatments are superposed. The ash content of unbleached pulp is lowered somewhat by

TABLE 2

Analytical Results for Pulps

Pulp batch	Fine fibers removed (%)	Bleachability (permanganate units)	Pentosan content of unbleached pulp (%)	Resin and fat contents of pulps: (%): unbleached: extract in dichloroethane	Resin and fat contents of pulps: (%): unbleached: extract in ether + acetone	Resin and fat contents of pulps: (%): bleached: extract in dichloroethane	Resin and fat contents of pulps: (%): bleached: extract in ether + acetone	Lignin contents of pulps: (%): unbleached	Lignin contents of pulps: (%): bleached	Contents of α-cellulose (%) in: unbleached pulp	Contents of α-cellulose (%) in: after chlorination	Contents of α-cellulose (%) in: after alkaline treatment	Contents of α-cellulose (%) in: after hypochlorite bleach	Average degree of polymerization: unbleached pulp	Average degree of polymerization: after chlorination	Average degree of polymerization: after alkaline treatment	Average degree of polymerization: after hypochlorite bleach	Ash content (%): unbleached pulp	Ash content (%): after chlorination	Ash content (%): after alkaline treatment	Ash content (%): after hypochlorite bleach
	0	35.0	6.54	1.70	1.89	0.45	0.52	3.07	0.25	87.5	86.44	94.73	94.07	903	832	1051	908	0.257	0.12	0.07	0.49
	5.0	27.8	6.47	1.13	1.19	0.42	0.50	1.29	0.25	88.38	87.67	95.42	94.86	943	900	1014	790	0.240	0.14	0.14	0.30
	11.17	27.5	6.43	0.58	0.73	0.32	0.44	0.79	0.043	88.7	88.07	95.61	95.01	961	974	1030	841	0.237	0.10	0.12	0.23
	18.46	29.2	4.26	0.48	0.75	0.28	0.32	0.47	0.022	89.16	88.31	94.85	93.94	937	931	1017	867	0.234	0.11	0.13	0.60
	0	46.0	5.57	1.31	1.73	0.32	0.42	3.32	0.23	88.3	86.92	94.94	93.52	1019	971	1147	934	0.30	0.10	0.09	0.69
I	6.47	40.0	5.31	1.02	1.05	0.31	0.41	1.55	0.065	89.1	87.91	95.38	94.81	1098	1052	1107	931	0.258	0.16	0.17	0.38
	9.13	40.4	4.98	0.71	0.74	0.30	0.40	1.29	0.065	89.37	87.84	95.56	94.67	1080	1016	1129	894	0.27	0.16	0.14	0.32
	17.40	37.6	3.97	0.51	0.65	0.26	0.39	0.66	0.12	89.45	88.55	95.14	94.35	1038	1059	1160	980	0.25	0.08	0.12	0.33
GOST specifications for refined viscose pulp grade:																					
I	—	—	—	—	—	0.55	—	—	0.65	—	—	—	91.5	—	—	—	—	—	—	—	0.19
II	—	—	—	—	—	0.7	—	—	0.75	—	—	—	89.0	—	—	—	—	—	—	—	0.26

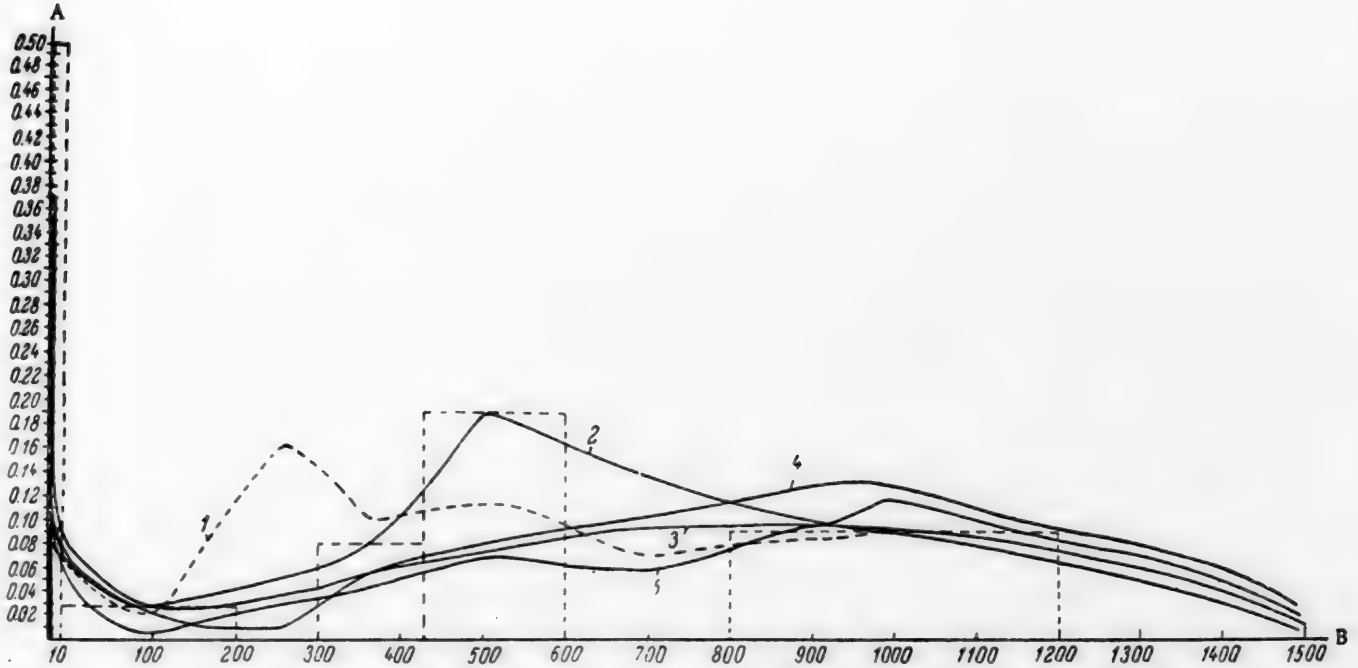

Distribution of cellulose fractions by degree of polymerization: A) ratio of percentage contents of fractions to changes of degree of polymerization; B) degree of polymerization; pulps: 1) original unbleached; 2) original bleached; 3, 4 5) bleached with fine fibers removed; amounts of fine fibers removed (%) 3) 5, 4) 11.17, 5) 18.5.

fractionation. The higher ash content of bleached and refined cellulose is due to the fact that we omitted the acid treatment after the hypochlorite bleach.

It follows from the data in Table 2 that preliminary fractionation of unbleached pulp improves the quality is almost every respect and that the best results were obtained after removal of 18.46 and 17.40% of fine and accompanying large fibers.

It should be remembered that the average degree of polymerization as determined by the Dearing cuprammonium method, is an aggregate value which does not take molecular heterogeneity into account.

Akim and Kil'kki [15] demonstrated convincingly the influence of molecular heterogeneity of sulfite viscose pulp on its reactivity. Akim [16] carried out an extensive study of the molecular heterogeneity of cellulose by the method of stepwise dissolution in phosphoric acid solutions of definite concentrations [17]. This method was used to characterize molecular heterogeneity, by fractionation according to molecular weight, of unbleached pulp Batch I (without preliminary treatment), the same pulp after bleaching and hot alkaline refining, and bleached pulps after pretreatment. The results of fractionation by molecular weight are plotted in the diagram, where the ratios of the percentage contents of the fractions (F) to changes in the degree of polymerization (ΔDP) are taken along the ordinate axis, and the degree of polymerization (DP) along the abscissa axis.

TABLE 3

Determination of Chlorine Consumption for Pulp Chlorination

Pulp batch	Fine fibers removed (%)	Bleachability (permanganate units)	Chlorine consumption for chlorination (%)	
			of total chlorine consumption	on fiber weight
I	0	35.0	100	2.3
	5.00	27.8	90	1.7
	11.17	27.5	90	1.7
	18.46	29.2	90	1.7
II	0	46.0	100	2.6
	6.47	40.0	90	2.1
	9.13	40.4	100	2.3
	17.4	37.6	90	2.0

TABLE 4

Results of Experiments on Hot Alkaline Treatment of Fractionated Pulp

Pulp batch	Fine fibers removed (%)	Yield (% on original pulp)		Total losses (%)	Relative decrease of losses (% relative to original unfractionated pulp, with 7.5% alkali consumption)	α-Cellulose contents (%)		Average degree of polymerization	
		after alkaline treatment	after hypochlorite bleach			after alkaline treatment	after hypochlorite bleach	after alkaline treatment	after hypochlorite bleach
I	0	85.21	85.21	14.79	25.45	92.34	91.82	—	930
	5.0	85.56	85.56	14.44	27.2	94.22	93.58	1008	783
	11.17	85.45	85.25	14.75	25.6	94.35	93.77	999	796
	18.46	89.76	89.58	10.42	47.5	93.97	93.25	987	821
II	0	85.67	85.67	14.33	22.6	92.90	92.14	—	861
	6.47	85.62	85.62	14.38	22.4	94.31	93.88	1088	918
	9.13	86.33	86.33	13.67	26.2	94.04	93.63	1112	861
	17.4	88.18	88.18	11.82	36.2	93.61	92.76	1100	912

The rectangles marked by dash lines in the diagram represent the product $(F/\Delta DP)\cdot\Delta DP = F$, the percentage content of each fraction.

It follows from the diagram that preliminary removal of fine fibers from unbleached pulp lowers the content of low-molecular fractions (up to DP 200) in bleached and refined pulp. Moreover, the distribution curves are shifted toward higher degrees of polymerization. Thus, the pulp becomes more homogeneous and the fractional composition is improved.

The chlorine consumption for chlorination of pulps after removal of fine fibers was determined; the results are given in Table 3.

Table 3 shows that after removal of fine fibers the chlorine consumption falls relatively by 26 and 23.1%, respectively.

In view of the fact that preliminary treatment of unbleached pulp by fractionation according to fiber length removes, before bleaching and hot refining, the greater proportion of harmful impurities and also the fine-fiber fraction which, in our opinion, is totally or partially dispersed and is the main source of mechanical and chemical losses in production, we studied the possibility of finding milder conditions of alkaline treatment in order to lower alkali consumption and to reduce chemical losses further. Experiments were carried out in which previously fractionated pulp was subjected to hot alkaline treatment with a 33.3% reduction of alkali consumption, i.e., with 5% alkali on the fiber weight; as before, fiber losses were taken into account and the α-cellulose contents and the average degree of polymerization were determined.

The results are given in Table 4.

It follows from the results of Table 4 that as the result of preliminary fractionation of unbleached pulp the alkali consumption in hot refining can be reduced considerably, and another important step toward a sharp reduction of chemical losses can be taken. The total relative decrease of chemical losses as the result of fractionation of the unbleached pulp and the use of milder conditions of alkaline treatment was 47.5 and 36.2% respectively for the pulps tested. As the data on the α-cellulose contents show, the resultant pulp quality is considerably above the GOST specifications. The average degree of polymerization conforms to the specifications for viscose pulp.

In addition to decreased consumption of bleaching agents and alkali as the result of removal of fine fibers, the consumption of heat in hot refining and of electric power should show corresponding decreases.

It is to be expected that under production conditions mechanical losses, in addition to chemical losses, should be reduced substantially.

SUMMARY

1. Chemical losses during bleaching and hot alkaline treatment of viscose pulp, without preliminary fractionation and after preliminary fractionation of the unbleached pulp to various degrees according to fiber length, were determined under laboratory conditions.

2. As the result of preliminary fractionation of unbleached pulp, and the consequent possibility of using milder conditions for hot alkaline refining, chemical losses of fibers can be reduced considerably (by 36.2–47.5%), the consumption of chlorine (by 23.1–26.0%) and of alkali (by 33.3%) can be lowered, and the quality of the viscose pulp can be improved.

3. Industrial trials of the production of viscose pulp by the method described may be recommended on the basis of these results.

LITERATURE CITED

[1] I. Koskinen, Pappers och Trävareitidskrift för Finland, 21, 857 (1938).

[2] V. P. Derevyagina and S. L. Talmud, J. Appl. Chem. 27, No. 5, 501 (1954).*

[3] S. L. Talmud and É. M. Ioffina, Trans. Leningrad Technol. Inst. 4, 143 (1956).

[4] S. L. Talmud, A. M. Ivanyushkina, L. A. Popova and L. P. Yazuvaeva, Proc. Acad. Sci. USSR 92, No.2, 397 (1953).

*Original Russian pagination. See C. B. Translation.

[5] Olavi Perila, Paperi ja Puu 35, 4a, 139 (1953).

[6] S. L. Talmud, A. N. Turzhetskaya, and A. A. Kuleshova, Colloid J. 19, No. 1, 118 (1957).*

[7] P. Sarten, Das Papier 8 (1954).

[8] Z. A. Rogovin, Fundamentals of the Chemistry and Technology of Artificial Fiber Production [in Russian] (State Light Industry Press, 1957) p. 210.

[9] Z. A. Rogovin, Paper Ind. 7, 2 (1957).

[10] S. L. Talmud and N. F. Gracheva, Trans. Leningrad Technol. Inst. 5, 79 (1958).

[11] M. G. Aizenshtadt, É. M. Ioffina, E. A. Kuz'mina, A. I. Lavrent'ev, S. L. Talmud, and A. N. Turzhetskaya, Trans. Leningrad Technol. Inst. 7 (1959).

[12] M. Dubach and M. Rutishauser, Das Papier 3/4, 37 (1957).

[13] H. Sihtola, A. Saarinen, I. Wigren, T. Ulmanen and E. Saxen, Paperi ja Puu 39, 8, 383 (1957).

[14] E. Treiber, A. Stenins and I. Rehnström, Svensk Papperstidning, 61, 3, 55 (1958).

[15] L. E. Akim and V. E. Kil'kki, Paper Ind. 10, 5 (1953).

[16] N. I. Nikitin, Chemistry of Wood [in Russian] (Izd. AN SSSR, 1951) p. 96.

[17] A. Ekenstam, Svensk Papperstidning, 45, 61 (1942).

Received October 28, 1958

*Original Russian pagination. See C. B. Translation.

POTASH SULFATE PULP

Yu. N. Nepenin and L. N. Vybornova

The S. M. Kirov Academy of Wood Technology

The influence of the nature of the alkali used for alkaline delignification of wood has been studied very little. In 1941 Larocque and Maass [1] cooked black-spruce chips with a large excess of 2 M alkali and determined the rate constants of delignification, regarded as a monomolecular reaction. If the constant for cooking with caustic soda is taken as unity, the corresponding values are 0.62 for cooking with lithium hydroxide and 1.13 with caustic potash.

Also in 1941, a short note was published by Brintzinger [2], who performed a large number of experiments on cooking of different woods in order to compare the delignifying effects of caustic soda and caustic potash. It was found that the mechanical properties and viscosity of "potash" pulp are better than those of soda pulp made under the same conditions. Comparative cooks by the sulfate process were also performed, and it was again confirmed that "potash sulfate" pulp has considerably better properties than ordinary "soda sulfate" (kraft) pulp.

Since the reserves of potash salts in the Soviet Union are considerable, and economically efficient methods for their winning and production (including potassium sulfate) are now available, the question of the use of caustic potash for production of sulfate pulp is of practical as well as of theoretical interest. This fact prompted us to carry out this limited investigation, conducted in the laboratory of the Pulp and Paper Department of the Academy of Wood Technology.

Comparative Kinetic Studies of the Cooking of Wood Chips in Solutions of Caustic Soda and Caustic Potash

For determination of the kinetic relationships, several series of laboratory cooks were performed in a battery of steel autoclaves, 160 ml in capacity, heated on a glycerol bath. Each autoclave was charged with 100 ml of alkali and 20 g (bone-dry weight) of pine chips 20 x 10 x 2 mm in size. Analysis of the wood gave the following results (% on bone-dry weight): ash 0.27, resin (by ether extraction) 3.20, lignin (in resin-free wood, by the method with 72% sulfuric acid) 27.75, pentosans (by the bromide–bromate method) 11.9. The average moisture content of the chips was 8%. The caustic liquors were made from chemically pure reagents. The autoclaves were immersed simultaneously into the previously-heated bath in such a manner that after a short time (10 minutes on the average) the required ("final") cooking temperature became established in them, and this was then maintained constant. The cooking time was reckoned from the instant of immersion of the autoclaves in the bath. At the end of a fixed time (1, 2, 4, and 8 hours) the autoclaves were cooled in a stream of cold water to stop the cooking. The products were washed and screened, and the following were determined: yield, amount of uncooked wood, and lignin in the separated fibers and the uncooked wood (by the method with 72% sulfuric acid).

The cooking experiments were in three groups:

a) comparative cooks with NaOH and KOH, with equal consumptions of active alkali, equivalent to 25% NaOH on the bone-dry wood, at two different temperatures: 160 and 170°;

b) comparative cooks with NaOH and KOH, at the same temperature of 170° and with two different consumptions of active alkali, equivalent to 20 and 25% NaOH on the bone-dry wood;

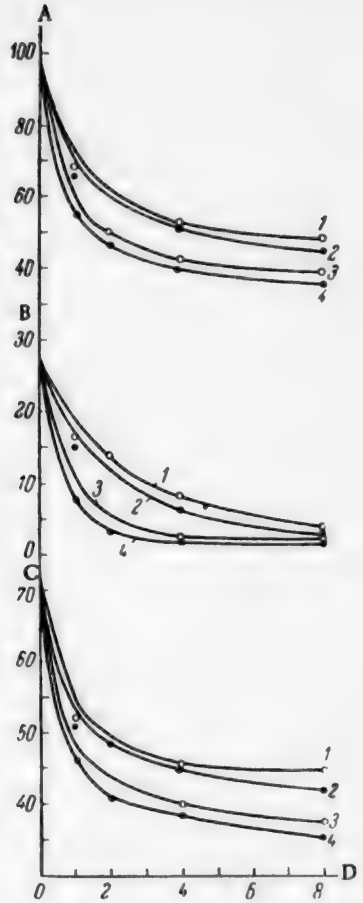

Fig. 1. Comparative cooks at active alkali consumption equivalent to 25% NaOH on the weight of bone-dry wood, at 160 and 170°: A) total yield (%); B) residual lignin (% on wood); C) residual carbohydrates (% on wood); D) cooking time (hours); 1) NaOH at 160°; 2) KOH at 160°; 3) NaOH at 170°; 4) KOH at 170°.

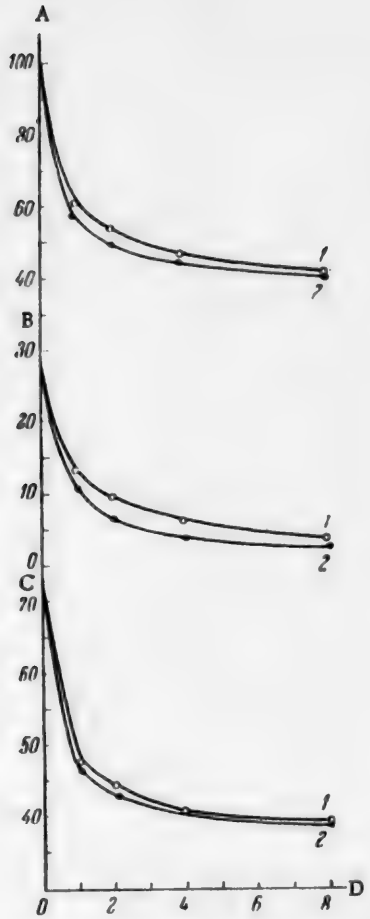

Fig. 2. Comparative cooks at active alkali consumption equivalent to 20% NaOH on the weight of bone-dry wood, at 170°: A) total yield (%), B) residual lignin (% on wood), C) residual carbohydrates (% on wood), D) cooking time (hours); 1) NaOH, 2) KOH.

c) comparative cooks by the sulfate process, with NaOH + Na_2S and KOH + K_2S, at 170°, with active alkali consumption equivalent to 25% NaOH on the bone-dry wood, 25% sulfidity.

The results are plotted in Fig. 1-3, showing the course of "dissolution " of lignin and carbohydrates (the contents of the latter were found from the difference between the total yield and the lignin content), and of the wood as a whole (from the total yield).

It is clear from the graphs that under all the cooking conditions used, cooking is accelerated when caustic potash is used rather than caustic soda. Both the "dissolution" of wood as a whole, and the dissolution of its principal components—lignin and carbohydrates—are accelerated. Among the separate pairs of cooks, the greatest relative acceleration is found for cooks with the lower consumption of active alkali (20% on the wood, in NaOH units, see Fig. 2), and the least relative acceleration is found for sulfate cooks (Fig. 3).

TABLE 1

Kinetic Equations

Cooking conditions				Empirical kinetic equations $\lg \frac{a}{a-x} = A \cdot t^m$ for "dissolution" of		
kind of alkali	temperature (°C)	consump. of active alkali (as % NaOH)	sulfidity (%)	wood as a whole	lignin	carbohydrates
NaOH	160	25	0	$\lg \frac{100}{100-x} = 0.163 \cdot t^{0.31}$	$\lg \frac{27.75}{27.75-x} = 0.215 \cdot t^{0.64}$	$\lg \frac{72.25}{72.25-x} = 0.143 \cdot t^{0.19}$
KOH	160	25	0	$\lg \frac{100}{100-x} = 0.178 \cdot t^{0.31}$	$\lg \frac{27.75}{27.75-x} = 0.252 \cdot t^{0.64}$	$\lg \frac{72.25}{72.25-x} = 0.152 \cdot t^{0.19}$
NaOH	170	25	0	$\lg \frac{100}{100-x} = 0.254 \cdot t^{0.23}$	$\lg \frac{27.75}{27.75-x} = 0.505 \cdot t^{0.38}$	$\lg \frac{72.25}{72.25-x} = 0.187 \cdot t^{0.20}$
KOH	170	25	0	$\lg \frac{100}{100-x} = 0.274 \cdot t^{0.23}$	$\lg \frac{27.75}{27.75-x} = 0.587 \cdot t^{0.38}$	$\lg \frac{72.25}{72.25-x} = 0.204 \cdot t^{0.20}$
NaOH	170	20	0	$\lg \frac{100}{100-x} = 0.226 \cdot t^{0.23}$	$\lg \frac{27.75}{27.75-x} = 0.317 \cdot t^{0.48}$	$\lg \frac{72.25}{72.25-x} = 0.180 \cdot t^{0.17}$
KOH	170	20	0	$\lg \frac{100}{100-x} = 0.239 \cdot t^{0.23}$	$\lg \frac{27.75}{27.75-x} = 0.404 \cdot t^{0.48}$	$\lg \frac{72.25}{72.25-x} = 0.193 \cdot t^{0.17}$
NaOH + $+ Na_2S$	170	25	25	$\lg \frac{100}{100-x} = 0.298 \cdot t^{0.15}$	$\lg \frac{27.75}{27.75-x} = 0.770 \cdot t^{0.30}$	$\lg \frac{72.25}{72.25-x} = 0.191 \cdot t^{0.18}$
KOH + $+ K_2S$	170	25	25	$\lg \frac{100}{100-x} = 0.319 \cdot t^{0.15}$	$\lg \frac{27.75}{27.75-x} = 0.848 \cdot t^{0.30}$	$\lg \frac{72.25}{72.25-x} = 0.208 \cdot t^{0.18}$

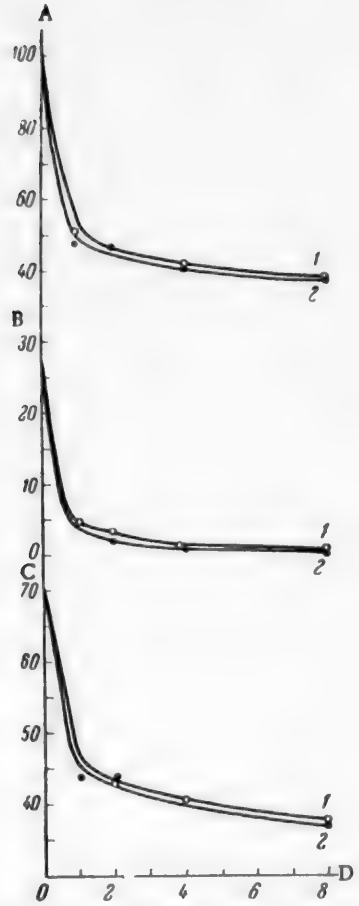

Fig. 3. Comparative sulfate cooks at active alkali consumption equivalent to 25% NaOH on the weight of bone-dry wood, 25% sulfide content, 170°: A) total yield (%); B) residual lignin (% on wood); C) residual carbohydrates (% on wood); D) cooking time (hours); 1) NaOH + Na_2S; 2) KOH + K_2S.

Empirical kinetic equations were derived in order to illustrate more clearly the difference in kinetics in cooking with NaOH and KOH. The rate constant for the first hour of the cook was calculated, as for a monomolecular reaction, from the equation

$$k_0 = \frac{1}{t} \cdot \ln \frac{a}{a - x},$$

where a is the initial amount of wood (lignin, carbohydrates), and x is the percentage of wood (lignin, carbohydrates) dissolved at time t = 1 hour. For the subsequent time intervals it was assumed that the rate constant decreases as a power function of time

$$k = k_0 \cdot t^n,$$

where n is a negative index (less than unity).

Correlation of the experimental results by this method gives, for the cooking conditions used, an empirical equation of the form

$$\lg \frac{a}{a - x} = A \cdot t^m,$$

where $A = \frac{k_0}{2.303}$ and $m = 1 + n$.

Such equations may be used for calculating the yield or residual amount of lignin (or carbohydrates) x at any time t from the start of the cook.

Table 1 contains kinetic equations derived in this manner; they characterize the rates of "dissolution" of lignin, carbohydrates, and wood as a whole under the cooking conditions used.

The index m in the equations found for each pair of comparative cooks is the same, and the pairs of equations differ only in the magnitude of the coefficient A in the right-hand side, which is proportional to the reaction rate constant for the first hour of cooking.

It follows that the ratio of the rate constants for the potash and soda cooks (the ratio k_{KOH}: k_{NaOH}) must remain constant for a given time instant, and it can be calculated most simply as the ratio of the corresponding coefficients A or of the rate constants for the first hour of cooking. These calculations are presented in Table 2.

It follows from Table 2 that the use of caustic potash has the greatest accelerating effect on the "dissolution" of lignin; the ratio of the constants is from 1.10 to 1.27 (according to Larocque and Maass this ratio is 1.13, see above), whereas for the "dissolution" of carbohydrates the ratio of the constants is 1.06-1.10. Therefore an increase of the pulp yield may be expected with the use of caustic potash for the same degree of cooking.

The over-all acceleration of cooking with the use of caustic potash may be estimated from the ratio of the constants for "dissolution" of wood as a whole. Table 2 shows that the rate constants are higher by 6-9% for the potash cook. This a fairly significant increase, which may be of practical value for shortening cooking time and the digester cycle.

TABLE 2

Calculation of the Ratio of the Rate Constants for Potash and Soda Cooks

Cooking conditions			Ratio of reaction rate constants with the use of caustic potash and soda (the ratio $k_{KOH}:k_{NaOH}$) for "dissolution" of		
temperature (°C)	consumption of active alkali (as % NaOH)	sulfidity (%)	wood as a whole	lignin	carbohydrates
160	25	0	1.09	1.17	1.06
170	25	0	1.08	1.16	1.09
170	20	0	1.06	1.27	1.10
170	25	25	1.07	1.10	1.09

TABLE 3

Values of the Temperature Coefficient

Cooking conditions			Temperature coefficients for t = 1 hour (ratio of the rate constants $k_{170°} : k_{160°}$) for "dissolution" of		
kind of alkali	consumption of active alkali (as % NaOH)	sulfidity (%)	wood as a whole	lignin	carbohydrates
NaOH	25	0	1.56	2.34	1.30
KOH	25	0	1.54	2.33	1.34

The temperature coefficients calculated for the soda and potash cooks from the results of the first two series (Table 3) proved to be almost the same, i.e, increase of the cooking temperature has the same accelerating effect in both cases.

Comparative Investigation of the Properties of Potash Sulfate and Soda Sulfate Pulps

For comparison of the chemical and mechanical properties of sulfate pulps made by cooking with potash and soda liquors respectively, three pairs of comparative cooks were performed, designed to yield pulps of high, moderate, and low bleachability (permanganate) numbers. A 2-liter electrically heated autoclave was used for the cooking. The autoclave was charged with 300 g of chips (calculated on the bone-dry weight) and 1500 ml of liquor. The amount of active alkali in each cook was 25% calculated as NaOH on the weight of the bone-dry chips, and the sulfide content of the liquor was 25%. The final temperature adopted was 170°, and the heating time to 170° was 2 hours 30 minutes. The time of cooking at the final temperature was varied in accordance with the degree of bleachability required. The pulp was washed and screened, and the following were determined: yield, amount of uncooked fiber, permanganate number (Bjorkman), viscosity (by the standard cuprammonium method), copper number (by the Staud and Gray method), lignin content (by the method with 72% sulfuric acid), pentosans (by the bromide–bromate method), resins (by ether extraction), and α-cellulose (by the Jentgen method).

The results are given in Table 4.

It is seen that with the use of potash liquor the total cooking time could be shortened by 30-45 minutes or about 6-10% for a given bleachability; i.e., the relationship found in the kinetic studies was confirmed. However, with regard to the pulp yield the advantage of cooking with potash liquor was not confirmed.

TABLE 4

Analytical Results for Potash Sulfate and Soda Sulfate Pulps

Cook No.	Liquor	Total cooking time (hr and min)	Yield of screened pulp (% on wood)	Uncooked fiber (% on wood)	Permanganate number	Lignin content (%)	Pentosan content (%)	α-Cellulose content (%)	Cuprammonium viscosity (millipoises)	Copper number	Ash content (%)
1	$NaOH + Na_2S$ . .	5—00	46.3	0.3	130	5.00	8.50	88.0	689	1.41	0.62
2	$KOH + K_2S$ . . .	4—30	46.5	0.4	130	4.82	7.62	92.0	684	1.80	0.59
3	$NaOH + Na_2S$ . .	6—00	46.0	0.0	104	3.20	7.82	88.5	451	1.21	0.56
4	$KOH + K_2S$ . . .	5—30	44.5	0.0	101	3.08	7.60	91.4	438	1.39	0.45
5	$NaOH + Na_2S$ . .	7—45	39.0	0.0	67	1.83	6.88	89.0	205	0.67	0.45
6	$KOH + K_2S$ . . .	7—00	38.4	0.0	67	1.80	6.60	91.2	149	0.72	0.34

TABLE 5

Results of Mechanical Tests on Handsheets

Specimen No.	Cooking liquor	Permanganate number	Grinding, °Sch-R	Grinding time (min)	Breaking length (m)	Extensibility (%)	Fold. endur. (double folds)	Tear strength (g)	Bursting strength (kg/cm^2)
1	$NaOH + Na_2S$	130	60	42	12500	3.4	3320	30.8	9.0
2	$KOH + K_2S$	130	60	30	14900	4.2	4597	31.6	10.0
3	$NaOH + Na_2S$	104	61	37	11320	3.0	2815	28.0	6.0
4	$KOH + K_2S$	101	62	28	14700	4.0	3092	28.8	7.0
5	$NaOH + Na_2S$	67	61	30	10700	2.7	2260	26.0	5.0
6	$KOH + K_2S$	67	60	22	10300	3.2	2270	25.2	5.8

TABLE 6

Properties of Bleached Pulp

Sample No.	Cooking liquor	Whiteness (%)	α-Cellulose content (%)	Pentosan content (%)	Cuprammonium visc. (mpoises)	Breaking length (m)	Extensibility (%)	Fold. endur. (double folds)	Bursting length (kg/cm^2)
	Hypochlorite bleaching of "easy" pulps								
5	$NaOH + Na_2S$	85	83.9	5.75	121	11000	2.90	1680	5.6
6	$KOH + K_2S$	85	85.0	5.32	102	10960	2.80	1550	6.2
	Chlorine – alkali bleaching of "moderate" pulps								
3	$NaOH + Na_2S$	90	85.3	8.05	148	11300	3.40	1250	5.8
4	$KOH + K_2S$	90	87.5	7.60	126	14090	2.85	900	5.5

Comparison of the individual chemical properties of potash and soda sulfate pulps reveals a large difference in the α-cellulose contents: this difference was 2.2% for samples of low permanganate number, 2.9% for moderate samples, and as much as 4.0% in favor of the potash pulps for samples of high permanganate number.

With regard to other chemical properties, there are no special differences between the potash and soda sulfate pulps. Potash pulp has somewhat lower contents of pentosans and ash, but its copper number is somewhat higher and the viscosity (for the most bleachable pulp) somewhat lower than those of soda pulp. This last fact, in conjunction with the higher content of α-cellulose, may be an advantage in the production of pulps for artificial fibers.

The results of mechanical tests on handsheets after grinding in a laboratory roll mill to 60° Schopper–Riegler are given in Table 5 (the numbers of the specimens correspond to the numbers of the cooks in Table 4).

It follows from the table that potash sulfate pulp has better beatability than ordinary soda sulfate pulp; the time of grinding to 60° Schopper–Riegler is considerably less (by 25-30%) for potash sulfate pulp in all cases. The mechanical characteristics:breaking length, extensibility, bursting and flex strength, are appreciably higher for potash sulfate pulps than for soda sulfate pulps of the same bleachability. The difference in mechanical strength is especially prominent for the least-bleachable specimens: this difference is 16% with respect to tensile strength and 28% with respect to flex strength, in favor of the potash suflate pulp.

In conclusion, bleaching experiments were carried out with pulps of low and moderate permanganate number. The most bleachable samples (No. 5 and 6) were subjected to two-stage hypochlorite bleaching. The consumption of active chlorine was 4.8% on the weight of the bone-dry fiber; two thirds of this amount was used at the first stage. The pulp concentration was 10% at the first and 6% at the second bleaching stage. The first stage was effected at room temperature until the chlorine was completely consumed; the duration of the first stage was 2 hours 15 minutes for both samples. The second stage was performed at 30° and was continued for 2 hours, also in both cases.

The pulp samples of medium bleachability (No. 3 and 4) were bleached by the chlorine–alkali method. The chlorination was effected by means of chlorine water with 6% chlorine on the fiber weight, at 2% pulp concentration and 20° for 50 minutes. The chlorinated pulp was washed with cold water and then treated with caustic soda at 8% concentration for 2 hours, with an alkali consumption of 2% NaOH on the fiber weight. The pulp was washed with hot water, then subjected to a two-stage hypochlorite bleach with chlorine consumption of 2.3% on the fiber weight; it was then acidified with hydrochloric acid (0.5% on the fiber weight), washed, and analyzed.

The bleached pulp was tested for α-cellulose and pentosan contents, cuprammonium viscosity, whiteness, and mechanical properties of handsheets after 50 minutes of grinding in a "Iokro"* mill at 125 revolutions / minute. The results are given in Table 6.

The whiteness of the potash and soda pulps was approximately the same, both after hypochlorite and after chlorine–alkaline bleaching. It follows that the two types of pulp are of equivalent bleachability.

The difference between the α-cellulose contents of unbleached samples of potash sulfate and soda sulfate pulps persisted in the bleached pulp samples: the potash sulfate pulps contained 1.1-2.2% more α-cellulose than the soda sulfate pulps. The pentosan contents of all the samples decreased only slightly (compare Table 5), and approximately to the same extent in the potash and the soda pulps. On the other hand, the viscosity decrease was considerable, and in both cases the bleached potash sulfate pulps had somewhat lower viscosities than the corresponding soda pulps. The mechanical properties of Samples No. 5-6, made from easily bleachable pulp by hypochlorite bleaching, were approximately the same. The potash sulfate pulp Sample No. 4, made by chlorine–alkali bleaching of moderate pulp had considerably greater breaking length than the corresponding soda sulfate Sample No. 4, but was somewhat inferior to the latter in extensibility and folding endurance.

The pulp losses in bleaching were exactly the same in the pairs of experiments.

SUMMARY

1. Wood chips are cooked more rapidly in caustic potash than in caustic soda liquors. The ratio of the reaction rate constants for caustic potash and caustic soda ($k_{KOH}:k_{NaOH}$)is from 1.10 to 1.27 for the

*Transliteration of Russian – Publisher's note.

delignification reaction, from 1.06 to 1.10 for hydrolysis and dissolution of polysaccharides, and from 1.06 to 1.09 for "dissolution" of the wood as a whole. The temperature coefficients of the reaction rate are the same for potash and soda cooking. The rate of retardation of the process during cooking is also the same in both cases.

2. Because of the higher rate of the cooking reactions with the use of the potash sulfate method as compared with the soda sulfate method, the cooking time required to give the same bleachability can be reduced by 6-10 %. The yield of pulp from wood remains almost unchanged.

3. Unbleached potash sulfate pulp differs from soda sulfate pulp in having a considerably higher content of α-cellulose (by 2-4 %), easier beating (the beating time is shortened by 25-30%), and better mechanical properties, especially for pulps of high permanganate number.

4. The bleachability of potash sulfate and soda sulfate pulps is the same. Bleached potash sulfate pulp has a higher α-cellulose content and somewhat lower viscosity than soda sulfate pulp, while their mechanical properties are similar.

LITERATURE CITED

[1] G. L. Larocque and O. Maass, Canad. J. Res. 19, B., 1, 1 (1941).

[2] H. Brintzinger, Kolloid-Zeitsch. 95, 2, 212 (1941).

Received March 7, 1958

DETERMINATION OF THE PERCENTAGES OF 1,4 AND 1,2 UNITS IN DIFFERENT FRACTIONS OF SODIUM BUTADIENE RUBBER

A. I. Yakubchik and V. A. Filatova

Butadiene rubbers contain 1,4 and 1,2 units:

$$-CH_2-CH=CH-CH_2- \quad \text{1, 4 units} \qquad \text{(I)}$$

$$-CH_2-\underset{\displaystyle CH_2}{\overset{\displaystyle |}{\underset{\displaystyle |}{CH}}}- \quad \text{1, 2 units} \qquad \text{(II)}$$

In investigations of the microstructure of butadiene rubbers by the ozonolysis method [1-6], it has been established that the macromolecules of butadiene rubbers contain 1,4 – 1,4; 1,4 – 1,2 – 1,4 ; 1,4 –$(1,2)_2$ – 1,4 regions and 1,4 – 1,4 regions branched at the α-methylene group. The available information on the chemical structure of butadiene rubbers was obtained in studies of nonfractionated rubbers.

The present investigation was concerned with the chemical structure of different fractions of sodium butadiene rubber (made at 40°); the object was to determine whether the fractions (of different molecular weights) differ in chemical structure. For this purpose we fractionated sodium butadiene rubber (made at 40°) and isolated eight fractions the molecular weights of which are indicated in the table.

The fractionation was carried out by the procedure developed by Zhukov et al. [7]. Kinetic curves for oxidation of the nonfractionated rubber and the fractions by benzoyl hydroperoxide were determined, and these curves were used for calculating the percentages of internal double bonds.

It was shown earlier that the rate of oxidation of unsaturated compounds by benzoyl hydroperoxide depends on the degree of substitution of the hydrogens attached to carbon atoms joined by double bonds, by radicals. Tetrasubstituted compounds are oxidized at the highest rate, and monosubstituted at the lowest [8-10].

In butadiene rubbers the double bonds in 1,4 units are oxidized by benzoyl hydroperoxide at a greater rate than double bonds in 1,2 units. Kinetic curves for oxidation by benzoyl hydroperoxide are used for determining the percentage of 1,4 units, while the percentage of 1,2 units is the difference between 100 (the total number of units) and the percentage of 1,4 units. The percentage of 1,2 units was determined by this method so that it was possible to compare the percentage of 1,2 units found by the ozonolysis method and infrared spectroscopy, respectively.

There are several methods for interpreting the experimental data obtained in the oxidation of unsaturated compounds by benzoyl hydroperoxide [11].

Our method was to compare the kinetic curves for oxidation of rubbers by benzoyl hydroperoxide with the kinetic curve for oxidation of a model compound by benzoyl hydroperoxide. The model compound was 1-vinyl-cyclohexene-3. It is formed by combination of butadiene molecules in the 1,4 and 1,2 positions, i.e., its

molecule contains a unit with an internal double bond and a unit with an external double bond. An internal double bond is one contained in a unit of type (I), and an external one is one contained in a unit of type (II).

It was shown that the double bond in the 1-vinylcyclohexene-3 ring is oxidized at the same rate as the double bond in an open-chain disubstituted ethylenic compound.

The curves for oxidation of 1-vinylcyclohexene-3 are used to find the time required for oxidation of 50% of 1-vinylcyclohexene-3 (when all the double bonds in the ring have been oxidized), and it is assumed that the same time (under precisely the same conditions) is required for oxidation of all the internal double bonds in the rubber. The value of the ordinate drawn from the point corresponding to oxidation of 50% of 1-vinylcyclohexene-3 to the intersection with the curve for oxidation of the rubber gives the percentage of 1,4 units.

TABLE

Characteristics of Sodium Butadiene Rubber Fractions

Fraction No.	Molecular weight	Percentage of double bonds, determined by different methods					
		internal			external		
		oxidation by benzoyl hydroperoxide	infrared spectroscopy	ozonolysis	oxidation by benzoyl hydroperoxide	infrared spectroscopy	ozonolysis
I	835000	34.0	32.1	33.2	66.0	67.9	66.8
II	665000	29.0	29.8	—	71.0	70.2	—
III	480000	31.0	29.6	—	69.0	70.4	—
IV	391000	28.5	28.4	—	71.5	71.6	—
V	304000	30.0	27.7	—	70.0	72.3	—
VI	195000	30.5	30.8	—	69.5	69.2	—
VII	105000	30.0	28.0	30.0	70.0	72.0	70.0
VIII	около 200000	29.0	30.0		71.0	70.0	—
Nonfractionated rubber	400000	31.0	30.0	31.0	69.0	70.0	69.0

Columns 3 and 6 of the table give the percentages of 1,4 and 1,2 units determined in the rubber fractions from the kinetic curves for oxidation by benzoyl hydroperoxide. Columns 4,5,7, and 8 give the percentages of 1,4 and 1,2 units determined by other methods [12-14].

It follows from the table that the respective percentages of 1,4 and 1,2 units are almost the same in different fractions of sodium butadiene rubber made at 40°.

EXPERIMENTAL

The investigation was carried out with sodium butadiene rubber made at 40°, and eight fractions isolated from it. The average molecular weight of each fraction was determined from its viscosity [7] (see Table).

Benzoyl hydroperoxide was prepared from benzoyl peroxide (m.p. 103.5-104°) which had been previously recrystallized twice from chloroform. Alcohol-free chloroform was used for the recrystallization [11].

The benzoyl hydroperoxide solution was prepared in a mixed solvent containing 90% chloroform and 10% benzene; the latter was added to prevent formation of phosgene and other oxidizing agents [11]. The concentration of the original benzoyl hydroperoxide solution was 2 N. The rubber was dissolved in chloroform; the concentration was 0.135 g per 50 ml. The oxidation of nonfractionated rubber and of the fractions by benzoyl hydroperoxide was carried out in a thermostat at 20°. To 50 ml of the rubber solution an equal volume of benzoyl hydroperoxide solution was added. The mixture was placed in a thermostat, and 5 ml samples were taken at definite intervals; the unchanged benzoyl hydroperoxide in these samples was determined iodometrically. A blank experiment was carried out at the same time as a check on the behavior of the hydroperoxide in this solution.

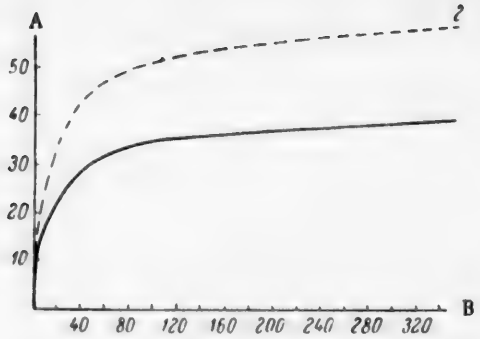

Curves for the oxidation of Fraction I of sodium butadiene rubber and of 1-vinylcyclohexene-3 by benzoyl hydroperoxide: A) percentage of rubber oxidized; B) time (minutes); oxidation of: 1) Fraction I of sodium butadiene rubber; 2) 1-vinylcyclohexene-3, by benzoyl hydroperoxide.

The percentage of oxidized rubber was calculated from the following equation [11]:

$$\%\ \text{of oxidized rubber} = \frac{T_{Na_2S_2O_3} \cdot C \cdot A \cdot 100}{b \cdot x},$$

where T is the titer of the thiosulfate calculated as oxygen; this was 0.000822 in our case; C is the amount of thiosulfate (in ml) taken for titration of the blank sample less the amount of thiosulfate (in ml) taken for titration of the sample with rubber; A is the total volume of rubber solution (in ml); b is the volume of rubber solution in the sample (in ml); x is the amount of oxygen (in g) required for oxidation of the rubber present in the sample taken.

The model compound used was 1-vinylcyclohexene-3 (b.p. 66.5 at 100 mm, d_4^{20} 0.8310, n_D^{20} 1.4642). It was oxidized under the same conditions as the nonfractionated sodium butadiene rubber and the isolated fractions. The molar concentrations of the model compound and of benzoyl hydroperoxide were the same as in the experiments with the rubber. The curves for oxidation of 1-vinylcyclohexene-3 (see Figure) were used to find the time required for oxidation of 50% of the double bonds in 1-vinylcyclohexene-3, i.e, all the double bonds in the ring. This time was found to be 80 minutes in our experiments. The contents of 1,4 units in the nonfractionated rubber and in the isolated fractions were determined as the amounts of double bonds oxidized in 80 minutes. Kinetic curves for oxidation by benzoyl hydroperoxide were plotted for the nonfractionated rubber and for the eight fractions isolated from it.

The figure shows the kinetic curves for the oxidation of 1-vinylcyclohexene-3 and of the first fraction by benzoyl hydroperoxide; this graph was used to find the percentage of 1,4 units in this fraction. The same procedure was used to find the percentages of 1,4 units in the nonfractionated rubber and in the other fractions.

SUMMARY

1. The percentage contents of 1,4 and 1,2 units (in sodium butadiene rubber made at 40°), determined by titration of double bonds by benzoyl hydroperoxide, coincide within the limits of experimental error with the percentage contents of 1,4 and 1,2 units determined by infrared spectroscopy and by the ozonolysis method.

2. It follows from these results that the respective percentages of 1,4 and 1,2 units are almost the same in nonfractionated sodium butadiene rubber made at 40° as in eight fractions isolated from it.

LITERATURE CITED

[1] A. I. Yakubchik, V. M. Zhabina and A. E. Mal'tseva, Synthetic Rubber 4, 6, 50 (1935).

[2] C. S. Marvel, W. M. Schilling, D. J. Shields et al., J. Org. Ch. 16, 6, 838, 854 (1951).

[3] Rabjohn, J. Am. Chem. Soc. 69, 2, 314 (1947).

[4] A. I. Yakubchik and N. G. Kasatkina, J. Gen. Chem. 25, 1473 (1955).*

[5] A. I. Yakubchik and N. I. Sorokina, J. Gen. Chem. 26, 2421 (1956).*

[6] A. I. Yakubchik, N. G. Kasatkina, G. I. Demidova and G. B. Fedotova, J. Gen. Ghem. 27, 1195 (1957).

[7] I. I. Zhukov, I. Ya. Poddubnyi and A. V. Lebedev, Colloid J. 11, No. 3, 151 (1949).

[8] N. A. Prilezhaev, Organic Peroxides and their Use for Oxidation of Unsaturated Compounds [in Russian] (1912).

*Original Russian pagination. See C. B. Translation.

[10] I. M. Kolthoff, T. S. Lee, and M. A. Mairs, J. Polym. Sci. 2, 199, 206, 220 (1947).

[11] I. M. Kolthoff, T. S. Lee and M. A. Mairs, J. Polym. Sci. 2, 206 (1947).

[12] M. P. Burgova and A. A. Korotkov, Bull. Acad. Sci. USSR, Phys. Ser. 14, 452 (1950).

[13] A. I. Yakubchik, Collective Volume on the 80th Birthday of Academician S. V. Lebedev [in Russian] (Izd. AN SSSR, 1954) p.197.

[14] A. I. Yakubchik and V. A. Filatova, J. Gen. Chem. 29 (1959).*

Received February 7, 1959

*See C. B. Translation.

CATALYTIC POLYMERIZATION OF POLYCHLOROPHENYLDIMETHYL SILOXANES

K. A. Andrianov, S. Dzhenchel'skaya
and Yu. Petrashko

Hydrolysis of phenyltrichlorosilane and dimethyldichlorosilane, separately or jointly, by water in an acid medium results in the formation of cyclic polyphenyldimethyl siloxanes. Conversion of these cyclic compounds into high polymers is usually effected by heating at high temperatures. However, soluble polymers of high molecular weight are not obtained by this method. Usually, the polyphenyldimethyl siloxanes formed by thermal condensation of the products of joint hydrolysis of phenyltrichlorosilane and dimethyldichlorosilane are of low viscosity. Attempts to increase the viscosity of the polymer by further heating result in its conversion into an insoluble form.

The high viscosity of the polymer is associated with a number of properties of lacquers and electrical insulation materials made from it. In this connection, studies of the catalytic polymerization of the products of joint hydrolysis of di- and trifunctional compounds, and in particular of dimethyldichlorosilane with phenyltrichlorosilane, in order to obtain soluble polymers of higher viscosity are of great interest. The cyclic compounds formed by hydrolysis of difunctional monomers (dimethyldichlorosilane, phenylmethyldichlorosilane) [1] are capable of regrouping, with ring scission, in presence of a number of catalysts—antimony pentachloride [2], caust potash [3], and ferric chloride [4].

The polymerization of the cyclic compounds formed from dimethyldichlorosilane in presence of alkalies proceeds according to the scheme:

$$(R_2SiO)_x + O\overline{H} \longrightarrow HOSiR_2OSiR_2—OSiR_2—O^-.$$

Hydrolysis of trifunctional compounds (ethyltriethoxysilane [5] and pentachlorophenyltrichlorosilane [6]) yielded the crystalline cyclic polymers $(C_2H_5SiO_{1.5})_8$ and $(C_6Cl_5SiO_{1.5})_6$.

Joint hydrolysis of phenyltrichlorosilane with dichlorophenyltrichlorosilane and dimethyldichlorosilane in an acid medium, and joint hydrolysis of phenyltrichlorosilane with dimethyldichlorosilane, results in the formation of cyclic polymers of a mixed type:

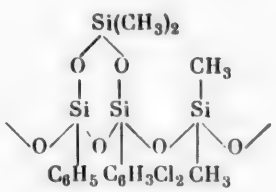

The alkali-catalyzed polymerization of the products of joint hydrolysis of phenyltrichlorosilane with dimethyldichlorosilane in 1:1 molar ratio has been studied [7]. It was found that under the action of caustic soda, in amounts from 0.1 to 0.9%, at 20° these products are converted into polymers of high viscosity. These polymers retain high solubility in the usual organic solvents. The polymers formed by catalytic polymerization are converted into the insoluble state at different viscosities, in accordance with the amount of alkali taken for the reaction (Fig. 1).

TABLE 1

Variation of Relative Viscosity with Duration of the Polymerization Reaction

Expt. No.	Molar proportions of starting materials			Duration of polymerization (min)	η_{rel} of 10% solution in toluene on gel formation
	dimethyldichlorosilane	phenyltrichlorosilane	dichlorophenyltrichlorosilane		
1	1.0	1.25	–	105	3.2
2	1.0	1.0	0.25	195	4.16
3	1.0	0.75	0.50	370	5.15
4	1.0	1.0	–	48	2.8
5	1.0	0.75	0.25	180	3.7
6	1.0	0.50	0.50	420	3.8

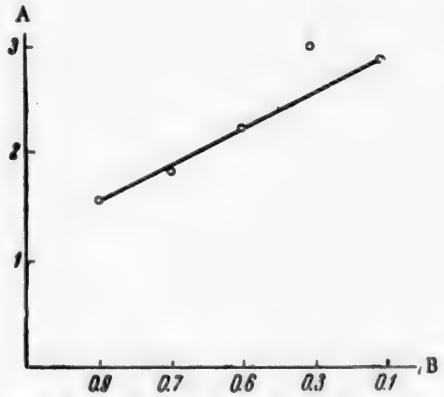

Fig. 1. Variation of viscosity with the amount of alkali taken: A) relative viscosity; B) amount of alkali (%).

In Fig. 2 the time after which the polymer loses solubility is plotted against the amount of alkali added.

It follows from Fig. 1 and 2 that with the use of 0.9% NaOH the relative viscosity (η) of a 10% solution of the polymer in toluene is 1.57, and the polymer loses its solubility after 0.5 hour; with 0.1% NaOH the relative viscosity of the product is over 2.8, and solubility is lost after 5.7 hours.

Investigation of the alkali-catalyzed polymerization of the joint hydrolysis products of dichlorophenyltrichlorosilane with dimethyldichlorosilane in 1.25:1 molar ratio, at 20°, with 0.3% NaOH, and with 59.6% of polymer in toluene solution showed that the polymer viscosity was not increased appreciably. The reaction proceeded only when the temperature was raised to 90°.

If dichlorophenyltrichlorosilane is partially replaced by phenyltrichlorosilane, catalytic polymerization proceeds at 20° under the conditions described. This reaction was studied with the component ratios indicated in Table 1.

Fig. 3 represents variations of the relative viscosity of polymer solutions during polymerization of the products of joint hydrolysis of dimethyldichlorosilane, phenyltrichlorosilane, and dichlorophenyltrichlorosilane with the di- and trifunctional compounds in 1:1.25 molar ratio.

It is clear from Fig. 3 that the rate of increase of polymer viscosity falls sharply with increase of the amount of dichlorophenyltrichlorosilane. The product of joint hydrolysis of phenyltrichlorosilane with dimethyldichlorosilane becomes insoluble in 1.75 hours at a relative viscosity of 3.2; with 0.25 mole of dichlorophenyltrichlorosilane the insoluble state is reached in 3.25 hours at a viscosity of 4.16, and with 0.5 mole of dichlorophenyltrichlorosilane, in 6.15 hours at a viscosity of 5.15.

Fig. 4 represents variations of the relative viscosity of polymer solutions during polymerization of the products of joint hydrolysis, with di- and trifunctional compounds in equal molar ratios (Table 1, Experiments No. 4-6).

It is clear from Fig. 4 that here again the rate of viscosity increase falls sharply with increase of the amount of dichlorophenyltrichlorosilane.

The product of joint hydrolysis of phenyltrichlorosilane with dimethyldichlorosilane becomes insoluble in 0.75 hour; with the addition of 0.25 mole of dichlorophenyltrichlorosilane the time is 3 hours, and with 0.5 mole, 7 hours.

The product of joint hydrolysis of phenyltrichlorosilane with dimethyldichlorosilane becomes insoluble in 0.75 hour; with the addition of 0.25 mole of dichlorophenyltrichlorosilane the time is 3 hours, and with 0.5 mole, 7 hours.

The mechanism of the catalytic polymerization of the products of joint hydrolysis of phenyltrichlorosilane, dichlorophenyltrichlorosilane, and dimethyldichlorosilane can probably be represented as follows.

The first reaction stage under the action of alkali is coordination of the donor hydroxyl group of caustic soda with a silicon atom. This results in cleavage of the weakened silicon–oxygen bond.

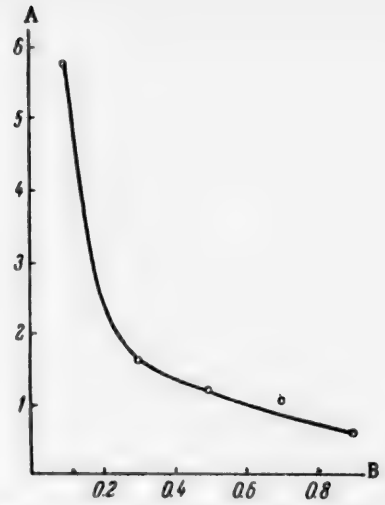

Fig. 2. Variation of the time to loss of polymer solubility with the amount of alkali taken: A) time to gel formation (hours); B) amount of alkali (%).

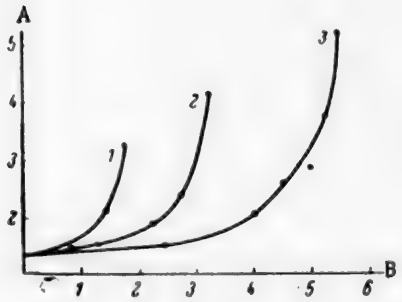

Fig. 3. Variations of the relative viscosity of polymer solutions with polymerization time, with different molar ratios of the starting substances: A) relative viscosity; B) polymerization time (hours); molar ratios: 1) $(CH_3)_2SiCl_2$: $C_6H_5SiCl_3$ = 1 : 1.25; 2) $(CH_3)_2SiCl_2$: $C_6H_5SiCl_3$: $Cl_2C_6H_3SiCl_3$ = 1 : 1 : 0.25; 3) $(CH_3)_2SiCl_2$: $C_6H_5Cl_3$: $Cl_2C_6H_3SiCl_3$ = 1 : 0.75 : 0.50.

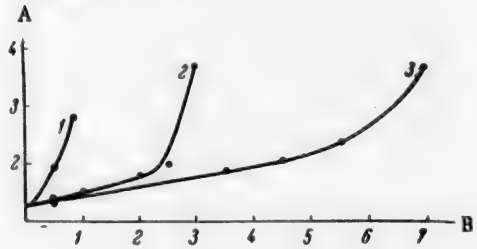

Fig. 4. Variations of the relative viscosity of polymer solutions with polymerization time, with equal molar ratios of di- and trifunctional compounds: A) relative viscosity; B) polymerization time (hours); molar ratios: 1) $(CH_3)_2SiCl_2$: $C_6H_5SiCl_3$ = 1 : 1; 2) $(CH_3)_2SiCl_2$: $C_6H_5SiCl_3$: $Cl_2C_6H_3SiCl_3$ = 1 : 0.75 : 0.25; 3) $(CH_3)_2SiCl_2$: $C_6H_5SiCl_3$: $Cl_2C_6H_3SiCl_3$ = 1 : 0.5 : 0.5.

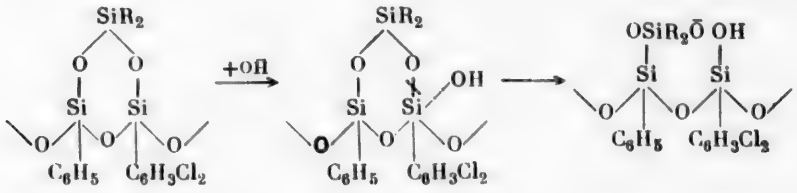

The ion formed attacks a second cyclic molecule, breaking the Si–O bond, and joins to it. The molecular chain grows and branches, and the process culminates in closure of the high-polymer molecule.

EXPERIMENTAL

Preparation of polydimethylphenyldichlorophenyl siloxanes. A hydrolysis vessel fitted with a cooling jacket, stirrer, thermometer, and dropping funnel contained 360 g of water and 180 g of toluene. The mixed

chloro compounds, dissolved in 180 g of dry toluene, were introduced into the vessel with continuous stirring. The amounts of chloro compounds are given in Table 2.

TABLE 2

Amounts of Chloro Compounds Used in the Polymerization Reaction

Expt. No.	Dimethyldichlorosilane (g)	Phenyltrichlorosilane (g)	Dichlorophenyltrichlorosilane (g)
1	59	120.9	–
2	56.8	92.5	30.8
3	54.4	66.5	59.1
4	68.4	111.6	–
5	64.9	79.9	35.2
6	61.9	50.7	67.4

The temperature of the mixture was maintained at 20°. After the addition the mixture was stirred during 1 hour; the organic layer was then separated from the aqueous, washed with water to a neutral reaction, and filtered, and toluene was evaporated off.

Catalytic polymerization of polydimethylphenyldichlorophenyl siloxanes. A round-bottomed flask with a side tube, fitted with a stirrer, contained 50 g of the joint-hydrolysis products (Table 2, Experiments 1-6) dissolved in toluene (the concentration was 59.4-60.1%).

Aqueous 39.3% caustic soda was added to the solution with vigorous stirring at 20°, in the proportion of 0.3% by weight to the amount of polymer. The temperature during the reaction was maintained at 20 ± 0.5°. Polymer samples were taken during the reaction, and the relative viscosity of 10% polymer solutions in toluene were determined by the Ostwald method. The reaction was terminated at the instant of gel formation. The results are presented in Fig. 3 and 4.

SUMMARY

1. The catalytic polymerization of cyclic polydimethylphenyldichlorophenyl siloxane under the influence of caustic soda was studied; it was found that the products of joint hydrolysis of dimethyldichlorosilane with dichlorophenyltrichlorosilane, taken in 1:1.25 molar ratio, do not polymerize in presence of 0.3% caustic soda at 20°, but polymerization takes place at 90°.

2. It was found that the low-molecular products of hydrolysis undergo chemical conversion with formation of compounds of higher molecular weight; the polymerization reaction is retarded appreciably by replacement of phenyltrichlorosilane by dichlorophenyltrichlorosilane.

3. The amount of catalyst taken for the reaction greatly influences the viscosity of the polymer in its transition into an insoluble form. The less catalyst is taken, the higher the polymer viscosity and the greater the time required for formation of an insoluble polymer.

LITERATURE CITED

[1] H. I. Fletcher and M. I. Hunter, J. Am. Chem Soc. 71, 2922 (1949).

[2] D. W. Scott, J. Am. Chem. Soc. 68, 2294 (1946).

[3] D. T. Hard, J. Am. Chem. Soc. 76, 249 (1954).

[4] British patent 658640; Chem. Abs. 46, 4848 (1952).

[5] M. Sprung and F. Guenther, J. Am. Chem. Soc. 77, 3996 (1955).

[6] K. Andrianov and V. Odinets, Bull Acad. Sci. USSR, Div. Chem. Sci. 6 (1957).

[7] K. Andrianov, S. Dzhenchel'skaya and Yu. Petrashko, J. Gen. Chem. 29, 685 (1958).

Received March 21, 1958

COPOLYMERS OF STYRENE WITH MALEIC ACID DERIVATIVES

A. Ya. Drinberg, B. M. Fundyler,
G. N. Gorelik and A. M. Frost

The potentialities of polystyrene as a coating material are restricted by its poor adhesion and inadequate compatibility with other resins and plasticizers. One possible way of removing the disadvantages of polystyrene while retaining all its valuable properties is by production of copolymers of styrene with various carboxylic monomers.

Acrylic or methacrylic acid [1,2] and maleic anhydride and its derivatives [3,4] may be used as the carboxylic copolymerization components. Introduction of maleic anhydride residues into the polystyrene chain improves coating adhesion, while the presence of carboxyl groups in the polymer makes possible the production of a whole series of derivatives (salts, esters, etc.).

There have been numerous investigations of the mechanism of copolymerization of styrene with maleic anhydride. Alfrey and Levin [5] suggested that polar and volume factors account for the fact that maleic anhydride does not polymerize but forms copolymers relatively easily.

Several workers have shown that the copolymer of styrene with maleic anhydride has an alternating structure, and the monomers enter the copolymerization reaction in equimolecular proportions. Bartlett and Nozaki [6] attributed the alternation effect to formation of intermediate active complexes due to electron transfer from donor radicals to acceptor monomers. Bamford and Barb [7] studied the influence of various factors on the rate of copolymerization of styrene with maleic anhydride. They showed that the copolymerization constants for this monomer pair increase with temperature. Bamford and Barb claimed that their copolymers were not of equimolecular structure, but that their composition varied in accordance with the reaction conditions.

Thus, despite the numerous investigations of copolymerization of styrene with maleic anhydride, there is no single and generally-accepted view concerning the mechanism of the process. Moreover, detailed data on the copolymer properties are lacking. The available information on the use of styrene–maleic anhydride copolymers in coatings is confined to a number of patents, which are mainly concerned with certain derivatives of the copolymer [8-11].

EXPERIMENTAL

The copolymer was synthesized from a styrene fraction boiling at 41-43° at 3-7 mm residual pressure, d_4^{20} = 0.908 g/cc, and n_D^{20} = 1.5461. The maleic anhydride used was chemically pure and melted at 52-54°.

Styrene was copolymerized with maleic anhydride in acetone solution at 50°, and in cyclohexanone at 100°. The monomer concentration in solution was 20%. The experiments were performed in sealed glass tubes. Benzoyl peroxide was added to the reaction mixture in the proportion of 1% on the monomer weight. To determine the effect of monomer ratio in the original mixture on the copolymer composition, maleic anhydride and styrene were taken in the following molar ratios: 0.1 : 0.9, 0.3 : 0.7, and 0.5 : 0.5.

The acid numbers of the original mixtures before the start of the reaction were determined, and the maleic anhydride contents of the mixtures were found from the results. Analytical data for the reaction mixtures are presented in Table 1.

TABLE 1

Analytical Data for the Original Reaction Mixtures

Molar contents of monomers in original mixture		Amount of mixture (g)	KOH taken for titration (ml)	Acid number (mg KOH)*	Maleic anhydride found in 1 g of original mixture (g)	Notes
styrene	maleic anhydride					
0.5	0.5	1.2510	21.2	107.6	0.0939	Copolymerization in cyclohexanone
0.5	0.5	1.001	17.8	111.5	0.0955	Copolymerization in acetone
0.7	0.3	0.985	10.2	65.4	0.0560	
0.9	0.1	0.971	3.3	21.5	0.0184	

* KOH solution contained 0.00632 g/ml.

TABLE 2

Variations of Refractive Index and Density of the Copolymerization Product with Reaction Time

Time from start of reac. (hours)		Refractive index		Density (g/cc)	
50°	100°	50°	100°	50°	100°
0	0	1.3890	1.4652	0.8431	0.955
0.5	0.5	1.3890	1.4659	0.8431	0.9809
1	1	1.3890	1.4667	0.8431	0.9822
1.5	1.5	1.3890	1.4675	0.8431	0.9842
2	2	1.3890	1.4676	0.8431	0.9858
3	3	1.3890	1.4689	0.8431	0.9872
6	4	1.3900	1.4697	0.8442	0.9914
9	6	1.3931	1.4701	0.8521	0.9918
12	8	1.3940	1.4707	0.8603	0.9958
15	10	1.3940	1.4712	0.8652	0.9971

TABLE 3

Copolymer Yield in Relation to the Reaction Time

Duration of copolymerization (hours)		Weight of copolymerization product (g)		Amount of copolymer (g)		Copolymer yield (%)	
in acetone	in cyclohexanone	in acetone	in cyclohexanone	in acetone	in cyclohexanone	in acetone	in cyclohexanone
0.5	0.5	—	10.2613	—	0.3871	0	18.9
1	1	—	8.5610	—	0.5474	0	31.9
1.5	1.5	—	8.5002	—	0.6234	0	36.6
2	2	—	8.0410	—	0.6420	0	40.0
3	3	—	6.7212	—	0.7156	0	53.4
6	4	—	7.3973	—	0.8713	0	59.1
9	6	13.31	6.4072	0.81	0.8013	30.5	62.6
12	8	12.25	7.0397	1.27	0.9237	51.8	65.9
15	10	12.16	6.4075	1.64	0.9161	67.4	71.7
18	12	13.05	6.3402	1.82	0.9241	69.7	72.9

TABLE 4

Effect of Copolymerization Time on Copolymer Composition

Duration of copolymerization (hours)		Weight of copolymer taken (g)		Acid number of copolymer (mg KOH)		Maleic anhydride content of copolymer (molar %)	
50°	100°	50°	100°	50°	100°	50°	100°
0.5	0.5	—	0.0879	—	508.6	—	45.8
1	1	—	0.05474	—	510.1	—	45.9
1.5	1.5	—	0.06234	—	508.6	—	45.8
2	2	—	0.06420	—	507.7	—	47.6
3	3	—	0.07150	—	507.9	—	45.7
6	4	—	0.0871	—	508.7	—	45.8
9	6	0.1015	0.8013	530	503.6	47.7	45.3
12	8	0.1035	0.9277	526	506.5	47.4	45.6
15	10	0.093	0.0916	530	504.0	47.7	45.4
18	12	0.100	0.07213	524	507.3	47.2	45.6

TABLE 5

Determinations of Maleic Anhydride in Filtrate and Copolymer

Duration of reaction (hours)		Maleic anhydride content (%)					
		of copolymer		of filtrate		total	
50°	100°	50°	100°	50°	100°	50°	100°
0.5	0.5	—	17.9	—	81.2	—	99.1
1	1	—	31.9	—	67.9	—	99.8
1.5	1.5	—	35.7	—	64.1	—	99.8
2	2	—	37.9	—	60.8	—	98.7
3	3	—	50.3	—	49.4	—	99.7
6	4	—	56.0	—	44.1	—	100.1
9	6	29.5	58.6	69.6	40.9	99.1	99.5
12	8	50.0	62.4	49.7	37.5	99.7	99.9
15	10	65.2	66.3	35.1	32.7	100.3	99.0
18	12	67.1	68.9	32.6	31.2	99.7	100.1

When the molar ratios of maleic anhydride to styrene are 0.1:0.9 and 0.3:0.7, pure polystyrene is formed together with the copolymer, and the composition of the copolymer is close to equimolecular. Therefore the subsequent experiments were carried out with 0.5:0.5 molar ratio of styrene to maleic anhydride.

The course of the copolymerization reaction was studied by determinations of the refractive index and density of the polymerization products. The relevant data are presented in Table 2.

It follows from these results that at 50° the polymerization reaction passes through an induction period during which the original properties of the reaction mixture remain unchanged. At 100° there is no induction period, as shown by changes in the refractive index density at the earliest stages of the reaction.

The copolymer was isolated by precipitation from solution by the action of 4-5 volumes of ligroine. The copolymer was then reprecipitated and dried at room temperature. The copolymer of styrene and maleic anhydride is soluble in acetone, cyclohexanone, dioxane, and pyridine.

For investigation of copolymerization kinetics, the copolymer was analyzed with respect to yield, the amount of maleic anhydride converted, and variations of specific viscosity; the amount of maleic anhydride in the filtrate was determined.

Data on the copolymer yield in relation to the reaction time are presented in Table 3.

TABLE 6

Specific Viscosity of Copolymers•

Duration of reaction (hours)		Efflux time of solution (sec)		Relative viscosity		Specific viscosity	
50°	100°	50°	100°	50°	100°	50°	100°
0.5	0.5	—	68.1	—	1.586	—	0.586
1	1	—	65.3	—	1.521	—	0.521
1.5	1.5	—	64.5	—	1.501	—	0.501
2	2	—	63.7	—	1.487	—	0.487
3	3	—	59.4	—	1.383	—	0.383
6	4	—	58.1	—	1.355	—	0.355
9	6	198	54.1	4.62	1.260	3.62	0.260
12	8	183	51.1	4.27	1.191	3.27	0.191
15	10	168	49.6	3.93	1.156	2.93	0.156
18	12	157	49.5	3.66	1.151	2.66	0.151

• The efflux time of cyclohexanone is 42.9 seconds.

The chemical composition of the copolymer was established from its maleic anhydride content, which was found from the acid number. For determination of the acid number a copolymer sample was weighed in acetone and titrated by aqueous caustic potash in presence of phenolphthalein.

The results of experiments on the effect of reaction time on copolymer composition are given in Table 4.

The experimental results show that the composition of styrene–maleic anhydride copolymer is equimolecular irrespectively of the reaction time.

The small deviation of the molar content of maleic anhydride from 50% may be attributed to the effect of end groups; this effect is greater if the reaction is conducted at 100° because the copolymer formed at that temperature should have lower molecular weight.

The filtrate obtained after precipitation and washing of the copolymer was analyzed for its content of free maleic anhydride which did not enter the copolymerization reaction. The corresponding contents of maleic anhydride in the copolymer were determined. The results of determinations of maleic anhydride in the filtrate and copolymer are given in Table 5.

The data in Table 5 give an idea of the kinetics of the copolymerization process. The amount of unconverted maleic anhydride gradually diminishes as the reaction proceeds. The amount of maleic anhydride entering the copolymerization reaction correspondingly increases.

Variations of the specific viscosity of the copolymer with reaction time and temperature were studied. The viscosity of 1% solutions of the copolymer in cyclohexanone was determined at 20°.

The results are given in Table 6.

The specific viscosity of the polymer gradually falls as the reaction proceeds, indicating a decrease of the average molecular weight. The most likely cause of the decrease of the molecular weight of the copolymer as the reaction proceeds is a decrease of monomer concentration in the reaction mixture. For a copolymer of equimolecular structure the molecular weight is proportional to the concentration of the monomers in the original mixture [12]. Therefore, as the monomers are gradually consumed, fractions of copolymer with progressively lower molecular weight are formed, decreasing the average molecular weight.

Because of the poor solubility of the copolymer and its high acid number it cannot be used as a film former in coatings. To improve the copolymer properties it was esterified by butyl and octyl alcohols. The esterification was performed in cyclohexanone solution, the reaction mixture being heated at 150-160° for 6-8 hours. The amount of alcohol in the reaction mixture was varied from a 2-fold to a 4-fold excess over the

TABLE 7

Results of Physical Tests on Coatings

Ground coating	Strength		Hardness	Resistance to 3% NaCl solution (days)	Water resistance
	flexural (mm)	impact (kg/cm)			
SM-1, based on monooctyl ester of the copolymer	1	50	0.71	3	Only traces of waterline corrosion after 3 months of exposure in water
VL-02, polyvinyl butyral	1	50	0.67	3	Continuous corrosion after 5 days of exposure in water

amount corresponding to the acid number of the copolymer. The experiments showed that, regardless of the amount of alcohol taken or the duration of the process, a monoester of the styrene–maleic anhydride copolymer is formed. The butyl monoester of the copolymer has an acid number of 240 mg KOH, and the octyl ester, 170 mg KOH. Monoesters of styrene–maleic anhydride copolymer can be used as film formers for coatings, as they are readily soluble in ethyl cellosolve, butyl acetate, acetone, and cyclohexanone; the octyl ester is also soluble in turpentine.

On the basis of the octyl monoester of the copolymer the following formulation for SM-1 ground coating was developed (in %): octyl monoester of copolymer 7.2, ground-coat zinc yellow 8.0, orthophosphoric acid (85%) 3.6, isopropyl alcohol 64.8, ethyl alcohol 16.4.

For preparation of the ground coating, the copolymer monoester is dissolved in isopropyl alcohol and the solution is mixed with zinc yellow and phosphoric acid solution in ethyl alcohol. The component mixture is put into a porcelain-ball mill and ground for 16-20 hours down to about 10 μ. Orthophosphoric acid serves as a stabilizer in the mixture, retarding formation of insoluble salts before application of the coating. When the coating is applied to the surface, the phosphoric acid combined with iron and the reaction shifts toward formation of the insoluble salt of the copolymer monooctyl ester. The physical properties of the coatings so formed were investigated. The impact strength, flexural strength, hardness, water resistance, and adhesion were determined [13]. Single coatings on steel were used for the tests. Patallel tests were performed on VL-02 polyvinyl butyral ground coatings, recently introduced in industry. The results of the tests are given in Table 7.

The results showed that ground coatings based on the monooctyl ester of the copolymer are not inferior to phosphatizing polyvinyl butyral ground coatings in quality, and are superior to the latter in water resistance.

SUMMARY

1. The copolymer of styrene with maleic anhydride was synthesized by the solvent method in acetone and cyclohexanone, with various monomer ratios in the original mixture and at different temperatures.

2. The course of the copolymerization was studied by variations of the refractive index and density of the copolymerization product. The copolymerization reaction at 50° is preceded by an induction period. There is no induction period at 100°.

3. The copolymer composition is constant and close to equimolecular, regardless of composition of the mixture and reaction conditions.

4. The copolymer viscosity continuously decreases during the reaction, owing to decrease of the monomer concentration of the original mixture.

5. A ground coating based on the monooctyl ester of the copolymer has been formulated; this is not inferior in properties to VL-02 polyvinyl butyral phosphatizing ground coating.

LITERATURE CITED

[1] E. C. Chapin, G. E. Ham and C. K. Mills, J. Polymer. Sci. 4, 597 (1949).

[2] A. Ya. Drinberg, B. M. Fundyler, and A. M. Frost, J. Appl. Chem. 31, No. 7, 1080 (1958).*

[3] T. Wagner-Jouregg, Ber. 63, 3213 (1930).

[4] R. B. Seymour, F. F. Harris and I. Branum, Ind. Eng. Ch. 41, 7, 1509 (1949).

[5] T. Alfrey and E. Lavin, J. Am. Chem. Soc. 67, 2044 (1945).

[6] R. D. Bartlett and K. Nozaki, J. Am. Chem. Soc. 68, 1495 (1946).

[7] C. H. Bamford and W. G. Barb, Disc. Faraday Soc. 14, 208 (1953).

[8] German Patent 571665 (1933).

[9] U. S. Patent 1976679 (1934).

[10] U. S. Patent 2399084 (1946).

[11] French Patent 763027 (1934).

[12] T. Alfrey, J. Bohrer and H. Mark, Copolymerization (IL, Moscow, 1953) pp; 67, 81, 212, 243 [Russian translation].

[13] S. V. Yakubovich, Testing Lacquer and Paint Materials and Coatings [in Russian] (1952).

Received January 16, 1958

* Original Russian pagination. See C. B. Translation.

VINYLATION OF CYCLIC HYDROCARBONS

P. P. Karpukhin and A. I. Levchenko

The V. I. Lenin Polytechnic Institute, Khar'kov

Vinylation of organic compounds, which was first studied in detail by Academician Favorskii, is now widely used in industry in the production of plastics, rubbers, insulating materials, and in the paint and varnish industry.

It is known from the literature [1] that alcohols, amines, esters, and acids of the aliphatic series can be vinylated. Organic compounds of cyclic structure, such as phenols, amines, carbazole, and others, can also be vinylated.

We found no descriptions in the literature of the vinylation of cyclic hydrocarbons such as fluorene, acenaphthene, or indene. However, vinylation of cyclic hydrocarbons containing mobile hydrogen atoms is possible on theoretical considerations. The development of a method for vinylation of the above-named compounds would have great practical significance, as it would provide a new material for the paint, varnish, and plastics industries from compounds such as fluorene, indene, and others, which are utilized little by industry.

It is known that coal tar contains over twice as much fluorene as anthracene [2]. Methods for isolation and purification of fluorene and acenaphthene have been worked out and described in the literature [3, 4]. It is known that fluorene and acenaphthene do not polymerize on heating [5], and therefore they cannot be used directly as film formers.

The object of this investigation was to verify the possibility of vinylation of fluorene, acenaphthene, and indene by acetylene. As the result of these experiments 9-vinylfluorene [6], vinylacenaphthene, and vinylindene were prepared. In addition, a mixture of carbazole and fluorene was vinylated, and a mixture of the vinyl derivatives of fluorene and carbazole was obtained.

The vinylation of fluorene, acenaphthene, and a heavy benzene fraction containing up to 40% indene was effected by the action of acetylene under 18-20 atmos pressure at 175-210° in toluene in presence of caustic alkali. The experiments showed that in vinylation of these compounds by acetylene the formation of vinyl compounds is accompanied by formation of acetate from the caustic alkali and acetylene.

EXPERIMENTAL

9-Vinylfluorene. This compound consists of yellow crystals of m.p. 76-78°, and polymerizes readily when heated to form a transparent pale yellow water-resistant film. On standing in air, 9-vinylfluorene polymerizes to a viscous yellow liquid. Both vinylfluorene and its polymers dissolve in organic solvents such as benzene, toluene, xylene, carbon tetrachloride, chloroform, and acetone, with formation of yellow solutions.

The formation of 9-vinylfluorene from fluorene and acetylene can be represented as follows:

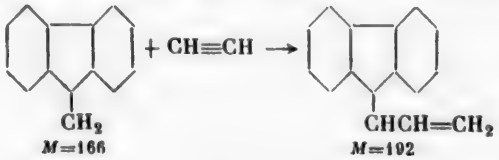

TABLE

Results of Experiments on Vinylation of Fluorene

Expt. No.	Autoclave charge: fluorene (g)	toluene (ml)	KOH (g)	NaOH (g)	water (ml)	Maximum pressure (atmos)	Maximum temperature (°C)	Heating time (hours)	Yields (%): 9-vinyl-fluorene	acetate
1	150	500	60	—	—	54	175	36	61.3	92.4
2	150	500	60	—	—	18	200	16	27.0	75.3
3	150	500	60	—	—	36	200	22	54.3	92.8
4	75	500	—	30	—	20	200	10	45.9	44.0
5	75	500	—	20	5	24	210	10	74.9	87.3
6	75	500	—	20	5	22	210	7	70.4	81.1
7	40	500	—	10.7	5	26	210	7	92.0	79.2

The structure of 9-vinylfluorene is proved by its elementary composition, molecular weight, bromine number and analysis of the dibromo derivative, and the ability of vinylfluorene in contrast to fluorene, to polymerize easily because of the presence of a vinyl group.

In vinylation of fluorene by acetylene in presence of caustic potash the yield of 9-vinylfluorene was 50-60%, and of potassium acetate, 75-92% of the theoretical. In vinylation of fluorene by acetylene in presence of caustic soda the yield of 9-vinylfluorene was 70-92%, and of sodium acetate, 79-87% of the theoretical. The vinylation of fluorene is largely completed after 6-7 hours of heating. Further heating may lead to polymerization of vinylfluorene. The best yields of 9-vinylfluorene and acetate were obtained when the autoclave was charged with one mole each of fluorene and alkali to three moles of acetylene.

The relationships between temperature, pressure, and heating time in vinylation of fluorene are plotted in Fig. 1 and 2.

The formation of acetates during vinylation of cyclic compounds by acetylene may be represented by the following scheme, given in the literature [7]:

$$CH{\equiv}CH + KOH + H_2O \longrightarrow CH_3COOK + H_2.$$

Confirmation of this course of the reaction is confirmed by the reaction products – acetate and hydrogen; over 20% of the latter was found in the exit gas.

Fluorene was vinylated by acetylene in a 2.5 liter autoclave, which was charged with fluorene, toluene, caustic potash or caustic soda, and water. The amounts of chemicals taken are given in the Table. The autoclave was closed, nitrogen was blown through to remove air, and acetylene was then blown in. The autoclave was placed on a horizontal electric heater, heated during 1-2 hours to the maximum temperature indicated, and then held at that temperature to the end. To agitate the reaction mass, the autoclave was rotated by means of an electric motor. At the end of the vinylation the autoclave was cooled to room temperature, a sample of the exit gas was taken for analysis, and the rest of the gas was released. The autoclave contents were discharged into a porcelain beaker, and the autoclave was rinsed out several times with toluene, which was collected separately. The reaction product had the appearance of a thick yellow mass, containing a considerable amount of gray acetate precipitate. The toluene solution of 9-vinylfluorene was separated from the acetate by filtration, and the acetate was washed thoroughly, first with the toluene used for rinsing of the autoclave and then with pure toluene.

The toluene solution of 9-vinylfluorene and unconverted fluorene was fractionated under vacuum. Toluene was distilled at 10-15 mm and 45-50°, fluorene at 150-175°, and 9-vinylfluorene was then collected. To prevent polymerization of 9-vinylfluorene, a small amount of hydroquinone was added during distillation. Vinylfluorene and fluorene can also be separated by means of methyl or ethyl alcohol.

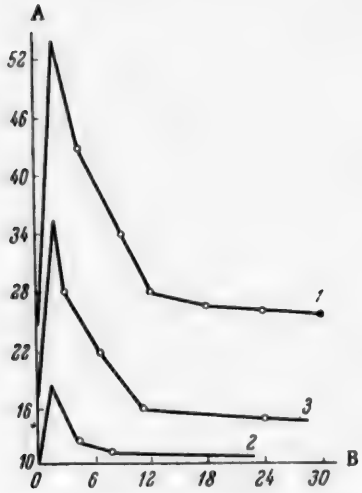

Fig. 1. Vinylation of fluorene in presence of caustic potash: A) pressure (atmos); B) duration (hours); the numbers of the curves correspond to the experiment numbers in the Table.

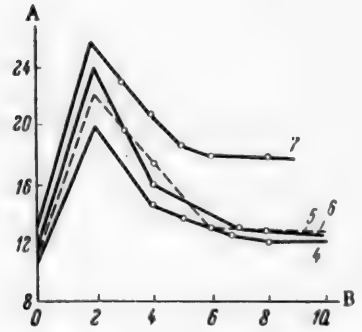

Fig. 2. Vinylation of fluorene in presence of caustic soda: A) pressure (atmos); B) duration (hours); the numbers of the curves correspond to the experiment numbers in the Table.

The acetate residue was dissolved in distilled water and separated by filtration from a small amount of brown substance, insoluble in water, which contained iron and was probably formed from impurities in the alkali. The aqueous solution of acetate was evaporated to dryness and dried to constant weight. The acetate was obtained as a white anhydrous powder.

The results of fluorene vinylation are given in the Table.

The 9-vinylfluorene used for analysis was recrystallized 3 times from ethyl alcohol and had m.p. 78°.

Found %: C 93.04, H 6.4; M 190 bromine number 82.8. $C_{15}H_{12}$. Calculated %: C 93.75, H 6.25; M 192, bromine number 83.3.

The dibromo derivative of 9-vinylfluorene was prepared and its bromine content determined.

Found %: Br 45.42. $C_{15}H_{12}Br_2$. Calculated %: Br 45.43.

The acetate content was determined by treatment of a weighed portion of the substance with phosphoric acid, with subsequent distillation of the acetic acid and titration by 0.1 N caustic soda solution.

Vinylacenaphthene consists of yellow acicular crystals of m.p. 87° after twofold recrystallization from ethyl alcohol. Vinylacenaphthene polymerizes on heating to from a hard water-resistant transparent pale yellow film. Vinylacenaphthene is easily soluble in benzene, toluene, xylene, chloroform, and other organic solvents.

The formation of vinylacenaphthene may be represented as follows:

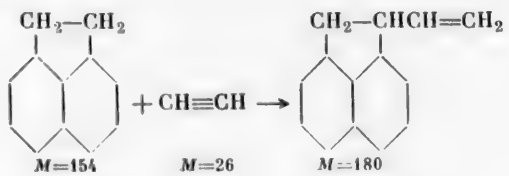

This structure is confirmed by the molecular weight, bromine number, the presence of one vinyl group which makes vinylacenaphthene capable of polymerization, and by the bromine content of the dibromo derivative of vinylacenaphthene.

The same method and the same autoclave as those used for vinylation of fluorene were used for vinylation of acenapththene (m.p. 92°) by acetylene under pressure. Two experiments were performed, one with the use of caustic soda and the other with caustic potash. The autoclave was charged with 39 g of acenaphthene, 500 ml of toluene, 11 g of caustic soda, and 3 ml of water; 94.9% of vinylacenaphthene and 99.0% of sodium acetate (of the theoretical yields) were obtained at 19 atmos maximum pressure and 210° during 7 hours. In the experiments with the same amounts of substances, but with caustic potash instead of caustic soda the yields were 96.2% of vinylacenaphthene and 86.3% of potassium acetate. The relationship between temperature, pressure, and vinylation time for acenaphthene is plotted in Fig. 3.

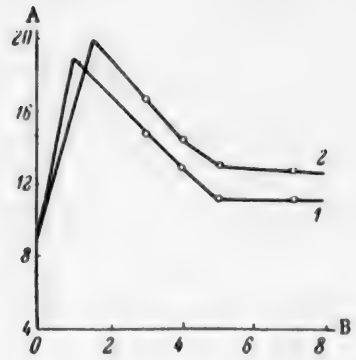

Fig. 3. Vinylation of acenaphthene at 210°: A) pressure (atmos); B) duration (hours); vinylation in presence of: 1) NaOH; 2) KOH.

The analytical data below refer to vinylacenaphthene recrystallized 3 times from ethyl alcohol, of m.p. 87°; the bromine content of the dibromo derivative was also determined.

Found %: Br 46.9. $C_{14}H_{12}BR_2$. Calculated %: Br 47.1. Found: M 176, bromine number 88.3. $C_{14}H_{12}$. Calculated: M 180, bromine number 88.8.

The determination of acetates was performed in the same manner as before.

Vinylindene is a viscous yellow liquid, sp. gr. 0.993; it polymerizes readily to form a hard water-resistant film. Both the liquid and the solid polymer are readily soluble in organic solvents—benzene, toluene, chlorobenzene, and carbon tetrachloride.

Vinylindene was prepared by vinylation of a heavy benzene fraction of b.p. 180° (sp. gr. 0.965), containing up to 40% indene, at 210° and 18 atmos pressure. Two hours after the maximum temperature had been reached the pressure dropped from 18 to 12 atmos (Fig. 4).* Calculation of the amount of acetylene consumed indicates that one vinyl group was introduced into indene, and that the amount of acetate formed would agree with that found. In addition, the molecular weight, bromine number, and analysis of the dibromo derivative indicated that the product was probably vinylindene.

The formation of vinylindene may be represented as follows:

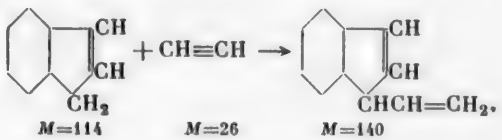

The vinylation of the heavy benzene fraction was performed in the same autoclave as before, in toluene in presence of caustic potash. The autoclave was charged with 200 ml of heavy benzene fraction, 300 ml of toluene, 11 g of caustic potash and 3 ml of water; the yield of vinylindene was 94.7%, and of potassium acetate, 80% (of the theoretical) at 18 atmos pressure and 210°. The toluene solution of the products formed by vinylation of the heavy benzene fraction can be used directly as a varnish, as it hardens in air after 20 minutes with formation of a hard pale yellow film. Hardness tests showed that the vinylindene film is equal in quality to oil varnish films.

The vinylindene was analyzed.

Found: M 134 $C_{11}H_{10}$ Calculated: M 142. Found: bromine number 111.5, Br 50%. $C_{11}H_{10}Br_2$. Calculated: bromine number 112.5, Br 50%.

Vinylation of a mixture of carbazole and fluorene. Experiments were performed on vinylation of equal amounts of carbazole and fluorene by acetylene under 39-55 atmos pressure at 195° in toluene in presence of caustic potash. These experiments were prompted by the hypothesis that, since fluorene has the lower melting point, it may facilitate melting and dissolution of carbazole. The formation of better plastics from copolymers of vinylfluorene and vinylcarbazole may be expected. Moreover, the copolymer should be free from the harmful properties ascribed to carbazole polymer.

In these experiments a mixture of vinylfluorene and vinylcarbazole was obtained in yields up to 60% of the theoretical, while the acetate yield was 92.4% calculated on the alkali taken.

The mixture of vinyl compounds consisted of yellow crystals which polymerize readily on heating or on exposure to air. The mixture was found to contain up to 45% vinylcarbazole, by determination of nitrogen.

*Fig. 4, omitted in the Russian original — Publisher.

The same method and autoclave as those used for vinylation of fluorene were used for vinylation of fluorene and carbazole.

SUMMARY

1. A method has been developed for vinylation of cyclic hydrocarbons: fluorene, acenaphthene, and indene; two important products—the vinyl compound and potassium or sodium acetate—are obtained simultaneously.

2. The following new vinyl compounds were prepared: vinylfluorene, vinylacenaphthene, and vinylindene; these may be of practical importance in the paint and varnish industry and in plastics production.

3. A mixture of fluorene and carbazole can be vinylated, with simultaneous production of a mixture of vinylcarbazole and vinylfluorene and the acetate.

LITERATURE CITED

[1] V. V. Korshak, General Methods of Polymer Synthesis [in Russian] (Izd. AN SSSR, 1955).

[2] P. P. Karpukhin, Proceedings of Conference on Cyclic Raw Materials, Acad. Sci. USSR [in Russian] (Izd. AN SSSR, 1936).

[3] P. P. Karpukhin and P. I. Mikhailenko, Trans. Khar'kov Inst. Chem. Tech. 1, 19 (1939).

[4] A. I. Kiprianov and M. M. Dashevskii, Aniline Dye Ind. 2, 8/9 (1932); P. P. Karpukhin and L. I. Slominskii, Ukrain. Chem. J. 10, 392 (1935).

[5] R. E. Burk, Progr. Chem. 8, 83 (1939).

[6] P. P. Karpukhin, Author's Certif. No. 9018 (1948).

[7] J. Nieuwland and R. Vogt, Chemistry of Acetylene (IL., 1947) p.195 [Russian translation].

Received January 13, 1958

EFFECTIVENESS OF 3,5-DI(TERT-BUTYL)-4-HYDROXYTOLUENE AND PROPYL GALLATE AS ANTIOXIDANTS FOR LARD

D. G. Knorre, Yu. N. Lyaskovskaya,
V. I. Piul'skaya, and N. M. Emanuel'

Institute of Chemical Physics, Academy of Sciences USSR
and the All-Union Scientific Research Institute of the Meat Industry

Oxidation processes which develop in edible fats and other fat-containing food products during storage cause enormous losses in the food industry. Therefore the question of prevention of oxidative deterioration of fats has for a long time attracted the attention of research workers. The most effective way of preventing oxidative deterioration of fats is by the use of antioxidants. The oxidation of fats is a chain process in the first stage of which hydroperoxides are formed

$$R^{\bullet} + O_2 \longrightarrow RO_2^{\bullet}, \quad (1)$$

$$RO_2^{\bullet} + RH \longrightarrow RO_2H + R^{\bullet}, \quad (2)$$

here RH is a molecule of the original fat. According to modern theories, antioxidants are capable of terminating the chains as the result of interaction with the radicals involved in the chain process.

The mechanism of interaction of free radicals with inhibitor molecules cannot as yet be regarded as finally established. It is probable that the free radical either detaches an H atom from the inhibitor molecule, or joins to the inhibitor molecule at the double bond with formation of an inactive free radical, incapable of continuing the chain. As a result, the reaction chain is terminated and the chain process is arrested. Thus, the reaction of $RO_2^{\bullet}$ with an inhibitor molecule I can be provisionally represented as follows:

$$RO_2 + I \longrightarrow \text{inactive radical} \quad (3)$$

As an objective measure of the degree of oxidative deterioration of fats it is reasonable to take the extent of the oxidative processes, i.e., the amount of oxidation products accumulated in the fat. Since a fat becomes unfit for use as food even at the early stages of oxidation, when the principal oxidation products are still peroxides, the peroxide number may be adopted as a measure of the degree of oxidative deterioration. As a rule a fat is spoiled when the peroxide number reaches a value of about 0.1. The time during which the fat still remains fit for use is of the principal practical interest. Therefore the oxidative processes which develop in fats may be characterized by the time τ required to reach a peroxide number of 0.1.

The effectiveness of an antioxidant may be represented as the ratio of time τ_a, required to reach a peroxide number of 0.1 in presence of the antioxidant, to time τ_0, required to reach a peroxide number of 0.1 in absence of the antioxidant.

Since under practical storage conditions τ_0 is measured in many months and τ_a is much greater still, determinations of antioxidant effectiveness under these conditions would take several years. Therefore, in general, antioxidant effectiveness is evaluated by an accelerated method, the oxidation being performed at elevated temperatures. Therefore, determination of the dependence of antioxidant effectiveness of temperature is of great interest.

TABLE

Effectiveness of Propyl Gallate and Butylhydroxytoluene as Antioxidants for Lard

Temperature (°C)	τ_0 (hr)	τ_a for 0.01% propyl gallate (hr)	$\frac{\tau_a}{\tau_0}$	τ_a for 0.01% butylhydroxy-toluene (hr)	$\frac{\tau_a}{\tau_0}$
90	11.9	—	—	36.2	3.0
100	4.9	42.6*	8.7	16.6	3.3
110	2.8	19.0	6.8	9.2	3.3
120	1.3	10.7	8.2	4.0	3.1
		Mean	7.9		3.2

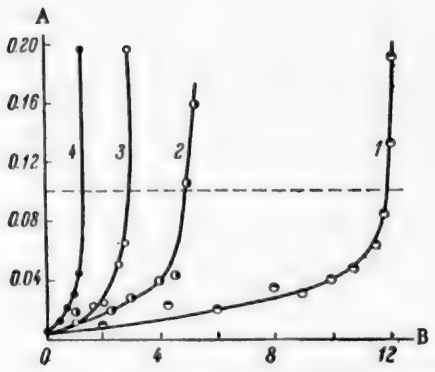

Fig. 1. Kinetics of peroxide accumulation during oxidation of lard at various temperatures: A) peroxide number; B) time (hours); temperature (°C) : 1) 90; 2) 100; 3) 110; 4) 120.

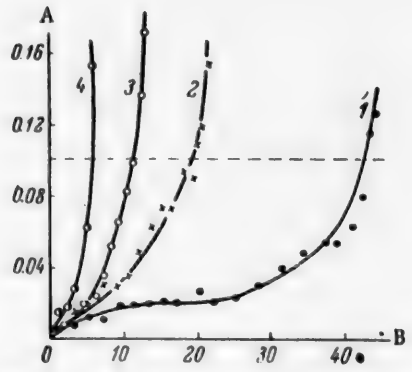

Fig. 2. Kinetics of peroxide accumulation during oxidation of lard in presence of 0.01% propyl gallate at various temperatures: A) peroxide number; B) time (hours); temperature (°C) : 1) 99; 2) 110; 3) 120; 4) 130.

We have studied the dependence of antioxidant effectiveness on temperature in the case of butylhydroxyanisole [1] and of a mixture of butylhydroxyanisole with ascorbyl palmitate [2].

In the present investigation we studied the effectiveness of action, and its dependence on temperature, of two food antioxidants—propyl gallate and di- (tert-butyl)-hydroxytoluene.

As previously [1-3], we studied the kinetics of peroxide accumulation in fat samples during oxidation. The process was conducted in an oxidation cell contained in a thermostat. The cell contained 20 g of fat, and air was blown in at the rate of 7 liters/hour through a porous glass filter sealed into the bottom of the cell. At definite time intervals samples of oxidized fat were taken and their peroxide number determined. With the aid of kinetic curves it was easy to determine τ corresponding to a peroxide number of 0.1.

Propyl gallate of m.p. 146° and 3,5-di-(tert-butyl)-4-hydroxytoluene of m.p. 70° were used in the experiments.

The value of τ decreases with rise the temperature. It had already been shown in our earlier papers that the effect of temperature on τ both in absence and in presence of antioxidants is satisfactorily represented by the Arrhenius equation

$$\tau = Ae^{\frac{K}{RT}},$$

where E is the activation energy of the process.

The value of E varies somewhat for different fat samples (between 20 and 25 kcal/mole). Therefore the same batch of fat must be used in determinations of τ in presence and in absence of antioxidant for determination of antioxidant effectiveness.

Fig. 1 shows kinetic curves for oxidation of lard at 90-120°. Fig. 2 and 3 show kinetic curves for oxidation of the same lard sample in presence of 0.01% propyl gallate at 100-130° and 0.01% tert-butylhydroxytoluene at 90-120° respectively.

Values of τ for all three cases and the antioxidant effectiveness at different temperatures are given in the table.

In Fig. 4 the time τ is plotted against temperature in the Arrhenius coordinates $\log \tau - 1/T$. It is seen that the points fit satisfactorily on straight lines in all cases, confirming the applicability of the Arrhenius equation. The values of the activation energy in this series of experiments were 21.4 kcal without antioxidant, 20.6 kcal in presence of 0.01% propyl gallate, and 21.0 kcal in presence of 0.01% di-(tert-butyl)-hydroxytoluene; i.e., they are almost identical.

These results are in full agreement with earlier data for butylhydroxyanisole and for mixtures of butylhydroxyanisole (0.01%) with ascorbyl palmitate (0.02%). In the former case the activation energy for the noninhibited and inhibited reaction was 23.0 and 23.0 kcal respectively, and in the latter, 23.1 and 23.6 kcal.

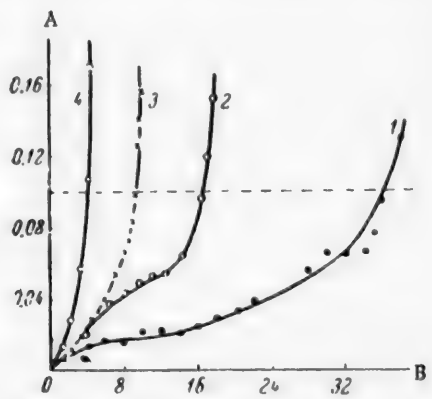

Fig. 3. Kinetics of peroxide accumulation during oxidation of lard in presence of 0.01 butylhydroxytoluene at various temperatures: A) peroxide number; B) time (hours); temperature (°C): 1) 90; 2) 100; 3) 110; 4) 120.

Thus it may be regarded as definitely established that the activation energy of oxidation at the initial stage of oxidation depends on the properties of the fat only, and is independent of the properties of the antioxidant.

The absence of a difference between the activation energies of oxidation in presence of different antioxidants is reasonably natural. According to the chain theory, the rate of oxidation in presence of an antioxidant is [4]

$$W = W_i \frac{K_2 [RH]}{K_3 [I]},$$

where W_i is the rate of chain inititation (in the case of fat oxidation this is, in practice, equal to the rate of hydroperoxide decomposition), K_2 and K_3 are the rate constants for Reactions (2) and (3), and [I] and [RH] are the concentrations of the antioxidant and the oxidized substrate respectively. The values of W_i and K_2 depend on the properties of the fat, and the value of K_3 depends on the properties of the antioxidant. Since all the antioxidants in question are similar in effectiveness, it follows that the activation energy for Reaction (3) should have virtually the same values. Therefore for a given batch of fat the effective energy of activation

$$E = E_i + E_2 - E_3$$

should be the same for all antioxidants.

The fact that the activation energies for inhibited and noninhibited oxidation coincide is more remarkable. As was noted in an earlier paper [5], this may be due to the fact that the process which is assumed to be noninhibited actually proceeds in presence of natural antioxidants retained in the fat during the rendering process.

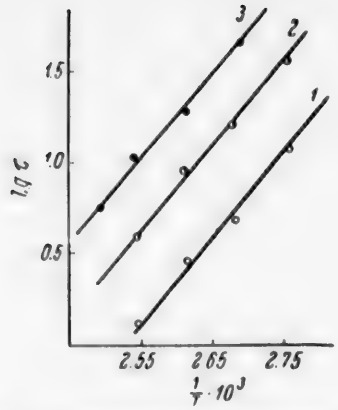

Fig. 4. Variation of the induction period τ (time to reach peroxide number 0.1) with temperature T: oxidation of fat: 1) without antioxidant, 2) in presence of 0.01% butylhydroxytoluene, 3) in presence of 0.01% propyl gallate.

SUMMARY

1. The effectiveness of di-(tert-butyl)-hydroxytoluene and propyl gallate as antioxidants for lard has been determined; with 0.01% antioxidant contents the values are 3.2 and 7.9 respectively.

2. The activation energy of oxidation in presence of propyl gallate and di-(tert-butyl)-hydroxytoluene is 20.6 and 21.0 kcal respectively, and the value in absence of inhibitor is 21.4 kcal.

3. In conjunction with our earlier data these results lead to the conclusion that the activation energy of the oxidation process depends only on the nature of the fat, and is independent of the presence of antioxidants for their nature.

LITERATURE CITED

[1] N. M. Émanuél', D. G. Knorre, Yu. N. Lyaskovskaya, and V. I. Piul'skaya, Meat Ind. USSR 6, 47 (1955).

[2] D. G. Knorre, Yu. N. Lyaskovskaya, V. I. Piul'skaya, and N. M. Émanuél', Bull. Acad. Sci. USSR, Div. Chem. Sci. 1422 (1958).*

[3] N. M. Émanuél', D. G. Knorre, Yu. N. Lyaskovskaya, and V. I. Piul'skaya, Meat Ind. USSR 5, 44 (1955).

[4] D. G. Knorre, Z. K. Maizus, L. K. Obukhova, and N. M. Émanuél', Progr. Chem. 26, 416 (1957).

[5] D. G. Knorre, Yu. N. Lyaskovskaya, and N. M. Émanuél', Bull. Acad. Sci. USSR, Div. Chem. Sci. 678 (1957).*

Received February 7, 1958

* Original Russian pagination. See C. B. Translation.

REACTION MECHANISM OF THE THERMAL DEPOLYMERIZATION OF POLYCAPROLACTAM*

N. D. Katorzhnov and A. A. Strepikheev

All-Union Scientific Research Institute of Artificial Fibers

Thermal depolymerization of polycaprolactam leads to a number of undesirable complications in the technological process of capron fiber production. Clarification of the mechanism of this reaction is important in relation to theoretical aspects of methods for improving the process.

There is no published research information on the reaction mechanism of depolymerization, but only a number of hypotheses.

According to Carothers [3] the depolymerization reaction proceeds in absence of activators by a "transpositional" mechanism of radical redistribution (analogously to transesterification and transamidation reactions, etc.), both between individual macromolecules and within the polymer macromolecules, which leads to removal of rings of different sizes, in the extreme case containing a single structural unit of the original macromolecule.

However, depolymerization by this mechanism is impossible, because, as has been shown for a number of examples [2, 3, 4], cyclic and linear amide linkages are kinetically inhibited in absence of activated.

It has been demonstrated in numerous investigations that polymerization of caprolactam can be activated by a variety of compounds: water (or compounds which split off water at elevated temperatures), alcohols, mineral and organic acids, amines [3, 4], alkali metals [5], and alkali carbonates [6].

In dry polycaprolactam made by polymerization of caprolactam in presence of water, free amino and carboxyl functional groups are present at the ends of the macromolecules.

Functional amino and carboxyl groups, especially in presence of water, being activators of one reaction of radical redistribution – ring polymerization – should also activate another type of radical redistribution, namely transamidation, which is involved in polycaprolactam depolymerization.

Strepikheev [4] examined the possible reaction schemes of polycaprolactam depolymerization from the theoretical aspect, and concluded that all such schemes must involve free functional amino and carboxyl end groups.

In the present investigation the fundamental reaction mechanism of the thermal depolymerization of polycaprolactam was established experimentally.

EXPERIMENTAL

Kinetic data on depolymerization of unstabilized polycaprolactam with free functional amino and carboxyl end groups were published earlier [7].

The present paper contains the results of a study of the kinetics of thermal depolymerization of polycaprolactam stabilized (by blocking) during polymerization of caprolactam by means of various compounds (monocarboxylic acids, normal monoamines, their salts, and amides).

*Communication 2 in the series on the thermal depolymerization of polycaprolactam.

TABLE 1

Conditions for Preparation of Polymers Stabilized by Various Additives

Stabilizer	Amt. (% on wt. of caprolactam)		Polymerization conditions		Polymer yield (%)	Monomer content (%)	Specific viscosity of 0.5% polymer solution in cresol
	stabilizer	activator (water)	temperature (°C)	time (hours)			
Acetic acid	0.5	1.0	260	10	92.4	7.6	0.350
	1.0	1.0	260	10	91.4	8.6	0.253
n-Butylamine	0.6	1.0	260	10	94.0	6.0	0.427**
	1.2	1.0	260	10	93.7	6.3	0.312**
n-Butylamine acetate	1.1	—	260	30	93.5	6.5	0.360
	2.2	—	260	30	94.2	5.8	0.252

*Despite the use of equimolar proportions, the specific viscosities of the polymer made with n-butylamine were higher than those of the polymer stabilized by acetic acid, because of losses of amine due to partial evaporation when the ampoules were filled.

TABLE 2

Kinetics of Thermal Depolymerization of Polycaprolactam, Stabilized by Acetic Acid, in Presence of 0.034% Water

Depolymerization temperature (°C)	Initial specific viscosity of polymer	Caprolactam formed (%) during time (hours)			
		0.5	1	3	5
230	0.350	0.91	1.05	1.73	2.07
	0.253	1.1	1.90	2.15	2.58
240	0.350	1.24	1.37	2.16	2.67
	0.253	1.23	1.79	2.92	3.53
250	0.350	1.08	1.93	2.85	3.74
	0.253	1.53	2.30	3.55	4.33

The amino groups in polycaprolactam macromolecules were blocked by addition of acetic acid, carboxyl groups were blocked by means of n-butylamine*, and both end groups by means of butylamine acetate. Conditions for preparation of caprolactam polymers stabilized by various additives are given in Table 1.

The kinetics of the thermal depolymerization of polycaprolactam was determined from the amount of caprolactam formed in relation to the initial molecular weight of the polymer, its water content, and the temperature and time of heating. The methods used were described earlier [7].

Polycaprolactam stabilized by acetic acid was thermally depolymerized in presence of 0.034% water.

The results are given in Table 2.

Polycaprolactam stabilized by n-butylamine and by n-butylamine acetate was thermally depolymerized in presence of 0.135% water. The results are shown in the figure.

*We are deeply grateful to Prof. G. Ya. Vanag of the Latvian University for kindly supplying n-butylamine.

TABLE 3

Effect of Functional End Groups in the Polymer Macromolecules on Formation of Caprolactam in Thermal Depolymerization of Polycaprolactam

Stabilization of polycaprolactam	Nature of free end groups	Initial specific viscosity of polymer	H_2O cont. of polymer during depolymerization (%)	Amount of caprolactam formed (in %) during 5 hours of heating at (°C)		
				230	240	250
Not stabilized	—COOH	0.400	0.037	2.45	3.35	4.2
	$-NH_2$	0.350 *	0.037	2.70 *	3.60 *	4.70 *
Stabilized by acetic acid	—COOH	0.350	0.034	2.07	2.67	3.74
Stabilized by n-butylamine	NH_2	0.427	0.135	2.51	3.44	4.81
	NH_2	0.350 **	0.135	3.40 **	4.40 **	5.30 **
Stabilized by butylamine acetate	—	0.350	0.135	0.85	1.41	2.212

*Extrapolated data.

**Interpolated data.

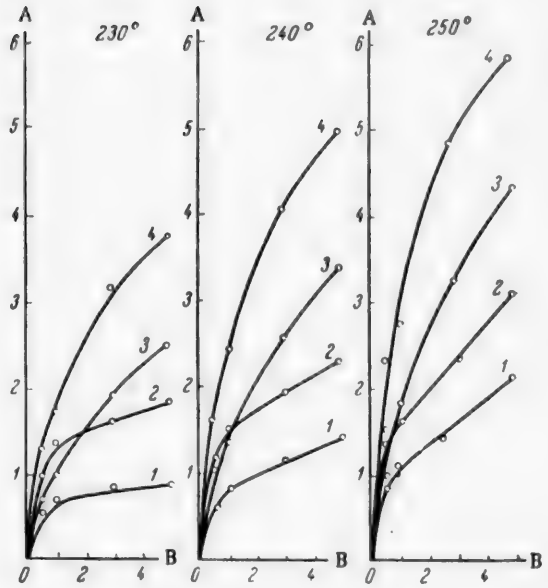

Kinetics of thermal depolymerization of polycaprolactam, stabilized by butylamine and butylamine acetate, in presence of 0.135% water: A) amount of caprolactam formed (% of polymer weight), B) duration of thermal depolymerization of polycaprolactam (hours); specific viscosity of original polymer: stabilized by butylamine acetate, 1) 0.360, 2) 0.252; stabilized by butylamine, 3) 0.427, 4) 0.312.

DISCUSSION OF RESULTS

It is evident from the data in Table 2 and the figure that the thermal depolymerization of polycaprolactam stabilized by different additives and with one or both end groups in the polymer chain in the blocked state does not differ in character from the thermal depolymerization of unstabilized polycaprolactam [7]. The same relationships hold: the rate of caprolactam formation increases with decrease of the average molecular weight of the polymer (expressed in terms of the specific viscosity of a 0.5% polymer solution in cresol), with increase of the reaction temperature, and with increase of water content.

Comparative data on the influence of functional end groups on the rate of caprolactam formation, for a thermal depolymerization time of 5 hours at reaction temperatures of 230, 240, and 250°, are presented in Table 3. Graphical analysis of the results shows that:

a) elimination (blocking) of one of the two functional groups in the polycaprolactam macromolecule by conversion into an inactive alkyl amide group lowers the rate of caprolactam formation, but only to a small extent;

b) the rate of monomer formation is the same for polycaprolactam with blocked amino groups (stabilized by acetic acid) as for polycaprolactam with blocked carboxyl groups (stabilized by n-butylamine;

c) elimination (blocking) of both functional end groups in the polycaprolactam macromolecule sharply retards the rate of caprolactam formation.

Because the activator (water) is present in the proportion of 0.135% of the polymer weight, the process does not stop completely.

The results of experiments in which water was removed almost completely by heating of the stabilized polycaprolactam in ampoules under vacuum for 7 hours at 260° showed that during subsequent additional heating for 9 hours at 260°, i.e., under much harsher conditions than in any of preceding experiments, the amount of caprolactam increased by only 2% in the polymer of specific viscosity 0.207, and by 1.5% in the polymer of specific viscosity 0.252. In unstabilized polymer 5-7% of monomer is formed under these conditions.

These experimental results indicate that the amount of monomer formed during thermal depolymerization of polycaprolactam of given molecular weight depends mainly on the influence of functional amino and carboxyl end groups, and the splitting effect of these groups is intensified in presence of activator (water). This result leads to the conclusion that, as was suggested by Strepikheev, the principal mechanism in the depolymerization of polycaprolactam is interaction of functional end groups in the macromolecules with the last amide linkages in the same macromolecules (a mechanism of "rolling up" of the functional amino and carboxyl end groups) with liberation of caprolactam according to the scheme

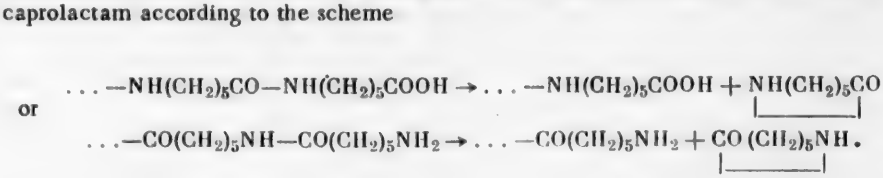

The acceptance of this mechanism as the principal mechanism of the thermal depolymerization of polycaprolactam makes it possible to account for the inverse relationship between the amount of monomer formed and the molecular weight of the polycaprolactam [7].

In accordance with this reaction mechanism, the greatest amount of monomer is formed per unit time in unit weight of polymer in polycaprolactam with the greatest amount of end groups, i.e., of the lowest molecular weight.

Means of inhibiting thermal depolymerization are also entirely consistent with this mechanism. Elimination of one active end group in the macromolecule retards to some extent the rate of monomer formation. However, depolymerization continues owing to the activating action of the remaining free end groups.

Blocking of both functional end groups in the macromolecule and their conversion into inactive alkyl amide groups results in the formation of a "kinetically inhibited" polymer, incapable of change in absence of activator (water).

In presence of water, which is difficult to remove completely from the polymer in practice, hydrolysis of the amide linkages in the macromolecules leads to formation of amino and carboxyl end groups, which assist the thermal depolymerization reaction in accordance with the mechanism described above. Therefore inhibition of monomer formation when the method of "kinetic" stabilization of polycaprolactam is applied in practice is more effective if as much water as possible is removed from the polymer.

It must be pointed out that blocking of both end groups of the polycaprolactam macromolecule not only retards sharply the process of monomer formation, but effectively stabilizes the molecular weight. The molecular weight (specific viscosity) of such polymers does not change on prolonged heating, in contrast to polycaprolactam containing one or both functional end groups in its macromolecules.

The principle of "kinetic" stabilization may be of practical utility in the production of polycaprolactam and capron fiber, especially in processes of continuous polymerization of caprolactam and melt spinning of fibers after evacuation of the monomer.

SUMMARY

1. Strepikheev's hypothesis concerning the reaction mechanism of thermal depolymerization of polycaprolactam has been confirmed experimentally. It is shown that the principal mechanism of this reaction consists of interaction of free amino and carboxyl end groups of the macromolecules with the last amide linkages of the same macromolecules ("rolling up" of functional amino and carboxyl end groups), with liberation of caprolactam.

2. The principle of "kinetic" stabilization of caprolactam has been worked out; this consists of blocking of both active end groups in the macromolecule and their conversion into inactive alkyl amide groups, incapable of causing, in absence of water, depolymerization of polycaprolactam with monomer formation.

Salts of normal monoamines and monocarboxylic acids, and N-n-alkyl amides of monocarboxylic acids can be used as stabilizers.

LITERATURE CITED

[1] W. H. Carothers and F. J. van Natta, J. Am. Chem. Soc. 52, 314 (1930); W. H. Carothers, Chem. Rev. 8, 353 (1931); W. H. Carothers and J. W. Hill, J. Am. Chem. Soc. 55, 5043 (1933).

[2] A. A. Strepikheev and A. V. Volokhina, Proc. Acad. Sci. USSR 92, 3, 407 (1954).

[3] I. Knunyants, Z. Rogovin, Yu. Rymashevskaya and É. Khait, J. Gen. Chem. 17, 987 (1947); 17, 1316 (1947).

[4] A. A. Strepikheev, Candidate's Dissertation [in Russian] (All-Union Sci. Res. Inst. Artif. Fibers, 1950).

[5] W. Hanford and R. Joyce, Polymer Sci. 3, 167 (1948).

[6] O. Wichterle, Faserforsch u. Textiltechnik 6, 237 (1955).

[7] N. D. Katorzhnov and A. A. Strepikheev, J. Appl. Chem. 32, No. 3,625 (1959).*

Received May 9, 1958

*Original Russian pagination. See C. B. Translation.

REMOVAL OF IMPURITIES FROM POTASSIUM BY THE IONIC-MOBILITY METHOD

B. P. Konstantinov and V. S. Rylov

The Leningrad Institute of Technical Physics, Academy of Sciences, USSR

The purification of salts of chemical elements by the ionic-mobility method essentially consists of separation of mixtures of the elements, contained in electrolytes, by the action of an electric field. The mixture of elements to be separated is placed in the form of an electrolyte solution into a glass tube. When a direct electric current is passed through the electrolyte, the cations of the element with the highest ionic mobility outstrip the cations of other elements and collect in a separate column in the tube. This column is followed by cations of the element with a somewhat lower ionic mobility, etc. According to Kohlrausch [1], the ratio of cation concentrations in adjoining columns is equal to the ratio of the transference numbers of these cations, i.e.

$$\frac{C_1}{C_2} = \frac{T_1}{T_2}, \tag{1}$$

where C_1 and C_2 are the concentrations (in terms of normality) and T_1 and T_2 are the transference numbers of the cations in the first and second columns respectively.

The relationship (1) becomes established automatically in accordance with the concentration of the electrolyte nearest to the cathode.

Under the steady conditions represented by (1) at the boundary between two adjoining columns the concentrations change from C_1 and C_2 virtually to zero. Because of ion diffusion, the boundary between the electrolytes is diffuse. The diffuseness of the boundary, i.e., its width, may be calculated by means of Eq. (2)*, derived by B. P. Konstantinov for solution of the equations for migration of ions in an electrolyte under the influence of an electric field.

$$\frac{C_1}{C_1 + C_2} = \frac{1}{1 + e^{Ax}}, \tag{2}$$

$$A = \varepsilon E \frac{e}{kT}, \tag{3}$$

where ϵ is the relative difference of mobilities of cations from two adjacent columns, E is the potential of the electric field along the x coordinate, x is the coordinate along the tube length, T is the absolute temperature of the electrolyte, k is the Boltzmann constant, and e is the electronic charge.

Suppose that a column of potassium ions is followed by a column of sodium ions. For these ions $\epsilon \approx 0.4$. When $E \approx 10$ v/cm and $T \approx 300°$, we have, from Eq. (3), $A \approx 160$.

Hence it is easy to calculate from Eq. (2) that the concentration of sodium in the column of potassium ions at a distance of less than 1 mm from the boundary with the sodium column ($x = 0$) is $\frac{C_2}{C_1 + C_2} < 10^{-4}$ %.

*The derivation of Eq. (2) is given in the Appendix (see p. 1403).

TABLE 1

Concentrations of Impurities in the Original KCl

Potassium content (mg/liter)	Impurities in mg/liter										in g/liter		
	Na	Ca	Mg	Mn	Cu	Fe	Ni	SiO_3''	Al	Cr	SO_4''	NO_3'	HCl
100	5	5	3	2	20	10	5	20	5	5	0.1	0.1	5

Apart from ion diffusion, the width of the boundary may be appreciably influenced by the dynamic counterflow used to balance the migration of the ions under the action of the electric field, and the temperature gradient across the tube, leading to ion convection. These factors, which lead to additional mixing of the ions, must be eliminated in purification; this can be achieved if:1) separation tubes containing fillers, such as quartz sand(with grains smaller than 0.1 mm), or agar gel are used; 2) if the electric current passed through the tube does not exceed the value at which the filler becomes ineffective (fusion of gel, formation of gas bubbles in sand).

The minimum time necessary for removal of cation impurities from an electrolyte column containing a given cation is

$$t_{\min} \approx \frac{l}{\epsilon \cdot v}, \qquad (4)$$

where l is the length of the electrolyte column, v is the velocity of the cation in the tube without counterflow, and ϵ is the relative difference between the mobilities of the given cation and the impurity cation.

Preliminary Purification of Potassium Chloride. The composition of the original potassium chloride, subsequently purified by the ionic-mobility method, is given in Table 1.

The ionic-mobility method is ineffective for removing rubidium and cesium impurities from potassium chloride, as the mobilities of the respective ions differ little. Removal of anionic impurities from the electrolyte column (Table 1) presents no difficulty, as anions move in the opposite direction to cations during the purification.

The mobility of potassium cations is greater by several tenths than the mobilities of the cations indicated in Table 1. Of the elements in Table 1, the sodium ion has the closest mobility to the potassium ion. It follows that if sodium can be removed from potassium by the ionic-mobility method, the other impurities can be removed all the more easily.

The presence of relatively large amounts of impurities, the contents of which may vary from sample to sample, in the original potassium salt (Table 1) made preliminary purification necessary. This was performed by the ionic-mobility method in a gel-filled glass tube. The impurity content was lowered to $\leq 0.1\%$ by purification in the gel-filled tube. The maximum losses of potash were 2-5%. The apparatus with the separating tube filled with agar gel is shown schematically in Fig. 1. The internal diameter of the tube was 7 mm, and the length was 350 mm. The gel contained 18 g NH_4Cl and 3 g agar per 90 ml of water. The tube was filled with this gel up to the mark a. The original "impure" KCl solution, containing not more than 0.7 g of KCl, was poured in from above into the wide portion of the tube. Hydrochloric acid must first be removed from the original KCl solution by evaporation. The KCl solution in the tube was filled with quartz sand, which was then covered with 1 N $CuCl_2$ solution. The lower end of the tube was inserted into the cathode vessel containing 1 N HCl.

When a current of 400 ma was passed through the tube, the ions of potassium and of the impurity elements were separated in the following sequence: potassium ions were followed by sodium ions, then calcium, copper, and the other elements.

The boundary between the potassium and sodium columns can be seen distinctly in a shadow projection. When this boundary reached a distance of 10 cm from the lower end of the tube the purification was terminated. The gel column, containing KCl with some NH_4Cl, was squeezed out of the tube up to the boundary with sodium

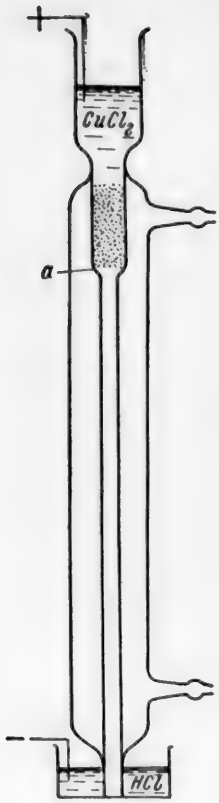

Fig. 1.

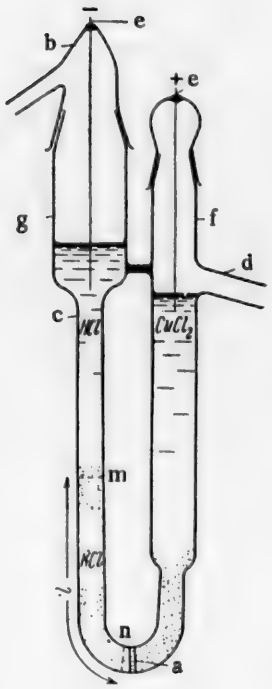

Fig. 2.

Fig. 1. Gel-filled tube for preliminary purification of KCl; a) upper boundary of agar gel in tube.

Fig. 2. Tube with quartz sand for final purification of the KCl electrolyte column: a) filter, b) cover, c) cathode limb of tube, d) side tube, e) electrodes, f) anode vessel, g) cathode vessel; m and n) boundaries of the KCl column being purified.

into a small quartz flask. To remove organic matter and ammonium chloride from the KCl sample so obtained, it was heated at 600°.

Final Purification of Potassium Chloride. The final purification of KCl was also effected by the ionic-mobility method, in a quartz U-shaped tube 8 mm in internal diameter (Fig. 2). The tube was partially filled with quartz sand (0.1-0.05 mm grain size). The filter a served to prevent displacement of the sand along the tube. The cover b protected the cathode limb of the tube against accidental contamination. The side tube d from the anode vessel f served to maintain the anolyte level and to remove the chlorine formed at the anode. The electrodes e were made of platinum.

The sand in the tube was first filled with 3 N $CuCl_2$ solution. The KCl sample, containing not more than 0.7 g in 3 ml of solution, was introduced through the limb b by means of a pipet and then sucked into the sand by means of a water-jet pump. The cathode vessel g was then washed out thoroughly with water and hydrochloric acid, and 3 N $CuCl_2$ solution was added into the cathode vessel. The difference between the electrolyte levels in the anode and cathode vessels was 2-3 cm, which ensured hydrodynamic counterflow to the electrical migration of the cations.

The current passing through the tube was maintained constant at 250 ma. For cooling, the tube was immersed in a vessel containing water at room temperature. During the purification the column of KCl solution of

TABLE 2

Sensitivity of the ISP-22 Spectrograph

	Impurities in KCl						
	Ca	Mg	Cu	Fe	Ni	Si	Al
Sensitivity of analysis (%)	$10^{-3} - 10^{-4}$	$\sim 10^{-3}$	$\sim 10^{-3}$	$\sim 10^{-2}$	$\sim 10^{-2}$	$\sim 10^{-3}$	$\sim 10^{-3}$

length l (Fig. 2) was in the sand, and mainly in the cathode half of the tube. The purification was continued for 6-8 hours.

For collection of the purified KCl, the column of KCl solution was withdrawn by means of an electric current into the tube c out of the sand so that its height (from the sand surface to the boundary with HCl, easily seen in a shadow projection) was 50-60% of the height of the KCl column remaining in the sand (from the sand surface to the colored boundary with $CuCl_2$). With the KCl column in this position, hydrochloric acid was removed (as far as the boundary with KCl) from the cathode vessel, and the column of KCl solution over the sand was transferred by suction into a quartz siphon.

From the quartz siphon the KCl solution was transferred into a quartz weighing bottle and evaporated to dryness. The part of the KCl column remaining in the sand (about 50%), containing Na, Ca, and other impurities, was extracted from the tube and used again. Irrecoverable losses of KCl during purification in the sand tube were 5-6%.

The degree of purification was tested simultaneously by means of the ISP-22 and ISP-51 spectrographs. It was found that the sodium content of the purified KCl samples was usually $\leq 10^{-4}$ %. Therefore if no impurities are introduced into the KCl during collection and subsequent treatment of the purified salt, the contents of the other impurities (see Table 1) can also be assumed to be $\lesssim 10^{-4}$%.

Table 2 contains our data on the sensitivity of the ISP-22 instrument in determinations of the impurities in KCl.

The impurities indicated in Table 2 were not detected in the purified KCl samples.

With regard to the anionic impurities (Table 1), these are removed from the KCl column considerably before the cationic impurities if the catholyte (hydrochloric acid) is reasonably pure.

APPENDIX

Suppose that a column of electrolyte with cations 1 contains an admixture of cations 2, the atomic fraction of which is α. Then the average velocity of the electrolyte column containing the two cations under the influence of an electric field E is

$$v_{av} = v_2 \alpha + v_1 (1 - \alpha), \tag{5}$$

where $v_1 = u_1^+ \cdot E$, $v_2 = u_2^+ \cdot E$, u_1^+ and u_2^+ are the mobilities of the corresponding cations.

The velocity of the impurity cations 2 relative to the moving electrolyte column is

$$v_2' = v_2 - v_{av}$$

and, from Eq. (5), we have

$$v_2' = (1 - \alpha)(v_2 - v_1), \tag{6}$$

which means that the velocity with which the impurity cations leave the electrolyte column with cations 1 under the influence of the electric field is proportional to the atomic fraction of cations 1.

Under steady-state conditions, the flow of cations 2 from the electrolyte column containing cations 1 is balanced by the opposing diffusional flow of cations 2, i.e.

$$\alpha \cdot v_2' - D_2 \frac{d\alpha}{dx} = 0, \tag{7}$$

where D_2 is the coefficient of diffusion of cations 2 in the electrolyte. Substituting Eq. (6) into (7) we have

$$\frac{d\alpha}{\alpha(1-\alpha)} = \frac{v_2 - v_1}{D_2}\, dx. \tag{8}$$

Under the given conditions for separation of cations 1 and 2 it may be assumed that D_2 is constant. At the end of the separation process, when the relative concentration of cations 2 in the column of electrolyte with cations 1 is small, i.e., $\alpha \ll 1$, we have $v_2 - v_1 = E(u_2^+ - u_1^+) \approx$ const. thus integrating (8), we have

$$\frac{\alpha}{1-\alpha} = B \cdot exp\left[\frac{v_2 - v_1}{D_2} x\right]. \tag{9}$$

If the origin of the x coordinate (x = 0) is taken to be the boundary between the electrolytes of cations 1 and cations 2 at which the concentration of cations 1 is equal to the concentration of cations 2, i.e. $\alpha = 0.5$, then in Eq. (9) the integration constant B = 1.

By the Einstein formula

$$D_2 = \frac{u_2^+ \cdot k \cdot T}{Ze}, \tag{10}$$

where Z is the valence of the cation.

Substituting Eq. (10) into (9) and putting

$$A = \frac{Z \cdot e \cdot E(u_2^+ - u_1^+)}{kT \cdot u_2^+} = \frac{Z \cdot e \cdot E}{kT} \epsilon,$$

we have

$$\frac{\alpha}{1-\alpha} = exp(Ax). \tag{11}$$

If C is the total concentration of cations 1 and 2 in the electrolyte column of cations 1, then we have $C_1 = C(1-\alpha)$, $C_2 = C\alpha$.

Therefore from Eq. (11) we obtain Eq. (2)

$$\frac{C_1}{C_1 + C_2} = \frac{1}{1 + e^{Ax}}.$$

LITERATURE CITED

[1] F. Kohlrausch, Ann. der Physik 62, 209 (1897).

Received April 2, 1958.

VACUUM-THERMAL PRODUCTION OF SODIUM AND POTASSIUM

V. M. Gus'kov, A. I. Voinitskii, N. M. Zuev,

A. Yu. Taits and V. M. Chel'tsov

The alkali metals are becoming increasingly important in various branches of industry and new technological processes.

Sodium is used as a reducing agent in the production of titanium, zirconium, and other refractory rare metals, and in the production of synthetic rubber, tetraethyllead, and ethyl fluid. Potassium is used in the production of peroxides, which are becoming ever more important in modern technology.

The production of alkali metals in our country lags behind their possible consumption. The low technological level of production does not conform to the rising standards for these metals.

The production of potassium by the sodium thermic process involves a high consumption of caustic potash and metallic sodium. The degree of utilization of the starting materials is low, the operating conditions are difficult, and the equipment used industrially for this process is inefficient.

The production of sodium by electrolysis of sodium chloride or caustic soda involves a high consumption of electric power. With the existing types of cells, high current efficiencies are not obtainable, the hygienic labor conditions are abnormal, and metal of such purity that it could be used without further purification for such purposes as titanium production cannot be obtained.

Therefore in 1951-1957 extensive investigations were carried out in the All-Union Aluminum and Magnesium Institute on the vacuum-thermal method for production of sodium and potassium. This method should yield alkali metals of a high degree of purity, with the use of much the same equipment and processes, at a high economic efficiency and under normal hygienic operating conditions.

The chlorides of potassium and sodium are used as the starting materials in the vacuum-thermal production of the metals. The reducing agents may be silicon (ferrosilicon), aluminum or its alloy with silicon, calcium carbide or its mixtures with ferrosilicon. Essential components in the production of sodium and potassium are lime and the fluorides of sodium, potassium, calcium, or aluminum.

The basic conditions for preparation of the briquets for reduction were determined during these investigations. Limestone was crushed and then calcined in a rotary kiln at 1100-1200° until the carbonates were completely decomposed. The chlorides and calcium fluoride were dried at 200-250° to constant weight. The materials were ground in closed ball mills. The chlorides were passed through a 30-50 mesh screen, and the reducing agent, lime, and calcium fluoride through a 100 mesh screen.

The charge components were mixed thoroughly in the required proportions, and molded under a pressure of 400-600 kg/cm^2 into briquets 30-75 mm in diameter and 30-40 mm high. The briquetting was performed by means of an industrial mechanical continuous tabloid press with a rotating table, with a capacity of 500 kg/hour.

More than 20 charge compositions for sodium production, 170 charge compositions for potassium production, and 4 compositions for production of sodium – potassium alloys were tested under laboratory conditions.

The simultaneous processes taking place between the individual components in the vacuum-thermal production of sodium and potassium are complex and diverse. They are typical heterogeneous reactions involving gaseous, liquid, and solid compounds.

Thermodynamic calculations and their experimental verification show that the reduction process primarily involves alkali chlorides in the solid and vapor states, solid calcium oxide, and liquid or solid (aluminum or silicon) reducing agent. Interaction of the original compounds yields vapors of the alkali metals, calcium chloride, and calcium aluminate or silicate by the principal reactions

$$4MeCl + 4CaO + Si = 4Me + 2CaCl_2 + 2CaO \cdot SiO_2, \quad (I)$$

$$18MeCl + 14CaO + 6Al = 18Me + 9CaCl_2 + 5CaO \cdot 3Al_2O_3, \quad (II)$$

where Me represents sodium or potassium.

The principal reactions between the original components are accompanied by a number of side reactions. The most important of these are the processes of formation of calcium aluminide and silicide ($CaAl_2$ and $CaSi_2$). The intensity of the side reactions directly depends on the proportions of the components in the charge and the conditions of the thermal process.

The thermal process of alkali metal production is greatly influenced by the relative proportions of the charge components; both a deficiency and an excess of calcium oxide or reducing agent have adverse effects. In the former case the conversion of the salt, and in the latter, the conversion of calcium oxide and reducing agent is decreased sharply. The consequent increase of charge consumption per unit weight of metal produced sharply lowers the output rate of the equipment and raises the cost of the metal produced.

For industrial use, the most promising charge compositions are those in which the molar ratio of calcium oxide to chloride is close to 0.8, and the molar ratio of reducing agent to chloride is 0.8-0.9. Reduction of sodium and potassium begins at temperatures close to 650°. The reaction rates rise sharply with increase of temperature. When the temperature in the reaction zone is below 800° the reduction of alkali metals is slow and most of the sodium or potassium chloride leaves the reaction zone unchanged. With increase of temperature the chemical activity of the interacting compounds increases more rapidly than the evaporation rate of the salt. The charge activity becomes sufficiently high at temperatures above 850°. As a result, despite the high evaporation rate of the salt, the degree of extraction of metal in the charge increases, and the duration of the reduction decreases sharply. The optimum reduction temperature is 800-850° for sodium and 900-950° for potassium.

Reduction of pressure has a strong influence on the nature of the reduction processes. It shifts the equilibrium in reactions (I) and (II) to the right. For example, the isobaric potential of the system corresponding to reaction (I), when the vapor pressure of potassium chloride is 0.5 mm and the temperature is 850°, alters by about 20 kcal relative to the isobaric potential for the process performed without pressure reduction. Apart from changing the isobaric potential, pressure reduction favors evacuation of the forming metal vapor from the reaction zone. This disturbs the equilibrium between the original components and the reaction products and favors more complete and rapid course of the reactions represented by Eq. (I) and (II).

The alkali metal and salt vapors are fractionally condensed in the cold zones of the furnace, forming a solid sublimate of the salt and the liquid metal. Separation of chlorides and metal condensed from the gas phase is improved considerably on reduction of pressure. This is especially important in the case of potassium, in the production of which the boundary between the salt sublimate and the metal in the condenser is usually indistinct. The reduction of the alkali metals is most complete at residual pressures below 0.5 mm Hg. Higher pressures in the reaction zone lower the reaction rate and the effectiveness of the thermal process.

The reactivity of the charge components increases considerably with decreasing particle size of the calcium oxide and reducing agent. The particle size of the chloride has no practical influence on the thermal process. This is because of the heterogeneous character of the reactions involved and the physicochemical properties of the interacting compounds. Subdivision increases the contact area of the components and favors completion of the reactions taking place on the surface of the solid particles. The favorable effect of subdivision of the charge components becomes increasingly prominent at higher reduction temperatures. At low temperatures decrease of particle size has little effect.

The effectiveness of the thermal process for production of alkali metals can be improved considerably by addition of fluorides to the charge. Even small amounts of fluorides (up to 5%) sharply increase the reduction rate and metal extraction. The influence of such additions is especially effective if the thermal process is conducted at low temperatures.

The influence of fluorides is very complex, and depends in a considerable measure on the nature and the amount of the salt in the charge, the nature of the reducing agent, and the temperature at which the thermal process is carried out. It affects not only the kinetics of the processes taking place, but also the properties of the charge briquets and the solid residues after the reduction.

Reduction of a mixture of potassium and sodium chlorides by ferrosilicon yielded a sodium-potassium alloy; the degree of extraction of the metals from the charge was up to 62.5%, the specific consumption of the reducing agent was 1.7, and the charge consumption was 7 kg per kg of alloy. Sodium-potassium alloys of any desired composition may be obtained by variation of the proportions of sodium and potassium chlorides in the charge.

Trials of the separate production of sodium and potassium were conducted in large-scale laboratory experiments; retorts fitted with Silit (carbon) heaters were charged with 20-25 kg of the reaction mixture, and resistance-heated retorts, with 100 kg. The following results were obtained: sodium yield 84-85%, specific consumption of reducing agent, 0.9-1.0, and charge consumption 6.0-6.6 kg per kg of sodium.

The purpose of the semiworks experiments was to obtain data for industrial adoption of the vacuum-thermal process of potassium production. The trials were conducted in the experimental electrothermal unit of the Dnepropetrovsk aluminum works. The reaction equipment was based on experimental electrical vacuum retorts which had been formerly tried in the production of magnesium by reduction with ferrosilicon.

The principal problem of equipment design was the design of the condensation unit which should ensure complete separation of the salt and metal condensate without clogging of the reaction space. In the case of the vertical vacuum retort the problem of condensation of the reaction products was solved as follows: the stream of salt and metal vapors was directed downward, a salt condenser with a series of screens being installed in the lower part of the retort, in the 800-400° zone, and below this, a condenser for the metal, cooled to 60-100°.

In comparative trials,the reaction mixture was charged either in containers or directly into the retort. Direct charging of the mixture into the retort proved effective with regard to heat-transfer conditions and consequently to the rate of the process, energy consumption, and utilization of the retort space.

The briquets were charged into the heated furnace. During the first stage of the process, when the charge was heated up to 780°, a higher residual pressure was artificially maintained. The pressure was then reduced sharply and the temperature was gradually raised to 950°; under these conditions the evaporation of the salt was at a minimum. The metal, salt condensate, and charge residues were discharged from the hot retort, without cooling, at the end of the process.

The optimum duration of the process was 8 hours, charging and discharging took 2 hours, and the whole cycle took 10 hours. Six series of experiments were carried out in the vertical vacuum retort.

In the first series of experiments the briquets were enclosed in a container, and in the second and third they were charged directly into the retort. The potassium yields were 25-35%. The yield could not be increased by doubling of the ferrosilicon-potassium chloride ratio in the charge, or by increase of the process time from 14 to 24 hours, or by grinding the charge down to 200 mesh.

The charge used in the fourth series of experiments was of the normal particle size, but with additions of 4.7 and 9.1% of calcium fluoride. This produced a favorable result. The potassium yield and all the other characteristics were improved sharply even on addition of 4.7% calcium fluoride.

In the fifth and sixth series of experiments a different reducing agent, silicon-aluminum alloy, was used. The potassium yields were: without calcium fluoride, 40-44%; with calcium fluoride, about 60%.

The principal average results for the optimum processes are given in the table (the reduction time was 8 hours).

The main impurity in the metal was sodium, about 3%. Chlorine or calcium were not detected.

The results of these trials were used for comparing the economic characteristics of the existing methods of production of sodium and potassium by the vacuum-thermal process. It was found that the method is very promising for production of metallic potassium. Plans have been put into operation for construction of an industrial plant for production of metallic potassium by the vacuum-thermal process. An industrial furnace with an output of 500 kg of metallic potassium per cycle is under construction.

Charge composition (%)					Furnace charge (kg)	Metal obtained (kg)	Yield of metal (%)	Consumption per kg of metal		
KCl	lime	CaF_2	FeSi	SiAl				charge (kg)	reducing agent (kg)	electric power (kw-hr)
42.0	32.3	4.7	21.0	—	240	32.0	62.0	7.5	1.5	15.8
49.5	31.5	4.7	—	14.3	243	37.1	59.0	6.55	0.94	13.75

The production of metallic sodium by the vacuum-thermal process is rational provided that chlorine production is not tied up with it. Since sodium can be produced at lower temperatures than potassium, natural gas or powdered fuel can be used rather than electricity for heating the furnace.

Received April 29, 1958

INFLUENCE OF AMMONIUM FLUORIDE ON THE PHYSICO-CHEMICAL PROPERTIES OF IRON ELECTROLYTE

N. A. Solov'ev

Despite the considerable interest in iron plating as a possible economic method for restoration of machine parts which have changed dimensions as the result of wear, up to the present time this process has been studied less than other electroplating methods and its applications are therefore limited.

The first attempts to apply electroplating to restoration of tractor parts in the USSR were made in 1940-1941 [1], but because of the defects which became apparent in the process, iron plating was not widely adopted. The following defects were found: peeling of the deposited layer at various stages of treatment and during use, instability of the electrolyte composition, and low hardness of the deposited layer.

Electrodeposited iron also has some positive qualities: a) the deposits can be applied in thin layers, b) its thermal conductivity is twice that of ordinary steel, c) the corrosion resistance is considerably higher than that of steel, d) the deposited layer is suitable for surface oxide finishing and application of various electrocoatings.

At the present time, chloride and sulfate electrolytes are used for iron plating, and in the United States, fluoborates are used [2-5]. The main operating conditions are: for chloride and sulfate electrolytes, pH 1.8-3.5, operating temperature 80-105°, current density 5-25 amp/dm^2; for fluoborate electrolytes, pH 3.0-3.7, temperature 60-80°, current density 2-9 amp/dm^2.

The published data on the wear resistance and hardness of iron deposits are contradictory. Kazartsev reported that the wear of electrodeposited iron is almost twice as great as of 45 grade steel and 12-15 times as great as of electrodeposited chromium, and therefore he did not recommend iron plating for restoration of machine parts [6]. The opposite view is held by Kudryavtsev and Yakovleva [7], who reported that the wear of specimens iron-plated by their method is considerably less than that of chromium-plated parts. With regard to the hardness of iron coatings deposited from the usual sulfate and chloride electrolytes, we may agree with the data published by Tope [8], who stated that the microhardness varies from 140 to 370 kg/mm^2.

The electrolytes used at present are very unstable to the action of atmospheric oxygen. The electrolyte pH alters continuously, whether it is being used for iron plating or not. Ferrous iron is oxidized to ferric, undergoes hydrolysis, and is precipitated.

Research workers are now directing their efforts toward developing electrolytes of stable composition which give deposits of increased hardness.

The adherence of the coating to the basic metal is greatly influenced by surface preparation of the parts to be plated. The parts are subjected to machining and further preparatory processes including chemical or electrochemical etching.

The methods being used at the present time for preparation of parts for iron plating are laborious. In one detailed paper on iron plating [9], 15 laborious operations of surface preparation are described.

The purpose of this investigation was to find an electrolyte which would yield fairly hard and strong iron deposits and would remain relatively stable.

TABLE 1

Effect of Ammonium Fluoride Content on Electrolyte Stability

Electrolyte components	Contents (g/liter)	pH of electrolyte		
		freshly prepared	after 168 hours	after 480 hours
$FeCl_2 \cdot H_2O$	200	2.4	No data	
NaCl	200		Electrolyte oxidized	
$FeCl_2 \cdot H_2O$	200	5.75	6.1	4.55
NaCl	200			
NH_4F	8			

EXPERIMENTAL

In studies of the known chloride and sulfate electrolytes, we reached the conclusion that it is difficult to obtain hard deposits, with good adherence to the surface, from such electrolytes. This is not only because the electrolytes are unstable in operation, but also because the deposition takes place in strongly corrosive media. The corrosiveness of the electrolytes is due to their high acidity and the high operating temperatures in presence of active chloride ions. Such electrolytes actively attack steel and iron surfaces, especially at the instant of immersion.

It has been noted by other workers and confirmed by our experimental investigation on iron plating that the lower the electrolyte pH the narrower the operating conditions which can be used, and the more difficult it is to obtain good quality coatings under mass-production conditions.

On the basis of experimental data obtained previously, we investigated the possibility of obtaining iron deposits at relatively high pH values.

The specimens used for the iron-plating experiments were made from KP-10 steel band 0.25 mm thick. The specimens were weighed on the AD-200 balance before and after iron plating for determination of the deposit thickness. The microhardness of the specimens was determined by means of the PMT-3 microhardness tester.

Chloride electrolytes made in distilled water with various additives were used for the experiments. The $FeCl_2 \cdot 4H_2O$ concentration was 200 g/liter, as it was intended to obtain the hardest possible deposits.

The electrolyte pH was determined by means of the P-5 pH-meter with an antimony electrode. Every day the electrode surface was polished with fine emery paper and powdered antimony before the determinations. The cleaned electrode was kept for 1 hour in distilled water. The anodes were strips of KP-08 steel 1 mm thick.

Glass beakers were used for the iron plating at the first stages of the investigation, and enameled vessels lined with a double coating of black No. 177 stove lacquer in subsequent experiments. Uncoated enamel was attacked by fluorides, and visible cracks formed in iron deposits obtained in enameled unlined vessels.

Before the iron plating, the specimens were degreased and subjected to anodic etching in 25-30% sulfuric acid under the following conditions: 1) exposure for 3-5 minutes at 4-5 amp/dm^2 current density; 2) exposure for 2-3 minutes at 20-25 amp/dm^2. The washed specimens were immersed in the electrolyte at a low current.

Of the numerous additives tested, ammonium and sodium fluorides gave the best results. Because of the greater solubility of ammonium fluoride, it was preferred to sodium fluoride in the subsequent experiments.

When ammonium fluoride is added to the iron electrolyte, its pH increases by 2-3 units. Particularly good results with regard to pH increase were obtained when ammonium fluoride was added together with certain other components, such as NaCl, Na_2SO_4, etc.

In presence of ammonium fluoride, the electrolyte pH remains unchanged for a long time in open glass beakers (Table 1). In electrolytes protected from access of air, the pH remains almost without change for months. A brownish film is gradually formed on the electrolyte surface, and this is one of the factors retarding interaction

TABLE 2

Effects of Ammonium Fluoride Concentration on Electrolyte pH and Stability*

Electrolyte comp. (g/liter)			pH of electrolyte				
$FeCl_2 \cdot 4H_2O$	NaCl	NH_4F	freshly prepared	after 48 hours	after 96 hours	after 114 hours	after 192 hours
200	Nil	Nil	2.85	No data (electrolyte oxidized)			
200	Nil	4	4.4	3.65	3.35	3.25	—
200	Nil	7	5.0	4.05	3.65	3.5	—
200	200	4	6.0	6.0	6.0	6.05	5.8
200	200	7	6.6	6.6	6.6	6.6	6.4

*The electrolytes were prepared in glass 0.1 liter beakers from $FeCl_2 \cdot 4H_2O$ (GOST 4149-48) and NaCl (GOST 4233-48). For preparation of the electrolyte the solution was heated to 80° and when the salts dissolved it was cooled to 18°. Between the pH determinations the beakers were kept in a closed cupboard.

of atmospheric oxygen with the electrolyte. If sufficient NH_4F is present, the electrolyte is quite clear both at room temperature and at 90°.

On addition of ammonium fluoride to the electrolyte the pH gradually increases with the NH_4F content, as Table 2 shows. At sufficiently high contents of NH_4F, the electrolyte pH increased with time, even if the electrolyte was kept in glass beakers.

Electrolytes of the following composition (in g/liter) were used for iron plating: $FeCl_2 \cdot 4H_2O$ – 200, NaCl – 200 (GOST 153-41), NH_4F – 5-8. $FeCl_2 \cdot 4H_2O$ was prepared from KP-10 steel shavings and technical HCl. The electrolyte pH was taken to 5.8-6.0 by addition of ammonium fluoride. A wide range of temperatures and current densities was used at pH 5.8-6.0. At electrolyte temperatures from 20 to 60° and current densities from 5 to 20 amp/dm^2 the microhardness of the deposits varied from 200 to 900 kg/mm^2. The most elastic and strongest iron deposits were formed at electrolyte temperatures of 55-60°, and the hardest deposits were obtained at 20°.

In addition to current density and temperature, the electrolyte pH has a strong influence on the quality and hardness of the deposits. At pH 5.8-6.0, electrolyte temperature 60°, and current density 9 amp/dm^2 the average microhardness of the layer was 417 kg/mm^2, and at 15 amp/dm^2 the microhardness rose to 635 kg/mm^2. At pH 4.8, electrolyte temperature 60°, and current density 15 amp/dm^2 the microhardness of the layer fell to 385 kg/mm^2, and at electrolyte temperature 95° and current density 40 amp/dm^2 it fell to 300 kg/mm^2. The average thickness of the iron layer on all the specimens was 0.2 mm. None of the deposits peeled off when the specimens were flexed 18 times through an angle of 180°. A greater number of flexings was not used, as the basis metal cracked even after 18 bends. Patches were formed on the deposits at electrolyte pH above 6.0, and there was pitting at pH below 5.6; therefore we consider that the best electrolyte pH is 5.8-6.0.

SUMMARY

1. An electrolyte composition has been formulated which can be used for electrodeposition of iron layers with microhardness from 200 to 900 kg/mm^2.

2. The presence of NH_4F in the electrolyte confers a high pH value and stabilizes the electrolyte against atmospheric oxidation. The probable explanation of the stability of the electrolyte against oxidation and of the stability of its pH is that the solubility of oxygen in this electrolyte is low owing to the high total salt concentration. The high salt concentration favors displacement of oxygen from the electrolyte, while the brownish film which forms on its surface in presence of fluorides retards access of atmospheric oxygen to it.

3. The observations of other investigators have been confirmed: the higher the electrolyte pH, the wider the range of permissible operating conditions. With the high operating pH range of 5.8-6.0 attained in our experiments the current density could be varied from 5 to 20 amp/dm^2, and the electrolyte temperature from 20 to 60°.

4. Black No. 177 lacquer is suitable for lining of cells used for iron electrolytes containing fluoride and chloride ions.

5. As the result of the increased hardness of the iron deposits obtained, in comparison with those known previously, it is possible to extend the applicability of iron plating both in repair work and in the production of new parts without the need for heat treatments, for replacement of hard nickel and hard chromium coatings by iron, etc.

LITERATURE CITED

[1] M. P. Melkov, Restoration of Automobile Parts by Electrolytic Steel Plating [in Russian] (Ministry of Communal Economy Press, Moscow, 1954).

[2] N. T. Kudryavtsev, Electroplating Technology [in Russian] (State Light Industry Press, 1940).

[3] V. I. Lainer and N. T. Kudryavtsev, Fundamentals of Electroplating 2 [in Russian] (Metallurgy Press, 1957).

[4] J. Beach, Plating 43, 5, 616-617 (1956).

[5] V. P. Revyakin and P. D. Myasnikov, Bull. Machine Construction 4, 64-65 (1957).

[6] V. I. Kazartsev, Bull. Machine Construction 1, 63-65 (1956).

[7] N. T. Kudryavtsev and L. A. Yakovleva, Trans. GOSNIIGVF* 14, 26-34 (Moscow, 1957).

[8] N. A. Tope, The Inspection Engineer 21, 4, 74-79 (1957).

[9] V. M. Yanson, É. A. Tseske and S. Ya. Timshans, Trans. Latvian Agric. Acad. 5, 97-106 (1956).

Received February 10, 1958

*State Scientific Research Institute of the Civil Air Fleet.

BRIEF COMMUNICATIONS

THERMAL DECOMPOSITION OF MAGNESIUM SULFATE IN A CURRENT OF STEAM IN PRESENCE OF MANGANESE OXIDE

A. B. Suchkov, B. A. Borok, and Z. I. Morozova

Thermal decomposition of magnesium sulfate for production of sulfuric acid may be of definite importance if the reaction temperature could be lowered. We investigated this reaction in a current of steam with the addition of various oxides.

EXPERIMENTAL

The apparatus used for the principal experiments is depicted in Fig. 1.

The apparatus was made of quartz. It consists of a microburet A with two stopcocks 1 and 2, a reaction tube B with a socket for a thermocouple and a porous sintered-quartz partition 3, a condenser C with a stopcock 4 and receiver 5, a U-tube D, and bubblers E packed with Raschig rings. The tube B is contained in a thermoregulated furnace. A steam superheater F is attached to its lower portion.

TABLE 1

Results of Certain Experiments on Decomposition of $MgSO_4$ in Presence of $MnO.H_2O$; rate 0.1 ml/minute

Material	Component ratio (molar)	Temperature (°C)	H_2SO_4 yield (η in molar %) in reaction time (min)					
			10	20	30	40	50	60
$MgSO_4 + MnO$	1 : 1	500	—	—	—	—	—	0.083
		600	0.25	0.60	0.88	1.20	1.48	1.70
		700	1.17	2.57	3.86	5.08	6.30	7.23
		800	7.6	13.7	19.0	23.6	27.8	32.2
		900	2.8	10.6	20.7	31.6	42.3	56.6
$MgSO_4 + MnO$	1 : 0.5	600	0.25	0.60	0.88	1.20	1.48	1.70
$MgSO_4 + MnO$	1 : 0.2	600	0.16	0.31	0.46	0.59	0.70	0.80

The experimental procedure was as follows. The material for investigation was placed in the tube B, the U-tube D was filled with dry sodium chloride, the bubbler E contained 3% hydrogen peroxide, and the microburet A was filled with water. The sodium chloride was used for absorption of SO_3, and hydrogen peroxide for absorption of SO_2 [1].

The assembled apparatus was tested for air tightness. When the required temperature had been reached, water was fed into the tube B. Samples of the acid formed were taken at definite intervals from the receiver 5. After removal of SO_2 these samples were analyzed; the NaCl and H_2O_2 were also analyzed for their H_2SO_4 content. The solid residue from the reaction was analyzed by chemical, electron-diffraction, and petrographic methods.

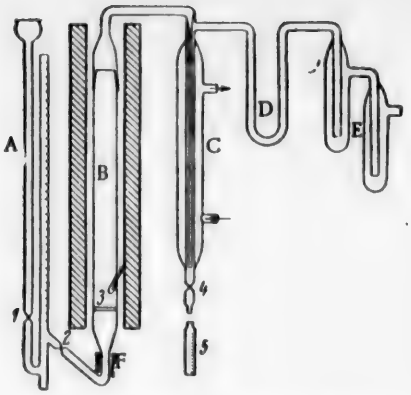

Fig. 1. Apparatus for thermal decomposition of magnesium sulfate.

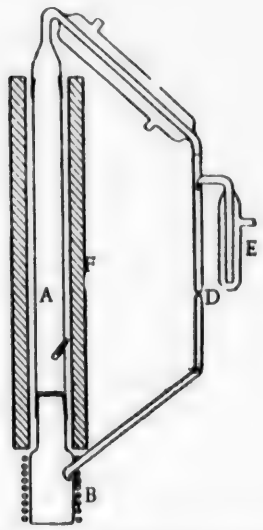

Fig. 2. Apparatus for production of concentrated sulfuric acid by the circulation method.

The following conditions were varied in the experiments: composition of the reaction mixture (sulfate – oxide), water feed rate, temperature, granulometric composition, and methods used for preparation of the starting substances. The magnesium sulfate and MnO were of chemically pure grade. In preliminary experiments they were shown to contain no free sulfuric acid or other sulfates. It was also confirmed that the water of crystallization formed by dehydration of magnesium sulfate does not contain H_2SO_4.

In a number of cases, experiments were performed on the production of concentrated sulfuric acid by the circulation method in the apparatus shown in Fig. 2.

This apparatus consists of a reaction tube A 800 ml in capacity, a receiver B, a condenser C, a siphon valve D, and a bubbler E containing hydrogen peroxide. The tube A is contained in a thermoregulated furnace F, and the receiver B is also enclosed in a small furnace.

Before the start of an experiment, the tube A was filled with the material for investigation, and the receiver B with water. When the required temperature had been reached in tube A the heater of the receiver B was switched on and the temperature in it was maintained at 190° during the experiment. At this temperature only water is evaporated from $H_2SO_4 - H_2O$ mixtures [2]. The steam passing through the material took sulfur oxides with it. Sulfuric acid, with an admixture of sulfurous, was condensed in the condenser C. A part of the SO_2 which did not dissolve in H_2O entered the bubbler E. The H_2SO_4 formed flowed down into the receiver B, where water was evaporated. Finally concentrated H_2SO_4 remained in the receiver and solid reaction products in tube A.

DISCUSSION OF RESULTS

It was found in preliminary experiments that during decomposition of $MgSO_4$ and of $MgSO_4$ with additions of CuO, Fe_2O_3, Cr_2O_3, MnO_2, Mn_2O_3 sulfur oxides appear in the vapor-gas phase at 800°. If MnO is added, this temperature falls to 500°.

Table 1 gives an idea of the results of experiments on the decomposition of $MgSO_4$ in presence of MnO. This table contains data on H_2SO_4 yields at various temperatures and $MgSO_4$: MnO ratios. The acid yield is expressed in molar percentages:

$$\eta = \frac{\text{number of moles of } H_2SO_4 \cdot 100}{\text{number of moles of } H_2SO_4 \text{ in original sulfate}}$$

Similar weights of $MgSO_4$ were used in the experiments. The heights of the columns of material were kept equal as far as possible from experiment to experiment. The particle size was kept constant within a fairly narrow range (0.08-0.1 mm).

Comparison of these results with the data of other authors on the thermal decomposition of $MgSO_4$ [3-6] shows that the process is accelerated and can be carried out at lower temperatures by the use of steam in presence of MnO.

To establish the course of $MgSO_4$ decomposition in presence of MnO and H_2O it is necessary to consider the following possible reactions:

$$MgSO_4 + H_2O \rightleftarrows Mg(OH)_2 + SO_3, \quad (I)$$

$$MgSO_4 + H_2O \rightleftarrows MgO + H_2SO_4, \quad (II)$$

$$MgSO_4 + MnO \rightleftarrows MgO + MnSO_4, \quad (III)$$

$$MgSO_4 + 3MnO \rightleftarrows Mn_3O_4 + MgSO_3, \quad (IV)$$

$$nMgSO_4 + mMnO \rightleftarrows (n-x)MgSO_4 + xMgO \cdot yMnO + (m-y)MnO + xSO_3 \quad (V)$$

and to compare them with the reaction

$$MgSO_4 \rightleftarrows MgO + SO_3. \quad (VI)$$

Calculations show that the changes of the thermodynamic potentials of reactions I-VI (with the exception of reaction V, Table 2) are:

TABLE 2

Changes of Thermodynamic Potential for Reactions I-VI

Temperature (°K)	Values of Δ°_{ZT} for reactions				
	I	II	III	IV	VI
800	41200	35800	1400	94100	30800
900	39700	34900	1500	91200	26400
1000	38500	34600	1600	88300	22400
1100	36200	33300	1700	83900	17600
1200	34500	32800	1800	80800	13600

TABLE 3

Yields of H_2SO_4 After Different Reaction Times

Material	Yield of H_2SO_4 (molar %) after reaction time (min)					
	10	20	30	40	50	60
$MnSO_4$	1.05	1.56	1.68	1.77	1.86	1.95
$MnSO_4 + MgO$ (1 : 1)	9.1	15.6	21.2	24.9	26.4	27.2

The data in Table 2 indicate that reaction III undoubtedly predominates in our case.

Analysis by petrographic and electron-diffraction methods showed that the solid reaction products consist of the following phases: MgO, $Mg(OH)_2$, MnO, MnO(OH) and $MgSO_4$. All the phases are distributed in the form of individual grains; the presence of these phases indicates that binary compounds of magnesium and manganese oxides cannot be formed.

Determinations of the amounts of H_2O introduced into the reaction and formed in the reaction indicates that water does not interact chemically during the reaction with manganese and magnesium sulfates and oxides. Hydroxyl groups are formed while the reaction mass cools over the water remaining in the receiver; when the reaction mass rapidly removed from the system is cooled, analysis reveals only MgO, MnO, $MgSO_4$ and higher manganese oxides formed in secondary reactions.

The ratio of SO_2 to SO_3 liberated in the process conforms to the equilibrium constant for the reaction

$$SO_3 \rightleftarrows SO_2 + \frac{1}{2} O_2.$$

Hence it is clear that the oxidation – reduction reaction IV does not occur.

In a stream of argon, SO_3 and SO_2 are found in the vapor-gas phase at 900°; liberation of sulfur oxides from the system $MgSO_4$ + MnO is weaker than in a current of H_2O.

All the experimental and calculated data indicate that mutual loosening of bonds in the system $MgSO_4$ + + MnO + $MnSO_4$ + MgO takes place. In this case water not only favors weakening of the bonds but also binds the sulfur oxides and loosens the oxide films. It must be pointed out that the reverse reaction

$$MnSO_4 + MgO \rightarrow MgSO_4 + MnO$$

also proceeds with liberation of SO_3 and SO_2 much more intensively than the thermal decomposition of $MnSO_4$. This is illustrated by data on decomposition at 800° (Table 3).

It is clear from Table 1 that decrease of the relative amount of MnO in the range of molar ratios of $MgSO_4$: MnO between 1 : 1 and 1 : 0.5 does not affect the efficiency of the process; when the $MgSO_4$: MnO ratios is 1 : 0.2 the reaction rate slows down appreciably.

It must be noted that in the circulation unit, $MgSO_4$ is decomposed completely within 2 hours at 700°. Concentrated H_2SO_4 accumulates in the receiver in 70% yield. The reaction products, MgO and MnO, can be completely separated by fractional elutriation; MnO can be used again in the process.

SUMMARY

1. Apparatus is described for high-temperature decomposition of sulfates in steam, with collection and concentration of sulfuric acid.

2. It is shown that the oxides of magnesium and manganese sharply lower the decomposition temperatures of manganese and magnesium sulfates respectively.

3. As the reaction products (MgO and MnO) can be separated, the proposed method can be used for the production of concentrated H_2SO_4.

LITERATURE CITED

[1] F. N. Kel'man, Industrial Lab. 18, 1316 (1952).

[2] K. M. Malin, N. L. Arkin, G. K. Boreskov and M. G. Slin'ko, Sulfuric Acid Technology [in Russian] (Goskhimizdat, 1950).

[3] G. Marchal, J. Chim. Phys. 22, 325 (1925).

[4] L. A. Bhatt and H. E. Watson, J. Indian Inst. Sci. A 10, 128 (1928).

[5] S. D. Shargorodskii, Ukrain. Chem. J. 16, 310 (1950).

[6] R. M. Gruber, J. Am. Ceram. Soc. 34, 353 (1951).

Resubmitted October 4, 1958

THE pH VALUES OF AMMONIUM SULFITE-BISULFITE SOLUTIONS

B. A. Chertkov, D. L. Puklina, and T. I. Pekareva

Ammonium sulfite – bisulfite solutions are used for collection and concentration of sulfur dioxide, and also in the production of caprolactam, paper, and other chemical products.

The principal characteristics of these solutions are the total salt concentration and the bisulfite – sulfite ratio. In particular, the cyclic ammonia process for extraction of SO_2 from flue gases and other industrial gases is based on variation of this ratio.

The ratio of ammonium bisulfite to sulfite in solution is usually represented as the S/C ratio [1].

In the limiting cases, when the solution contains sulfite only, and 1 mole of SO_2 is combined with 2 moles of NH_3, the S/C ratio if 0.5; if the solution contains bisulfite only, and 1 mole of SO_2 is combined with 1 mole of NH_3, the S/C ratio is 1.

The composition of any mixture of these salts in solution can be expressed in terms of the S/C ratio from 0.5 to 1.

It is easy to show that in this notation the molar content of bisulfite in solution is $2S - C$, and the molar content of sulfite is $C - S$. Hence the percentage of bisulfite in solution must be

$$\frac{(2S - C)\,100}{S} \quad \text{or} \quad \left(2 - \frac{1}{S/C}\right) 100.$$

In some industries the composition of such solutions is expressed in terms of molar or weight ratios of sulfite to bisulfite. These ratios are

$$\frac{116\,(C - S)}{99\,(2S - C)} \quad \text{or} \quad \frac{1.171\,(1 - S/C)}{2S/C - 1}.$$

Determination of the S/C ratio is the principal step of production control, and forms the basis for regulation of absorption of SO_2, regeneration of the liquor, and addition of fresh ammonia to balance losses. The S/C ratio is also important in relation to oxidation of sulfite – bisulfite solutions and decomposition of the spent liquor into ammonium sulfate and elemental sulfur. Its value is generally found from analytical data for the individual liquor components, determined by the accelerated method developed in the Scientific Research Institute for Gas Purification (by S. M. Golyand, A. E. Strakhova, T. K. Krapivina, et al.).

It is quite natural to seek a simpler control method for the production process, for example, one based on determinations of solution pH, which can be performed automatically by means of an instrument. The problem is therefore to determine the variation of pH with the S/C ratio at different solution concentrations and in presence of impurities in the solution. Some data on the pH of ammonium sulfite – bisulfite solutions are to be found in Johnstone's paper [2]. He found a linear relationship between pH and the S/C ratio, conforming to the following empirical equations:

$$\text{pH} = -4.62\ \text{S/C} + 9.2$$

or

$$\text{S/C} = 2 - 0.22\ \text{pH}.$$

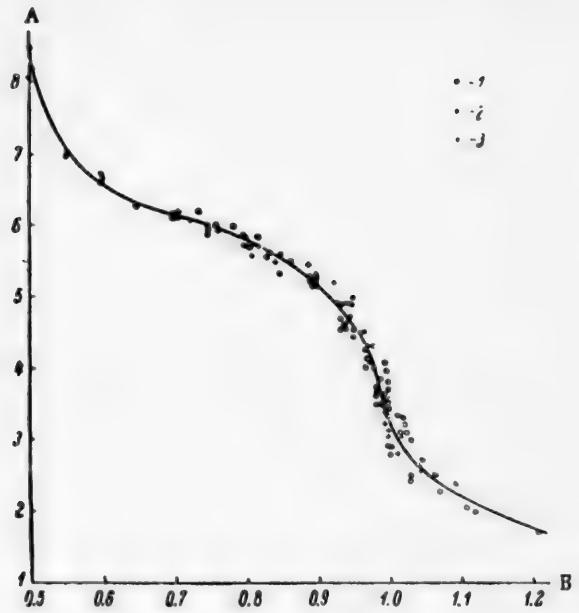

Fig. 1. Relationship between S/C ratio and pH of artificially prepared ammonium sulfite – bisulfite solutions: A) pH, B) S/C ratio.

solution	NH_3 eff	NH_3 tot	$(NH_4)_2SO_4$	$(NH_4)_2S_2O_3$
(moles/liter)				
1	2.5—6	2.7—6.5	0.1—0.2	0
2	5—9	5.7—10	0.2—2.6	0
3	3—4.5	3.3—5.2	0.1—0.4	0

It should be noted that Johnstone determined pH over a relatively narrow S/C range, from 0.7 to 0.9, and that this equation cannot be extrapolated to either the more acid or the more alkaline regions.

The pH values of ammonium sulfite – bisulfite solutions used in equipment for extraction of SO_2 from the flue gases were determined earlier by us jointly with T. K. Krapivina. These determinations were performed over a wider range of S/C ratios than those of Johnstone – from 0.5 to 0.95. It was confirmed that over the S/C range from 0.7 to 0.9 the relationship between pH and S/C is linear and is represented by the following equation:

$$S/C = 2.22 - 0.25\ pH.$$

However, the existence of a linear relationship between pH and S/C over a single narrow range does not reflect the true general variation of pH with S/C, which in reality proved considerably more complex (Fig. 1 and 2).

In addition, it was found that pH changes very little with changes of the total solution concentration and that the presence of ammonium sulfate thiosulfate in the quantities found in practice likewise has no influence on pH.

The pH values of ammonium sulfate, sulfite, and bisulfite solutions (each individually) were also determined by Kuz'minykh, Yakhontova, and Vorob'eva [3]. They found that the pH of pure ammonium sulfite is 8.0 and is independent of the solution concentration; the pH of pure bisulfite solution also depends little on the concentration, and varies from 3.0 for 5% solution to 2.7 for 45% solution.

In our investigations of the oxidation rates of ammonium sulfite – bisulfite solutions and of their decomposition into ammonium sulfate and elemental sulfur numerous determinations of the pH of solutions of various concentrations and compositions were performed*. In some of the samples the S/C ratio often reached 1 and sometimes exceeded this value (when free sulfurous acid was present in addition to bisulfite) owing to the operating conditions; accordingly, the range of pH determinations was considerably wider than in the preceding investigations (Fig. 1 and 2).

It is clear from Fig. 1 and 2 that all the experimental points fit reasonably accurately around a curve of a shape characteristic for such determinations – with sharp breaks at critical points corresponding to the appearance of new compounds in the solution, in this instance at S/C = 0.5 and S/C = 1.

It should also be noted that the curve in Fig. 1, which refers to artificially prepared solutions, hardly differs from the curve in Fig. 2 for production liquors. Thus, the presence of fairly large amounts of ammonium sulfate and thiosulfate and small amounts of inhibitor and light ash in the production liquor has virtually no effect on its pH, because of its high buffer effect. The total ammonium sulfite – bisulfite concentration likewise has little practical effect on the solution pH.

*The MOSKIP apparatus with the LP-5 electronic potentiometer was used; all the determinations were performed at 20-22°.

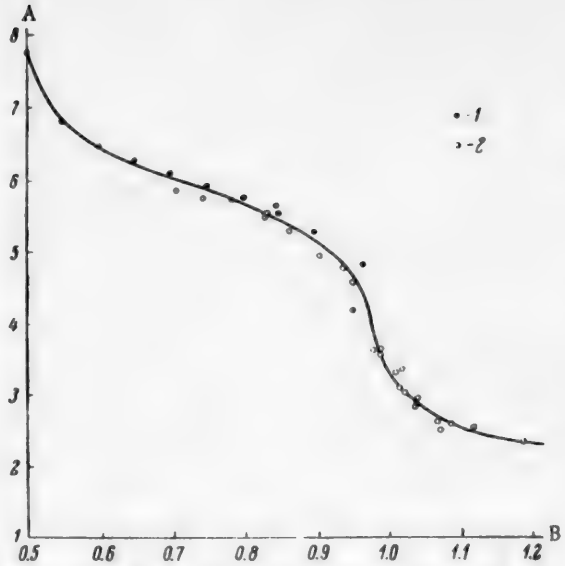

Fig. 2. Relationship between S/C ratio and pH of production ammonium sulfite – bisulfite liquors: A) pH, B) S/C ratio.

solution (moles/liter)	NH_3 eff	NH_3 tot	$(NH_4)_2SO_4$	$(NH_4)_2S_2O_3$
1	2.3	7.0	2.25	0.07
2	1.1—4	7—7.9	1.7—2.9	0.05—0.21

The second-stage dissociation constant of sulfurous acid and the dissociation constant of ammonia differ relatively little (at 25° they are $5 \cdot 10^{-6}$ and $1.8 \cdot 10^{-5}$ respectively). Therefore it can be assumed for practical calculations without serious error that at a given S/C ratio the pH is independent of the total salt concentration.

This fact is very convenient in relation to the use of pH determinations as a means of production control, regulation of SO_2 absorption, and regulation of the liberation of SO_2 from the liquors on heating.

For this purpose the S/C ratio corresponding to the determined pH value must be found from the curve of Fig. 2 for the production liquor or from data compiled from this curve, and the operating conditions are then regulated accordingly.

The data for the curve in Fig. 2 (production liquor) are presented below.

It should be noted that our value for the pH corresponding to pure bisulfite does not agree with literature data. According to our results, the pH at S/C = 1 is approximately 3.5.

pH	7.8	7.6	7.4	7.2	7.0	6.8	6.6	6.4	6.2	6.0	5.8	5.6
S/C	0.5	0.51	0.52	0.53	0.54	0.56	0.58	0.62	0.65	0.71	0.75	0.8
pH	5.4	5.2	5.0	4.8	4.6	4.4	4.2	4.0	3.8	3.6		
S/C	0.85	0.89	0.92	0.94	0.955	0.965	0.97	0.98	0.985	1.0		
pH	3.4	3.2	3.0	2.8	2.6	2.4	2.2					
S/C	1.005	1.02	1.04	1.06	1.08	1.12	1.20					

It is also often stated in the literature that the pH of pure ammonium bisulfite is 4.6-4.7. However, Johnstone gives pH = 4.1 for pure ammonium bisulfite [2], while Kuz'minykh et al. [3] found pH values from 2.7 to 3.0. We consider that these discrepancies depend on the method used for determination of the solution composition at the point corresponding to pure bisulfite rather than on the method of pH determination. The slightest inaccuracy in the former determination, as is clear from Fig. 1, results in a large pH difference, as the curve has a sharp break in this region.

In future this determination must be performed with particular care, with precautions against oxidation of the solution, desorption of SO_2, and other factors which might cause changes in the composition of the solution during the actual determination.

LITERATURE CITED

[1] B. A. Chertkov, J. Appl. Chem. 30, No. 10, 1496 (1957).*

[2] H. F. Johnstone, Ind. Eng. Ch. 27, 5, 587 (1935).

[3] I. N. Kuz'minykh, E. L. Yakhontova and V. T. Vorob'eva, Trans. Mendeleev Inst. Chem. Tech., Moscow, 22, 203 (1956).

Received November 21, 1957

*Original Russian pagination. See C. B. Translation.

PICKLING OF FERROUS METALS WITH ADDITIONS OF GLUTAM

R. G. Genes and Yu. B. Lukov

The organic additive glutam B was studied. Vinasse, after removal of calcium salts, is evaporated to sp. gr. 1.2-1.4 with addition of yeast; the product is glutam B, which is a sirupy liquid readily soluble in water and aqueous acids (H_2SO_4, HCl).

EXPERIMENTAL

The protective action of glutam was determined in studies of its influence on the weight loss of metal during pickling of polished specimens, and on the rate of scale removal. The tests were performed at 50, 65, and 80° in 10 and 20% H_2SO_4 solutions without glutam and with additions of glutam in the proportions of 10, 20, and 30 ml per liter of solution.

The specimens (49×49×1×1.5* mm) were made from hot-rolled steel of the following chemical composition (in %): C 0.56, Si 0.02, Mn 0.50, P 0.021, S 0.025. The polished specimens were washed in ligroine, dried in a current of air, degreased by means of magnesium oxide, washed in water, and subjected to chemical or cathodic (at 2 amp/dm²) pickling for half an hour; they were then again washed in water and dried in a current of air. Specimens coated with scale were degreased anodically (at 5-6 amp/dm²) in 10% NaOH solution at 80-90°, and were then subjected to the same treatment as the polished specimens. All the specimens were weighed on an analytical balance before and after the pickling. Average results for 10 specimens were taken.

The influence of glutam on pickling and descaling is shown in Table 1.

TABLE 1

Metal Losses (in g) for Single Specimens During Chemical and Cathodic Pickling with and without Glutam for 30 Minutes

Temperature (°C)	Metal losses (in g) in 20% H_2SO_4		Loss ratio	Metal losses (in g) in 10% H_2SO_4		Loss ratio
	without glutam	with 10 ml of glutam		without glutam	with 10 ml of glutam	
Chemical pickling						
50	0.72	0.11	~ 7	0.19	0.0370	~ 5
65	1.65	0.21	~ 8	1.32	0.0900	~ 15
80	2.60	0.70	~ 4	1.54	0.1900	~ 8
Cathodic pickling						
50	0.0390	0.0060	~ 7	0.0130	0.0031	~ 4
65	0.5300	0.0071	~ 75	0.0500	0.0038	~ 13
80	0.6100	0.0074	~ 90	0.4000	0.0100	40

Note: In all the experiments definite amounts of glutam were added per liter of 10 and 20% H_2SO_4.

*As in original – Publisher's note.

TABLE 2

Effect of Glutam on Descaling Time in Cathodic and Chemical Pickling

Temperature (°C)	Pickling time (min)							
	in 20% H_2SO_4				in 10% H_2SO_4			
	without glutam		with 10 ml of glutam		without glutam		with 10 ml of glutam	
	cathodic	chemical	cathodic	chemical	cathodic	chemical	cathodic	chemical
50	8	15	11	15	20	25	9	11
65	7	10	5	7	5	7	7	7
80	6	9	4	5	8	4	7	5

TABLE 3

Effect of Glutam Concentration on Metal Losses During Cathodic and Chemical Pickling in 20 and 10% H_2SO_4 Solutions for 30 Minutes

Temperature (°C)	Loss of metal per single polished specimen (in g) in pickling with glutam concentrations of (ml)							
	0		10		20		30	
	cathodic	chemical	cathodic	chemical	cathodic	chemical	cathodic	chemical
	Pickling in 20% H_2SO_4							
50	0.0390	0.72	0.006	0.11	0.0046	0.06	0.0037	0.05
65	0.53	1.65	0.0071	0.21	0.0057	0.16	0.0042	0.12
80	0.61	2.60	0.0074	0.70	0.0510	0.34	0.0053	0.27
	Pickling in 10% H_2SO_4							
50	0.0300	0.1900	0.0031	0.0370	0.0033	0.0280	0.0050	0.037
65	0.0500	1.3200	0.0038	0.0900	0.0032	0.0670	0.0033	0.070
80	0.4000	1.5400	0.0100	0.1900	0.0600	0.1650	0.0120	0.0160

Effect of Pickling With and Without Glutam on the External Appearance of the Specimens. Polished specimens pickled in 20% or 10% H_2SO_4 without glutam became coated with a large amount of sludge which could not be washed off by water, with a considerable amount of surface attack (especially at the faces) and disappearance of luster. Similar pickling with glutam resulted in slight sludge formation without noticeable surface corrosion, but also with loss of luster.

It is clear from Table 1 that when glutam is used in chemical pickling the metal losses are decreased 5 to 15-fold. Gas liberation is also slight. In cathodic pickling without glutam the polished specimens had slight roughness on the faces; this roughness increased with increase of the solution temperature and cracks appeared on the faces. There was no sludge formation in pickling with glutam. The specimens were free from visible corrosion and retained their polish.

Table 2 shows that glutam does not increase descaling time to any appreciable extent; this time is 5-15 minutes. Descaling by cathodic and chemical pickling with addition of glutam proceeded with slight gas evolution and without sludge formation; the specimens were free from visible corrosion. In chemical descaling without glutam there was considerable sludge formation and the specimens became roughened; this was not observed in cathodic descaling under analogous conditions.

It follows from the data in Table 3 that metal losses in pickling in 20% H_2SO_4 solution decrease considerably with increase of glutam concentration. The protective action of glutam, in absolute values, is more prominent in chemical than in cathodic pickling.

TABLE 4

Consumption of H_2SO_4 in Pickling in 20% H_2SO_4 With and Without Glutam

Surface treated (dm^2)	With 10 ml of glutam			Without glutam		
	average weight loss per specimen (g)	iron dissolved (g)	H_2SO_4 consumption (g)	average weight loss per specimen (g)	iron dissolved (g)	H_2SO_4 consumption (g)
2.5	0.21	—	—	1.65	—	—
50	0.21	—	—	0.83	—	—
100	0.15	48	84	0.12	148	259
200	0.105	84	147	—	—	—

TABLE 5

Descaling Time in Determination of the Duration of Action of the Pickling Solution Containing 20% H_2SO_4

Surface treated (dm^2)	Descaling time (minutes)	
	with 10 ml of glutam	without glutam
2.5	7-8	7-8
50	7-8	24-25
100	11-12	26-27
200	16-17	—

TABLE 6

Thermal Stability of Glutam

Type of pickling	Temperature (°C)	Weight loss per specimen (g)	
		before boiling	after boiling
Chemical	50	0.11	0.10
	65	0.21	0.26
Cathodic	50	0.006	0.004
	65	0.007	0.006

Duration of the Action of Glutam in Pickling Liquors. The duration of the effect of glutam was investigated by the pickling of a large number of specimens in the same solution. Two solutions were tested: 20% H_2SO_4 with glutam (solution 1), and without glutam (solution 2), at 65°. The volume of each solution was 1.2 liter. Five polished specimens were pickled simultaneously for 30 minutes. The total amount of iron dissolved was calculated from the loss in weight. The acid consumption was calculated from the amount of iron dissolved. The descaling time was determined after 2.5, 50, 100 and 200 dm^2 of metal had been treated. A metal area of 200 dm^2 (400 specimens) was treated in the first solution, and 100 dm^2 (200 specimens) in the second. The results are given in Tables 4 and 5.

It follows from Table 4 that 147 g of pure H_2SO_4 was consumed in the pickling of 200 dm^2 of metal in 20% H_2SO_4 with glutam; one liter of 20% H_2SO_4 contains 274.8 g of pure H_2SO_4, so that the concentration of the residual acid was about 10%. The weight loss was almost the same (Table 1) as in freshly prepared 10% H_2SO_4 solution with glutam (0.090 g). It follows that glutam does not lose its protective properties after prolonged pickling, and it is not necessary to add more during the process. After 100 dm^2 of metal had been treated in 20% H_2SO_4 solution without glutam, nearly all the acid had been consumed (15.8 g remained). In a corresponding solution containing glutam, 190.8 g of H_2SO_4 remained after treatment of 100 dm^2, and 127.8 g after treatment of 200 dm^2. It follows that acid consumption is decreased 3 to 4-fold on the average with the use of glutam.

The Thermal Stability of Glutam was determined after a solution containing 10 ml of glutam in 1 liter of 20% H_2SO_4 had been boiled for 1 hour at 103°. Separate portions of the solution were used for chemical and cathodic pickling at 50 and 60° (Table 6).

Table 6 shows that the protective properties of glutam remain virtually unchanged as the result of boiling.

Effect of Glutam Films on Adherence of Metal Coatings to the Basis Metal. Specimens descaled by chemical pickling in 10% H_2SO_4 with glutam were washed in cold running water and plated with nickel or zinc from acid electrolytes. Neither the zinc nor the nickel coatings peeled from the basis metal when rubbed with a file or bent through 180°.

Anodic Pickling. In experiments on anodic pickling of polished specimens in 20% H_2SO_4 containing glutam, the metal losses were considerable (greater than in chemical pickling). A thick layer of sludge was formed, which was not removed by subsequent cathodic treatment in the same solution. Therefore the influence of glutam in anodic pickling was not studied further.

SUMMARY

1. Additions of glutam in the proportion of 10 ml per liter of pickling liquor at 50-80° decreases metal losses 4 to 8-fold in 20% H_2SO_4, and 5 to 15-fold in 10% H_2SO_4; in cathodic pickling the weight losses are reduced 7 to 90-fold in 20% H_2SO_4, and 4 to 40-fold in 10% acid.

2. The descaling time is not increased appreciably by the use of glutam.

3. Glutam is thermally stable and retains its protective properties during the entire service life of the pickling liquor.

4. Acid consumption is decreased 3 to 4-fold by the use of glutam.

5. Zinc and nickel coatings on metal pickled with addition of glutam have good adherence to the basis metal.

6. The effectiveness of glutam is confirmed by experiments on cold pickling in H_2SO_4 and HCl solutions with added glutam.

7. The decrease of gas evolution and the consequent reduction of the amount of acid mist formed on addition of glutam improves the working conditions considerably.

8. The use of glutam as an additive to pickling liquors in drawing, forging, and thread-cutting workshops is economically very advantageous owing to the sharp reduction of H_2SO_4 consumption.

Resubmitted December 31, 1958

EFFECT OF POLARIZATION OF STRESS CORROSION OF BRASS

V. V. Romanov

This paper, like the preceding communications [1, 2] is concerned with a study of the effects of cathodic and anodic polarization on the rate and character of stress corrosion of metals and of the influence of polarization on the electrode potential and elongation of the metal during cracking.

The metal chosen for the investigation was brass of the following composition (in %): Cu – 61.44, Zn – 38.46, Mn – 0.01.

The metal was in the form of semifinished sheet and was not subjected to special heat treatment. The specimens were cut in the direction of rolling in the form of Gagarin specimens, and had the following dimensions (in mm): length 72, width of the working portion 4, thickness 1.5. They were polished successively with emery paper (the last polishing was performed lengthwise with No. 14 paper), degreased, and placed in a desiccator for 15-20 hours.

The prepared specimens were placed horizontally in a rectangular polystyrene vessel containing the corrosion medium. The vessel was covered with a glass lid with an opening for the tip of the electrolyte bridge leading to the reference electrode. The potential was determined by the compensation method relative to a saturated calomel electrode, and then recalculated on the hydrogen scale. Polarization was effected by means of a storage battery. The auxiliary electrode consisted of a platinum coil wound uniformly around the working portion of the specimen.

The electrical circuit was so designed that the current density could be varied as required. Tensile stresses were created by uniaxial extension of the specimens by means of a device with an indicator which gave the elongation; the initial tensile stress was 18 kg/mm^2. The investigation was performed with 27% ammonia solution to which 5 g of H_2O_2, 10 g of K_2CrO_4, and 0.015 g of $CuSO_4$ per liter were added to accelerate cracking [3].

The rate of stress corrosion was estimated from the time to total destruction of the specimens. The microsections for investigation were prepared by the usual method, with subsequent electrochemical etching.

The average results for five parallel determinations are considered.

EXPERIMENTAL RESULTS

The cathodic branch of the polarization curve (Fig. 1) shows that at the initial low current densities (0.025 ma/cm^2) cracking is accelerated at first. On further increase of current density the time to cracking increases steadily and at 0.85 ma/cm^2 the alloy becomes protected*. The scattering of the points was greatest, about 50%, over the region of the curve from the minimum time to cracking to complete protection, whereas for other points on the curve it did not exceed 10%.

The anodic branch of the polarization curve shows that the time to cracking decreases continuously with increase of current density. The curve has an inflection which indicates that high current densities have relatively less effect than the initial values on the cracking rate.

*The current density required to protect the alloy against cracking was taken to be the value at which no cracking occurred for over 20 hours.

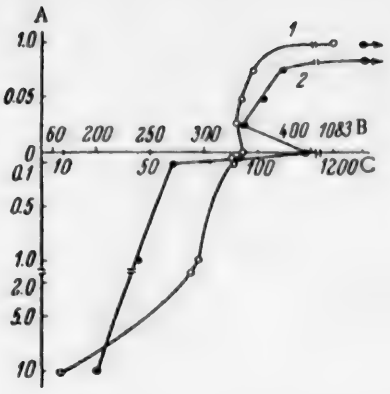

Fig. 1. Effects of anodic and cathodic polarization on the rate of stress corrosion and electrode potential of brass: A) D_a and D_c (in ma/cm^2), B) electrode potential (mv), C) time to cracking (minutes); 1) electrode potential, 2) time to cracking.

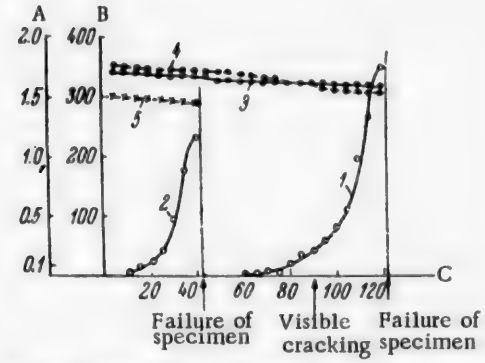

Fig. 2. Effects of anodic polarization on the start and absolute magnitude of the elongation of brass: A) elongation (mm), B) electrode potential (mv), C) time (minutes); elongation: 1) in absence of polarization, 2) with anodic polarization at D_a = = 1.0 ma/cm^2; potential: 3) unstressed brass in absence of polarization; 4) brass in absence of polarization under a stress of 18 kg/mm^2; 5) brass with anodic polarization under a stress of 18 kg/mm^2.

The same figure shows the values of the potential at the corresponding current densities for a time of 28 minutes, which corresponds to the highest rate of stress corrosion at a current density of 10 ma/cm^2. These results show that the potential curve is of the same shape as the cathodic-polarization curve: at low current densities the potential becomes more positive at first, and then more negative on further increase of current density. The potential changes continuously in the positive direction with increase of anodic current density.

Data on elongation of the specimens in absence of polarization (Fig. 2) indicate that it begins at about half the total time to cracking and continues smoothly, the rate being especially high during the last 10-15 minutes. The elongation curves with anodic polarization are of the same shape as before, but with increase of current density they contract and shift toward the coordinate origin, i.e., increase of the anodic current density reduces contraction and causes it to begin earlier; at D_a = 10 ma/cm^2 it commenced almost at the same time as polarization.

At insufficient cathodic polarization, which increases the time to cracking, the elongation curve is of the same shape as in the previous cases but the elongation begins later and has a greater absolute value than in absence of polarization.

The potential – time curves in Fig. 2 show that in absence of polarization the initial potential is somewhat more negative for stressed than for unstressed metal, but the values converge after some time and at the instant of visible crack formation the potential of the unstressed metal is more negative than that of the stressed.

During the first few seconds after failure of the specimens, both in presence and in absence of polarization, there is no sudden change of the potential in the negative direction such as is observed in 18/8 steel; this may be attributed to differences in the properties of the protective films on the surfaces of the respective metals. Cracks situated at equal distances from the main one were selected for microscopic investigation. These investigations showed that with and without polarization the cracks appear predominantly within the crystals (Fig. 3-5).

The influence of polarization on the nature of corrosion cracks is illustrated by Fig. 3-5.

The most pronounced influence is that of insufficient cathodic polarization, which increases the time to cracking as compared with absence of polarization: the cracks have blunted ends and tend to expand laterally across the grains (Fig. 4). Cathodic polarization appears to retain their progress at the ends. In absence of polarization (Fig. 3), the cracks are considerably narrower than with insufficient cathodic polarization, more elongated, and their ends pass into small narrow slits.

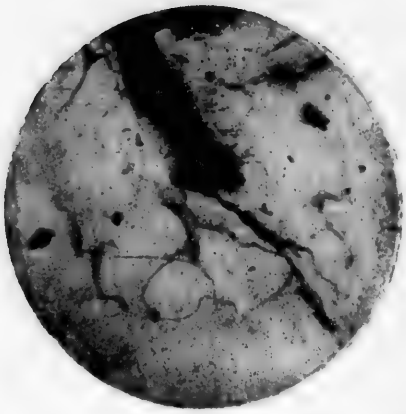

Fig. 3. Corrosion crack in absence of polarization (× 150).

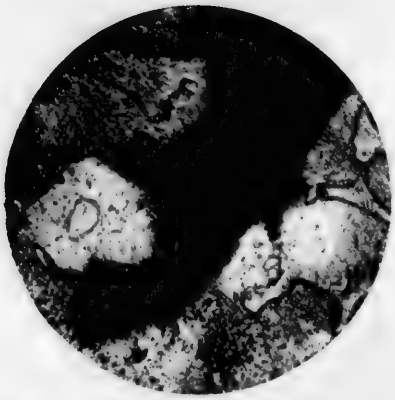

Fig. 4. Corrosion crack at insufficient cathodic polarization, at which the time to cracking was greater than in absence of polarization (one discarded result from data for D_c = 0.85 ma/cm^2) (× 150).

Fig. 5. Corrosion crack with anodic polarization D_a = 10 ma/cm^2 (×150).

In anodic polarization the cracks are even narrower than in absence polarization, and the narrow slits at their ends are even more elongated (Fig. 5).

DISCUSSION OF RESULTS

The shape of the polarization curve (of both the cathodic and the anodic branches) resembles that observed earlier in investigations of the cracking of MA2 magnesium alloy [4] and 18/9 steel [2], and is probably to be explained similarly. The causes of ennoblement of the potentials at the initial cathodic-current densities at which the time of cracking was less as compared with the time in absence of polarization are not clear, but the very fact that the potential is shifted in the positive direction at this stage of polarization makes it possible to explain the course of the cathodic branch of the polarization curve over its entire length by means of the polarization diagram for stress corrosion of metals [5, 6].

The influence of polarization on the nature of the corrosion cracks, consistent with earlier data [1, 2], provides a clear demonstration of the electrochemical nature of the stress corrosion of metals. The fact that the acceleration of the start of elongation and its decrease with increasing anodic current density is accompanied by a slight increase of the number of cracks and a substantial increase of the cracking rate probably indicates that this influence of anodic polarization on elongation is associated mainly with an increase of the rate of crack growth and to a lesser extent with an increase of the number of cracks.

The opposite influence of cathodic polarization may be explained conversely.

The data on the influence of polarization on elongation are fully consistent with data on the influence of polarization on the cracking rate and the shape of the corrosion cracks, and provide further experimental proof of the electrochemical nature of stress corrosion of metals*.

*I thank V. P. Romanova for assistance in the experimental work.

LITERATURE CITED

[1] V. V. Romanov, J. Appl. Chem. 29, 1191 (1956).*

[2] V. V. Romanov and V. V. Dobrolyubov, Metal Science and Treatment 7, 19 (1958).

[3] A. V. Bobylev, Stress Corrosion of Brass [in Russian] (Metallurgy Press, 1956).

[4] V. V. Romanov and V. V. Dobrolyubov, J. Appl. Chem. 5, 743 (1958).*

[5] V. V. Romanov, "Strength of metals," [in Russian] (Collected papers, Institute of Metals, Acad. Sci. USSR, 1956) p. 162.

[6] V. V. Romanov, Coll. Trans. Voronezh Section, D. I. Mendeleev All-Union Chem. Soc. 1, 105 (1957).

Received April 12, 1958

*Original Russian pagination. See C. B. Translation.

EFFECT OF LIGHT ON THE CORROSION OF ZINC AND CADMIUM

N. P. Fedot'ev, S. Ya. Grilikhes, and É. F. Orekhova

A number of workers have reported that light has an influence on metal corrosion. Investigation of the corrosion of iron in a solution of caustic soda and disodium phosphate showed that the corrosion rate increases under illumination by a fluorescent lamp. It has been suggested that light has a catalytic effect on the anode and cathode reactions. These reactions may include oxidation of ferrous iron to ferric by oxygen, and removal of hydrogen from the cathode surface as a consequence of an increase in the amount of ferric ions due to activation of oxygen and intensification of its depolarizing action [1]. The influence of light on electrochemical processes has been considered in relation to hydrogen peroxide formation [1].

In the present investigation the influence of light on zinc and cadmium galvanic coatings has been studied. Steel specimens were coated with zinc or cadmium in acid electrolytes of the usual composition. The coatings were 15μ thick. The tests were performed on specimens semi-immersed in 3% NaCl solutions in beakers. The specimens were divided into three groups; the first group was illuminated by a 1500 w spotlight lamp, the second by a PRK-2 ultraviolet lamp, and the third was shielded from light by several layers of dense black paper. The distance between the specimens and the light source was 30 mm. The test temperature was 35-37°. The corrosion resistance was estimated from the weight changes of specimens of the first and second groups. Before the second weighings the corrosion products were removed from the specimens by the action of 10% potassium persulfate solution, and the specimens were then washed in water and dried. Potential – time curves were determined for all three groups of specimens.

Fig. 1 and 2 show that the greatest weight loss was found in specimens kept in darkness. Both for zinc and for cadmium the difference is slight at the beginning of the tests. It reaches its maximum values after 80 (zinc) to 140 (cadmium) hours, and then gradually decreases again.

The course of the potential – time curves (Fig. 3 and 4) is of the usual type found in corrosion investigations for zinc and cadmium. The rapid rise of potential in the case of zinc during the first few hours is due to dissolution of the metal. Dark bands appear on the specimen surface 2-3 hours after immersion in NaCl solution. After 4-5 hours the formation of white loose corrosion products is observed. The potential reaches its highest negative value at this time. As the corrosion products increasingly cover the metal surface and protect it from the action of the corrosive medium, the potential becomes more positive. Subsequently, the loose corrosion products partially fall away from the surface, exposing isolated regions of the metal and making them again liable to corrosion attack. Removal of these products from some regions and their formation on others is marked by relative stabilization of the potential.

Examination of curves in Fig. 3 and 4 confirms that the corrosive breakdown is more rapid in specimens not exposed to light. Specimens coated with cadmium and zinc and kept in darkness have higher negative potentials than corresponding illuminated specimens. This difference becomes more prominent beyond the inflection on the curves, which coincides with the appearance of white corrosion products on the specimens. Subsequently, after some increase, the potential difference between the exposed and unexposed specimens becomes stabilized.

To determine how far the influence of light on corrosion is associated with formation and presence of insoluble corrosion products on the metal surface, experiments were carried out with zinc-plated specimens immersed in 0.125% H_2SO_4 solution. In this case, of course, the corrosion products are soluble in the electrolyte. The weight-loss curves in Fig. 1 for exposed and unexposed specimens almost coincide. It is evident that the

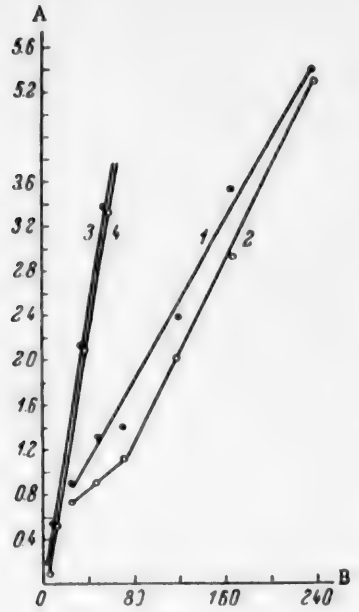

Fig. 1.

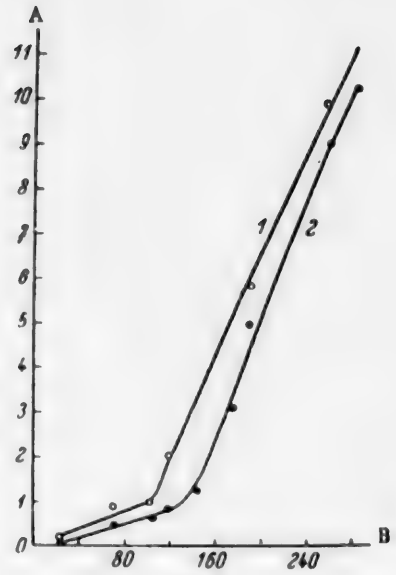

Fig. 2.

Fig. 1. Effect of light on corrosion of zinc-plated specimens: A) weight loss (mg/cm^2), B) duration of tests (hours); in 3% NaCl solution: 1) in darkness, 2) in light; in 0.125% H_2SO_4 solution: 3) in darkness, 4) in light.

Fig. 2. Effect of light on corrosion of cadmium-plated specimens: A) weight loss (mg/cm^2), B) duration of tests (hours); in 3% NaCl solution: 1) in darkness, 2) in light.

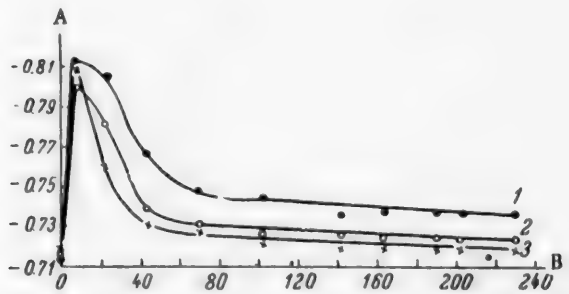

Fig. 3. Potential – time curves for zinc-plated specimens: A) potential (v), B) duration of tests (hours); 1) in darkness, 2) on exposure to light from PRK-2 lamp, 3) on exposure to light from a spotlight lamp.

corrosion products formed on the surface of the coating in NaCl solution are influenced differently by light and darkness. In contrast to its usual catalytic effect, in this instance light retards corrosion of zinc and cadmium coatings. Similar results are obtained in corrosion of specimens of metallurgical zinc.

When the experimental results are considered, it should be noted that the white corrosion products of zinc and cadmium contain compounds of these metals which are semiconductors. It is possible that the peculiar influence of light on corrosion is associated with the presence of these compounds on the metal surface.

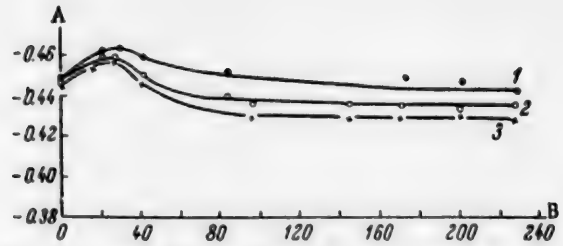

Fig. 4. Potential – time curves for cadmium-plated specimens; A) potential (v), B) duration of tests (hours); 1) in darkness, 2) on exposure to light from PRK-2 lamp, 3) on exposure to light from a spotlight lamp.

LITERATURE CITED

[1] Werkstoffe und Korrosion 8, 5, 277 (1957).

[2] I. B. Rabinovich and V. I. Veselovskii, J. Phys. Chem. 30, 2 (1956).

Received September 19, 1958

USE OF SOLID ELECTROLYTES IN STUDIES OF THE THERMODYNAMIC PROPERTIES OF ALLOYS BY THE ELECTROMOTIVE-FORCE METHOD*

M. F. Lantratov and A. G. Morachevskii

In studies of the thermodynamic properties of liquid or solid alloys, the use of solid electrolytes has undoubted advantages over the use of salt melts as electrolytes [2-4]. For this reason, cells with solid electrolytes have been used in numerous electrochemical investigations of alloys. For example, in determinations of the activity of sodium or potassium in binary and ternary alloys, glasses containing Na_2O or K_2O are widely used [5, 6]. Vierk [7] used glass containing Tl_2O as the electrolyte in studies of Tl – Sn and Tl – Bi alloys by the emf method. Kubaschewski and Hugler [4] use a glass containing silver ions in an electrochemical study of the system Ag – Au. Wacter [8] used solid silver chloride as the electrolyte for the same system.

It is known that the electrochemical method can be used for studies of the thermodynamic properties of alloys only if the electrolyte has purely ionic conductance and conforms strictly to the Faraday law [2, 4]. In all the investigations cited, these conditions were completely fulfilled. It has now been conclusively established that alkali silicate and borate glasses are purely ionic conductors [9, 10]. It is also known that, in addition to alkali-metal ions, silver and thallium ions can carry the current [4, 7]. Solid silver chloride is known to be a pure cationic conductor [8].

In the light of the foregoing there is no justification for using aluminum oxide as the solid electrolyte, as was done by Musikhin, Esin, and Lepinskikh [1] in emf determinations of the cell Al | Al_2O_3 | Fe, C_{sat}, Al, Me, where Me – Mn, P, Si.

The authors' reference [1] to the use of glasses in such investigations does not prove that Al_2O_3 may be used for investigating aluminum alloys. Extension of the concepts of the conduction mechanism of alkali glasses not only to Al_2O_3 but to alkali-free glasses in general is not valid. For example, it has been shown by Mazurin, Pavlova, Lev, and Leko [11] that a glass of the composition (in %): SiO_2 45, Al_2O_3 10, B_2O_3 10, CaO 30, Fe_2O_3 5, has pure electronic conductance.

It is known from the literature that Al_2O_3 is a semiconductor with electronic conductance [12-14]. The electronic nature of the conduction of aluminum oxide is retained at temperatures of 900-1300° [15], which is the temperature region used in the paper cited [1]. There is no reason to assume that the nature of the conduction may change at higher temperatures [16].

Thus Al_2O_3, being an electronic conductor, cannot be used as the solid electrolyte in electrochemical investigations of the thermodynamic properties of alloys. In other words, in the cell Al | Al_2O_3 | Fe, C_{sat}, Al, Me there is no transfer of aluminum from pure aluminum (in the standard state) to the alloy, and therefore, despite the claim made [1], the basic thermodynamic equation is inapplicable:

$$E = \frac{RT}{3F} \ln \frac{1}{a_{Al}} .$$

*With reference to the paper by V. I. Musikhin, O. A. Esin, and B. M. Lepinskikh: "Influence of Mn, P, and Si on the activity of aluminum in liquid crude iron."

LITERATURE CITED

[1] V. I. Musikhin, O. A. Esin and B. M. Lepinskikh, J. Appl. Chem. 31, 689 (1958).*

[2] O. Kubaschewski and E. Evans, Metallurgical Thermochemistry (IL, Moscow, 1954) [Russian translation].

[3] C. Wagner, Thermodynamics of Alloys (Metallurgy Press, Moscow, 1957) [Russian translation].

[4] O. Kubaschewski and O. Hugler, Z. Elektroch. 52, 170 (1948).

[5] A. F. Alabyshev, M. F. Lantratov and A. G. Morachevskii, Progr. Chem. 27, 921 (1958).

[6] A. F. Alabyshev and A. G. Morachevskii, J. Inorg. Chem. 2, 669 (1957).

[7] A. L. Vierk, Z. Elektroch. 54, 436 (1950).

[8] A. Wacter, J. Am. Chem. Soc. 54, 4609 (1932).

[9] W. Eitel, The Physical Chemistry of the Silicates (Chicago, 1954).

[10] K. S. Evstrop'ev and N. A. Toropov, Silicon Chemistry and Physical Chemistry of the Silicates [in Russian] (Industrial Construction Press, 1956).

[11] O. V. Mazurin, G. A. Pavlova, E. Ya. Lev and E. K. Leko, J. Tech. Phys. 27, 2702 (1957).

[12] G. Bush, Progr. Phys. Sci. 47, 258 (1952).

[13] W. Hartmann, Z. Phys. 102, 709 (1936).

[14] P. T. Oreshkin, J. Tech. Phys. 25, 2447 (1955).

[15] N. P. Bogoroditskii and N. L. Polyakova, Proc. Acad. Sci. USSR 95, 257 (1954).

[16] A. R. Regel', in the book: Theory and Investigations of Semiconductors and Processes in Semiconductor Metallurgy [in Russian] (Izd. AN SSSR, 1955).

Received October 26, 1958

*Original Russian pagination. See C. B. Translation.

EFFECT OF THIOUREA ON ELECTRODEPOSITION OF NICKEL

A. V. Pamfilov, O. É. Panchuk and G. G. Kossyi

Laboratory of Physical Chemistry, Chernovits University

Many of the known additives used for deposition of bright electrolytic nickel deposits contain sulfur [1]. One such brightener is thiourea, which causes formation of bright deposits even at a concentration of 0.15 g/liter and greatly increases the cathode potential [2]. The brightening effect of thiourea was also reported by Denise and Leidheiser [3]. Its influence on nickel deposition was studied more fully by Antropov and Popov [4], Elze [5], and Morgart [6].

The data in the cited publications on the dependence of polarization on the concentration of the additive are incomplete and not easily comparable. The brightness is not evaluated quantitatively. It was therefore desirable to study the influence of thiorea on electrodeposition of nickel in greater detail.

The electrolyte used for nickel deposition had the following composition (in g/liter): $NiSO_4 \cdot 7H_2O$ – 200, $NiCl_2 \cdot 6H_2O$ – 15, H_3BO_3 – 30. The effect of thiourea in concentrations of 0.02, 0.05, 0.1, 0.3 and 0.5 g/liter on cathodic polarization and brightness of the nickel deposits was studied. For each concentration, data were obtained on brightness (at current densities of 1, 2, 3, 4 and 5 amp/dm^2) and cathodic polarization (in the current-density range of 0.06-2.0 amp/dm^2, at temperatures of 25, 40 and 55°, and pH = 5.5-0.1). It was found that the influence of thiourea on brightness was best at a concentration of 0.3 g/liter; the effects of acidity on polarization and brightness were studied at this concentration for the same current densities and temperatures. The polarization curves were determined by the compensation method. The deposits were formed on brass specimens

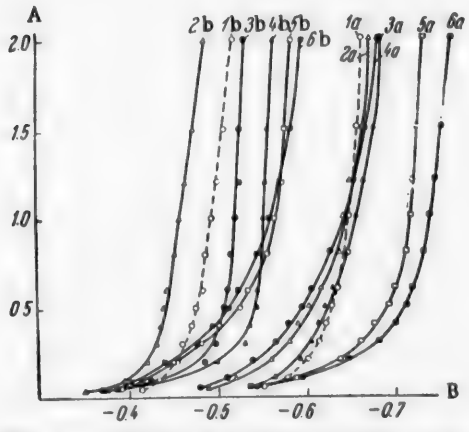

Fig. 1. Variation of cathode potential with current density in the electrodeposition of nickel in presence of different amounts of thiourea: A) current density (amp/dm^2), B) overvoltage (v); concentration of additive (in g/liter): 1) 0, 2) 0.02, 3) 0.05, 4) 0.1, 5) 0.3, 6) 0.5; in the curve, numbers a correspond to 25° and b to 55°.

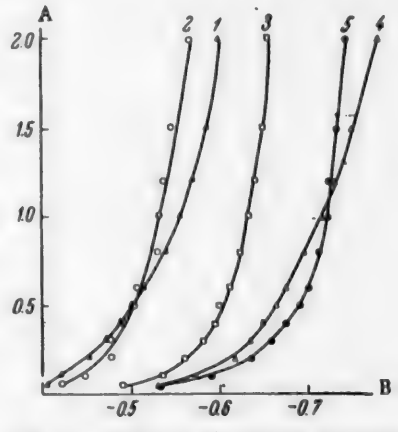

Fig. 2. Variation of cathode potential with current density in the electrodeposition of nickel in presence of 0.3 g thiourea per liter; temperature 25°; A) current density (amp/dm^2), B) overvoltage (v); electrolyte pH: 1) 2, 2) 3, 3) 4, 4) 5, 5) 5.5.

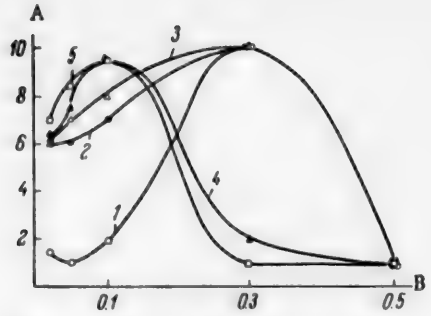

Fig. 3. Variation of the brightness of nickel deposits with the thiourea concentration; the numbers on the curves correspond to the current densities (in amp/dm^2); temperature 25°: A) brightness, B) thiourea concentration (g/liter).

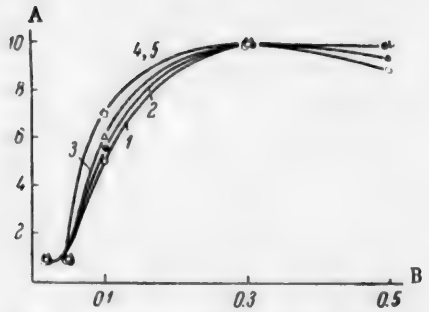

Fig. 4. Variation of the brightness of nickel deposits with the thiourea concentration; the numbers on the curves correspond to the current densities (in amp/dm^2); temperature 55°: A) brightness, B) thiourea concentration (g/liter).

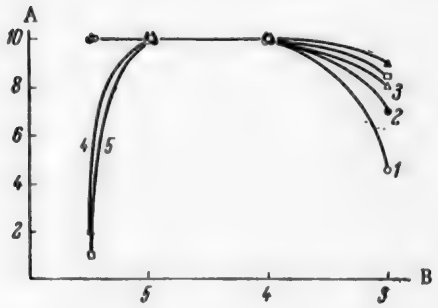

Fig. 5. Variation of the brightness of nickel deposits formed in an electrolyte containing 0.3 g thiourea per liter with the electrolyte pH; the numbers on the curves correspond to the current densities (in amp/dm^2); temperature 25°: A) brightness, B) pH.

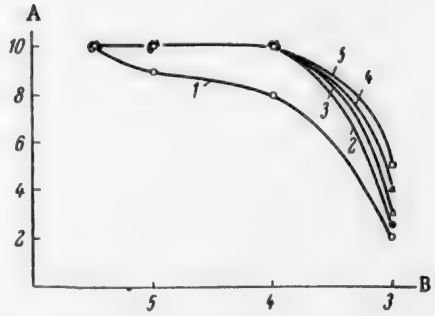

Fig. 6. Variation of the brightness of nickel deposits formed in an electrolyte containing 0.3 g thiourea per liter with the electrolyte pH; the numbers on the curves correspond to the current densities (in amp/dm^2); temperature 55°: A) brightness, B) pH.

10 cm^2 in area, mechanically polished and degreased by cathodic treatment; the deposit thickness was 10 μ. The brightness was determined by comparison with a series of 10 standard specimens [7].

It had been shown in our laboratory [1, 7, 8] that the role of sulfur-containing additives consists of formation of colloidal nickel sulfide by interaction with the nickel cathode, and it was suggested that the layers of nickel become leveled and brightened as the result of periodic adsorption and reduction of this sulfide. It was therefore assumed that cathodic polarization and brightness of electrolytic deposits are directly connected with the amount of stable colloidal nickel sulfide formed under the given conditions. The present results are considered from this standpoint.

The decomposition of thiourea in presence of Raney nickel proceeds as follows [9]:

$$(NH_4)_2CS + NiH_n \rightarrow NiS + NH_3 + CH_3NH_2 + CH_4.$$

A nickel cathode the surface of which is continuously renewed and saturated with hydrogen can be considered as being similar to Raney nickel, and in this instance the above reaction should be accompanied by a decrease of cathode potential. On the other hand, adsorption of the decomposition products of thiourea (mainly

colloidal nickel sulfide) retards the discharge of nickel ions, and this increases the cathodic polarization. With regard to other potential-determining processes, it is necessary to take into account the possible reduction of nickel sulfide, which should lead to depolarization. The polarization curves represent the aggregate effect of all the processes taking place at the cathode.

The depolarization observed at low current densities in presence of thiourea (Fig. 1) is probably due to predominance of the reduction effect in this case. The considerable increase of overvoltage at current densities of 1-2 amp/dm^2 should be ascribed to increased adsorption of positively charged colloidal nickel sulfide at these current densities. With regard to variations of the cathode potential with the thiourea concentration, at low concentrations, when little nickel sulfide is formed, the curves are shifted in the positive direction because the reduction effect predominates. However, with increase of the thiourea concentration,retardation of the electrode process begins to have a more pronounced effect, and at concentrations of 0.3-0.5 g/liter the curves are shifted into the region of negative potentials.

When the influence of acidity on polarization is considered, it is seen that the polarization curves are shifted in the positive direction with increase of electrolyte acidity (Fig. 2). The brightness of the deposits decreases considerably under these conditions. It may be assumed that increase of hydrogen-ion concentration leads to complete or partial dissolution of colloidal nickel sulfide, and this in its turn influences the potential and the formation of the deposit.

It was shown in our laboratory [7] that conditions which favor formation and increased stabilization of colloidal nickel sulfide also tend to increase brightness of the deposits, and conversely. When thiourea is used as brightener, the relationship between electrolysis conditions and brightness which was found for naphthalene-sulfonic acids again holds, and is even more pronounced, as is clear from Fig. 3-6.

SUMMARY

Addition of thiourea to electrolytes used for electrodeposition of nickel increases cathodic polarization. At low current densities,depolarization occurs because of the decomposition of the additive at the cathode with formation of colloidal nickel sulfide.

The relationship between brightness and deposition conditions of nickel deposits is explained in terms of the influence of electrolysis conditions on the amount and stability of nickel sulfide.

LITERATURE CITED

[1] A. V. Pamfilov and R. M. Morgart, Ukrain. Chem. J. 23, 684 (1957).

[2] E. Raub and M. Wittum, Z. Elektrochem. 46, 71 (1940).

[3] F. Denise and H. Leidheiser, Jr., J. Electrochem. Soc. 100, 490 (1953).

[4] L. I. Antropov and S. Ya. Popov, J. Appl. Chem. 27,206 (1954).*

[5] J. Elze, Metall. 8, 519 (1954).

[6] R. M. Morgart, Sci. Mem. Chernovits Univ., Chem. Ser. 20, 45 (1956).

[7] A. V. Pamfilov and O. É. Panchuk, Ukrain. Chem. J. 24, 266 (1958).

[8] A. V. Pamfilov and O. É. Panchuk, Ukrain. Chem. J. 23, 391 (1957).

[9] J. Bougault, A. Cattelain and P. Chabrier, Bull. Soc. Chim. France [5], 7, 78 (1940).

Received March 18, 1958

*Original Russian pagination. See C. B. Translation.

ELECTROLYTIC COPPER PLATING OF IRON IN AN ACID ELECTROLYTE

D. N. Gritsan and D. S. Shun

Institute of Chemistry, Khar'kov State University

Acid copper electrolytes are among the simplest and most stable with regard to composition and behavior. However, such electrolytes cannot be used for formation of dense, strong, and adherent deposits directly on iron and steel surfaces. Methods have recently been proposed for prevention of contact deposition of copper on iron in acid electrolytes [1-4], and thereby some advance was made toward the replacement of cyanide electrolytes by others. However, these methods are not free from important disadvantages and their adoption in practice involves serious difficulties.

In studying the effects of various surface-active substances on the electrodeposition of metals, we found that certain detergents and wetting agents can be used in electroplating as additives with very effective influence on the electrodeposition process and the structure of the deposited metal. For example, when DB or NB wetting agents are added to solutions of lead nitrate or acetate it is possible to obtain dense microcrystalline lead deposits directly on iron [5].

The present communication contains the results of a study of the influence of certain synthetic detergents and wetting agents on the electrodeposition of copper from solutions of its simple salts, carried out in order to determine whether they can be used in electrolytic copper plating of iron and steel articles.

A glass cell 150 ml in capacity was used for the experiments. The cathodes were iron plates 4 and 8 cm^2 in effective area. The anode was a copper spiral, the effective area of which was usually 10 times that of the cathode. The iron cathodes were cleaned, polished with emery paper, and degreased electrochemically [6] before the deposition. The electrolyte contained 200 g of copper sulfate and 50 g of sulfuric acid per liter. The solutions were prepared from chemically pure reagents in distilled water. The electrode potentials, current efficiencies, and adherence of the deposits to the cathodes were determined, and the microstructure and appearance of the deposits were studied. The quality of the coatings was also evaluated in terms of thickness and porosity.

It was found that the synthetic wetting agents and detergents DB and OP-10 have a strong influence on the electrodeposition and structure of copper, but cannot completely prevent dissolution of iron or contact deposition of copper on it. The coatings formed had poor adherence to the basis metal. To prevent contact deposition of copper, we passivated the iron specimens immediately before deposition and subjected them to the action of current of high density, a so-called "shock", for a short time before the normal electrolysis. The specimens were suspended in the solution with the current flowing. A solution formed by the mixing of equal volumes of 1 M sulfuric acid and saturated potassium dichromate solution was used for passivation. The time of exposure of iron specimens to the passivating solution depends on the temperature of the latter. For example, at 1-3° an exposure time of 3 minutes is needed, and at 18-20°, not more than 5 seconds.

The density and duration of the initial high "shock" current are of great importance for the production of good coatings with firm adherence to the basis metal. The influence of these factors on the quality of electrolytic copper deposits and their adherence to iron is illustrated in Table 1.

The data in the table show that the strongest, most even, brightest, and most compact copper deposits are formed at a "shock" current density of 5 amp/dm^2, or about 10 times the operating current density, applied for 15-30 seconds.

TABLE 1

Influence of Initial Current Density and Its Duration on the Quality of Copper Coatings on Iron. Electrolyte Composition: $CuSO_4 \cdot 5H_2O$ 200 g/liter, H_2SO_4 50 g/liter, DB Wetting Agent 6 g/liter, Operating Current Density 0.5 amp/dm^2

Current density (amp/dm^2)	Duration of initial current (sec)	Characteristics of coating
2.5	3	Dark, uneven, peels easily
2.5	20	
5	3	Darkish, peels
5	16	Bright, even, peels after 4 bends through 90°
5	20	Bright, even, strong to failure of specimen
5	25	
5	60	Dark, peels on bending

TABLE 2

Influence of Operating Current Density and Electrolysis Time on Thickness and Porosity of Copper Deposits on Iron Electrolyte Composition: $CuSO_4 \cdot 5H_2O$ – 200 g/liter, H_2SO_4 – 50 g/liter, DB Wetting Agent – 6 g/liter

Operating current density (amp/dm^2)	Electrolysis time (min)	Number of pores per cm^2	Thickness of coating (μ)	Nature of coating
0.5	10	Many	1	Bright, strong to failure of specimen
0.5	20	2	2	
0.5	30	2	4	
0.5	60	1	10	
0.6	30	5	5	
0.75	10	Many	2	
0.75	15	1	3	
0.75	30	None	7	
0.75	60		15	
0.9	40		10	
0.9	60		20	
1	10	Many	3	
1	20	5	7	
1	30	1	13	

With the correct passivation and "shock" conditions and under suitable electrolysis conditions it is possible to obtain compact, strong copper deposits of fine appearance, which do not peel on bending up to failure of the specimen itself. The operating current density can be varied in the range of 0.3-1.3 amp/dm^2. At higher current densities the coating becomes dark and loose.

The effects of operating current density and electrolysis time on the porosity and thickness of the coatings are given in Table 2.

The deposits were formed at room temperature (18-25°) from stirred electrolyte. The current efficiency was about 100%.

It was found in special experiments that acid copper electrolyte containing DB wetting agent gives good coatings only after electrolytic purification. Without this operation the copper coatings adhere badly to the iron, and do not differ in quality from coatings obtained from standard acid electrolyte. The electrolytic purification should be continued until the electrolyte gives good coatings with firm adherence to iron. The time required for such treatment of a solution containing 1% of DB wetting agent is about 25 hours. With higher concentrations of the additive this time must be increased. The concentration of the additive gradually falls during electrolysis, and therefore it must be supplemented at intervals during operation and complete exhaustion must not be allowed to occur. Special purification of the electrolyte after addition of supplementary portions of DB is not necessary.

When OP-10 was added to acid copper electrolyte the coatings obtained were also of good appearance, strong, and compact. The best coatings were obtained from an electrolyte which contained 200 g/liter of $CuSO_4 \cdot 5H_2O$, 100 g/liter of H_2SO_4, and 45 g/liter of OP-10. If NB wetting agent (Nekal) is added to copper electrolyte, the deposits formed are bright and of good appearance, but do not adhere well to iron.

Experiments on electrodeposition of copper from its nitrate showed that compact copper deposits can be obtained only on copper cathodes. Coatings of adequate density could not be obtained on iron cathodes from this electrolyte, as the iron was rapidly dissolved in nitrate solution, and the dissolution could not be suppressed by any means.

The results of this investigation show that the detergents and wetting agents OP-10 and DB have a most effective influence on electrocrystallization of metals and the structure of electrolytic deposits. The formation of compact microcrystalline copper deposits from sulfate solutions in presence of these additives is apparently determined by the simultaneous influence of several factors. Adsorption of organic molecules on the growing crystals retards the electrode process and lowers interfacial tension at the metal – solution boundary, so that the deposit is more disperse. At the same time, adsorption of surface-active wetting agents ensures ideal contact between the metal and solution, owing to the chemical structure of these additives, which make the metal surface hydrophilic and improve wetting of the metal by the aqueous solution from which the ions are discharged.

SUMMARY

In a study of the effects of wetting agents and detergents on the electrodeposition of copper from solutions of simple salts it was shown that compact, level, and nonporous deposits of copper on iron can be obtained from acid sulfate solutions in presence of small amounts of DB wetting agent or OP-10 detergent.

LITERATURE CITED

[1] L. I. Antropov, Soviet Author's Certif. 102546.

[2] A. D. Rupasova, Soviet Author's Certif. 99518.

[3] L. I. Kadaner, Soviet Author's Certif. 77528.

[4] L. I. Antropov and Yu. V. Fedorov, Trans. Novocherkassk Polytech. Inst. 25, 109 (1954).

[5] D. N. Gritsan and D. S. Shun, Soviet Authors' Certif. 106225; D. N. Gritsan and D. S. Shun, Soviet Authors' Certif. 111483.

[6] V. I. Lainer and N. T. Kudryavtsev, Fundamentals of Electroplating 1 [in Russian] (Metallurgy Press, 1953).

Received May 13, 1958

PREPARATION OF CHLORINATED AND CHLOROSULFONATED PROPYLENE*

B. A. Krentsel', A. V. Topchiev and D. E. Il'ina

Among the synthetic materials of the greatest importance at the present time are the polyolefins, which are becoming increasingly significant. The various possibilities of modifying polyolefin properties are worthy of attention in this connection. One such possibility is the introduction of definite functional groups into polyolefins.

This type of conversion of polyolefin macromolecules is of theoretical interest in connection with the general problem of the relationship between the structure and properties of high polymers, and is of technical significance in relation to the production of modified polyolefins.

Chlorinated and chlorosulfonated polyethylene, which have a number of valuable properties, already have technical uses.

The discovery of methods for the synthesis of an essentially new class of polyolefins – stereoregular polypropylene and its analogs – have naturally aroused interest in studies of various chemical conversions of these important polymers.

Among the interesting conversions are chlorination and chlorosulfonation. Apart from their use for modifying polymer properties, these reactions may be of importance for production of intermediates for further synthesis of new polymers, and in particular graft polymers.

It is to be expected that chlorinated and chlorosulfonated polypropylenes are highly inert to various chemical reagents, are vulcanizable, permeable, etc.

The present communication deals with some aspects of the chlorination of polypropylene and the properties of the products formed, and with the method for preparation of chlorosulfonated polypropylene.

EXPERIMENTAL

The starting material in most of the experiments was polypropylene synthesized in our laboratory with the aid of $Al(C_2H_5)_3$ and $TiCl_4$ catalyst. The polymer had intrinsic viscosity 1.55, melting point 154°, and contained about 60% of the isotactic component (insoluble in boiling heptane). The chlorination was effected photochemically. The reaction was conducted in carbon tetrachloride solution in a reactor fitted with a stirrer, bubbler, thermometer, and reflux condenser. The reaction mass was irradiated by means of an ordinary incandescent lamp (75 w).

The calculated amounts of polypropylene and carbon tetrachloride** were put into the flask. The polymer was dissolved at 60-65° with vigorous stirring during 2 hours. The temperature of the reaction mass was then regulated to the required reaction temperature.

Chlorine (from a cylinder) was passed into the reactor, through drying flasks containing concentrated sulfuric acid, at a definite rate regulated with the aid of a rheometer.

*Communication I in the series on chemical conversion of polyolefin macromolecules.

**CCl_4 was chosen as the solvent because it is unaffected by chlorine and dissolves the original polymer relatively easily.

TABLE 1

Relationship Between the Amount of Chlorine Introduced Into the Polypropylene Macromolecule and the Amount of Chlorine Passed. Temperature 20-22°

Expt. No.	Polypropylene taken (g)	Chlorine passed			Chlorine reacted		Chlorine content of polymer (%)
		liters	g	g per g of polypropylene	g	%	
33	2	0.5	1.56	0.78	0.028	1.8	1.7
34	2	1.0	3.15	1.56	0.178	5.6	10.8
1	2	3.5	11.1	5.0	—	—	40.0
2	2	3.6	11.0	5.0	0.92	8.4	38.3
13	4	15.5	48.9	12.2	1.7	3.5	50.0
20	2	10.0	31.5	15.7	1.0	3.2	39.5
32	2	21.0	66.2	33.1	1.55	2.3	62.0

TABLE 2

Effect of Reaction Temperature on the Amount of Chlorine Introduced Into the Polymer

Expt. No.	Polypropylene taken (g)	Temperature (°C)	Chlorine passed (liters)	Chlorine content of polymer (%)
1	2	25	3.5	40.0
2	2	24	3.6	38.3
24	2	42	3.5	34.2
25	2	58	3.5	31.1

Unchanged chlorine and the hydrogen chloride formed passed through the reflux condenser, traps cooled in a mixture of solid carbon dioxide and isopropyl alcohol, and an absorber with water.

On the conclusion of the experiment, when the light had been switched off, nitrogen was blown through the system with stirring of the reaction mass in order to remove any chlorine which dissolved in carbon tetrachloride but did not react with polypropylene. The reaction mass was cooled and the polymer was filtered off on a Büchner funnel. The solid chlorinated polypropylene and the solvent were treated separately with water, 10% aqueous sodium carbonate, and water again to remove traces of chlorine and hydrogen chloride.

The polymer was dried at 75-80° to constant weight. The finished product was a fine white powder.

The properties of chlorinated polypropylene should depend on the amount of chlorine introduced into the original polyolefin macromolecule. The amount of chlorine introduced, in its turn, depends on the reaction conditions.

The first series of experiments showed that the amount of chlorine introduced into the polypropylene macromolecule at a given temperature and chlorine rate depends on the amount of chlorine passed; this is clear from the data in Table 1.

Whereas under analogous conditions polyethylene yields a chlorinated polymer containing less than 20% chlorine, up to 62% chlorine can be introduced into the polypropylene macromolecule.

Evidently the presence of tertiary carbon atoms in polypropylene facilitates chlorination.

It is significant that the content of the isotactic portion of the polymer decreases with increasing chlorination. This is due, in all probability, to regrouping at the tertiary carbon atoms, where hydrogen is in the first instance replaced by chlorine. This is a more likely explanation than the supposition that the effect is caused by electrostatic repulsion of chlorine atoms replacing hydrogen in the methyl groups. The cause of the loss of isotactic characteristics on replacement of hydrogen atoms by functional groups is of primary theoretical importance in relation to the problem of structure of isotactic polymers, and it will be discussed more fully in subsequent papers.

The temperature of the reaction mass, in the range studied, had relatively little effect on the amount of chlorine introduced into the polypropylene macromolecule; this is clear from the data in Table 2.

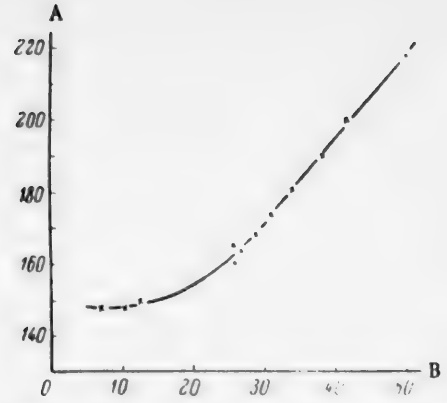

Fig. 1. Variation of melting point with the chlorine content of the polymer: A) melting point (°C), B) chlorine content (%).

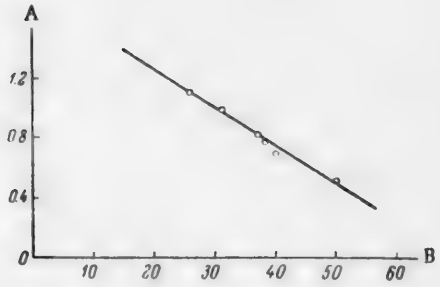

Fig. 2. Variation of intrinsic viscosity with the chlorine content of the polymer: A) intrinsic viscosity, B) chlorine content (%).

Introduction of chlorine into the macromolecule had a significant influence on some properties of the polymer, including the melting point. It follows from the data plotted in Fig. 1 that the melting point of the polymer rises sharply with increase of chlorine content.

It should be noted that when the chlorine content is less than 20% the melting point remains at almost the same level as that of the original polypropylene, or even decreases somewhat, but it rises with further increase of chlorine content. The melting point of chlorinated polypropylene containing 62% chlorine is above 250°.

The intrinsic viscosity* of the chlorinated products decreases with increasing chlorine content, and is lower than that of the original polypropylene. The results of these experiments are plotted in Fig. 2.

Polypropylene was chlorosulfonated in a laboratory unit which was almost the same as that used for chlorination. The chlorosulfonation agent was a mixture of SO_2 and Cl_2 formed in definite proportions in a mixer installed before the reaction vessel. At a molar ratio of $SO_2 : Cl_2 = 1 : 3$, chlorosulfonated polypropylene containing up to 4% sulfur and 40% chlorine was formed.

The melting point of chlorosulfonated polypropylene is 175°.

Studies of the chlorosulfonation reaction are continuing.

SUMMARY

1. The chlorination of solid polypropylene containing about 60% of the isotactic polymer has been studied, and it is shown that up to 62% chlorine can be introduced into the macromolecule of the original polymer.

2. It is shown that the melting point of polypropylene is raised by introduction of chlorine.

3. Chlorosulfonated polypropylene containing up to 4% sulfur and 40% chlorine was prepared.

Received July 10, 1958

*The intrinsic viscosity of chlorinated polypropylene was determined in decalin at 120°.

QUANTITATIVE DETERMINATION OF ACETONE AND METHYL ETHYL KETONE IN PRESENCE OF ALDEHYDES

L. N. Petrova, E. N. Novikova and A. B. Skvortsova

Determination of ketones in presence of aldehydes presents a rather complex problem. The usual procedure is to determine the total carbonyl compounds, to determine aldehydes by oxidation with silver oxide, and to find the ketone content by difference [1].

In this communication we describe a simple method for determination of volatile ketones – acetone and methyl ethyl ketone – in presence of aldehydes of various structures.

We have shown that under the action of bases such as aniline and o-toluidine all aldehydes are quantitatively converted into the corresponding azomethines (anils) with liberation of a mole of water per mole of aldehyde [2]. Most ketones do not react with the bases under the determination conditions used.

The following procedure is recommended for the determination. A sample of the mixture containing aldehydes and acetone or methyl ethyl ketone, weighing about 0.5 g, is put in a distillation flask [2] containing 15 ml of 15% aniline solution in benzene. The flask is connected through a condenser to a receiver containing 20 ml of 0.5 N hydroxylamine hydrochloride solution in 80% alcohol. The distillation flask is immersed in a bath containing petrolatum heated to 50-60°. The bath temperature is gradually raised to 150° and a mixture of benzene and acetone (or methyl ethyl ketone) is collected in the receiver. The heating at 150° is continued until distillation stops completely. The apparatus is allowed to cool, the condenser, still connected to the receiver, is rinsed out through the turned connecting tube with 15 ml of methyl or ethyl alcohol, and the hydrochloric acid liberated by the reaction of the ketone with hydroxylamine hydrochloride is titrated in the receiver by 0.5 N alcoholic KOH in presence of bromphenol blue indicator.

TABLE 1

Determinations of Acetone

Composition of mixture	Acetone content of mixture (g)	Acetone found	
		in g	% of the amount taken
Acetone + formaldehyde + water (30.4%)	0.0915	0.0926	101.2
	0.3891	0.3852	99.0
Acetone + acetaldehyde	0.0811	0.0823	101.4
	0.3299	0.3302	100.2
Acetone + propionaldehyde	0.1041	0.1059	101.3
Acetone + butyraldehyde	0.2908	0.2830	97.3
Acetone + benzaldehyde	0.0967	0.0941	97.5
	0.3580	0.3521	98.5

TABLE 2

Determinations of Methyl Ethyl Ketone

Composition of mixture	Content of methyl ethyl ketone (g)	Methyl ethyl ketone found	
		in g	% of amount taken
Methyl ethyl ketone + formaldehyde	0.1195	0.1195	100.0
	0.3442	0.3392	98.5
Methyl ethyl ketone + acetaldehyde	0.1183	0.1194	100.8
	0.5733	0.5711	99.6
Methyl ethyl ketone + propionaldehyde	0.1271	0.1297	101.5
Methyl ethyl ketone + butyraldehyde	0.2933	0.2881	98.0
Methyl ethyl ketone + citral	0.1637	0.1651	100.8
	0.2261	0.2243	99.3
Methyl ethyl ketone + benzaldehyde	0.1175	0.1140	97.0

In parallel with each series of determinations a blank experiment without mixture should be carried out in order to allow for the amount of aniline which distills over with benzene under these conditions. The results of the blank titration are added to the results of the analytical titrations.

Water, alcohols, esters, and acids in the samples do not interfere.

Tables 1 and 2 contain the results of analyses of mixtures of acetone or methyl ethyl ketone with various aldehydes.

SUMMARY

Acetone and methyl ethyl ketone in mixtures with aldehydes can be quantitatively determined by the oxime method if the aldehydes are first converted into nonvolatile Schiff bases by the reaction with aniline. Acetone and methyl ethyl ketone are distilled with benzene from the reaction mixture and then determined by the oxime reaction.

LITERATURE CITED

[1] W. Ponndorf, Ber. 64, 931 (1931); L. N. Petrova and V. D. Zhezmer, Industrial Lab. 17, 1 (1951).

[2] L. N. Petrova, E. N. Novikova and A. B. Skvortsova, J. Anal. Chem. 14, 348 (1959).*

Received July 29, 1958

*Original Russian pagination. See C. B. Translation.

INVESTIGATION OF THE RESISTANCE OF DIFFERENT STEELS UNDER CONDITIONS OF AMMONOLYSIS OF p-CHLOROBENZENE-SULFONAMIDE

Yu. P. Aronson and Yu. M. Rozanova

The S. Ordzhonikidze All-Union Chemico-Pharmaceutical Scientific Research Institute

The production of streptocide (sulfanilamide) by ammonolysis of p-chlorobenzenesulfonamide [1] is effected in an aqueous solution of NH_3 (27-28%) and NH_4Cl at 165° under 30 atmos pressure. The catalyst is a complex cuprous ammine.

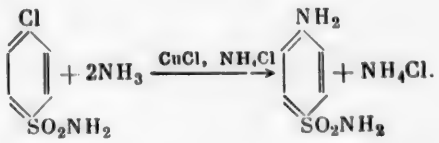

Through cracks formed in a tubular reactor made of 1Kh18N9T steel used for testing this process at the Akrikhin factory. It was necessary to find the causes of this effect and to look for a material which is more resistant under the reaction conditions.

Tests were performed on 1Kh18N9T, Kh18N11B, Kh18N12M2T, Kh18N12MZT, Kh18N28MZT, Kh18N28MZDZ, and Kh23N23MZDZ steels, and on tantalum. The investigations showed that if the ammonolysis is performed continuously and in accordance with the prescribed conditions, the corrosion of all these metals is slight and uniform over the entire surface. Strong intercrystallite corrosion with formation of deep cracks occurs if the NH_3 concentration decreases*, with decomposition of the cuprous ammine complex and appearance of free copper ions in solution; it is known that such ions cause this type of corrosion in stainless steel [3]. Copper is then displaced in powder form as the metal from the solution by iron.

The tests showed that intercrystallite corrosion intensifies with decrease of NH_3 concentration: the least resistant steels are 1Kh18N9T and Kh18N11B, and the most resistant are Kh23N28MZT and Kh18N28MZDZ, i.e., steels with the highest nickel and molybdenum contents. The ordinary low-carbon steels St 3, St 08, and St 20, and Armco iron, are not subject to intercrystallite corrosion at all. Displacement of copper and strong uniform corrosion of such steels occur only when the NH_3 concentration is 1.8%. Cuprous copper is partially oxidized to cupric during preparation of the catalyst. Cupric copper causes corrosion at lower NH_3 losses than cuprous.

It was subsequently found, however, that carbon steels can be strongly corroded, displacing copper from solution at NH_3 concentrations corresponding to the prescribed conditions, and even at higher concentrations. This occurs in two cases: 1) if, with complete immersion of the specimens in the reaction medium, the steel area exceeds 1.12 cm^2 per cc of solution; 2) if, with incomplete immersion, oxygen is present over the solution (carbon steel is quite resistant in absence of oxygen).

The most resistant material under conditions of ammonolysis of p-chlorobenzenesulfonamide is chromium – nickel steel containing 18-23% nickel and 2% molybdenum. If this steel is replaced by chromium – nickel steel

* Loss of NH_3 may occur if the operation is interrupted and the pressure falls without previous cooling of the solution [2].

without molybdenum, the ammonia concentration in the medium must not fall below 12%. If it is replaced by ordinary steel, atmospheric oxygen must not be allowed to enter the autoclave. If the prescribed conditions are observed strictly, air cannot enter the autoclave. The catalyst must be prepared in such a manner as to make oxidation of cuprous copper to cupric impossible.

LITERATURE CITED

[1] A. M. Grigorovskii and P. A. Gangrskii, Medical Ind. USSR 3, 93 (1955).

[2] Kh. L. Tseitlin, Proc. 2nd Conference on Corrosion [in Russian] I, 221 (1940).

[3] G. V. Akimov, Principles of Corrosion and Metal Protection [in Russian] (Metallurgy Press, Moscow, 1946) p. 398.

Received December 29, 1958

PREPARATION OF α-NAPHTHYLACETIC ACID AND ITS METHYL ESTER

Yu. A. Baskakov, V. N. Volkov and N. N. Mel'nikov

α-Naphthylacetic acid and some of its derivatives have varied uses in plant cultivation. The potassium salt of α-naphthylacetic acid is an active stimulant of root formation and is used in grafting and transplanting of fully-grown trees. It is used in practice for preventing fruit drop in apples and pears and to retard bud opening in fruit trees before the spring frosts. Another derivative of α-naphthylacetic acid, namely α-naphthylacetamide, is used with success for thinning of young fruits on apple and pear trees. Retardation of the sprouting of potatoes and other vegetables during prolonged storage by means of chemicals is of great economic importance. The substance most widely used for this purpose is the methyl ester of α-naphthylacetic acid, the main advantages of which over other chemicals are its high effectiveness and almost total absence of toxicity for humans[1].

Accordingly we undertook a study of methods for preparation of α-naphthylacetic acid and its methyl ester, suitable for production on the large scale.

Three methods are of the greatest interest for preparation of α-naphthylacetic acid: synthesis by way of α-naphthylchloromethane and naphthylacetonitrile [2], the Willgerodt reaction [3], and condensation of naphthalene with monochloroacetic acid. The first two methods have been studied in adequate detail and, under the conditions developed by us [2, 3], give high yields of α-naphthylacetic acid. However, the third of these methods is the simplest one-stage method for preparation of α-naphthylacetic acid. The subject of preparation of α-naphthylacetic acid by direct condensation of naphthalene with monochloroacetic acid is dealt with mainly in the patent literature, where in most cases even data on yields is lacking. According to information available in the literature, this condensation reaction proceeds at an adequate rate only in the presence of catalysts [4]; the recommended catalysts include ferric chloride or substances which form ferric chloride during the reaction [5, 6], potassium bromide [7], and salts of metals of atomic numbers from 22 to 28 – titanium, vanadium, chromium, manganese, cobalt, and nickel [8]. According to one publication [9], the reaction of monochloroacetic acid with naphthalene in presence of catalytic amounts of aluminum chloride gives very low yields of α-naphthylacetic acid. Krolik and Moiseeva developed a method for preparation of α-naphthylacetic acid by condensation in presence of aluminum powder [10]. The main disadvantage of this method is the high level of consumption of aluminum powder. The catalytic effect of iron oxides on the condensation reaction has been studied. The highest yield of α-naphthylacetic acid, 34% calculated on monochloroacetic acid, was obtained in presence of iron oxide with addition of potassium bromide [4].

We carried out experiments in order to determine the optimum conditions for synthesis of α-naphthylacetic acid in presence of various catalysts. Metal powders, and mixtures of metal powders with various additives, were tested as the catalysts. The results of some of the experiments are given in the table.

It is clear from the data in the table that when metal powders are used as catalysts the best results are obtained with zinc powder. In this case the yield is 14% calculated on monochloroacetic acid, whereas with iron powder the yield of α-naphthylacetic acid does not exceed 10%. However, addition of potassium bromide to zinc does not increase the yield appreciably, whereas the mixed catalyst consisting of iron + potassium bromide gives a 68-70% yield of α-naphthylacetic acid. The other additives: potassium iodide and potassium fluoride, have no appreciable influence on the course of condensation of naphthalene with monochloroacetic acid. We found that even in presence of catalysts and at high temperatures (185-220°), the reaction is very slow and is

Results of Experiments on Synthesis of α-Naphthylacetic Acid

Taken for reaction				Catalyst composition (g)	Molar ratio of naphthalene to monochloroacetic acid	Obtained		Yield of naphthylacetic acid (%)	
naphthalene		monochloroacetic acid				α-naphthylacetic acid (g)	naphthalene (g)	on monochloroacetic acid	on naphthalene
in g	moles	in g	moles						
57.6	0.45	14.1	0.15	0.1 Fe	3 : 1	3	46	10.5	18
57.6	0.45	14.1	0.15	0.1 Fe+0.5 KBr	3 : 1	15.3	41.4	55	65
57.6	0.45	14.1	0.15	0.1 Fe+0.5 KY	3 : 1	3.5	46	12.6	21
57.6	0.45	14.1	0.15	0.1 Fe+0.5 KF	3 : 1	6	44	21	30
57.6	0.45	14.1	0.15	0.1 $FeCl_3$+0.5 KBr	3 : 1	12	42	43	53
57.6	0.45	14.1	0.15	0.1 Al	3 : 1	2	50	7	18
57.6	0.45	14.1	0.15	0.1 Al+0.5 KBr	3 : 1	2	45	7	10.7
57.6	0.45	14.1	0.15	0.1 Zn	3 : 1	4	45	14	21.4
57.6	0.45	14.1	0.15	0.1 Zn+0.5 KBr	3 : 1	4.2	45.5	15.7	22.4
38.4	0.3	14.1	0.15	0.1 Fe+0.5 KBr	2 : 1	14	25	50	71
38.4	0.3	18.8	0.2	0.1 Fe+0.5 KBr	1.5 : 1	13	21	35	54
38.4	0.3	23.5	0.25	0.1 Fe+0.5 KBr	1.2 : 1	10	15	21.5	51
1152	9	283.2	3	2.0 Fe+10 KBr	3 : 1	330	830	59	70
3756	29	948	10.1	6.6 Fe+33 KBr	3 : 1	1256	—	68	—
2872	22.4	756	8	5.2 Fe+26 KBr	2.8 : 1	1026	—	69	—
3072	24.0	750.2	8	4 Fe+20 KBr	3 : 1	1012	1962	68	62

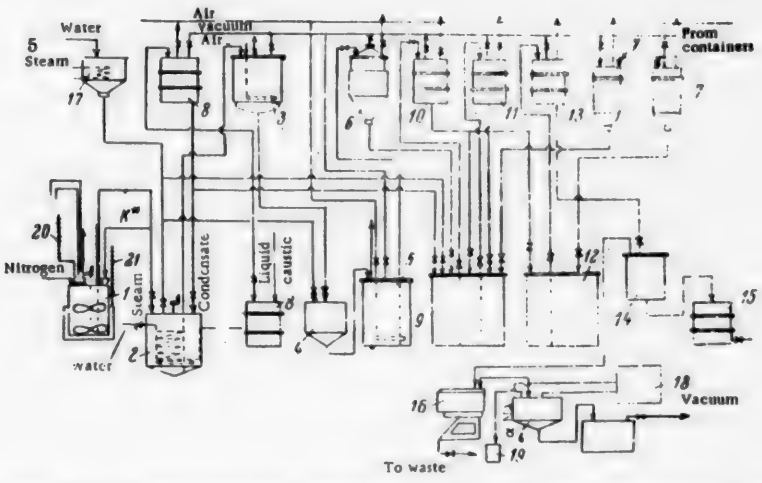

Flow sheet of α-naphthylacetic acid production: 1) reactor, 2) extractor, 3) settler for extract, 4) suction filter, 5) vacuum tank, 6) measuring tank for extract, 7) measuring tank for HCl, 8) measuring tank for NaOH solution, 9) neutralizer, 10) receiver for salt solution, 11) receiver for resins, 12) precipitating tank, 13) receiver, 14) vacuum filter, 15) vacuum tank for water collection, 16) centrifuge, 17) vacuum receiver, 18) heater, 19) plywood drum, 20) manometer, 21) thermometer, K*) catalyst (with naphthalene and monochloroacetic acid).

complete only after 20 hours. The ratio of the amounts of naphthalene and monochloroacetic acid taken for the reaction is important. For high yields a threefold excess of naphthalene is required. In the earliest experiments the catalyst used was potassium bromide with reduced iron. However, later it was found that the yields are not

reduced if, instead of reduced iron, powdered steel 3 is used, while the yields are even somewhat higher with cast-iron powder.

As the result of these experiments the following optimum conditions for preparation of α-naphthylacetic acid were established.

A flask fitted with an air condenser was charged with 3072 g of naphthalene, 750.2 g of monochloroacetic acid, 4 g of iron powder, and 20 g of potassium bromide. The mixture was heated on an oil bath. The temperature of the mixture (with a thermometer inside the flask) was slowly raised from 180 to 220° at an average rate of 2° per hour. The liberated hydrogen chloride was collected in absorbers containing water. The reaction was essentially complete after 20 hours. When the heating ended, the mixture was cooled to 110° and poured out, with stirring, into 2% NaOH solution (288 g NaOH and 14 liters of water) heated to 80-85°. The extraction was continued at the boil for 1 hour with mechanical stirring. The reaction mixture was then allowed to cool to room temperature with continued stirring (naphthalene did not solidify in lumps if the mixture was stirred during the cooling) and the naphthalene was filtered off and washed with 500 ml of water. The filtrate was made neutral to litmus and 500 ml of 10% calcium chloride solution was added until a transparent slightly yellowish solution was obtained. The precipitate was filtered off, and α-naphthylacetic acid was isolated by acidification of the filtrate with hydrochloric acid, for which 1100 g of 27% hydrochloric acid was required. The α-naphthylacetic acid was filtered off, washed with 300 ml of water, and dried at 80°. The yield was 1012 g or 68% calculated on the monochloroacetic acid taken. The recovered naphthalene was dried and purified by distillation. 1962 g of naphthalene was recovered. The α-naphthylacetic acid melted at 116-120°, and had a somewhat low molecular weight as indicated by titration with alkali. This was due to the presence of a small amount (from 5 to 8%) of 1,5-naphthylenediacetic acid, in addition to neutral impurities.

The methyl ester of α-naphthylacetic acid can be prepared from α-naphthylacetonitrile [11] or from α-naphthylacetic acid [12]. Direct esterification of α-naphthylacetic acid on heating in presence of sulfuric acid has been described. The ester was obtained in 64% yield [12]. To find the optimum conditions for preparation of the methyl ester of α-naphthylacetic acid, we studied the esterification reaction with different amounts of sulfuric acid and methyl alcohol. It was found that the yield of the methyl ester of α-naphthylacetic acid is increased considerably and approaches the theoretical if the esterification in presence of sulfuric acid is performed at room temperature.

The optimum conditions for preparation of the methyl ester of α-naphthylacetic acid were as follows.

To 186 g of α-naphthylacetic acid, 96 g of methyl alcohol and 35-40 g of sulfuric acid (d = 1.84) was added. The sulfuric acid was added gradually with thorough stirring so that the temperature of the mixture did not rise above 45°. After all this amount of sulfuric acid had been added the reaction mixture was stirred for 3-4 hours at room temperature. At the end of the stirring, the reaction mixture was poured into 500 ml of water. The liberated oil was separated off, washed with sodium carbonate solution and water, and dried. The yield was 194-195 g or 97-97.5%. The ester formed from crude α-naphthylacetic acid contained the dimethyl ester of naphthylenediacetic acid as an impurity, but it was almost equivalent in physiological activity to chemically pure methyl ester of α-naphthylacetic acid.

Our methods for production of α-naphthylacetic acid and its methyl ester were tested under works conditions, and the optimum synthesis procedure was confirmed in trials in a large-scale plant unit. It was found that when the condensation of naphthalene with monochloroacetic acid was effected in lead-lined equipment the yield of α-naphthylacetic acid was not decreased.

A specimen flow sheet for production of α-naphthylacetic acid is shown in the diagram.

SUMMARY

Under the optimum conditions found for the condensation of naphthalene with monochloroacetic acid in presence of a mixed catalyst consisting of iron + potassium bromide, it is possible to obtain α-naphthylacetic acid in yields of up to 70%, and by esterification of α-naphthylacetic acid by methyl alcohol in presence of sulfuric acid at room temperature, almost quantitative yields of the methyl ester of α-naphthylacetic acid can be obtained. The methods are suitable for large-scale production.

LITERATURE CITED

[1] N. N. Mel'nikov, Yu. A. Baskakov and K. S. Bokarev, Chemistry of Herbicides and Plant-Growth Stimulators [in Russian] (Goskhimizdat, Moscow, 1954).

[2] Yu. A. Baskakov and N. N. Mel'nikov, Proc. Acad. Sci. USSR 97, 543 (1954).

[3] Yu. A. Baskakov and N. N. Mel'nikov, J. Appl. Chem. 28, 1016 (1955).*

[4] J. Ogata and J. Ichiguro, J. Am. Chem. Soc. 72, 4302 (1950).

[5] British Patent 692341; Chem. Abs. 48, 7640 (1954).

[6] Federal German Patent 868298; Zbl. 126, 1841 (1955).

[7] U. S. Patent 2655531; Chem. Abs. 48, 11494 (1954).

[8] French Patent 1058915; Zbl. 126, 9199 (1955).

[9] J. Teijro, T. Kinijiro, M. Shinsi and K. J. Toshihide, Agron. Chem. Soc. Japan 18, 975 (1942).

[10] L. G. Krolik and Z. G. Moiseeva, Authors' Certif. No. 76549 (1952).

[11] Orescanin-Majhofer, Kemija u. industriji 2, 75 (1953).

[12] Baranowska, Przemysl Chem. 7, 291 (1951).

Received March 1, 1958

* Original Russian pagination. See C. B. Translation.